Impacts of Structurally Related Impurities on Crystal Growth and Purity in Acetaminophen: A Study of Single Crystal Stagnant Solution and Bulk Suspension Crystallisation

Layla Parsons

PhD Thesis

Thesis submitted to the Chemical and Process Engineering Department at the University of Strathclyde in accordance with the requirements for the degree of Doctor of Philosophy

2024

Declaration of author's rights

This thesis is the result of the author's original research. It has been composed by the author and has not been previously submitted for examination which has led to the award of a degree. The copyright of this thesis belongs to the author under the terms of the United Kingdom Copyright Acts as qualified by University of Strathclyde Regulation 3.50. Due acknowledgement must always be made of the use of any material contained in, or derived from, this thesis.

Signed:

Date:

Dedication

I wish to dedicate this thesis to my beloved daughter, Genevieve. Despite being just six years old, she is a constant source of inspiration, driving me to strive for success and persevere through challenges. My husband Gary is my unwavering support, always there to lend a helping hand in any way he can. Lastly, I am deeply grateful to my mum, who has always believed in me and provided unwavering support and encouragement. Without their continuous love and encouragement, I wouldn't be where I am today.

Acknowledgements

List of publications

Peer reviewed journal publications:

- Nguyen, T.T., Khan, A., Bruce, L.M., Forbes, C., O'Leary, R.L. and Price, C.J., 2017. The Effect of Ultrasound on the Crystallisation of Paracetamol in the Presence of Structurally Similar Impurities. *Crystals*, *7*(10), p.294-318.

- Ottoboni S, Chrubasik M, Mir Bruce L, Nguyen TT, Robertson M, Johnston B, Oswald ID, Florence A, Price C. Impact of Paracetamol Impurities on Face Properties: Investigating the Surface of Single Crystals Using TOF-SIMS. Crystal Growth and Design. 2018 Mar 26;18(5):2750-8.

Conference presentation contribution:

- Bruce, L. M., Price, C. J. and Binti. H. H. The impact of solvent systems, process conditions, and structurally related impurities on the growth rate and morphologies of paracetamol crystals. Oral presentation at the 12th International Workshop of the Crystal Growth of Organic Material and 47th Annual British Association of Crystal Growth Joint Conference, 26th – 30th June 2016, University of Leeds. Third place poster prize.

Conference poster contribution:

- Bruce, L. M., Price, C. J. and Binti. H. H. The impact of solvent systems, process conditions, and structurally related impurities on the growth rate and morphologies of paracetamol crystals. Poster presentation at the 12th International Workshop of the Crystal Growth of Organic Material and 47th Annual British Association of Crystal Growth Joint Conference, 26th – 30th June 2016, University of Leeds.
- Bruce, L. M., Price, C. J. and Nguyen. T.T.H. The use of ultrasound to actively remove structurally related impurities from paracetamol. Poster presentation at

the 4th Winter Process Chemistry Conference, 12th – 14th December 2016, University of Strathclyde.

- Bruce, L. M., Price, C. J. and Nguyen. T.T.H. Using ultrasound to remove impurities from paracetamol. Poster presentation at STEM for BRITAIN Conference, 13th March 2017, Houses of Commons.

Abstract

Crystallisation is a widely used technique in the purification, separation, and pre-formulation processes, yielding crystals with diverse shapes and sizes. The morphology of a crystal, including its faces and habits, determines its overall appearance. External factors like supersaturation, temperature, and solvent choice greatly influence the crystal habit. While it is possible to stabilise these factors, the removal of impurities presents a significant challenge, whether they originate from chemical sources or other origins. Although various methods, such as filtration, washing, and recrystallisation are employed to remove impurities, they have limitations.

Impurities exhibit varied effects in crystallisation systems, whether intentionally introduced or generated during the process. It is crucial not only to identify the source but also to understand the impact on drug solubility and crystal growth. Batch-to-batch variations can hinder downstream processes, making optimisation challenging. Changes in crystal habit can affect the compressibility and consolidation behaviour of drugs, resulting in the loss of valuable Active Pharmaceutical Ingredients (APIs). Impurities can also alter the flowability of fluids and the cake's permeability, leading to increased particle breakage.

In this study, the influence of metacetamol and acetanilide additives on the solubility of paracetamol in ethanol and isoamyl alcohol is investigated. Typically, drug substances exhibit higher solubility in alcohols compared to water, and evaluating solubility provides insights into dissolution rates in different solvents. Impurities were observed to have a modest effect on solubility at loadings of 1-4%. Metacetamol significantly reduced solubility in ethanol at low temperatures, while acetanilide decreased solubility at higher temperatures (25°C to 55°C). In isoamyl alcohol, the effects of impurities on solubility varied, with metacetamol generally increasing solubility at each temperature and acetanilide decreasing solubility from 25°C to 55°C.

Furthermore, the growth rates of single crystals in a stagnant ethanol solution was evaluated the influence of impurities (metacetamol and acetanilide) on habit modification and growth rates specific to crystal faces was also investigated. The growth of multiple crystal habits in a single system on several occasions was observed. As impurity concentrations increased, the growth rate of inhibited crystal faces decreased along with alterations in crystal habits. Additionally, the effect of an ultrasonic toothbrush was found to induced nucleation and growth of single crystals in all cases, leading to the formation of previously unseen habits.

Finally, the addition of ultrasound in a bulk suspension crystallisation system was explored to assess its impact on nucleation, temperature, crystal size distribution, habit, filtration rate, and product purity. Ultrasound increased the rate of nucleation, overall yield, and product purity, resulting in smaller particle sizes, reduced agglomeration, and a narrower particle size distribution. Metacetamol proved to be the most challenging impurity in terms of incorporation and its overall influence on nucleation, growth, and crystal habits.

These findings highlight the potential of sonocrystallisation to modify crystal habits and enhance the growth, purity, and yield of drug substances. Future studies examining the impact of ultrasound on purity will contribute to better control and optimisation of crystallisation parameters, thereby preventing the formation of undesired crystal habits and impurity concentrations.

Table of Contents

List of Symbols

Symbol (English)	Symbol (Greek)	Meaning	Page
	C	Speed of light in a vacuum or a medium (m s^{-1})	40
	f	Frequency of the wave (Hz) or (s^{-1})	40
	λ	Wavelength of light (nm or m)	40 110
	C	Speed of sound in the material/medium (m s^{-1}).	40 42
	K	Bulk modulus of the material, which is a measure of the material's resistance to compression. It is measured in pascals (Pa) or newtons per square meter (N m^{-2}).	40
	ρ	Is the density of the material/liquid, measured in kilograms per cubic meter (kg m^{-3}).	40 42
	E	Young's modulus of the material, which is a measure of its stiffness or elasticity in the direction of an applied force. It is measured in pascals (Pa) or newtons per square meter (N m^{-2}).	40
	G	Shear modulus of the material, which represents its resistance to deformation when subjected to shear stress. It is also known as the modulus of rigidity and is measured in pascals (Pa) or newtons per square meter (N m^{-2}).	40
	I	Intensity of the sound or light wave, measured in watts per square meter (W m^{-2}).	42
	P_o	The amplitude of the sound wave, which represents the maximum pressure variation from the equilibrium position. It is measured in pascals (Pa).	42

		Filtrate volume (m^3)	129 130
V		Filtrate volume (m^3)	129 130
	ΔP	Pressure difference along the filter axis (Pa)	129 130
	α	Cake resistance relating to cake filterability (m.kg^{-1})	129 130
	μ	Mother liquor viscosity (Ns m^{-2})	129 130
C		Concentration of solids (kg m^{-3})	129 130
A		Filtrate area of cake (m^2)	129 130
R_m		Resistance of the filter medium (m^{-1})	129 130
x		Mole fraction of the solute	131
	ΔH_f	Molar enthalpy of fusion of the solute (J mol $^{-1}$)	131
R		Gas constant (8.314 mol^{-1} K^{-1})	131
T_f		Fusion temperature (melting point) of the solute	131

List of Units/Abbreviations

Units	Meaning
kHz	Kilohertz
mm	Millimetres
µL/min	Microliters/minute
%w/w	Percent weight per weight
mol%	Mole Percent

Abbreviations	Meaning
API	Active pharmaceutical ingredient
B.S.C	Bulk suspension crystallisation
BFDH	Bravais-Friedel-Donnay-Harker
CLD	Chord length distribution
CNT	Classic nucleation theory
DoE	Design of experiment

DSC	Differential Scanning Calorimetry
emc	Electronic medicines compendium
FBRM	Focused Beam Reflectance Measurement
Fps	Frames per second
GRD	Growth rate dispersion
HPLC	High-Pressure Liquid Chromatography
MBSL	Multibubble Sonoluminescence
MLR	Multiple linear regression
MZ	Metastable Zone
MZW	Metastable Zone Width
PAA	p-acetoxyacetanilide
PSD	Particle Size Distribution
S.C.G.	Single Crystal Growth
TOF-SIMS	Time of Flight Secondary Ion Mass Spectroscopy
UK	United Kingdom
U.S.	United States
US	Ultrasound
XRD	X-ray diffraction
XRPD	X-ray powder diffraction

List of Tables

List of Figures

Chapter 1: Introduction

Summary:

This section presents the research background for this project with the overall aims and objectives.

Chapter 1: Introduction

1.0: Research background

Crystals are widely present in various contexts, ranging from natural occurrences like diamonds and quartz to everyday products such as salt and sugar. Crystallisation is a crucial technique in process industries to separate and purify products (1). The historical significance of crystallisation is evident as early as 1556, when Agricola described evaporative crystallisation in salt production (2).

The UK accounts for 2.6% of the global pharmaceutical market (3), with twelve of the top twenty pharmaceutical companies operating at fifty five sites in the country (4). Crystallisation plays a vital role in the manufacturing process of many products, aiding in removing hazardous or unwanted impurities. This purification occurs through molecular recognition and the rejection of impurities during crystal growth (5). Crystals are three-dimensional structures composed of regularly packed atoms, ions, or molecules with symmetrically arranged faces, forming a lattice at the core of the structure (6).

In most cases, impurity molecules are rejected at the growth site on the crystal surface due to a mismatch with the lattice. However, there are instances where the lattice mismatch is small enough for the impurities to attach to the crystal face. The presence of impurity molecules disrupts crystal growth by slowing down and partially obstructing growth at that specific location on the crystal face (5, 7-9). If the driving force for crystallisation significantly increases, the impurity can become overgrown and permanently incorporated into the crystal lattice (5). Impurities are commonly found in pharmaceutical products, with pharmaceutical companies often allowing up to 1% of impurities in their products and higher percentages in incoming feed solutions. The presence of impurities can have serious implications, such as reduced crystal growth rates, increased processing time, incomplete desupersaturation, and loss of product in waste streams (5). Biscans on behalf of the European Federation of Chemical Engineers highlighted that the improvement of crystal purity and increased efficiency in crystallisation processes are critical challenges to overcome (10).

Chapter 1: Introduction

This research investigates the growth of different crystal habits under identical conditions, with and without impurities. Various methods can be used to grow single crystals, typically using the cooling crystallisation technique at low temperatures (8, 11). However, limited research actively tracks the effects of different conditions on single crystals over time. When comparing stagnant and flow cells it was found that stagnant cells were better at enabling growth of single crystals. This lead to the discovery of stable forms and new habits of L-Glutamic acid (12). This project introduces a novel approach by utilising ultrasound to actively remove impurities from the crystal surface during the growth process. The objective is maintaining a crystal surface relatively free of attached impurity molecules by intervening at each active growth site (13). Ultrasound exhibits several beneficial effects, including increased molecular motion around the growing crystals, enhanced molecular transport to and from the crystal faces, reduced processing time, and improved product purity (14). Previous research on ultrasound in crystallisation has predominantly focused on nucleation, demonstrating reduced induction time and increased nucleation rates (15). Controlling nucleation with ultrasound has been found to improve product properties and filtration characteristics (16, 17).

This research paves the way for enhancing batch and continuous processes. The anticipated acceleration of crystallisation can potentially reduce batch cycle times, while continuous crystallisers can benefit from reduced residence time and crystalliser volumes (18). Using ultrasound in the growth of single crystals offers opportunities to improve crystallisation processes and achieve greater efficiency.

Chapter 1: Introduction

1.1: Research objectives

The research question underlying this PhD is:

"What are the implications of structurally related impurities in crystallisation systems, and to what extent do they affect solubility, crystal growth, and habit formation? Can sonocrystallisation effectively mitigate these impacts by preventing impurity incorporation, on the crystal surface during growth, thereby preserving the overall growth process?"

This question will be answered by:

- Determination of the overall effect selected impurities have on the solubility of the model compound, paracetamol, in ethanol.
- Analyse the impact of structurally related impurities (metacetamol and acetanilide) on individual crystal face growth rates and habits, in the presence and absence of ultrasound as a function of supersaturation and impurity loading in a single crystal stagnant cell.
- Scaling up the single crystal stagnant cell quantities to simulate batch production in the industry (bulk suspension crystallisation). Utilising an ultrasonic bath during cooling crystallisation to examine the effects of ultrasonic intervention on product purity, crystal habit, yield, and degree of crystal perfection.

1.2: Project funding and supervision

Chapter 1: Introduction

1.3: Thesis organisation

This thesis consists of seven chapters and accompanying appendices.

Chapter 1 lays the groundwork for this research by defining the research questions and outlining the corresponding experimental objectives.

Chapter 2 presents the concepts of crystallisation and sonocrystallisation. The chapter delves into the fundamentals of sonocrystallisation and the broader topic of crystallisation, discussing areas such as the workings of ultrasonic waves, sound propagation and velocity, acoustic intensity, sound absorption and attenuation, acoustic impedance, and the phenomena of reflection, refraction, and cavitation. It discusses the hot-spot theory, the impact of cavitation in liquid-solid systems, the correlation between frequency and cavitation, and the technical aspects of power ultrasound generation and the relevant equipment. Examining crystallisation processes with a particular emphasis on the role of impurities. Exploring how impurities affect various aspects of crystallisation, including solubility, supersaturation, metastable zone width, nucleation, crystal growth, crystal morphology, and polymorphism. The discussion concludes with a review of the crystallisation and characterisation techniques used in this research, and mutual influences of sonocrystallisation and traditional crystallisation methods.

Chapter 3 provides in-depth information about the materials and methodology employed in the investigations conducted in chapters 5, 6, and 7.

Chapter 4 presents experimental data regarding the solubility of paracetamol, metacetamol, and acetanilid. The chapter investigates the impact of introducing metacetamol and acetanilide impurities at 2 and 4 mol% on the solubility of paracetamol in ethanol and briefly discusses isoamyl alcohol.

Chapter 1: Introduction

Chapter 5 measures single crystal growth rates concerning different crystal habits of paracetamol. This encompasses conditions with and without the inclusion of metacetamol and acetanilide impurities. Additionally, the chapter explores the influence of ultrasound, delivered through an ultrasonic toothbrush, on crystal growth in the presence and absence of metacetamol and acetanilide.

Chapter 6 investigates the effects of ultrasonic intensity on paracetamol in bulk suspension crystallisation with and without metacetamol and acetanilide impurities at 2 and 4 mol% in an ethanol solution.

Chapter 7 provides a comprehensive review of the key findings from this research and offers recommendations for future work.

Chapter 2: Sonocrystallisation Principles and Crystallisation Science

2.0: Sonocrystallisation principles introduction

The common perception of ultrasound is as a diagnostic tool used for scanning unborn babies. However, ultrasound finds applications across various industries, including pharmaceutical (19), chemical (20), engineering (21) and food (22) sectors. Pioneering work on the physical, chemical, and biological effects of high-frequency acoustic waves (ultrasound), including the impact on the crystallisation of paraffin wax, was published by Richards and Loomis (134) and Wood and Loomis (135). Turner (134) reported that sugar solutions, which were typically resistant to crystallisation, could be induced to crystallise with a short burst of high-intensity ultrasound. In 1962, Pfizer obtained a patent for the first pharmaceutical application of ultrasound, demonstrating that ultrasound could produce a uniform size distribution and reduce the crystal size of procaine penicillin (23). In the same year, Principe and Skauen (24) investigated the hormone progesterone and sought an alternative method to reduce particle size without milling. They discovered that higher intensities of insonation led to the formation of smaller particles. Hem (136) proposed a theory that ultrasound's ability to create small, uniform crystals could be attributed to the formation of cavitation bubbles when ultrasound passed through the solution. Additionally, a latter paper suggested that the greater pressures generated upon the collapse of a cavitation bubble could induce nucleation by causing a change in the melting point of a solid.

Subsequently, there has been a notable increase in the application of ultrasound to enhance crystallisation processes, driven by the desire to understand, control, and achieve desired outcomes in various industries.

2.1: Acoustic Theory

2.1.1: Ultrasonic wave

Sound propagates through a medium with elastic properties (solid, liquid, or gas) through vibrations, forming a wave with a specific frequency. When a device generates sound, it necessitates some form of mechanical work; this mechanical energy transmitted through the medium gives rise to sound (25). The velocity of sound in air is 343 m s^{-1} but in liquids it is much higher, for example 1,497 m s^{-1} in water (26).

Acoustic waves are characterised by their frequency (number of cycles per second), wavelength (distance between cycles) and amplitude (wave height). These waveforms are classified based on the frequency into infrasonic (below the limits of human hearing, approximately 20 Hz), sonic (within the audible range) and ultrasonic (above the limits of human hearing, >20,000 Hz) (25, 27, 28). Figure 1 illustrates the minimum and maximum audible frequencies for various species, along with the frequency of sound output of selected species, phenomena, and equipment (25).
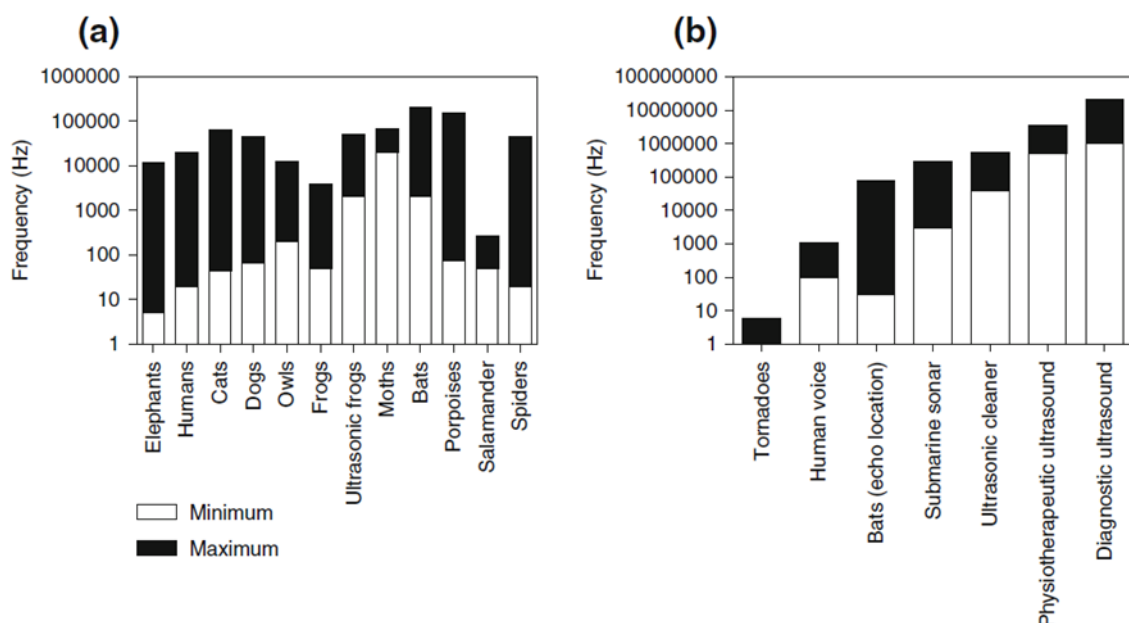
Figure 1: Acoustic frequency (a) Detection in various species (b) Emission in various species, phenomena, and equipment. The columns represent the minimum (white) and maximum (black) frequencies of detection and emission (25).

2.1.2: Wave propagation, velocity of sound and wavelength

Acoustic waves are characterised by their longitudinal nature, propagating through a medium by causing the localised displacement of molecules through oscillation around the equilibrium position. This process results in the transmission of energy through consecutive compression and rarefaction cycles, with the distance between two successive points corresponding to the wavelength λ (27).

The relationship between acoustic velocity, C (ms^{-1}), wavelength λ (m), and frequency f (s $^{-1}$) is described by Equation 1:

$$C = \lambda f$$ **Equation 1**

This equation illustrates that the wavelength of sound is inversely proportional to its frequency (27). The velocity at which sound travels through a liquid or gas is dependent on the material's bulk modulus K, which signifies its resistance to compression. The bulk modulus is the ratio between pressure increase and the resulting decrease in the material's volume, while ρ represents the density (Equation 2).

Equation 2

$$C = \sqrt{\frac{K}{\rho}}$$

When sound waves propagate through a solid, Young's modulus E is employed. Equation 3 illustrates the relationship between Young's modulus E and the bulk modulus (K), where G represents the shear modulus (25, 29):

Equation 3

$$E = K + \frac{4}{3}G$$

In a longitudinal wave, as depicted in Figure 2 (25), the molecules undergo displacement along the axis of the wave.
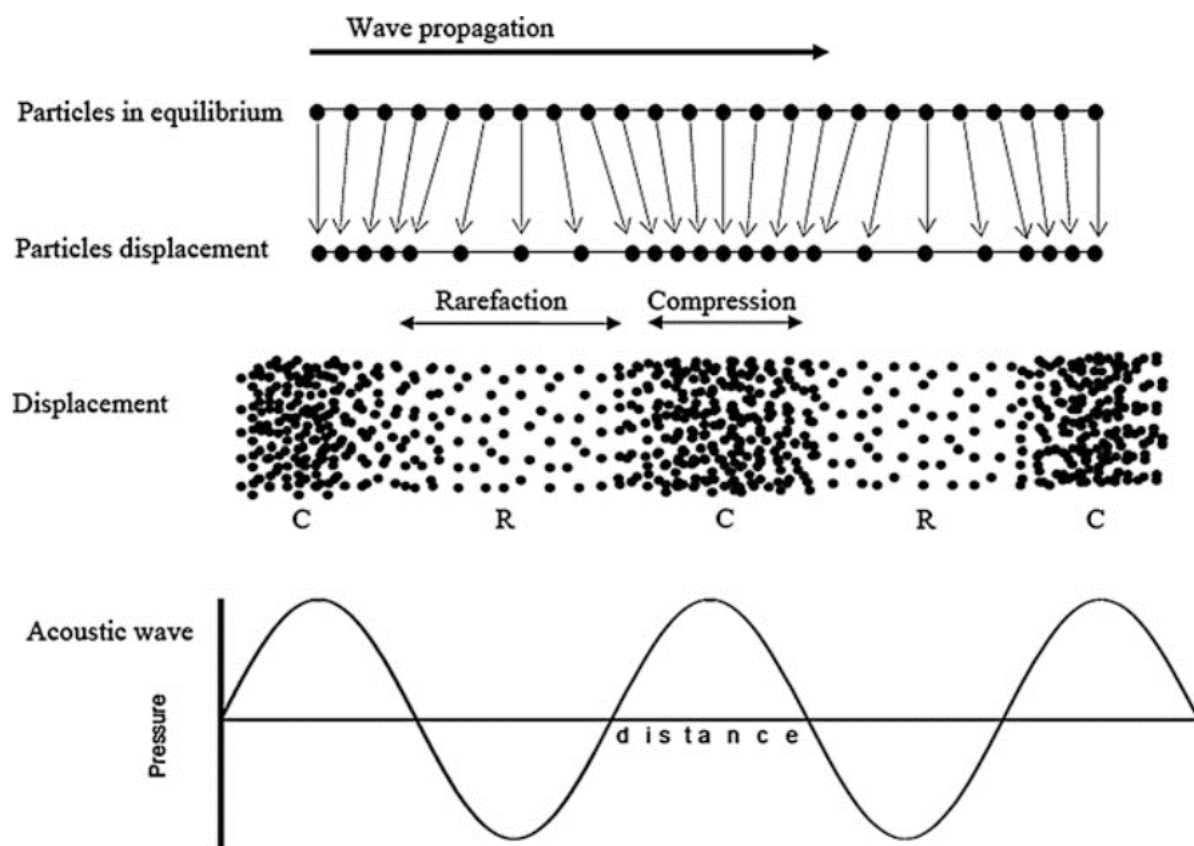
Figure 2: Depicts a longitudinal acoustic wave, with wave propagation initiating from the left and moving towards the right (25).

The mechanical vibrations (30) produce compression and rarefaction (expansion) phases in the wave, corresponding to its maximum and minimum amplitudes, respectively. In the compression phase, the molecules of the liquid experience a positive pressure, causing them to come closer together. Conversely, during rarefaction (expansion), the wave exerts a negative pressure on the molecules, drawing them away from one another (31).

2.1.3: Ultrasonic intensity

The ultrasonic intensity is directly related to the amplitude of vibrations produced by the ultrasonic source. Consequently, increasing the amplitude of vibration leads to a higher vibration intensity, resulting in an enhanced desired sonochemical effect (32). These vibrations carry kinetic energy derived from the waves themselves, and monitoring this energy enables the measurement of the intensity associated with the

ultrasonic field. This intensity is defined as the power delivered to the liquid through interaction with the surface of the ultrasonic transducer, and it is expressed in Equation 4 as the relationship between ultrasonic power or intensity and acoustic pressure:

$$I = \frac{P_o{}^2}{2_\rho C}$$

Equation 4

In the equation, I represents the power (intensity) of the sound wave, P_o is the acoustic pressure, ρ is the density of the liquid, and C is the speed of sound within the liquid. Showing that as the ultrasonic intensity increases, the acoustic pressure also increases (33).

2.1.3a Absorption and sound attenuation

As an ultrasonic wave propagates through a medium, such as a suspension of crystals in a solution, its intensity undergoes attenuation (reduction) with increasing distance from the source. This attenuation results from various factors, including scattering, reflection, diffraction, and refraction of the wave, as well as absorption and the conversion of the wave's kinetic energy into heat (34).

To calculate the intensity I at a distance *d* from the source, Equation 5 is used:

$$I = I_0 \exp\left(-2\alpha d\right)$$

Equation 5

In this equation, α represents the absorption coefficient, which is dependent on the frequency of the sound and the characteristics of the medium. The absorption coefficient and the velocity of sound in the medium are independent of the amplitude and geometry of the container or sample (35).

As the molecules within the medium vibrate in response to the ultrasonic sound waves, they interact and transform the acoustic energy into heat. Consequently, this heat energy leads to a bulk heating effect within the medium, causing a temperature increase of several degrees Celsius. To ensure accurate and controlled experimental conditions, effective thermostating is necessary (27).

2.1.3b Reflection and refraction of sound waves

When a transducer emits an ultrasonic wave, it will eventually encounter an interface between two different media. At this interface, a portion of the wave energy will be reflected into the first medium at the same speed, while the remaining energy will be transmitted into the medium beyond the interface, travelling with the velocity of sound in the new medium. This transmission and reflection phenomenon occurs due to the mismatch in acoustic impedance between the two media. If the sound wave strikes the new material at an angle other than 90°, it will be refracted either towards the normal if the velocity of sound is lower in the new medium or away from it if the velocity of sound in the new medium is higher.

Furthermore, when the ultrasonic wavelength is greater than or equal to the dimension of the reflecting object, the incident beam will undergo scattering (27).

2.1.4: Cavitation

Acoustic cavitation is a highly dynamic and intricate process (146), impacted by a myriad of factors, including frequency, power, mode of sonication, transducer type, reactor geometry, liquid volume, dissolved gas type and amount, solvent selection, solute concentration, and surface activity of solutes in the solution. This phenomenon encompasses the formation, growth, and implosion of bubbles within a liquid, with its dynamics intricately linked to the local environment. Depending on the circumstances, cavitation phenomena can yield advantageous or detrimental effects. The conditions created by cavitation play a pivotal role in facilitating sonochemical reactions (36) and have also been associated with significant erosion damage to hydraulic machinery and ship propellers, prompting extensive research since the 1950s (37).

When a sound wave passes through a liquid medium, it undergoes compressional and rarefaction cycles, causing the molecules to oscillate due to positive and negative pressure. In the rarefaction cycle, high negative pressure leads to the formation of cavitation bubbles, as depicted in Figure 3 (38). The intensity of the sound wave is represented by a grayscale at the top of the image, with darker sections indicating

higher intensity and lighter sections indicating lower intensity. The intensity correlates with the amplitude shown in the middle section of the figure, where increased amplitude results in greater positive and negative pressure. The size of the cavitation bubble oscillates with the frequency, known as stable cavitation. The volume change and the expansion and contraction of the bubble depend on the amplitude of the sound wave.

Cavity growth is affected by the sound intensity, and when the intensity is increased, a point is reached where transient cavitation occurs. During numerous expansion and compression cycles, gas diffuses into the bubble more than it diffuses out. The surface area of the bubble in the rarefaction cycle is greater than in the compression cycle, resulting in high pressure in the compressed state and low pressure in the expanded state. The bubble collects dissolved gas from the surrounding solution, leading to its growth through cycles, with the ability to also grow by coalescing with other bubbles. Eventually, a cavitation bubble reaches a critical size where it can no longer sustain itself, leading to a catastrophic collapse or implosion, as illustrated in Figure 3. At this point, the local conditions become extreme enough for chemical reactions to occur (36).

In the transient cavitation phase, when a bubble collapses near a crystal surface, shear stress creates cavitation centres, despite a potential reduction in local supersaturation resulting in secondary nucleation, a well-documented phenomenon (39-42). Additionally, various other outcomes are likely to occur, such as acoustic emissions, light emissions, surface erosion, free radical formation, and the generation of highly localised hot spots.

Ultrasonic cleaning is a common application of cavitation, where the asymmetric collapse of bubbles adjacent to a surface generates microjets of fluid, leading to the cleaning effect. After the cavitation bubble collapses, the remaining microbubble fragments are subjected to the next compression cycle of the ultrasonic wave, and the process repeats itself (38).
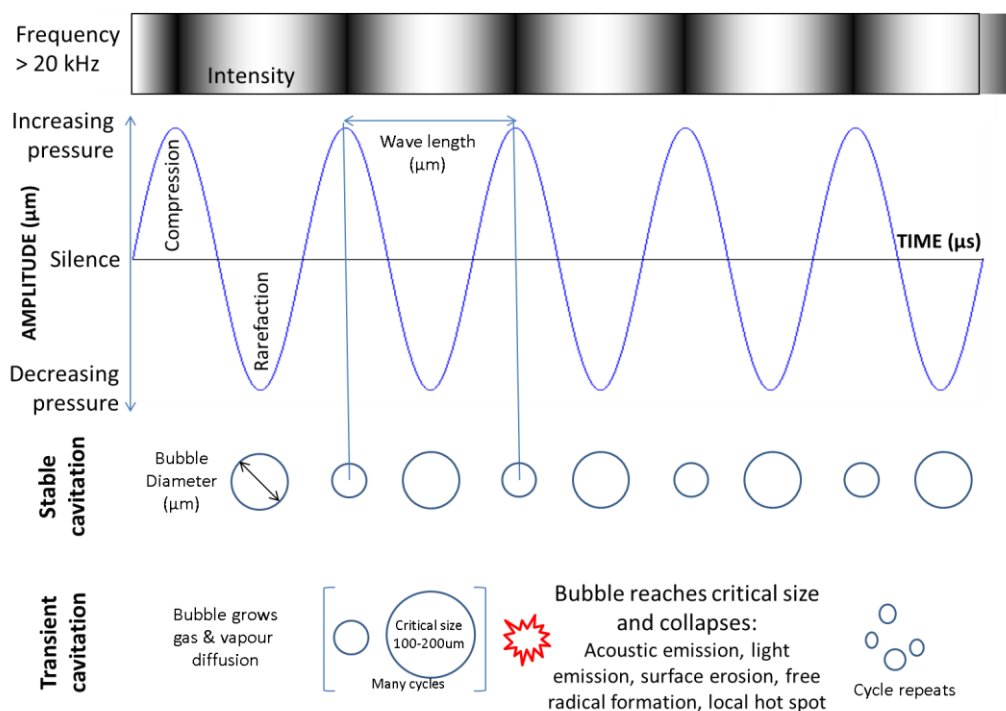
Figure 3: The intensity of a sound wave, illustrating how stable cavitation grows with the correlating amplitude/compression/rarefaction of the sound wave to eventually create transient cavitation where the bubble collapses creating a variety of outcomes (38).

2.1.4a Parameters that affect ultrasonic cavitation

Ultrasonic cavitation, a physical phenomenon, involves various critical parameters that must be taken into consideration:

1. Amplitude of the sound wave: High amplitudes generate intense cavitation, which may lead to chemical degradation and the violent collapse of cavitation bubbles. The violent collapse can result in localised heating and pressure spikes, potentially affecting the reaction environment and the materials involved. Careful control of the ultrasound amplitude is essential to avoid undesirable effects and ensure safe and effective ultrasonic applications (32, 43-45).

2. The frequency of the sound wave plays a crucial role in the generation of cavitation. Operating at high sonic frequencies in the MHz range often results in weak or no cavitation due to the short duration of the wave's expansion phase, which limits the stretching and pulling apart of liquid

molecules required for intense cavitation. In contrast, lower frequencies in the kHz range are more effective at inducing cavitation since they allow sufficient time for the expansion phase to create strong pressure variations. Although higher frequencies can reduce transducer thickness, which may impact heat exchange, they are less likely to generate violent cavitation with higher localised pressures during bubble collapse. However, it is essential to note that higher frequencies generally require higher energy levels to induce cavitation, as the energy required is related to the frequency and wavelength of the sound wave (31, 46-48).

3. Solvent properties: Solvents with high vapour pressure, low surface tension, and low viscosity favour the formation of cavities. However, the higher vapour pressure causes undercooling and evaporation of the solvent from the bubble's surface towards the core during expansion, resulting in the cavity filling with vapour and cooling the surface liquid. This leads to a cushioned, less violent collapse of the bubble (31, 43, 44, 46, 49).

4. External temperature increases the acoustic intensity required to induce cavitation in a liquid due to reduced viscosity. Cavitation activity may become more energetic and potentially damaging at higher temperatures. The vapour pressure of a liquid is independent of external temperature changes (31, 43, 46, 47).

5. External pressure raises the boiling point of a liquid, making it harder to induce cavitation. Cavitation occurs when the pressure drops below the vapour pressure of the liquid, leading to the formation, growth, and collapse of vapour bubbles within the liquid. When the pressure decreases to the vapour pressure, the liquid starts to vaporise, forming cavitation bubbles. However, as the external pressure increases, the boiling point of the liquid also increases, making it less likely for cavitation to occur since higher pressure is required to reach the vapour pressure and induce cavitation (31, 43, 49).

6. Gas properties: The presence of soluble gases dissolved in the insonated solution results in the formation of more cavitation nuclei. When the gas solubility is higher, more gas molecules dissolve in the liquid, forming larger and more stable cavitation bubbles. Larger bubbles can collapse more violently, generating stronger shockwaves upon bubble collapse. The heat

capacity ratio $(\frac{C_p}{C_v})$ or polytropic ratio $(\gamma = (\frac{C_p}{C_v}))$ and thermal conductivity of the gas influence the final temperature produced during bubble collapse. Gases with higher thermal conductivity will experience a decrease in temperature during collapse (31, 43, 44, 46, 47). Further information on specific gases is available in Vajnhandl's work (31).

Careful consideration of these parameters is essential to optimise ultrasonic cavitation conditions for specific applications.

2.1.4b Theories of sonochemical effects

Ultrasound can enhance catalyst activity through various mechanisms, including the enlargement of surface areas through particle breakage, efficient mixing of reagents, and improved transport to and from the catalyst surface, accelerating catalysed reactions. Additionally, ultrasound can increase reaction rates by promoting the formation of reactive radical species during cavitation, leading to the degradation of organic components (44, 50).

There are three main types of sonochemical processes:

1. Homogeneous sonochemistry occurs during ultrasound-induced cavitation in the liquid phase. It involves the formation of radicals and excited species within cavitation bubbles during collapse, leading to chemical reactions in the surrounding liquid. The process enhances chemical reactivity, heat, and mass transfer, and mixing efficiency, making it valuable for various applications, such as environmentally friendly synthesis and pollutant degradation. Understanding and controlling this process has led to significant advancements in sonochemical applications (44, 50, 51).

2. Heterogeneous sonochemistry occurs in a solid-liquid system where cavitation bubbles asymmetrically collapse near a solid surface. This phenomenon leads to the generation of high-speed microjets and localised shockwaves, resulting in mechanical effects such as erosion and

47

fragmentation of the solid material. These mechanical actions play a crucial role in processes like sonochemical cleaning, particle size reduction, and enhancing mass transfer at solid-liquid interfaces. Understanding heterogeneous sonochemistry is essential for optimising various applications that involve solid materials in contact with the liquid phase (44).

3. Mixed sonochemistry refers to a combination of both homogeneous and heterogeneous sonochemical effects occurring simultaneously in a system. In mixed sonochemistry, the cavitation bubbles collapse asymmetrically near both liquid and solid interfaces, leading to a combination of chemical and mechanical effects. This phenomenon is commonly observed in complex systems where both liquid-phase reactions and solid-phase interactions are involved, and it can result in unique and synergistic effects that enhance the overall efficiency and effectiveness of sonochemical processes.

The literature on sonochemistry proposes several theories to explain sonochemical reactions, including the "electrical" theory (52), the "plasma discharge" theory, the super-critical theory, and the hot-spot theory. These theories offer different perspectives on the mechanisms behind sonochemical reactions, such as plasma chemistry, pyrolytic decomposition, super-critical water oxidation, and hydroxyl radical oxidation (33, 43, 44). Among these theories, the hot-spot theory is widely used to explain the effects of insonation. It suggests that high-energy concentration occurs within cavitation microbubbles, acting as small microreactors that generate significant heat and pressure (reaching up to 5000 K and 1000 bar, respectively) upon their collapse. This process leads to the production of various reactive species, contributing to the overall sonochemical effects (19, 31, 43, 45).

The behaviour of a cavitation bubble is associated with three temperature profile zones, which will be further discussed and depicted in Figure 4 in the context of chemically treating a pollutant.
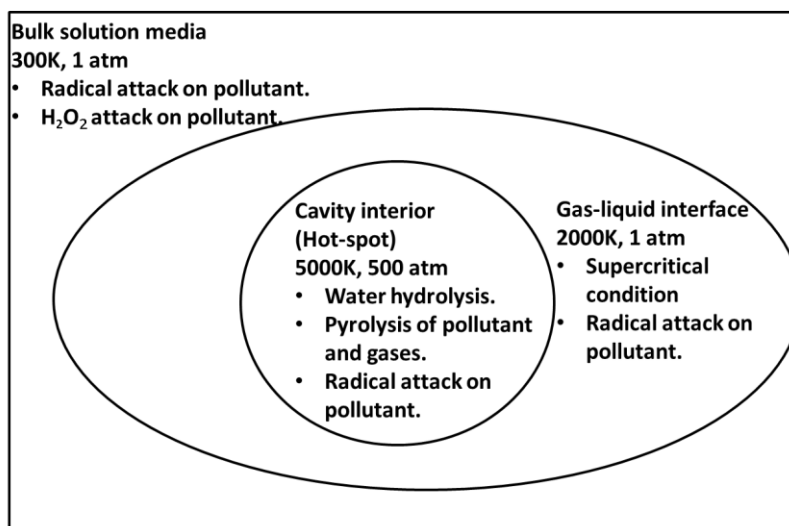
Figure 4: Illustrates the reaction zone in the cavitation process (53).

The cavitation process involves three distinct regions:

1. Hot-spot (thermolytic centre): During the final collapse of cavitation bubbles, the hot-spot or thermolytic centre experiences exceptionally high temperatures, around ~5,000 K and pressures of 1000 bar. The intense heat in this region causes the pyrolysis of water molecules, leading to the formation of highly reactive H and OH radicals in the gas phase. These radicals can then react with the surrounding substrate, resulting in various chemical transformations and contributing to the overall sonochemical effects (33, 43, 45).

2. Interfacial region: Positioned between the surface of the cavitation bubble and the surrounding bulk liquid, this zone experiences a localised temperature of approximately ~2,000 K and pressures of around ~1 atm during the final collapse of cavitation, representing a reduction in both temperature and pressure compared to the hot-spot region. Similar to the hot spot, thermolysis and oxidation reactions by OH radicals occur in this region, taking place in the aqueous phase. Hydrophilic and hydrophobic non-volatile compounds undergo these reactions, with hydrophobic compounds exhibiting higher concentrations compared to the bulk solution (33, 43).

3. Bulk region: Refers to the area surrounding the cavitation bubble where the pressure and temperature are close to ambient conditions since cavitation

follows an adiabatic process. During this stage, some OH radicals are generated due to the cavitation process, having the potential to form hydrogen peroxide (H2O2) or react with hydrophilic and ionic compounds present in the bulk solution. However, it is essential to note that OH radicals have a very short lifespan and may not penetrate deep into the bulk solution due to their high reactivity. As a result, the impact on chemical reactions in the bulk region is limited compared to the more localised and intense reactions occurring in the interfacial and hot spot regions (33, 43).

2.1.5: Ultrasonic generation and equipment

Acoustic processing equipment can be classified into various groups based on the design of the power generator (frequency, power input), the type of reactor used with the ultrasonic source (ultrasonic bath, ultrasonic probe) and the size and geometry of the treatment vessel.

2.1.5a Ultrasonic bath

Ultrasonic baths find everyday use in cleaning laboratory equipment, with numerous suppliers offer such equipment. The energy transmitted into a reaction vessel submerged in an ultrasonic bath via the vessel walls is typically relatively low, usually ranging between 1–5 W cm^{-2}. The power output in ultrasonic baths is deliberately limited to avoid damage to the bath walls caused by cavitation (27). Precise temperature control in ultrasonic baths is often challenging, necessitating additional heating and cooling to achieve the desired conditions (54).

The classic ultrasonic bath operates at a frequency range of around 40 kHz (32). For instance, Grant Instruments offers a range of digitally controlled bench-top ultrasonic baths, which offer a valuable degree of control over temperature and ultrasound intensity (55). Reactions performed in ultrasound baths usually involve glass reaction vessels placed within the bath, providing sufficient acoustic energy for most applications (27).

Certain ultrasonic baths provide a multi-frequency capability, where ultrasonic transducers simultaneously work at different frequencies, such as 25 and 40 kHz at the bottom and side, respectively. This configuration is reported to result in uniform ultrasonic power distribution (32). The intensity profile of ultrasound within an ultrasonic bath depends on the location of the transducers, making the placement of the reaction vessel within the bath a crucial variable to control.

Several techniques have been employed to measure the ultrasonic or cavitation intensity profile, including the use of a needle hydrophone, the optical and calorimetric method (25), (28), recording sonoluminescence, monitoring the increase in electrochemical current, or assessing the rate of sonochemical reactions (56, 57). Among the most widely used methods to determine the extent of cavitation is the aluminium foil test, where an aluminium foil sheet is placed inside an ultrasonic bath filled with water and the bath is operated normally. The areas of intense sonication can be identified by observing the erosion of the foil, the extent of erosion corresponds to the local acoustic intensity (32, 58, 59).

2.1.5b Ultrasonic probes

Ultrasonic probes offer greater versatility as they can be directly fitted into laboratory glassware and immersed in the sample solution. These probes are capable of emitting much higher ultrasound intensities ($\geq$several hundred W cm^{-2}) (32, 60). However, the intense cavitation field is limited to a few centimetres from the end of the probe, with typical operating face intensities ranging from 5×10^4 to 10^6 W m^{-2} at frequencies of 20-60 kHz (27).

Several important considerations arise when using a probe directly in the process solution:
  (1) Contamination, which can be achieved through indirect sonication, should be avoided.
  (2) Probe tip erosion is a concern, as the transducer horn is typically made from aviation-grade titanium. High intensities of 2 W cm^{-2} can lead to erosion and shedding of titanium particles into the product (61).

(3) Sample volume has practical limits, with the lowest recorded sonicated volume being 10 μL. Under such conditions, controlling the sample temperature becomes challenging.

(4) As ultrasound amplitude increases, so does the bulk temperature, the extent of which depends on the sample volume and ultrasound intensity. Uncontrolled temperature rise can lead to product degradation (32).

2.2: Crystallisation introduction

Crystallisation, a vital aspect of particle technology, finds extensive application in the chemical and pharmaceutical industries for the purification, manufacturing, and retrieval of solid substances. Controlling crystal size, shape, size distribution, and physical characteristics is essential in tailoring the product material to specific requirements (6, 62). The unique characteristics of each product crystal are determined by various crystallisation processes, including nucleation and growth, the polymorphic form that initiates nucleation, solvent selection and the presence of impurities in the solution during crystal isolation. The interplay of these factors significantly impacts crystal habit, crystal size distribution and other relevant properties of the final product crystals, as highlighted in Figure 5.
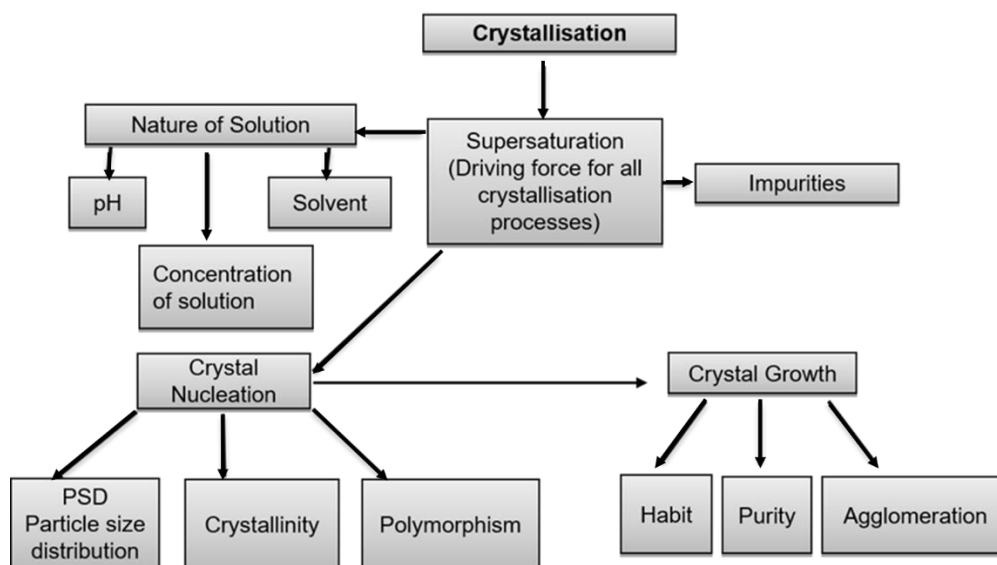
Figure 5: Diagrammatic flow chart of crystallisation conditions, which influence crystal properties.

2.3: Crystal structure and crystallography

2.3.1: Crystalline and amorphous solids

A crystal is characterised by the regular arrangement of its constituent atoms, ions, or molecules in a three-dimensional pattern with long-range order. In contrast, materials lacking this ordered arrangement are classified as amorphous (6). Crystalline solids in their pure form exhibit distinct melting points, marking their transition into the liquid state at specific temperatures. On the other hand, amorphous solids do not possess a precise melting point; instead, they undergo a more gradual melting process across a range of temperatures.
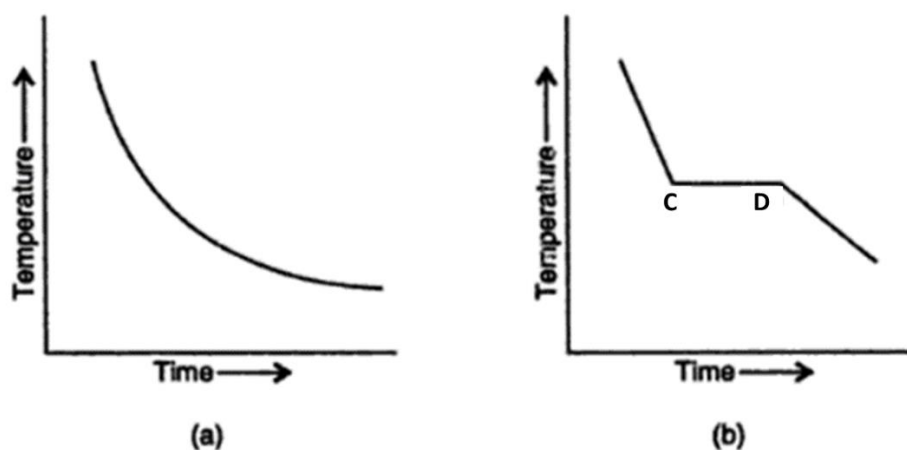
Figure 6: Cooling curve of (a) Amorphous solid (b) Crystalline substances (63).

Figure 6 illustrates the cooling curves for two types of materials: (a) an amorphous solid, showing a gradual and continuous cooling progression. Amorphous solids exhibit properties such as thermal conductivity, electrical conductivity, mechanical strength, coefficient of thermal expansion, and refractive index that remain the same regardless of orientation, making them isotropic. (b) In contrast, for a crystalline substance, two distinct breakpoints labelled 'C' and 'D' are evident. The line between these points remains steady, indicating a constant temperature during certain phases of the process. This constancy in temperature is attributed to the liberation of enthalpy of crystallisation (the energy associated with lattice formation) during crystallisation processes. Consequently, these properties can differ in different orientations for crystalline solids, rendering them anisotropic (64).

2.3.2: Crystal systems, lattices, and unit cells

The crystal lattice and the conditions of crystal growth greatly influence the resulting crystal. The precise arrangement of molecules within the lattice is characteristic of a particular substance, and this regularity of internal structure defines the crystal shape (7).

As early as 1666, Robert Boyle observed in his work "Origins of Forms and Qualities" that the crystal habit could be modified when crystals were formed in a liquid containing other salts in solution. Robert Boyle laid the foundation for the principle of 'habit modification' by 'impurities' (65, 66). Lowitz (67) later confirmed that supercooling or supersaturation is necessary for the initiation of crystal growth, and he also documented the characteristics of supersaturated solutions. Additionally, Lowitz explored the use of seeding and noted the differences between various nucleating agents. The field of crystallography was further formalised by Romeo de l'Lisle and Haüy's law of rational indices (68), which describes the orderly arrangement of crystal planes in space. These planes represent the faces of crystals and can be described within a three-coordinate-axes system (68). These fundamental concepts are exemplified by the seven types of unit cells described in Table 1.

Crystal system	Angles between axes	Length of axes	Number of lattice in the system	Shape
Regular	α = β = γ = 90°	a = b = c	3	
Tetragonal	α = β = γ = 90 °	a=b ≠ c	2	
Orthorhombic	α = β = γ = 90 °	a ≠ b ≠ c	4	
Monoclinic	α = β = 90° ≠ γ	a ≠ b ≠ c	2	
Triclinic	α ≠ β ≠ γ ≠ 90°	a ≠ b ≠ c	1	
Trigonal	α = β = γ ≠90°	a= b =c	1	
Hexagonal	α = β = 90, γ = 120°	a=b ≠ c	1	

Table 1: The seven crystal systems: adapted from (1).

Miller indices provide a unique way to designate each face of a crystal using three numbers, which are the reciprocals of the intersections of that face with the crystallographic axes, denoted as a, b, and c (6). Miller (69) proposed a unique identification system for specific planes or surfaces on a crystal using three numbers: h, k, and l, collectively known as Miller indices. The general notation (hkl) represents a particular crystal plane's orientation within the lattice. For instance, (100) denotes a plane parallel to the x-axis, (010) represents a plane parallel to the y-axis, and (001) corresponds to a plane parallel to the z-axis.

Conversely, square brackets [hkl] denote a family of equivalent crystal faces resulting from symmetry within the lattice. These equivalent faces share the same Miller indices but may occur at different positions within the crystal lattice due to the presence of symmetry elements.

In crystals with cubic symmetry, planes with identical Miller indices but different orientations are considered equivalent. For instance, [100], [010] and [001] represent crystal planes parallel to the x-axis, y-axis, and z-axis, respectively.

On the other hand, {hkl} denotes a collection of equivalent crystallographic directions within the crystal lattice. These directions are defined by three integers, h, k, and l, known as Miller indices, which specify the vector's orientation relative to the crystal lattice. The notation {hkl} includes all equivalent directions that share the same Miller indices but may appear in different regions of the crystal due to symmetry. These are defined as follows in Figure 7 and Equation 6.

$$h = \frac{a}{X}, k = \frac{b}{Y} \ and \ l = \frac{c}{Z}$$

<div align="right">Equation 6</div>

For Example:

	h	k	L
	3A	2B	2C
Reciprocal numbers:	$\frac{1}{3}$	$\frac{1}{2}$	$\frac{1}{2}$
Indices of the plane (Miller):	(2	3	3)
Direction of indices:	[2	3	3]
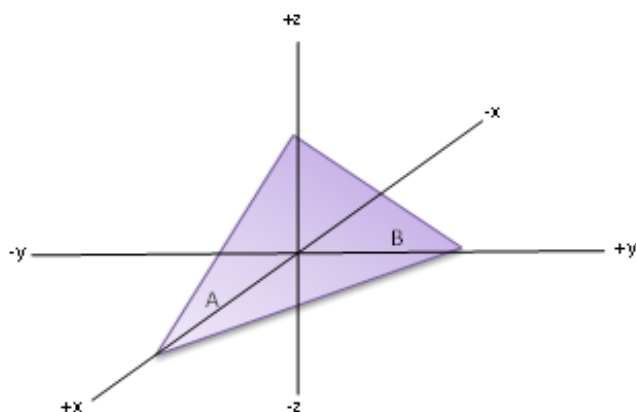
Figure 7: Miller indices intercept of planes on the crystallographic axes.

2.4: Crystallisation processes and potential impacts

2.4.1: Solutions and solubility

A solution is a homogeneous mixture of two or more substances, typically involving solvents and dissolved solutes, crucial for crystallisation processes (7). Controlling crystallisation relies on manipulating solubility variations. Organic compounds can be crystallised using a wide range of organic solvents. For instance, Zhang (26) investigated the metastable zone width of lovastatin in methanol, ethanol, and acetone. They observed an increase in the metastable zone width with saturation temperature and cooling rate for all solvents. Zhang (26) identified different nucleation mechanisms: instantaneous in ethanol and acetone and progressive in methanol. The crystal habits were similar across all solvents, attributed to the competition of adsorption between solvents and solute molecules during crystal growth. However, the focus on only three solvents and lack of consideration for impurities limit the generalisability of the findings, warranting further research to explore the effects of other solvents and impurities, on nucleation and crystal formation (70).

Lovette (71) highlights significant progress in engineering tools for improved crystallisation processing design. Molecular simulation and mechanistic modelling allow for predicting steady-state crystal shapes, accounting for single solvents and tailor-made additives on crystal shapes. The fast computation of mechanistic modelling makes it feasible for product and process development. Most molecular organic crystals' shapes are determined by surface integration rates rather than bulk transport limitations. Real-time feedback control through online shape measurement and image analysis techniques presents a promising future for model-predictive crystallisation control.

Choosing a suitable solvent is essential for effective separation during crystallisation, regardless of the crystalliser's quality or process design. Undesirably, the solvent molecules may incorporate into the crystal lattice, leading to the formation of a solvate to avoid this, an alternative solvent must be selected (72).

Ideally, the optimal solvent choice should have high solubility for the solute at elevated temperatures, enabling a good yield upon cooling. Moreover, it should exhibit temperature-dependent solubility and possess low toxicity, flammability, and viscosity while being cost-effective and non-corrosive. Water fulfils many of these criteria and is commonly used, especially for crystalline materials with some level of aqueous solubility. However, water's solubility may be limited for most pharmaceutical compounds, reducing its suitability as a crystallisation solvent. Water use also comes with potential drawbacks, such as the possibility of hydrolysis reactions and undesired hydrate formation, depending on hydrate stability (73).

In industrial practices, the chemical similarity between solvents and the compound being crystallised provides an initial indication of suitability. However, the final solvent selection requires precise measurement of the solute's solubility in the solvent.

In conjunction with carefully selected parameters, such as solvent choice, ultrasound can play a crucial role in the transformation of allicin, a pharmacologically active compound found in garlic. Ilic (74) explored different methods to transform allicin, including conventional techniques, ultrasound, and microwaves. Investigating the impact of organic solvents (acetonitrile, acetone, methanol, and chloroform) at different temperatures (room temperature, 45 °C and 55 °C) on the kinetics of allicin transformation.

A noteworthy finding found ultrasound to significantly affect the transformation rate of allicin. While microwaves led to the fastest allicin transformation, ultrasound proved to be even more effective, causing allicin to transform three to four times faster than conventional methods in all solvents used (74).

Furthermore, Ilic (74) highlighted the influence of solvent selection on the stability of allicin. Different solvents affected the transformation process differently, with ultrasound and higher temperatures, like 55 °C, accelerating the transformation of allicin.

2.4.2: Supersaturation

Supersaturation, the concentration in excess of the thermodynamic equilibrium, is the driving force for all crystallisation processes. When a solution is saturated at a specific temperature, the solution is in thermodynamic equilibrium with the solid phase. The solution must be in a supersaturated state to accomplish the first step in crystallisation (nucleation) (75). Supersaturation, the extent to which the solution concentration exceeds the equilibrium value, has been represented by several expressions, the most common are described as follows:

Equation 7 defines the concentration driving force for crystallisation (Δc).

$$\Delta c = C(T) - C^*(T)$$

Equation 7

Where C is the actual solution concentration at the selected temperature and C^* is the equilibrium saturation of the solution at the selected temperature (1, 7).

This can also be expressed by Equation 8 as a Supersaturation (S) ratio.

$$S = \frac{C}{C^*}$$

Equation 8

And Equation 9 the relative or absolute Supersaturation (σ).

$$\sigma = \frac{\Delta C}{C^*} = S - 1$$

Equation 9

Figure 8 is a diagrammatic view of the solubility-supersolubility curve; this figure will be discussed in terms of three sections.
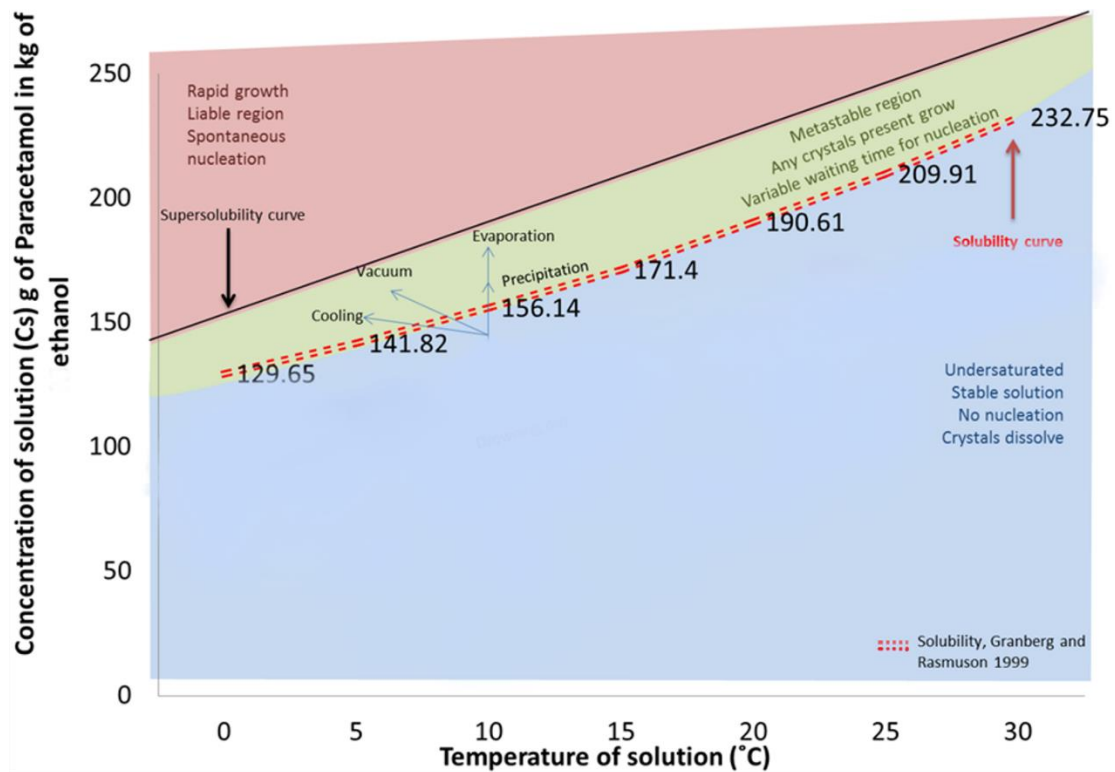
Figure 8: Diagram of solubility and supersolubility of paracetamol in ethanol, showing three regions red (unstable) supersaturated zone; green the metastable zone and blue (stable) undersaturated zone adapted from (32).

In this illustration, the three zones can be characterised as follows:

1. Undersaturated Zone: The solution contains insufficient solute crystals in this region, and any added crystals would dissolve.
2. Metastable Zone: This is a supersaturated region where existing solute crystals continue to grow. Nucleation is possible if no solute crystals are present, but it is not spontaneous.
3. Liable Zone: In this area, spontaneous nucleation occurs, and any solute crystals present will experience rapid growth.

In the stable region (depicted in blue), the solution has the capacity to dissolve a specific amount of solute at a given temperature, which is greater than the amount of dissolved solute currently present. This zone is located below the solubility curve, and the solution is considered undersaturated, meaning crystallisation will not occur as the concentration is below the equilibrium solubility.

The supersaturated region is above the solubility curve (represented by the green and red zones) and supersaturation is a prerequisite for crystallisation to occur. This region can be further divided into two areas. The first is the metastable zone (shown in green), which exists between the solubility and super-solubility curves. In this zone, the solution is in a supersaturated state, allowing any existing crystals to grow. However, spontaneous nucleation does not occur when no crystals are present. If multiple crystals are present, secondary nucleation from crystal-crystal collisions can happen. Inducing growth and additional nucleation within this region is possible by introducing seed crystals.

The second region in the supersaturated area is the unstable or labile zone (depicted in red). Here, primary nucleation and subsequent crystal growth occur spontaneously due to the high level of supersaturation in the solution (1, 6, 7).

In the context of supersaturation, Zhong (76) emphasised the influence of ultrasound on the crystallisation of sucrose in a supersaturated state. Supersaturation occurs when a solution holds more solute than it can typically accommodate at a given temperature. The researchers noted that as supersaturation increased, the crystallisation time decreased, and ultrasound played a significant role in further augmenting this effect.

The experimental results demonstrated that ultrasound had a notable influence on the nucleation and growth rates in supersaturated environments. In the presence of ultrasound, the nucleation rate increased, leading to the formation of a large number of sucrose crystals per unit time. This increase in nucleation rate resulted in smaller crystal sizes and created difficulties in crystal growth, leading to a decrease in the growth rate of the crystals (76).

Furthermore, the study found that higher concentrations of the solution produced a higher level of supersaturation upon mixing with the anti-solvent, thereby accelerating the rate of nucleation (76). This finding suggests that ultrasound can intensify the supersaturation state, enhancing the crystallisation process even further.

The effect of ultrasonic power on supersaturation was also investigated. The nucleation rate reached a maximum when the ultrasonic power reached a specific level, with a further increase in ultrasonic power reducing the nucleation rate. This observation indicates that there is an optimal ultrasonic power level that can maximise the nucleation rate in the supersaturated solution.

Moreover, the kinetic analysis revealed that ultrasound reduced the activation energy of anti-solvent crystallisation of sucrose. This reduction in activation energy indicates that the energy barrier for nucleation and crystal growth was lowered in the presence of ultrasound, making the process more favourable.

2.4.3: Solubility

Various methods exist to measure solubility, and the shape of the equilibrium line, or the solubility curve, as shown in Figure 8, is crucial in determining the crystallisation process. This curve can vary significantly:

1. Steep Curve: A steep solubility curve, indicating strong temperature dependence, often necessitates 'cooling crystallisation'.
2. Wide Metastable Zone: Common in large organic molecules like sucrose, where adding seed crystals is beneficial for consistency.
3. Flat Curve: A flat curve, showing low temperature dependence, usually calls for 'evaporative crystallisation', particularly in solutions like sodium chloride.
4. Antisolvent Crystallisation: This involves changing the solvent composition to achieve crystallisation; understanding the solubility relationship is key here.
5. Reactive Crystallisation: Occurs through a chemical reaction, often leading to rapid crystallisation or 'precipitation'.
6. Melt Crystallisation (Fractional Crystallisation): This is used for purifying organic compounds in a multi-component mixture without a solvent, driven by cooling the melt (77).

Each crystallisation process has its unique advantages and limitations. Selecting the appropriate method requires consideration of these factors (7, 78).

Chapter 2: Sonocrystallisation Principles & Crystallisation Science

Granberg and Rasmuson (79) conducted a well-known study on paracetamol solubility in pure solvents, which was used for comparison with the solubility data discussed in this thesis. Their research aimed to investigate paracetamol's solubility in twenty-six organic solvents and water from -5 °C to 30 °C. Providing crucial data for drug formulation and manufacturing processes.

The findings revealed significant variations in paracetamol solubility across different solvents and temperatures. Nonpolar hydrocarbons and chlorinated hydrocarbons showed relatively low solubility, whereas polar solvents like dimethyl sulfoxide, diethylamine, and N,N-dimethylformamide exhibited notably higher solubilities. In the case of alcohols, solubility decreased with increasing carbon chain length. Surprisingly, water, despite being a polar solvent, demonstrated low solubility for paracetamol, which is attributed to complex interactions between paracetamol's aromatic ring and methyl group with the water molecules (79).

The researchers calculated the ideal solubility of paracetamol, which solely depends on temperature, and estimated the solute's activity coefficient in saturated solutions. The activity coefficient indicated the comfort of the paracetamol molecule within the solvent environment. High activity coefficients are correlated with low solubility, as seen in water, due to weak entropy effects. Conversely, low activity coefficients, as observed in methanol, indicated higher solubility, reflecting stronger entropy effects. Additionally, the solubility decreased with increasing temperature across all solvents (79).

Acknowledging certain limitations, the article focused on pure solvents rather than solvent mixtures commonly encountered in real-world crystallisation processes. The limited temperature range might not fully capture extreme temperature behaviours. Moreover, the purity of the paracetamol and solvents used in the experiments could potentially influence the solubility measurements (79).

If the solubility of an impurity is similar to or lower than that of the product, it becomes less likely to be eliminated during the crystallisation process. The positive or negative effects of impurities, if they alter the solubility, remain a subject of debate. According to Hendriksen (11), impurities can indeed modify the solubility of the solute, potentially

affecting the crystallisation process that results in the formation of the solid solute. However, Hendriksen's study did not specifically focus on the impact of impurities on solubility; instead, it concentrated on the effects on nucleation, incorporation, and growth processes. It does not represent the behaviour of larger crystals or different morphologies. In contrast, Keshavarz (80) observed a slight increase in paracetamol's solubility with the addition of impurities 4-nitrophenol and 4'chloroacetanilide. However, it was noted that these impurities did not significantly affect the overall solubility of paracetamol.

According to Pereira (81), ultrasound has been found to effectively enhance the solubility of poorly water-soluble drugs in solid dispersions. The researchers used Piroxicam as a model drug and conducted a complete factorial design to assess the impact of sonication parameters on drug solubility and dissolution rate. The results demonstrated a significant increase in Piroxicam's solubility and dissolution rate within the solid dispersion. Specifically, certain sonication conditions led to a maximum fourfold increase in solubility and a sixfold increase in dissolution rate. Notably, characterisation indicated that sonication did not adversely affect the drug or alter its polymorphic form. The study's generalisability to other drugs, the absence of in vivo data, and the considerations for scaling up the process should be further investigated. Sonication showed promise for enhancing drug solubility, but additional research is necessary to fully comprehend the mechanisms and implementation.

2.4.4: Metastable Zone Width (MZW)

Over the years, extensive research has been conducted on the solubility and MZW of common solute-solvent systems (7, 70, 82). The MZW, also known as the ΔC_{max} supersolubility curve, is often reported alongside the solubility curve and represents the region between the solubility curve and the onset of nucleation. Within this region, a solute remains in solution until sufficient supersaturation is achieved and maintained for a certain period (the induction period) to induce spontaneous nucleation (83). Determining the MZW involves cooling a saturated solution until nuclei are detected, the temperature difference between the saturation temperature and nucleation temperature provides the sub-cooling expression of MZW (70).

Measuring the MZW serves multiple purposes, including determining the crystallisation's operation window and analysing nucleation kinetics (70, 82, 84, 85). Various process parameters can influence the MZW, such as: the rate of supersaturation generation (86), solute-solvent interactions in solution (70), the presence of impurities (87) and the application of external forces like ultrasound (88). Different methods have been employed to measure the MZW, such as Nyvlt's (82) technique, which investigated the oxalic acid-water system's solubility and metastable zone characteristics. The solubility data was correlated with temperature, and the following thermodynamic parameters were determined: enthalpy of dissolution, enthalpy of fusion and enthalpy of mixing. The high enthalpy of mixing indicated strong solute-solvent interactions. The metastable zone width was measured using an ultrasonic method and correlated with cooling rate and equilibrium temperature. Nucleation parameters were also derived from the metastable zone data. However, the research was limited to the oxalic acid-water system and needed more in vivo data, reducing its broader applicability. Despite these limitations, the study utilised appropriate experimental methods and statistical analyses to yield valid results, offering valuable insights into crystallisation processes and industrial applications of oxalic acid in water.

Maharana (89) conducted a study to explore how ultrasonic amplitudes impact metastable zone width (MZW) and induction time during batch cooling Sonocrystallisation of pyrazinamide from its acetone solution. The experimental setup involved varying saturation temperatures, cooling rates, and different ultrasonic amplitudes (10%, 30%and 50%). The findings demonstrated that higher cooling rates expanded the MZW, whereas elevated saturation temperatures narrowed it. Additionally, increasing ultrasonic amplitudes decreased the MZW. The application of ultrasound also increased the nucleation rate, suggesting early nucleation and the potential formation of dimers in pyrazinamide. Nevertheless, the study's reliance on classical nucleation theory assumptions for data analysis may constrain a comprehensive understanding of nucleation phenomena during Sonocrystallisation. As a result, while the research provides valuable insights, its general applicability to various systems and real-world scenarios necessitates further investigation.

The induction time (t_{ind}) is another crucial aspect defined as the time elapsed between achieving a specific fixed level of supersaturation and detecting the first nucleation event in the solution kept at that constant level of supersaturation (90). The induction time is influenced by several parameters, including solute concentration in the solution, temperature, mixing, and solvent identity (91). It is closely related to the critical size of nuclei and serves as a valuable tool for evaluating nucleation kinetics (92).

2.4.5: Nucleation

Crystallisation is a two-stage phenomenon, with nucleation constituting the initial phase, where crystal nuclei form in a supersaturated solution (93). This step plays a crucial role in determining the crystal's structure and size distribution. Numerous factors influence this process, including: the choice of solvent for the supersaturated solution, the presence of foreign particles, the use of crystal seeding, the concentration and nature of impurities, hydrodynamics (such as agitation rate and vessel and agitator geometry), as well as cooling rate and temperature control (70, 82, 94). Figure 9 provides a schematic overview of both primary and secondary nucleation processes.
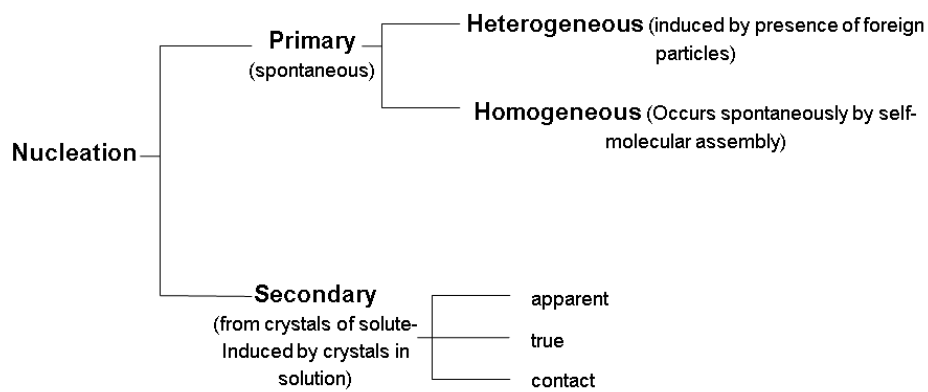
Figure 9: Schematic flow chart of the classification of nucleation stages within crystallisation processes (14)**.**

2.4.5a Primary nucleation

For primary nucleation to take place, the solution must be free from crystals. Homogeneous nucleation spontaneously occurs when nuclei form in the bulk of the solution. In contrast, heterogeneous nucleation happens when nuclei form on substrates, such as finely divided foreign particles (dust particles) or on the walls of the crystalliser (94).

2.4.5b Classic Nucleation Theory (CNT)

Classical primary nucleation is explained by the CNT, represented schematically in Figure 10. This theory originated from the study of droplet nucleation from supersaturated vapours (94). When a supersaturated vapour condenses into a liquid phase, microscopic liquid droplets (clusters) emerge in a process called condensation nucleation. However, due to the extremely high vapour pressure at the surface of these clusters, they tend to evaporate despite the surrounding vapour being supersaturated. Consequently, new nuclei form as the old ones evaporate, and this process continues until stable droplets are formed through locally high vapour supersaturations or droplet coalescence (7). Nucleation commences once a cluster reaches a critical size (r*). Notably, higher supersaturation results in smaller critical nuclei, thereby promoting nucleation. This phenomenon is known as the Gibbs-Thomson effect, which determines the critical size value (Equation 10) (94, 95).

$$r^* = \frac{2\Omega\gamma}{KTln\beta}$$

Equation 10

Where Ω is the volume of a molecule inside the crystal (m^3) and γ is the crystal solution interfacial free-energy (J m^{-2}) K is Boltzmann's constant, T is the temperature, and β is the supersaturation (94).

2.4.5c Two step nucleation

Despite its simplicity, the classical theory faced challenges with experimental results, as indicated by Dixit (55) and Knezic (54). Additionally, Auer and Frenkel (59) observed that CNT did not accurately predict absolute nucleation rates compared to their computer simulations. To address these limitations, Ten Wolde and Frankel (96) proposed a more intricate two-step mechanism for protein crystallisation. In this mechanism, a region of dense, disordered liquid phase forms initially, and then fluctuations in density in the bulk solution give rise to clusters that represent a liquid-liquid phase separation. Over time, these clusters reorganise into structured clusters, as depicted in Figure 10. Moreover, Knezic (97) discovered that the induction time for lysosome droplets was random, and the nucleation rate calculated based on Turnbull's model (98) showed significant inconsistency.
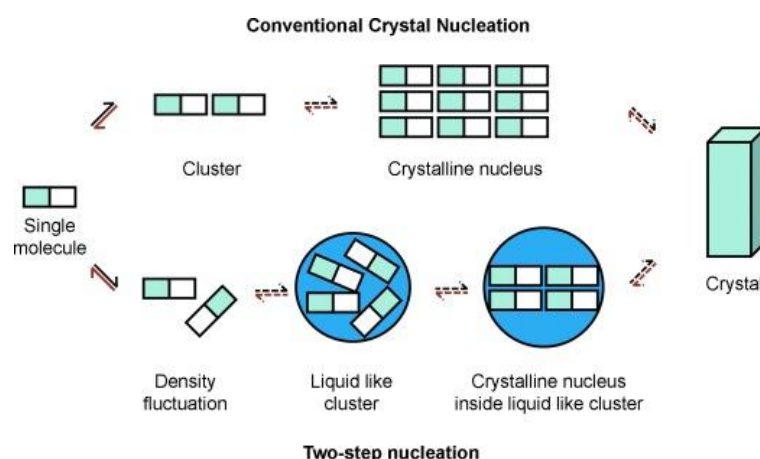
Figure 10: Schematic representation of two alternating models for cluster formation during nucleation in supersaturated solutions. CNT is represented at the top and two step nucleation at the bottom (95).

The model presented in Figure 10 illustrate the dynamic process of cluster formation in a supersaturated solution during crystal nucleation. In the two-step nucleation process, local density fluctuations are separated from the bulk solution, resulting in initially formed clusters that are liquid-like and disordered, a phenomenon known as liquid-liquid demixing. The crystalline order emerges later once these clusters are established. CNT relates the formation of clusters and their molecular order to the polymorphism of the initially formed crystal (95).

Several equations describe the crystal nucleation rate, denoted as J and have been extensively used in the literature (94, 95, 97, 99, 100). One of the most widely used equations for homogeneous nucleation is represented by Equation 11.

$$J = A \exp\left(-\frac{B}{In^2\ S}\right)$$

<div align="right">**Equation 11**</div>

Davey (95) defined the crystal nucleation rate in a supersaturated solution, denoted as J, as the number of crystalline particles that form per unit of volume per unit of time ($s^{-1}.ml^{-1}$). The supersaturation ratio, S, quantifies the deviation of the supersaturated system from equilibrium. In Equation 12, A and B are constants, while the exponent is given by Equation 12.

$$\frac{B}{In^2\ S} = \frac{W}{kT}$$

<div align="right">**Equation 12**</div>

The dimensionless nucleation work, represented by the exponent ($B/In^2 S$), signifies the dimensionless energy barrier for nucleation. The likelihood of nucleation occurring is determined by ($B/In^2 S$) which represents the natural logarithm of the number of accessible microstates S raised to the power of 2, W denotes the statistical weight or number of microstates associated with the critical nucleus, while k stands for Boltzmann's constant, and T indicates the absolute temperature of the system. As a result of these factors, the nucleation rate J responds non-linearly to the supersaturation ratio S, implying that even minute changes in the supersaturation can lead to significant variations, spanning several orders of magnitude, in the nucleation rate (95).

2.4.5d Secondary nucleation

Secondary nucleation arises when crystals of the same phase are already present in the slurry, which can result from primary nucleation or intentional seeding by the operator. This process is energetically favoured over heterogeneous and homogeneous nucleation, enabling the production of crystals at much lower supersaturation levels (7, 94). Early studies on nucleation, such as the work by Ting

and McCabe (101), highlighted that a solution of magnesium sulfate heptahydrate easily nucleated at moderate supersaturation levels when seeds were introduced. Kane et al., (102), also observed that seeding a supercooled solution proved to be an effective way to measure the kinetics of secondary nucleation. The impact of introducing a crystal into a supersaturated solution (seeding), which would not spontaneously crystallise, was discussed by Mason and Strickland-Constable (103). They proposed that the increase in the number of particles indicates the presence of additional nuclei, a phenomenon referred to as 'secondary nucleation,' which has been found to occur through various mechanisms.

2.4.5e Kinetic measurements, MZW and induction time

Various methods for evaluating secondary nucleation are documented in the literature. One widely used approach, as described by Kane et al. (102), involves measuring the metastable zone width (MZW), which represents the maximum acceptable supersaturation before spontaneous nucleation, and the induction time of nucleation. This denotes the time elapsed between creating supersaturation and solid phase formation in the presence of seed crystals. This assessment helps determine a practical working supersaturation level, enabling the design of an optimal cooling profile to remain within the MZW, thus preventing excessive crystal nucleation and ensuring a narrow crystal size distribution (93, 104, 105). However, the MZW's sensitivity to various parameters, such as temperature, impurities, rate of supersaturation and mixing, should be considered. Although the metastable zone is commonly used to characterise homogeneous nucleation, Poornachary (93) noted that it is often assumed that, at the moment nucleation is first detected, the rate of desupersaturation equals the rate of nucleation. Supersaturation is consumed not only by the birth of nuclei but also by the growth of existing crystalline particles.

2.4.5f Effect of impurities on nucleation and induction time

Impurities can have diverse effects on crystal nucleation, which are commonly assessed by studying changes in the metastable zone width (MZW) and induction time. The existing literature discusses these impacts through adsorption-based mechanisms. For example, Prasad (62) observed that soluble impurities in aqueous

solutions impede nucleation. Mullin (7) elaborated on this, noting how impurities can alter the solution's structure and equilibrium solubility, as well as the chemical or physical adsorption onto heterogeneous and homogeneous nuclei. Sangwal and Mielniczek-Brzoska (106) found that impurities obstruct active growth sites on the crystal surface, increasing the supersaturation barrier for homogeneous nucleation. In contrast, Poornachary (93) proposed that impurities adsorbed onto the crystal surface increase interfacial tension, especially for near-critical nuclei clusters. In both cases, impurity-doped solutions demonstrate an increased MZW and prolonged induction time.

In Hendriksen's (11) investigation, the influence of impurities on the crystal habit of paracetamol and their integration within the crystal structure were explored. The results indicated that the presence of impurities disrupted the hydrogen bonding network, leading to decreased stability in emerging nuclei. Additionally, the study examined how structurally related compounds affected the crystallisation of paracetamol from aqueous solutions, investigating aspects such as crystal shape, additive uptake, morphological changes, and nucleation inhibition caused by different additives. The findings revealed distinct interactions between the additives and paracetamol crystals, affecting adsorption, docking onto the crystal surface, or disrupting the emerging nucleus. The results suggested that the molecular similarity between additives and paracetamol played a role in determining their effects. However, the study had limitations, including a narrow focus on specific additives and conditions as well as limited structural analysis. Nevertheless, the study provided valuable insights into paracetamol crystallisation and identified areas for further research to gain a comprehensive understanding of the complexities involved in the crystallisation process.

2.4.6: Crystal growth

Crystal growth, the second stage in the crystallisation process, plays a crucial role in determining the final size of the crystal. This growth process involves the transportation of solute molecules to the crystal surface, where they are then oriented and integrated into the crystal lattice. Similar to nucleation, the driving force for growth

is supersaturation, which allows nuclei to develop into microscopic crystals (27). The shape or habit of a crystal is influenced by the varying rates at which growth can occur in different directions. When growth is more favourable in one direction, the face perpendicular to that direction tends to be smaller (107). The combination of these face growth rates dictates the overall crystal shape, and the crystal's size is controlled by both the growth time and the level of supersaturation.

The growth process is influenced by internal and external factors. Internal factors encompass how atoms or molecules incorporate onto the growing crystal surface. These ultimately determine the strength of the intermolecular interactions between the crystal surface and the solution (108). On the other hand, external factors involve various aspects:

   (i)   Mass transport of solute molecules towards the boundary layer neighbouring the crystal surface.
   (ii)   Solute diffusion through the boundary layer is due to the concentration gradient.
   (iii)   Adsorption of the solute molecule onto the crystal surface.
   (iv)   Diffusion over the crystal surface to select an energetically favourable binding site.
   (v)   Attachment to a step site of the crystal surface.
   (vi)   Diffusion along the surface step site.
   (vii)   Attachment to the kink site of the crystal surface (1).

However, in the growth process of some materials, not all these steps (i) to (vii) are necessary. Solute molecules can bypass stages (iv) and (v) by directly incorporating onto a kink site, or some stages may occur more rapidly than others (1). External factors impact interactions at the solid-liquid interface such as: temperature, solvent, supersaturation, impurities, pH, and stirring rate (108).

For a considerable time, researchers have been exploring ways to influence single crystal growth for diverse purposes. The ability to control the growth process empowers scientists to customise the crystal's size, shape, and orientation, resulting in materials with specific and exceptional properties suitable for various applications. Moreover, single crystals serve as a valuable platform for fundamental research,

allowing the study of material properties at the atomic level and the investigation of phenomena like crystallography and phase transitions. Manipulating single crystal growth is crucial for device fabrication, enabling the creation of high-quality films with controlled orientations for enhanced performance in electronic and optoelectronic devices. Additionally, scientists can engineer functional materials by influencing single crystal growth to augment properties such as piezoelectricity and ferroelectricity. Furthermore, optimising growth conditions can reduce defects and impurities, leading to higher-performing crystals.

Milisavljevic (109), introduced solid-state-single-crystal growth (SSCG) as a promising alternative to conventional melt and solution-growth techniques for producing single crystals. SSCG offers cost-effective and straightforward processing, allowing the fabrication of single crystals with complex chemical compositions and unique properties. The demand for high-quality single crystal materials in diverse applications, including electronics, optics, and optoelectronics, has spurred a keen interest in SSCG. This technique utilises conventional sintering equipment, offering advantages in net-shape production. However, SSCG is still in its developmental stage, with limited research and understanding of its mechanisms, presenting challenges in achieving full control. Despite these obstacles, SSCG has already succeeded in commercially producing piezoelectric single crystals and exhibits potential for further research and broader application across various material systems.

No prior investigations have specifically examined the impact of sonocrystallisation on single crystal growth, which will be addressed in detail in Chapter 5 of this thesis. However, existing literature extensively discusses the positive contribution of sonocrystallisation to overall crystal growth. Notably, Yadva (110) conducted a study focusing on the effects of ultrasound on ascorbic acid crystallisation. The use of ultrasound during crystallisation resulted in notable improvements in product quality, evident in finer particles, increased surface area, and a narrower size distribution compared to conventional cooling crystallisation. Ultrasound also reduced the induction time for nucleation, while the process's temperature profile significantly influenced the final product attributes. The study highlighted the vital roles played by ultrasound's duration and amplitude in determining particle size and distribution, where longer insonation periods and higher amplitudes led to finer particles. However, it was

observed that the increase in temperature caused by ultrasound-induced heat generation could also dissolve nuclei, consequently impacting the particle size distribution. Moreover, the cooling rate exerted an influence on the crystallisation process, as a slower cooling rate of 0.5 °C min^{-1} yielded smaller particles and a narrower size distribution. Overall, this research provided valuable insights into the effects of ultrasound and thermal conditions on crystallisation, contributing to a deeper understanding of growth control to customise product attributes. It is essential to acknowledge that the focus was limited to ascorbic acid as a model system, necessitating further research to validate these findings across diverse materials and conditions.

2.4.6a Effect of impurities on crystal growth

The influence of impurities on crystal growth, morphology, and nucleation kinetics has been widely recognised (8, 62, 72). Mullin (7) defines impurities as substances other than the material being crystallised, which includes the solvent mixture from which the crystals grow. Generally, impurities tend to suppress crystal growth (111, 112) and may have selective effects on different crystallographic surfaces, thereby modifying the crystal habit (7). Sangwal and Benze (113) state that all crystals, regardless of their structure, bonding nature, or growth phases, will contain impurities, whether unintentional or deliberately introduced (113). Introducing impurities into a system can serve specific purposes, such as controlling crystal size distribution (7, 8).

The Kossel model, represented in Figure 11, provides a valuable framework for understanding crystal growth, distinguishing between three types of crystal surfaces: flat (F), kinked (K) and stepped (S). This model applies to molecular and inorganic crystals, as the crystal growth maximises intramolecular interactions of incoming growth units. The availability of sites for incorporation and the strength of interactions at each site determines the growth rate of crystal surfaces. Consequently, some faces grow faster than others, influencing the overall crystal habit. Flat faces have low binding energies, offering only one interaction opportunity for incoming molecules. In contrast, kinked and stepped faces provide three and two binding sites, respectively, making them more favourable locations for molecular attachment (114).

Impurities significantly affect crystal growth rates by adsorbing onto favourable attachment sites on the crystal surface, inhibiting the subsequent attachment of solute molecules, and blocking active growth sites. Moreover, the presence of impurities in a solution can alter solubility and supersaturation, as well as the growth rate on individual faces. Impurities with molecular similarity are likely to be incorporated into the crystal structure, and tend to selectively adsorb onto different crystal faces, retarding their growth. Achieving overall face coverage is not necessary to significantly impede the growth of a face (7, 115). Even a few impurity molecules occupying specific sites along the length of a step can slow down the advancing step (64).

According to the Kossel model, to hinder growth on a flat face, only one impurity molecule may be enough to hold back the growth of a spiral growth step progressing across that face. Blocking growth on a stepped face requires halting growth on each step independently, and on a kinked face, blocking each point of attachment sites would be necessary (7, 93).
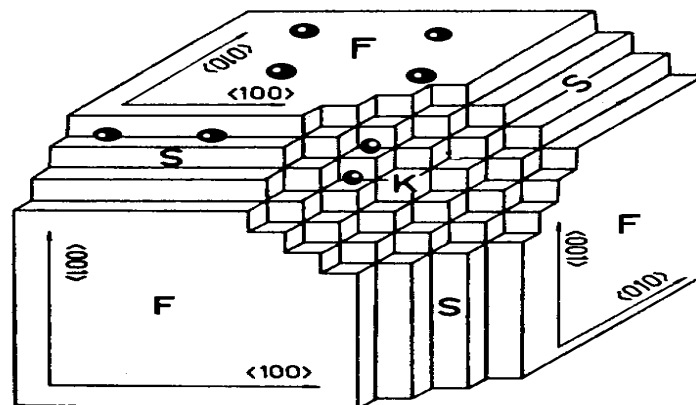
Figure 11: Modified image of impurity adsorption sites F- flat face, K- kinked face and S- stepped face, or on a ledge between steps. Image modified from (116).

In a study by Finnie (117), the morphology of monoclinic paracetamol crystals was investigated using theoretical and experimental methods, focusing on the effects of varying supersaturation levels. The findings revealed that different crystal faces

dominate at different supersaturation levels, and the growth mechanism significantly influenced the crystal morphology. However, the modelling calculations' reliance on specific force fields and the assumption of equivalent growth rates for all faces might introduce limitations to the predictions.

Despite the limitations, the study's experimental observations and microscopic examinations offer valuable insights into the micromorphological changes and growth mechanisms. The research shows consistent morphological changes across different growth media, indicating minimal solvent influence on crystal morphology. While the paper contributes valuable knowledge to paracetamol crystal growth, a more comprehensive understanding of the underlying mechanisms and accurate force field models would further enhance the findings' validity.

2.4.6b Diffusion reaction theory

The diffusion reaction theory is a concept used to explain crystal growth, particularly in crystallisation from solutions or vapour phases. It combines diffusion and chemical reaction phenomena to describe how solute molecules interact, diffuse, and incorporate into the growing crystal lattice. Diffusion involves the movement of solute molecules from regions of higher concentration to regions of lower concentration, driven by concentration gradients. Once the solute molecules reach the crystal surface, they undergo chemical reactions to become part of the crystal structure. This theory is essential in understanding the kinetics of crystal growth and how factors like temperature, concentration, and supersaturation influence the growth rate. Different rates of diffusion and chemical reactions at various crystal faces lead to variations in growth rates, ultimately determining the crystal's morphology and habit. Moreover, the theory considers the influence of impurities or other molecules present in the solution or vapour phase, which can impact crystal growth and its resulting quality (7).

Controlling crystal growth is crucial for producing high-quality crystals with specific properties. The diffusion-reaction theory guides researchers and manufacturers in optimising crystal growth conditions to achieve desired material characteristics (7). Industries such as pharmaceuticals and electronics heavily rely on single crystal growth to create materials with tailored properties. Understanding the processes of solute diffusion and chemical reactions during crystal growth enables researchers to tailor crystal growth processes to meet specific application requirements.

The diffusion reaction theory offers valuable insights into crystals' kinetics, morphology, and quality. By understanding how solute molecules diffuse and react during crystal growth, researchers can optimise growth conditions and control the properties of resulting crystals for various industrial applications. The theory's historical roots can be traced back to the pioneering work of Noyes and Whitney (118), who proposed that crystal growth is driven by diffusion, postulating that crystallisation is the reverse process of dissolution, both influenced by the difference in solute concentration at the solid surface and in the bulk solution (7).

$$\frac{dm}{dt} = k_m A(C - C^*)$$

Equation 13

The rate of crystal mass deposition over time (dm dt^{-1}) can be mathematically described by Equation 13, with k_m as the coefficient of mass transfer, *A* as the crystal's surface area, C as the solute concentration in the solution, and *C** as the equilibrium concentration. Building upon their work, Nerst (119) introduced modifications to the theory, considering a thin stagnant liquid film adjacent to the growing crystal face, through which solute molecules would diffuse (Figure 12). This led to the revised Equation 14, where *D* represents the diffusion coefficient of solute molecules, and δ is the thickness of the stagnant film. The thickness of the stagnant film (δ) is dependent on the relative solid-liquid velocity or degree of system agitation (118).

$$\frac{dm}{dt} = \frac{D}{\delta}A(C - C^*)$$

It is now understood that crystallisation is not merely the reverse process of dissolution, as substances generally dissolve significantly faster than they crystallise under the same conditions of relative supersaturation or undersaturation and temperature (7). The essential processes in crystal growth are diffusion and adsorption (surface integration). Solute molecules are transported from the bulk of the supersaturated liquid phase to the crystal's surface by diffusion, driven by a concentration gradient. The adsorption process, incorporating solute molecules into the crystal surface, occurs in the absorption layer immediately adjacent to the crystal (Figure 12). Together, these steps determine the rate of crystallisation, influenced by the degree of supersaturation and mixing (63).
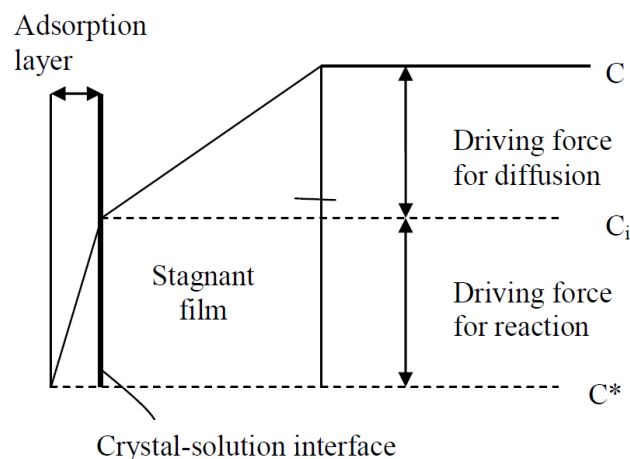
Figure 12: Concentration driving force for diffusion and adsorption stages in crystal growth from solution (7).

When diffusion governs the growth rate, increasing the velocity of the supersaturated solution relative to the crystal surface results in an accelerated crystal growth rate. However, if further increases in the solution velocity have no effect on the growth rate, the growth process becomes surface integration controlled. The interplay between diffusion and adsorption processes significantly affects the speed of crystallisation under specific conditions.

An investigation by Car (120) focuses on microscopic calculations of impurity defect reactions and diffusion mechanisms of dopant impurities in silicon (Si). Impurity diffusion is crucial in electronic device fabrication, but the underlying mechanisms in Si have remained poorly understood, relying on empirical programmes developed over time. This research aimed to provide a detailed understanding of diffusion mechanisms to enhance device design. The investigation centres on impurity diffusion through vacancies and self-interstitials. Vacancies were found to mediate impurity diffusion via impurity vacancy pairs, while self-interstitials contribute through the "kick-out" mechanism, ejecting substitutional impurities into interstitial channels. The study challenges previous assumptions regarding the primary role of "interstitialcy" in self-interstitial contributions.

The paper explains that diffusion at normal atomic sites is governed by defects that induce marked atoms to move to different sites. The activation energy for impurity diffusion can be smaller than the self-diffusion activation energy due to complex mechanisms arising from impurity-defect reactions. Phosphorus and aluminium were used as representative impurities, and the calculated results align well with measured activation energies for intrinsic and extrinsic Si. The researchers provided detailed information about diffusing species, their atomic configurations, charge states, and migration paths (120).

The role of vacancies in self-diffusion was investigated, revealing that substitutional impurities diffuse through impurity-vacancy pairs. The study explores self-interstitial-mediated diffusion, considering various configurations of impurity and silicon atoms. The lowest-energy configuration involved the impurity atom in the channel site, leading to reduced activation energies. The findings suggest that complex mechanisms involving impurity-defect reactions account for the observed reduction in activation energy for impurity diffusion. The study sheds light on enhanced diffusion processes and oxidation-enhanced diffusion in Si. While the paper provides valuable insights into impurity diffusion, further research should validate theoretical assumptions and consider experimental verification (120).

In a separate study by Coleman and Roy (121), mass transfer by ultrasound agitation during electrodeposition in a narrow inter-electrode gap was investigated. The study employed polarisation experiments to identify the mass transfer limiting current. The gathered data was used to calculate mass transfer boundary layer thicknesses and develop correlations. Indicating that lower ultrasound powers, ranging from 9 to 18 W cm^{-2}, were more effective at agitating the solution in narrower electrode gaps compared to higher powers exceeding 18 W cm^{-2}. When a side-on ultrasound probe was used, Sherwoods correlations revealed the presence of turbulent flows near the electrode surface. Developing turbulence was observed for larger inter-electrode spacing, while narrow electrode gaps showed fully turbulent correlations.

However, the study encountered limitations, particularly in detecting a limiting current plateau when the electrodes were positioned closely together or when the ultrasound probe was in proximity to the electrodes. This difficulty may be attributed to distortions in polarisation data caused by the metallic ultrasound probe. As a result, the applicability of the limiting current technique for measuring mass transfer limitations in electrochemical systems using ultrasound was called into question. Further analysis and research are necessary to fully understand the precise mechanism of ultrasound agitation at the electrode surface and address potential distortions in potential measurements (5).

The validity of the results is supported by the experimental data, correlations, and modelling analysis presented in the paper. The study highlights the significant enhancement in mass transfer achieved through ultrasonic agitation, making it a promising technique for various applications. Nevertheless, it underscores the importance of careful consideration in equipment design and the proximity of ultrasound sources to substrates or workpieces to avoid potential distortions and ensure accurate and reliable results. As this investigation opens new possibilities for improving mass transfer in electrochemical processes, further research and development could lead to valuable advancements in various industrial applications.

2.4.6c Crystal defects

Crystal defects, irregularities, or disruptions in a crystal lattice's atomic arrangement profoundly impact material properties and performance. They influence mechanical properties, either strengthening or weakening the material. Electrical properties are affected by introducing charge carriers through point defects, while optical properties undergo alterations due to energy levels created by defects within the band gap. Defects also influence thermal conductivity by scattering phonons and impacting chemical reactivity, serving as more reactive sites with unsaturated atoms and acting as diffusion pathways that affect mass transport. In electronic devices, defects can affect performance and reliability with controlled defects deliberately introduced for specific electronic properties.

Moreover, defects can act as catalytic sites in heterogeneous catalysis. Crystal defects play a crucial role in determining material behaviour and characteristics, necessitating the understanding and control in materials science and engineering to tailor materials for specific applications. In bulk crystalline materials, despite the favourable energy conditions for a perfect lattice, the molecular arrangement deviates, resulting in the presence of defects. These defects are challenging to eliminate once they form during crystal growth due to the limited mobility of molecules in solids (122).

Table 2: Summary of crystal defects (7).

Point (Zero-dimensional)	Line (One dimensional)	Surface (Two-dimensional defect (area, plane, or volume))
• Vacancies: i.e. vacant lattice sites. • Interstitials: Additional atom inclusions not on lattice sites. • Impurities: Inclusion of foreign species into the lattice	• Screw and edge dislocations	• Stacking faults: odd number of atoms (twinning) • Inclusions

Table 2 presents three common types of point defects, or vacancies. Vacancy defects occur when holes within the crystal lattice and growth units are missing from the lattice sites (15). This defect governs the migration of atoms or molecules in the crystal lattice, as solid-state diffusion requires target sites with vacancies for atoms or molecules to move from one lattice site to another. The rate of solid-state diffusion is significantly influenced by the presence of vacancies (98). Vacancy defects also impact the properties of solid materials, including electronic and mechanical properties, due to the larger internal energies compared to crystals with closely packed atoms (10). Another type of defect is interstitials, where foreign atoms or molecules occupy positions in the interstices between the matrix atoms of the crystal, leading to lattice distortion in most cases. On the other hand, substitutional defects occur when an impurity molecule occupies the site of a matrix atom (15).

In crystal growth, slip or shearing is facilitated by two primary types of line defects, known as edge and screw dislocations, which can occur separately or together. These dislocations are abundant in large numbers due to surface and internal stress (15). Figure 13 illustrates an edge dislocation, which involves the insertion of an extra half-plane of atoms above or below the dislocation line.
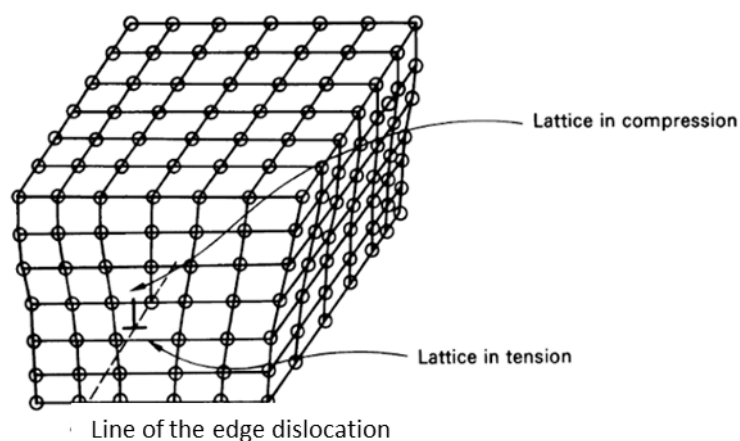
Figure 13: Line of the edge dislocation where there is one more vertical plane of atoms above the dislocation line (99).

This dislocation, Figure 13, constitutes a region of higher energy compared to the surrounding lattice. This energy disparity arises because the lattice above the dislocation line experiences constant compression, while below the line, it undergoes constant tension. Consequently, irregular inter-atomic distances form below the dislocation line, providing an ideal "sink" for chemical impurities and interstitial atoms to accumulate (99).

On the other hand, the screw dislocation, as depicted in Figure 14, involves a transformation where atoms are displaced along the dislocation line rather than at right angles to it, as observed in the edge dislocation. Although no compressive or tensile stress is present, the screw dislocation does exhibit sheer stress (99). This dislocation creates a favourable site for the attachment of growth units on the crystal's face, leading to a spiral growth pattern (15).
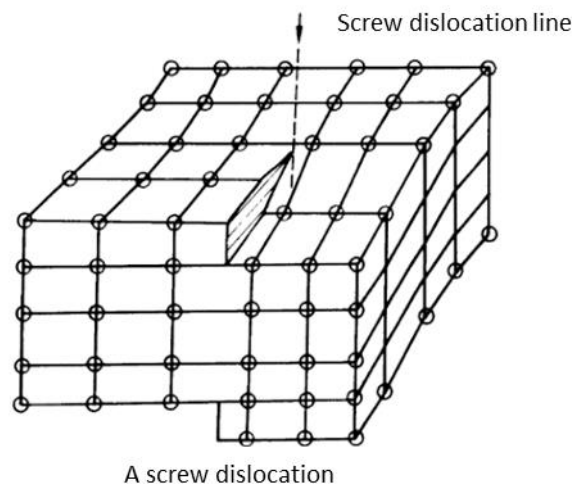
Figure 14: Screw dislocation (99).

In Figure 15, the Burgers vector is visualised as a closed loop encircling the dislocation line. This loop, often referred to as the Burgers circuit, is characterised by "equal integral lattice translations in each pair of parallel sides of a right-handed circuit around the direction of the dislocation line". According to Lovell (99) as the circuit traverses the crystal, it would normally close upon itself. However, in the presence of a dislocation, the circuit fails to close completely, and the extent of this failure is represented by the Burgers vector of the dislocation.
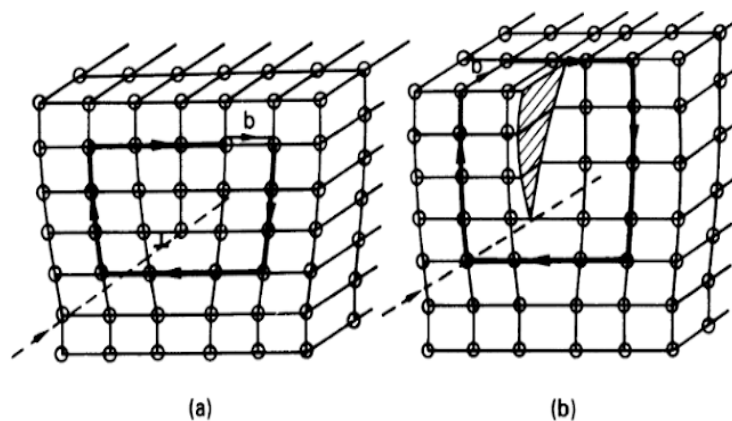
Figure 15: The Burgers vector of (a) Edge dislocation (b) Screw dislocation (99).

The Burgers vector is observed to be perpendicular to the line of distortion in cases of edge and screw dislocations. In contrast, for edge and screw dislocations, the Burgers vector runs parallel to the line of distortion.

Two-dimensional defects, also known as plane defects, can be more extensively incorporated into a crystal lattice compared to line or point defects. These defects may result from incorrect stacking arrangements or occur at growth sector boundaries. When successive close-packed layers follow the sequence ABCABCABC..., any deviation from this pattern, such as ABCBACBAC, leads to twinning. Twinning causes crystals to become mirror images of each other. Figure 15 illustrates a common plane called a twin plane, acting as a mirror image (10, 99, 100).

2.4.6d Crystal growth rate

The growth kinetics of crystals play a critical role in determining the distribution of crystal sizes (CSD) and the average crystal size (CMS) (123). There are various methods to express the rate of crystal growth, which depend on factors such as supersaturation, temperature, and the specific characteristics of the crystallised material.

In the literature, single crystals have been grown using slow evaporation over 3-4 weeks (124) or cooling crystallisation within 5-7 days (125-127). In this study, single crystals were grown and measured in real-time using pre-prepared saturated solutions

of impurity mixtures. Another commonly used method described in the literature involves seeding a system and subjecting it to different conditions, or doping (125). However, in this case, in-situ analysis proved more advantageous, as it observed a variety of crystal habits that would have otherwise gone unnoticed.

In the context of measuring in-situ single crystal growth rates, the choice of cell type plays a crucial role. Stagnant cells offer several advantages in comparison to flow cells. For example, a controlled and stable growth environment by eliminating flow-induced hydrodynamic effects such as convection and shear forces. This simplifies the experimental setup, reduces contamination risks, and allows for higher spatial resolution, enabling precise measurements and analysis of specific crystal faces or regions of interest. Stagnant cells also offer better stability for long-term measurements, making them suitable for prolonged observation. However, flow cells have their own merits, as they enable rapid mixing of solutions, induce supersaturation, and facilitate the observation of nucleation and subsequent growth of single crystals (74, 78).

For the specific research aim of investigating the effect of impurities on single crystal growth in-situ, a stagnant cell was selected over a flow cell. The choice was driven by the need for real-time analysis of single crystals growing in an undisturbed environment (1). Further details regarding this choice will be elaborated on in the single crystal growth chapter.

To visualise and capture images during the experiments, a Brunel SP-200XM metallurgical microscope was used. Microscopy emerged as a popular method for in-situ size characterisation of nucleating crystals or seeds due to its effectiveness in providing valuable insights (74, 79, 80).

Several techniques were employed to analyse single crystals in the bulk suspensions. The first technique, FBRM, enabled in-situ measurement of the crystal size distribution (128, 129). More information about the equipment used can be found in Section 2.7.3. Sympatec (QIPIC) was also used for particle sizing of the dry powder product. This offline particle sizing tool is widely used for analysing dry powder particles (130, 131). Further details regarding this technique can be found in Section 2.7.4.

2.4.7: Crystal morphology

The external appearance of a crystal, i.e., its overall shape, is described as its habit (needle-like or plate-like) or its morphology. In order to define the crystal morphology, face indexing is employed using X-ray diffraction; the angles between specific faces are characteristic; at an even more fundamental level, the angles between crystal axes and the length of the unit cell may be determined (131).

2.4.7a Molecular recognition at the crystal interface

The crystal habit represents the combination of the equilibrium morphology, that the crystal would assume when in equilibrium with its surroundings, and the growth morphology, where the crystal shape is influenced by the kinetics of dominant face growth (6).

Ristic (132) reported that the crystal morphology of paracetamol crystals depends on the crystallisation supersaturation. Figure 16 depicts paracetamol crystals grown in (a) low, (b) medium, and (c) high supersaturations, showing a clear alteration in habit based on supersaturations.
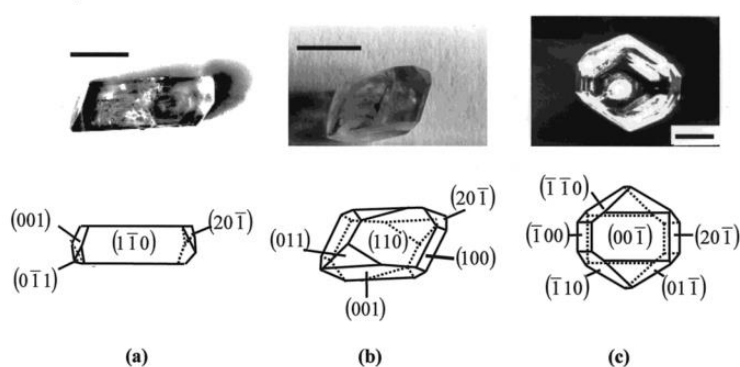
Figure 16: Paracetamol crystals grown at (a) Low (b) Medium (c) High supersaturations (132).

It is important to note that the crystal morphology has also been found to influence the bulk solid state properties and downstream processes such as filtration, drying, and final product production, e.g., tabletting and performance in the patient, in particular bioavailability (133).

Guo (134) explores how the shapes of drug nanocrystals (NCs) affect their behaviour in oral drug delivery, specifically examining their impact on aqueous solubility, dissolution rate, and oral bioavailability. Although the effects of particle shapes on these properties have been studied, their influence on the transport of NCs across intestinal barriers remains unclear. To address this, the researchers prepared and characterised spherical, rod-shaped, and flaky NCs (SNCs, RNCs, and FNCs). They also used fluorescence resonance energy transfer molecules to track the fate of intact NCs. The study found that particle shapes significantly influenced various aspects of NCs behaviour. Notably, RNCs exhibited the best absorption efficiency, surpassing SNCs and FNCs in mucus permeation, cellular uptake, and transmembrane transport.

2.4.7b Effect of impurities

Crystals within the same crystal system can exhibit different habits depending on the relative growth rates of their different crystallographic faces. Terms like cubic, plate-like, acicular, or tubular are commonly used to describe the general habit. Faces that grow relatively quickly contribute minimally or not at all to the overall habit, while slow-growing faces, potentially hindered by impurity incorporation at their active sites, dominate the habit. This is illustrated in Figure 17, where an impurity impedes the growth of face B, causing face A to protrude from the habit. The habit is defined by the crystal structure, crystallisation conditions (e.g., solvent used or impurities found), the degree of supersaturation, and the density of active growth sites (132, 135).
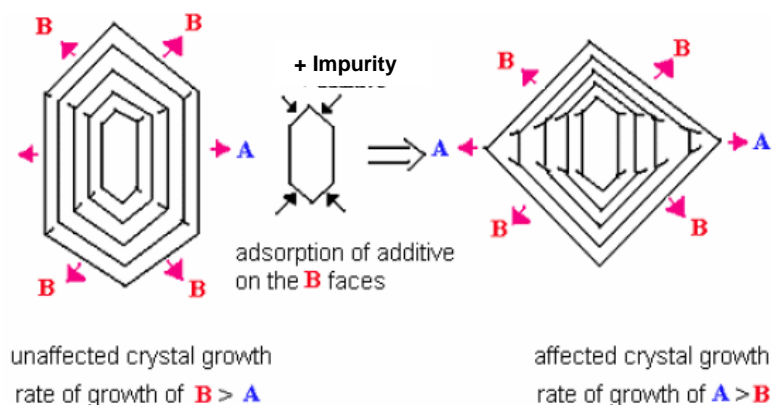
Figure 17: Schematic representation of crystal morphology adapted from Weissbuch (136).

The presence of impurities that can alter the overall crystal morphology poses a challenge in many cases, as it can have downstream impacts on processes such as filtration during isolation and compaction during tablet formulation, affecting the final drug product. During crystal growth, the surface of the growing crystal consists of "active sites" that enable specific interactions with molecules in the solution. The effectiveness of different analytical techniques in identifying the quantity and spatial distribution of impurities on crystal surfaces and any morphological and surface texture changes has been investigated by Ottoboni (125) this study found surface texture changes and the presence of small crystal agglomerates of the deposited impurity.

It is widely recognised that the presence of impurities in varying amounts can affect crystal growth, morphology, dissolution, and nucleation kinetics (16, 23, 45). Mullin (7) defines an impurity as any substance other than the material being crystallised, which in this case would also include the solvent mixture from which the crystals are growing.

In general, impurities tend to suppress growth (87, 88), although there are rare cases where certain impurities may enhance growth (89, 90). Impurities that suppress growth can have selective effects, acting differently on each crystallographic surface and modifying the crystal habit (15). Sangwal and Benze (91) state that all crystals, regardless of their structure, bonding nature, and growth phases, will contain impurities, whether by chance or design. It is possible to intentionally introduce impurities into a system for specific purposes, such as controlling crystal size distribution (15, 16).

The Kossel model of crystal surfaces, discussed previously and depicted in Figure 11 and Figure 18, provides a valuable framework for understanding crystal growth and picturing the incorporation of impurities onto specific sites.
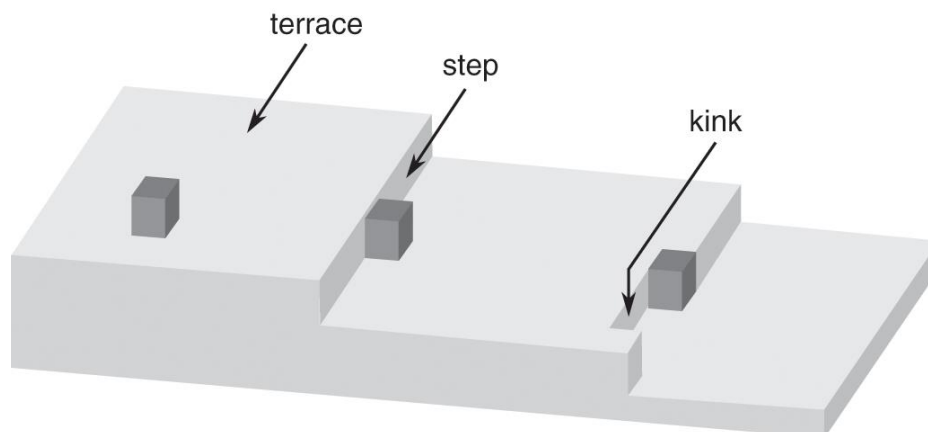
Figure 18: Terrace, step, and kink model (137).

The presence of impurities in a growing crystal lattice primarily acts as a growth inhibitor. These impurities are often closely related analogues of the active pharmaceutical ingredient or may be formed as degradants or by-products during the synthetic process (9). When incorporated onto the crystal faces, structurally related substances can have varying effects depending on the individual orientation of the molecules in the surface layer. Different crystal faces are influenced to different degrees, resulting in impurities affecting face-specific growth rates and morphology in a distinct manner. For instance, Finnie (95) observed that the impurity PAA (p-Acetoxyacetanilide) specifically influenced the growth of paracetamol, particularly on the (110) faces. This observation suggests that the presence of PAA plays a crucial role in shaping the crystal's surface and overall habit. Impurities like PAA can potentially alter growth rates and the morphology of specific crystal faces, which has important implications for the quality and production of paracetamol crystals (117).

2.4.8: Polymorphism

The first observation of a substance existing in different crystal forms was made by Martin Klaproth in the late seventeenth century, who examined CaCO3 as aragonite and calcite (138, 139). However, the term polymorphism was not used until 1823,

when Mitscherlich observed several structures of arsenate and phosphate salts (140). Polymorphism is defined by Davey and Garside (14) as crystals of the same chemical entity that can adopt more than one crystal structure. Each polymorph has its own unique combination of physical, thermal, and mechanical properties (6). These structures are composed of different stacking arrangements and, molecular conformations within the crystal lattice (141).

2.4.8a Challenges in industry

Polymorphism is a challenge for the pharmaceutical industry, as relatively few active pharmaceutical ingredients exhibit just one crystal form (1). Where multiple polymorphs of a compound exist, one will always be the most stable, and the others will be metastable with respect to that one. Polymorphism may also impact many physiochemical properties of the active ingredient, such as: solubility, density, stability, melting points, and dissolution rates (142). Reducing the solubility and dissolution kinetics in the patient's gut may reduce the rate of adsorption and lower bioavailability. Potential, changes in the polymorphic form of the formulated drug substance can occur in the interval between production, storage, and distribution (143, 144), making the characterisation of polymorphs and identification of the stable polymorph a critical step in drug development (145).

2.4.8b Ostwald's rule of stages

According to Ostwald's rule of stages, polymorphs interconvert from least to most stable forms. The most stable polymorphic form is being the least soluble. It is preferable to develop the most stable polymorph so that any unwanted phase transformations are avoided during processing and manufacturing. However, this is not always possible without intervention based on seeding with the most stable form; otherwise, the most metastable form will nucleate and grow first, and the following most stable form will nucleate until the most stable form is achieved. In polymorphic systems, kinetics favours the formation of metastable forms, while thermodynamics leads to transformation to the most stable form. During crystallisation or phase transitions, the kinetic behaviour influences the initial stages, promoting the formation of less stable, metastable polymorphs. In contrast, as the system reaches equilibrium

over time, the thermodynamic behaviour drives the conversion of metastable forms to the most stable polymorphic form, which has the lowest free energy and highest stability. Understanding these kinetic and thermodynamic factors is vital for controlling the final polymorphic form obtained during the manufacturing process (146-148).

2.5: Paracetamol

2.5.1: Introduction

Paracetamol $C_8H_9NO_2$, also known as acetaminophen (more commonly used in the USA), has a molecular weight of 151.16 g mol^{-1} and a melting point of 169 °C. Due to its widespread use and simple chemical structure, paracetamol has been extensively studied (125, 149). It serves as an active ingredient in various preparations, such as Calpol, commonly used as an infant suspension, and cold and flu remedies like Lemsip. The electronic medicines compendium (emc) lists over 263 products containing paracetamol, all licensed for patient use within the UK (150). These products are sold for self-medication, providing relief from common symptoms like headaches, colds, fever, and toothache. Paracetamol is considered safe in standard doses without the need for prescriptions. Unlike aspirin, it does not impact blood coagulation or irritate the stomach lining, kidney function, or fetal ductus (151). However, despite its widespread and diverse use, many people remain unaware of the potential risks associated with overdosing on paracetamol, which can lead to liver damage or even death (152,153).

In 1877, the synthesis of acetaminophen (paracetamol) was carried out at Johns Hopkins University in Baltimore. Initially, the synthesised compound held little significance until 1893, when Von Mering proposed its potential as a pain reliever. Further investigations confirmed its analgesic and antipyretic properties, though some side effects were observed. However, due to challenges in controlling the reaction, the product was initially overlooked. It wasn't until 1950 that the first paracetamol containing product was developed, following extensive tests conducted by American researchers in 1949 (154). Finally, in 1956, paracetamol became commercially

available in the UK under the trade name Panadol (8). Over the years, several common synthesis routes for this compound have been reported, with Ellis and Quartarone later contributing to the understanding of these methods (155, 156).

2.5.2: Polymorphism and habit

Paracetamol exhibits three distinct polymorphs: form I monoclinic (157), form II orthorhombic (158) and form III which is known for its high instability, requiring tightly controlled conditions for crystallisation (144, 159, 160). In the crystal structure of form I, molecules arrange themselves in a herringbone pattern, as depicted in Figure 21. On the other hand, form II appears in layered form, providing improved physical properties such as enhanced compressibility, making it favourable for tabletting, with a slight increase in solubility, aiding in bioavailability (161); However, form II is considered metastable compared to form I at all temperatures and ambient pressures, undergoing a phase transition to form I upon cooling in the presence of humidity (162, 163).

Agnew (161) successfully produced paracetamol form II using a multicomponent templating approach through cooling crystallisation with two templating molecules, metacetamol, and 4-fluorobenzoic acid. This innovative method used the difference in solubility between metacetamol and 4-fluorobenzoic acid in the selected solvent system. Metacetamol displayed higher solubility, allowing for higher concentrations of the templating material during the crystallisation process. As a result, they scaled up the production to a substantial volume of 800 mL, resulting in the synthesis of over 100 g of pure paracetamol form II see Figure 19.

The use of multicomponent templating not only facilitated the successful production of form II but also showcased its potential for large-scale applications. This approach opens doors for industrial processes aiming to access metastable forms in a controlled and scalable manner. However, it should be noted that while this method demonstrates significant progress in producing form II, there may still be opportunities for further optimisation to enhance the overall yield and reduce potential impurities. Additionally, consideration should be given to this approach's industrial applicability

and scalability when aiming for large-scale production of paracetamol form II. Nonetheless, the success achieved by Agnew in obtaining pure form II through this innovative templating strategy marks a noteworthy advancement in the field of crystallisation techniques (161).
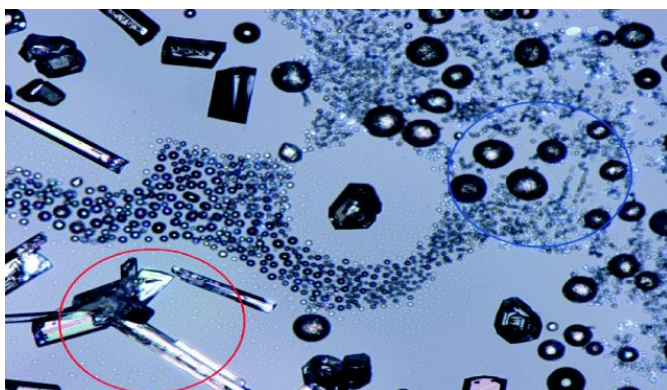
The habit of paracetamol form I varies to some extent, typically appearing as plate-like and needle-like structures depending on the specific crystallisation conditions.

Figure 19: Form I characteristic (elongated, thicker crystals), form II polycrystalline (round shapes) (161).

The prediction of paracetamol's external morphology was accomplished based on its internal crystal structure using the Bravis-Friedel-Donnay-Harker (BFDH) method. This method allows for the anticipation of a crystal's habit when its lattice structure is known, utilising symmetry operators and corresponding unit cell parameters (a, b, c, α, β and γ). By considering the symmetry and crystal lattice, a list of potential growth faces and their relative growth rates can be generated. An illustration of this process is presented in Figure 20, assuming that the relative growth rates R_{hkl} of the crystal faces are inversely proportional to the inter-planar spacing d_{hkl}. It is important to note that this approach does not account for the crystallisation environment; instead, the molecular packing arrangement of the crystal is deduced from the inter-planar spacing.
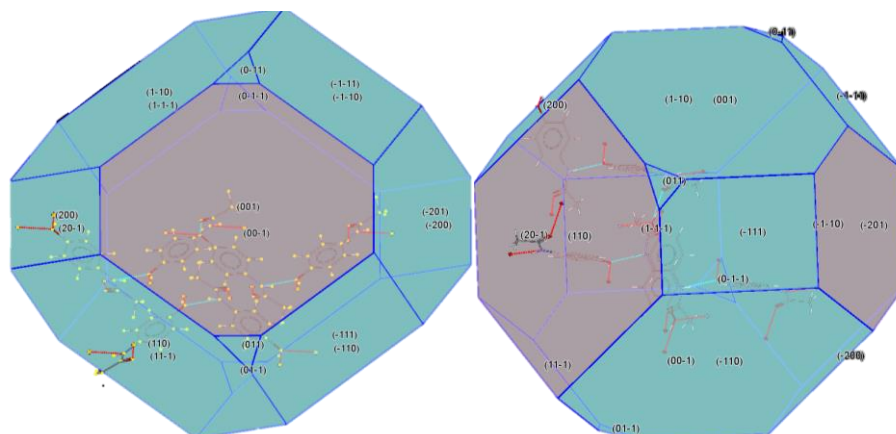
Figure 20: Paracetamol form **I** main facets. Predicted morphology using the Bravis-Friedel-Donnay-Harker (BFDH) method, assuming relative growth rates R_{hkl} of the crystal faces is inversely proportional to the inter-planar spacing d_{hkl}. The CCDC habit tool was used to predict the above structure.

2.5.3: Crystal structure

Paracetamol crystals belong to the space group $P2_1/n$, with four molecules in a monoclinic system. The unit cell of the crystal has lattice parameters a = 7.09($\dot{A}$), b = 9.39($\dot{A}$), c = 11.73($\dot{A}$), α=90°, β=97.49° and γ=90°. The primary feature of the paracetamol crystal structure is hydrogen bonding, leading to the formation of hydrogen-bonded chains of molecules packed in a herringbone conformation within the crystal structure. Additionally, hydrogen-bonded sheets are formed from these molecules and stacked in the [010] direction. These stacks are held together by Van der Waals interactions, as depicted in Figure 21.

The paracetamol molecule consists of a benzene ring centre, with one hydroxyl group and a methylamide group in the para position (117). The N-H (amide) and O-H (hydroxyl) groups act as hydrogen bond donors, while the C=O (carbonyl) acts as a hydrogen bond acceptor (125). Finnie (117) quantified the degree of hydrogen bonding occurring within the crystal to be 8.31 kcal mol^{-1}, which approximately corresponds to 30% of the total lattice energy (164). Structurally related impurities or additives that have the potential to disrupt the hydrogen bonding network may modify the overall crystal morphology and the crystal growth rates. These disruptions can have significant implications for the properties and behaviour of the paracetamol crystals.
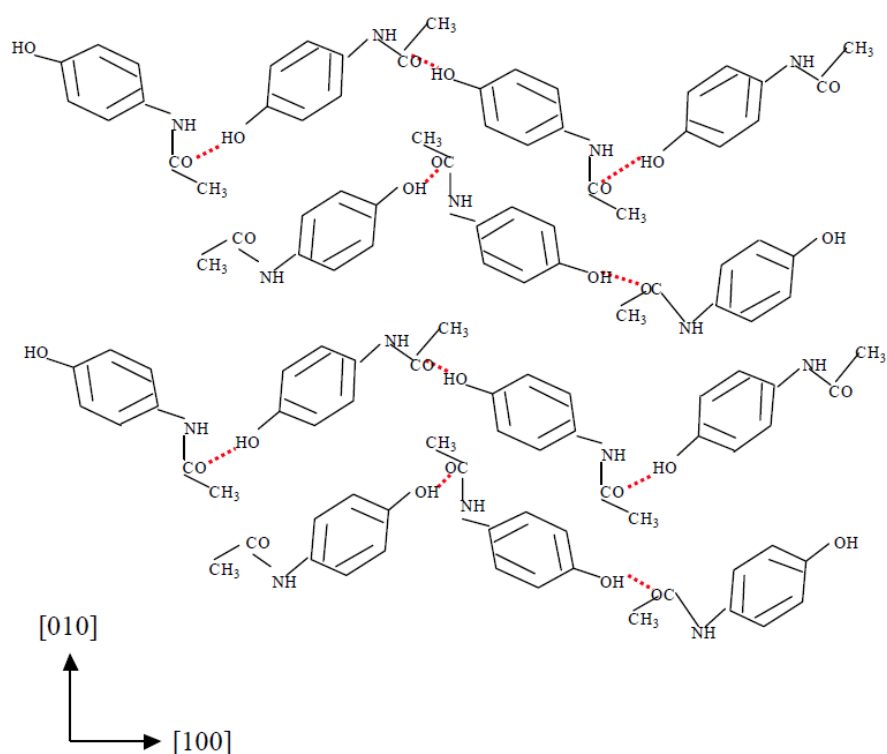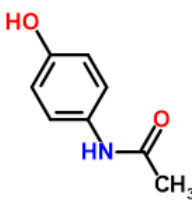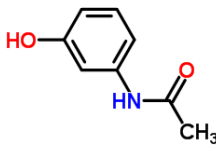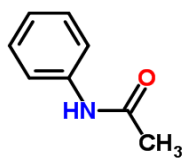
Figure 21: Paracetamol molecular packing on the (001) face; [010] and [100] directions are shown; the molecules are packed in a herringbone arrangement. In each layer, the molecules are held together with hydrogen bonds, represented by the dashed red lines (117).

2.5.4: Structurally related additives

Various structurally related additives, primarily impurities formed during the synthesis of paracetamol, have the potential to act as growth inhibitors, thus modifying the crystal habit. Among these compounds are orthocetamol, metacetamol, acetanilide, 4-aminophenol, 4-nitrophenol, and 4'-chloroacetanilide. For this study, metacetamol and acetanilide were chosen as the specific impurities due to their structural similarity. These impurities are conveniently available as pure entities from Sigma-Aldrich, and their structures and sourcing information can be found in Table 3.

Table 3: Paracetamol, metacetamol and acetanilide structure, purity, source, and batch number.

Material	Structure	Grade or purity	Source	Batch
Paracetamol		≥99.0% BioXtra	Sigma Aldrich	SLBH0785V
Metacetamol		97.0%	Sigma Aldrich	0512CHV
Acetanilide		99.0%	Sigma Aldrich	STBD0193V

2.6: Impact of ultrasound on crystallisation processes

The use of ultrasound-assisted chemistry has been reported to bring several key benefits, such as: waste reduction, energy saving, operation at ambient temperatures instead of elevated temperatures, enhanced safety, and improved mass transfer (165). Ultrasound has also been studied extensively for its positive impact on crystallisation processes, offering various advantages such as:

- Controlling the nucleation rate (49, 166-169)
- Narrowing the metastable zone width (MZW) (49, 168-170)
- Brief discussion on impurity incorporation (16, 128, 171)
- Assisting in controlling crystal size distribution, shape, and habit (19, 49, 50, 172, 173)
- Increasing the overall yield (50, 128, 174)
- Influencing polymorphism, promoting transitions from one form to a more desirable form (19, 49, 50, 161, 175-177)
- Elimination of the need for the addition of seed crystals (16, 50, 172, 178)

Overall, ultrasound presents a promising approach to enhance crystallisation processes and improve product quality, offering unique advantages not easily attainable through conventional methods. This thesis specifically focuses on investigating the impact of ultrasound in both single crystal growth settings and bulk suspension crystallisations. The primary objectives include studying the influence of structurally related impurities (metacetamol and acetanilide) on crystal growth rates and habits with and without ultrasound and scaling up single crystal growth settings to replicate industrial batch production using an ultrasonic bath. The investigation aims to assess product purity, crystal growth rates, yield, and habit formations under various conditions. The study will provide valuable insights into the potential benefits and applications of ultrasound in crystallisation processes, contributing to the advancement of this field of research.

2.6.1: Impact of ultrasound on nucleation

Numerous studies in the literature provide experimental evidence of the use of power ultrasound to induce primary nucleation in previously particle-free solutions and to enhance secondary nucleation, often at lower supersaturations than normally required (16, 49, 168, 169, 178-181). As previously mentioned, introducing ultrasound to a solution leads to the formation of acoustic cavitation bubbles that go through various stages of growth and eventual collapse. This process results in several effects, including regions of extreme molecular excitation, the release of shockwaves, and significant increases in temperature (up to $5000\,\text{K}$) and pressure (up to 2000 atm), along with microjets and improved mixing (16, 45, 182).

Ultrasound has demonstrated the ability to induce nucleation even in systems that are typically very resistant to nucleation, such as in the sugar industry, where the high viscosity of the sugar solution makes the formation of nuclei difficult. Additionally, Mullin (6) observed that nucleation resulting from scratching a vessel's side could potentially be attributed to cavitation effects. While various hypotheses have been proposed in the literature to explain why nucleation occurs due to these ultrasound-induced effects, the exact mechanism is not fully understood.

97

Ruecroft (16) provides a comprehensive overview of the application of power ultrasound to crystallisation processes, specifically focusing on its impact on crystal nucleation and growth. The study highlights one of the most significant effects of ultrasound: the induction of nucleation, enabling users to wield this influence strategically. Ruecroft emphasises the potential benefits of ultrasound in tailoring crystal size distribution and physical properties, positioning it as a valuable tool in pharmaceuticals and nanotechnology.

However, the absence of ultrasound in crystallisation processes introduces challenges, particularly in nucleation control. Ruecroft notes that nucleation events become challenging to control without ultrasound, and achieving specific crystal sizes and morphologies may prove difficult. Despite advancements in nucleation theories, the exact relationship between ultrasound-induced cavitation and nucleation remains incompletely understood (183-185).

Gielen (186) explores the use of pulsed ultrasound during the cooling crystallisation of paracetamol, focusing on pulse time and its effects on nucleation temperature, crystal size, and shape. The study contrasts silent conditions and continuous sonication with pulsed ultrasound, revealing intriguing findings. Notably, Gielen introduces the concept of pulsed ultrasound as an energy-efficient technique, reducing ultrasonic energy consumption while achieving similar nucleation temperatures. The pulse threshold, validated through bubble dissolution calculations, contributes to a vast reduction in energy consumption compared to continuous sonication.

Gielen's work delves into the role of bubbles in nucleation, indicating that bubbles can act as seeds for nucleation when present in the solution. Ultrasound's impact on particle size is multifaceted, involving improved nucleation, reduced Ostwald ripening, and breakage. The study suggests that ultrasound prevents Ostwald ripening, maintains small particles in the solution, and contributes to a reduction in particle size through cavitation bubble implosion and shockwaves (186).

Sanchez-garcia (187) aimed to investigate the effect of different ultrasound frequencies (20, 44, 98 and 142 kHz) and ultrasound powers (10, 20 and 30 W) on lactose nucleation. Lactose solutions (25% w v^{-1}) with traces of whey proteins (0.3%)

underwent sonication for 300 seconds. Crystallisation was induced by lowering the temperature from 30 to 15 °C, increasing the absolute supersaturation of lactose ($C\alpha$-$C\alpha s$) from 0.19 to 8.25 g/100g. The findings revealed that ultrasound significantly altered the molecular attachment frequency to form new nuclei k and the induction time.

The impact of ultrasound on lactose nucleation exhibited variations dependent on the ultrasound frequency or power applied. Notably, at 44 kHz, the most substantial changes were observed: an increase in the number of nuclei formed, a rise in the k-value to 0.1482 s^{-1} and a notable decrease in the induction time to 15 seconds. This frequency-dependent modulation of nucleation parameters highlights the intricate relationship between ultrasound conditions and lactose nucleation outcomes (187).

All three papers affirm ultrasound's role in inducing nucleation and enhancing nucleation rates, leading to the formation of more nuclei and smaller crystal sizes. However, challenges are acknowledged, such as the frequency and power dependence of ultrasound, introducing variations that may limit its general applicability.

Ruecroft (16) and Gielen (186) underscore the importance of carefully selecting ultrasound conditions to achieve desired nucleation outcomes. Ruecroft points to the need for further research to fully understand potential drawbacks and challenges in industrial settings. Gielen's introduction of energy-efficient pulsed ultrasound suggests a promising avenue for achieving nucleation control with reduced energy consumption.

Sanchez-garcia's study (187), focused specifically on lactose nucleation, providing insights into the frequency and power dependencies of ultrasound. The frequency-dependent alterations in nucleation parameters highlight the need for precise parameter selection in achieving desired nucleation outcomes. These comparative insights collectively contribute valuable perspectives on ultrasound's profound impact on crystallisation nucleation.

2.6.2: Impact of ultrasound on metastable zone width (MZW) and induction time

To assess the impact of ultrasound on nucleation, the metastable zone width (MZW) and induction time (t_{ind}) should be investigated (186).

Understanding the metastable zone (MZ) of a system is crucial for controlling the crystallisation process. In cooling crystallisation, the MZ width is defined as the temperature drop below the solubility temperature, marking the point where the crystalline phase spontaneously initiates (16). This width, also known as the metastable zone width (supersolubility limit), is specific to a given starting concentration value and cooling rate. Knowledge of the MZW provides an opportunity for precise control over crystallisation parameters.

Additionally, it has been observed that ultrasound irradiation of a solution leads to a decrease in the MZW (19). This reduction in the MZ is associated with improved product quality, manifesting as larger crystal sizes and less extreme crystal habits. The solute is less likely to precipitate out of the solution under these conditions, reducing the formation of fines (27).

Several studies have investigated the effect of ultrasound on the MZW (39, 88, 188, 189, 190). Kordylla (180) investigated the reduction of the MZW during crystallisation through the application of ultrasound. The results showed a clear reduction in the MZW due to ultrasound, which is consistent with findings reported by several other authors (88, 89, 190, 191). This suggests that ultrasound can effectively induce and control nucleation in the solution, leading to a narrower MSZ. Kordylla (180) explored the behaviour of this process under various ultrasonic parameters, with a focus on power output and frequency. The findings highlighted the importance of precise ultrasonic conditions, pointing towards a more focused and controlled crystallisation process with 200W power output and a frequency of 355.5 kHz, indicating the potential of ultrasound to optimise crystallisation outcomes.

Jordens (192) extended this exploration by investigating the impact of ultrasonic frequency on the nucleation and degradation of paracetamol under sonication. The study used three ultrasound transducers with frequencies ranging from 41 to 1140 kHz, with the aim to determine the most favourable frequency for enhancing nucleation rates and limiting degradation. Lower frequencies, particularly at 41 kHz, exhibited a more significant reduction in the metastable zone width (MZW), attributed to ultrasonic cavitation bubbles creating high supersaturation levels and enhancing nucleation. However, at higher frequencies, the effect on MZW diminished, possibly due to stable cavitation bubbles dominating the process.

Adding to this, Wohlgemuth and Ruether (193) found no significant changes in MZW with varying ultrasonic frequencies. Their paper primarily focused on the impact on nucleation control during crystallisation, particularly through power ultrasound and gassing techniques. While discussing the influence of ultrasonic frequency and insonation period on MZW, the study's main emphasis was on the role of the initial supersaturation ratio. The experiments demonstrated that the initial supersaturation ratio had a considerable effect on MZW during sonocrystallisation, resulting in a narrower MZW with lower ratios. However, the paper did not explicitly conclude that MZW was entirely independent of ultrasonic frequency or insonation period. Certain limitations, such as the unclear mechanism of power ultrasound.

Li (194) also found insonation to play a crucial role, though the frequency range did not result in significant changes in crystal nucleation and growth. This lack of effect was suggested to be due to the ultrasound wavelength being larger than the size of the nuclei and crystals. Li's study focused on "rapid sonocrystallisation," employing ultrasound as a mechanical aid during the salting-out crystallisation of a substance known as "MZW." By adjusting ultrasonic energy, duration, and mixture volume, Li demonstrated the possibility of controlling the mean size and size distribution of crystals. Sonocrystallised crystals exhibited well-defined shapes and minimal agglomeration, offering advantages over conventional methods where uncontrollable crystal growth and amorphous formations can arise.

These studies collectively highlight the intricate interplay of ultrasonic parameters, especially frequency, in influencing sonocrystallisation processes and nucleation control. While Kordylla (180) and Jordens (195) provide insights into specific frequency conditions, Wohlgemuth, Ruether (193) and Li (194) contribute by exploring broader factors impacting nucleation control and crystal growth during sonocrystallisation.

Ultrasound is known for its ability to shorten the induction time, which is the time it takes for nucleation and crystallisation to begin after reaching a specific level of supersaturation in a solution (169, 168, 7, 50).

Guo (189) revealed a significant reduction in the induction time during the anti-solvent crystallisation of roxithromycin when ultrasound was applied. This reduction implies that ultrasound accelerates the nucleation process, leading to a faster onset of crystal formation. Moreover, the increase in the nucleation rate constant (k_N) under ultrasonic conditions suggests an enhancement in the efficiency of the nucleation process.

Similarly, the study by Kaur Bhangu, Ashokkumar, and Lee (196) focused on paracetamol crystallisation, demonstrating a reduction in the induction time when ultrasound was introduced. The findings not only reinforce the idea that ultrasound expedites nucleation but also establish a correlation between cavitation activity and the rate of nucleation. Additionally, the study linked the modulation of induction time to the formation of different polymorphs of paracetamol under sonication.

A commonality between the two studies is the observed reduction in induction time under the influence of ultrasound. This shared outcome underscores the robust impact of ultrasound on expediting the initiation of crystallisation processes. The parallel increase in nucleation rate constants in both studies further supports the notion that ultrasound enhances the efficiency of nucleation, contributing to faster and more controlled crystal formation.

2.6.3: Impact of ultrasound on crystal growth and habit

When applied under carefully controlled and reproducible conditions, ultrasonic intervention initiates a precisely defined stage in the crystallisation process. Numerous research papers have explored various potential mechanisms by which ultrasound affects crystal growth (16, 40, 88, 197, 198). For instance, Boels (199) investigated the effects of ultrasound on the crystallisation of calcite under constant composition conditions. The research showed a significant increase (about 46%) in the rate at which calcite crystals form when treated with ultrasound. The study uses controlled variables to ensure reliable data, using scanning electron microscopy and particle size analysis to measure changes in crystal shape and size.

Bari's (168) research goes beyond just looking at how quickly crystals form, offering a comprehensive exploration of all the things that happen when ultrasound is used in the crystallisation process. The study demonstrates that ultrasound not only makes crystals form more quickly but also influences other processes, such as how crystals grow, break apart, and stick together. The paper gives a detailed understanding of these processes. However, it may be challenging to understand because the paper doesn't explain the statistical methods used very well. Despite this, the study highlights how ultrasound is helpful in making crystals form more efficiently and controlling their size and distribution.

Jordens (50) adds to the discussion by examining recent advancements in how ultrasound affects crystallisation. The paper discusses how ultrasound influences the start of crystal formation, crystals grow, and what kind of shapes can occur. The review acknowledges that there's still a lot we don't understand about how ultrasound works and that different studies sometimes have conflicting findings. The paper points out the challenges in drawing clear conclusions because different studies use different setups and equipment. The review also highlights how ultrasound can make crystals form quicker, affect their size and shape, with the potential to change the type of crystals that form.

All three papers together support the idea that ultrasound helps in making crystals form more efficiently, especially with how rapidly they form. Boels (199), Bari (168), and Jordens (50) agree that ultrasound can increase the rate of crystal formation, reduce formation duration, and offer a greater degree of control of crystal size distribution.

2.6.4: Impact of ultrasound on crystal size distribution, agglomeration, and breakage

Ultrasonic effects on crystal size distribution can be attributed to various factors, including: crystal breakage, agglomerate fragmentation, initiation of nucleation, sonication time, and irradiation intensity (178, 200).

Agglomerates, which are assemblies of loosely or potentially strongly bound crystals, play a significant role in crystal size distribution. Boels (201) reported that the application of ultrasound increased the volumetric growth rate of calcite crystals due to the alteration of the size and habit of seed crystals. With ultrasound, agglomerates experience attrition and breakage. Kusters (202) theorised that this breakage occurred when agglomerates were in close proximity to cavitation bubble collapses. Guo (203) attempted to confirm this hypothesis by studying the acoustic effects on large sugar crystals using high-speed video recordings. It was observed that the implosion of cavitation bubbles and the resulting vibrations and collisions caused deagglomeration. Such observations were made with high frame rates, corresponding to multiple cavitation cycles per frame. The disruption of aggregates and deagglomeration occurred due to the evolution of cavitation clusters, leading to erosion, pitting, and shear forces contributing to crystal fragmentation. Bartos and Horie (204) also observed similar fragmentation events with higher ultrasonic input power and longer exposure times.

Seeding is commonly used to control crystallisation processes and achieve a narrower crystal size distribution (180). Belca (177) compared conventional crystallisation with seeding and sonocrystallisation using ticagrelor as the API. Sonocrystallisation produced all three polymorphic forms faster and with a higher quality compared to

spontaneous and seeded crystallisation. The crystal size distribution could be 'tailored' by adjusting the duration of ultrasonic exposure. A short burst of ultrasound induced modest nucleation at lower supersaturation levels, allowing for the growth of larger crystals. Continuous or extended ultrasound bursts resulted in higher nucleation rates but limited crystal growth. Pulsed or intermittent ultrasound applications produced intermediate effects. Gielen (186) investigated the use of pulsed ultrasound during the cooling crystallisation of paracetamol and achieved a reduction of almost 70% in crystal size.

Ultrasound has been linked to the enhancement of primary and secondary nucleation, leading to the formation of more nuclei and smaller mean crystal sizes. Narducci and Jones (205) studied the effects of ultrasonic irradiation on Ostwald ripening, where large crystals are grown at the expense of smaller particles via molecular diffusion.

Sonofragmentation, the process of particle breakage induced by ultrasound, involves four mechanisms: interparticle collisions, horn-particle collisions, particle-wall collisions, and particle-shockwave interactions. Zeiger and Suslick (184) found that direct-particle shockwave interactions were the major contributor to particle breakage. Shockwaves, formed during cavitation bubble collapse, produce high local temperatures and pressures that result in interparticle collisions, damage to nearby objects, and sonofragmentation reducing the average particle size and size distribution (19).

2.6.5: Impact of ultrasound on impurity incorporation

Purification through crystallisation is a widely used method to eliminate impurities found in synthesised materials, allowing for the desired product in a pure state to be obtained, leaving unwanted impurities, which may be hazardous, in solution where they can be effectively filtered and washed. Subsection 2.4.7.b discusses how impurities can be incorporated into the crystal lattice. Commonly, industrial crystallisation feed streams exhibit impurity levels in the order of several mole%, leading to frequent interactions between impurity molecules and the developing crystal

surface. These interactions can yield undesirable consequences, such as impurity poisoning of growing crystal faces, resulting in prolonged processing times and delayed attainment of equilibrium. In some instances, a substantial amount of the product must be retained in solution and subsequently lost in the waste stream to maintain a feasible batch duration. Occasionally, the product may be sufficiently impure, necessitating a recrystallisation step to meet the specified quality standards (128).

The idea of using ultrasound to enhance purity was initially explored by Anderson (171) in a patent, wherein the application of low-intensity ultrasonic agitation during adipic acid crystallisation yielded a product of higher purity, smoother surfaces, and fewer inclusions and voids. It was discovered that the inclusion of impurities in the forming crystals can be minimised by introducing ultrasound to the crystallisation process (206). Nguyen (128) also found similar results through active intervention in the molecular process on growing surfaces; impurity removal from surfaces and entrapment within agglomerates were possible.

Similarly, Nalesso and Lee's (49) research explored numerous advantages of sonication in enhancing crystallisation and controlling the properties of the end product, including reducing crystal size, selecting desired polymorphs, improving purity, shortening induction time, and achieving better control over nucleation rates. Despite the evident effects of sonication on crystallisation, Nalesso and Lee (49) noted, like many others, that the underlying physical mechanisms remain unclear (5, 128, 207, 208).

Nalesso and Lee (49) discussed the presence of impurities in the crystallisation process, leading to agglomeration, stating impurities can get entrapped in liquid bridges between crystals, forming agglomerates that are challenging to break, resulting in reduced dissolution rates and lower product purity. However, "sono-deagglomeration" was highlighted as an effective way to break up agglomerates and keep particles dispersed during crystallisation, resulting in reduced agglomeration and smaller crystal sizes.

Ultrasound has the potential to enhance purity during crystallisation by preventing agglomeration and impurity entrapment, resulting in smaller crystal sizes and improved purity. While ultrasound has been mentioned to improve crystal purity (207), there is very limited data on ultrasound's effect on the purity of the final crystalline product. Ultrasound holds promise in addressing impurity-related challenges in crystallisation, and it is hoped that through this work, the potential for elevating the purity of pharmaceutical products through sonocrystallisation has been demonstrated.

2.7: Crystallisation characterisation and processing techniques

2.7.1: Differential Scanning Calorimetry (DSC)

Differential Scanning Calorimetry (DSC) is a valuable analytical method employed to aid in the identification of polymorphs and assess their thermal stabilities through the observation of phase transformations between different forms. In a DSC experiment, the heat flow into or out of a sample is carefully measured with a reference material as the temperature is systematically raised or lowered at a constant rate. The resulting endotherms and exotherms correspond to the phenomena of melting and recrystallisation, respectively, revealing distinctive characteristic temperatures (164).

2.7.2: High Performance Liquid Chromatography (HPLC)

High-performance liquid chromatography (HPLC) is a widely used method for effectively separating different components (analytes) within a mixture, facilitating the precise identification and quantification of each constituent present. In an HPLC setup, a dissolved sample is introduced into a continuously flowing mobile phase, propelled through a packed column containing fine particles, typically silica, acting as the stationary phase. This process occurs under high pressure. As the analyte molecules traverse the column, they undergo reversible adsorption onto the stationary phase.

Throughout their journey through the column, various analytes experience distinct durations of adsorption, leading to their separation based on differences in polarity. This separation mechanism is visually depicted in Figure 22. The analytes are detected as they exit the column, displaying characteristic retention times specific to the combination of elution conditions and the column used. The resulting HPLC data is represented in a chromatogram, which exhibits the time the eluted components emerge, with peak areas indicating the relative quantities of each component within the sample. By analysing these chromatograms, researchers can accurately determine the composition of complex mixtures and quantify the concentrations of individual analytes (209).
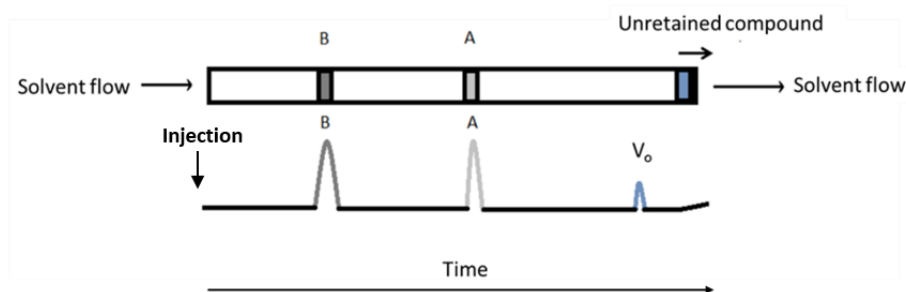
Figure 22: Schematic of HPLC column separation: A and B = components, V_o = void time altered from (114).

2.7.3: Focused Beam Reflectance Measurement (FBRM)

Focused beam reflectance measurement (FBRM) is used to determine particle size and number concentration within a crystal suspension. This analysis can be carried out in-situ, eliminating the need for sample preparation. The operating principle of FBRM is visually depicted in Figure 23. The FBRM probe comprises of a laser beam and a high-speed rotating lens, which directs light into the particle suspension. As the laser beam scans across a crystal, it scatters light back into the probe. By calculating the scanned chord trajectory length across the crystal, based on the scan speed and pulse width (time), data sets are collected every 2 seconds. This real-time information allows for tracking changes in the number and size of the crystals during the process. Consequently, updated chord length distributions (CLD) are obtained, which are crucial for monitoring and analysing crystal growth and evolution (210).
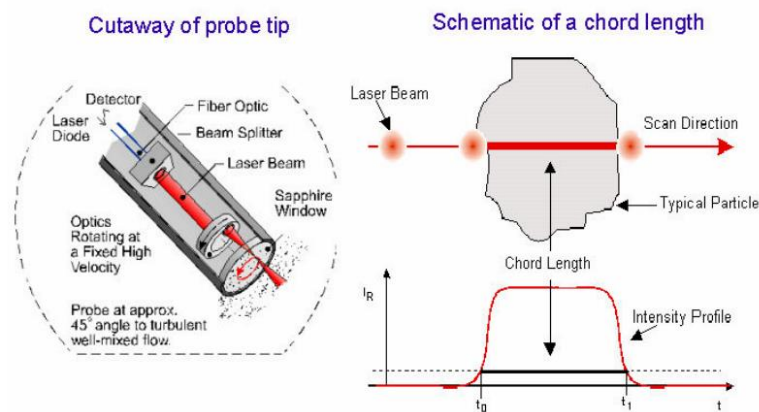
Figure 23: Focused Beam Reflectance Measurements (FBRM), probe tip (left) and chord length measurements (right) (210).

2.7.4: Sympatec (QIPIC)

QICPIC is an offline particle sizing instrument that uses image analysis to measure particle sizes within a wide range, from 1 µm to 34,000 µm. The instrument offers three different sample dispersion options:

1) Wet dispersion: (LIXEL)
2) Dry dispersion: Fine particles (RODES attachment)
3) Dry dispersion: Coarse particles (GRADIS attachment)

The RODES attachment was employed for the bulk suspension experiment detailed in this thesis due to some of the crystals being larger than 200 µm. The system is composed of: a light source, optics, a vacuum source, a venturi system to disperse particles, an aperture stop, and a camera. The samples are illuminated from below to produce silhouette outlines of the particles for accurate image analysis and sizing (211).

2.7.5: Single crystal and powder X-ray diffraction

Single crystal X-ray diffraction is a valuable technique that offers essential information, such as: unit cell dimensions, interatomic bond angles, bond lengths, and atomic positions (212).

X-ray diffraction relies on the constructive interference of a monochromatic X-ray beam as it passes through a crystalline sample. When the incident X-rays interact with the sample, they lead to the observation of both constructive interference and diffracted rays. Bragg's Law, expressed as Equation 15, defines the conditions for constructive interference in this context. This equation illustrated in Figure 24 relates to the wavelength of the incident X-rays λ, the spacing between the crystal lattice planes d, the angle of incidence θ, and an integer value n, representing the order of the diffraction peak. Valuable information can be obtained by analysing the diffraction pattern obtained from the crystal, including the unit cell dimensions, interatomic bond angles, bond lengths, and atomic positions (212).

$$n\lambda = 2\,d \sin\theta$$

Equation 15
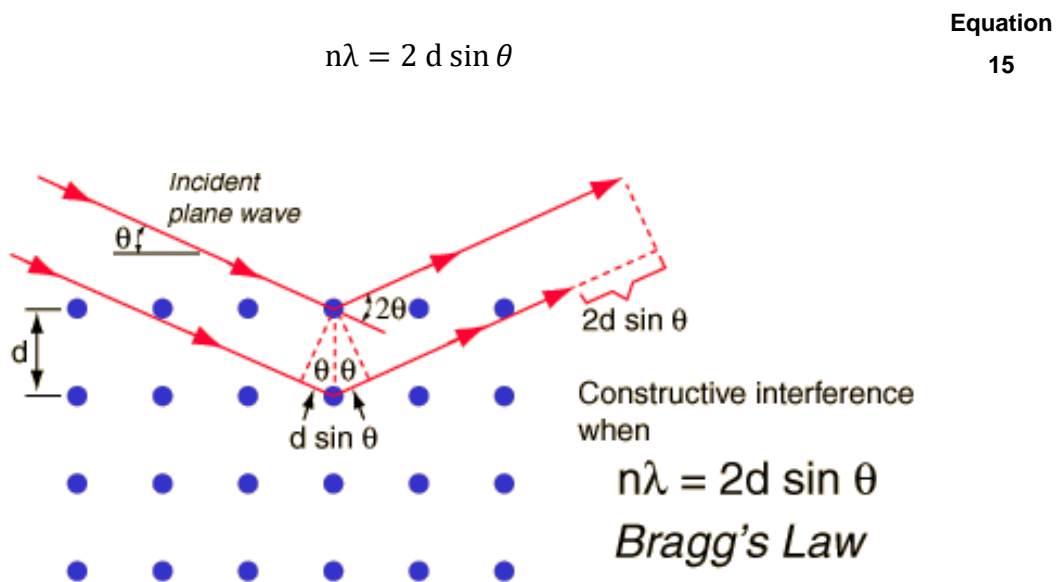
Figure 24: Bragg's law incident beam and reflected beams from lattice spacing (213).

Single crystal X-ray diffraction provides valuable information about the crystal structure of a material at an atomic level. However, it does not provide a comprehensive representation of the bulk material. To complement this, other methods are employed

to identify and confirm the purity of a compound. Powder X-ray diffraction is a widely used technique to obtain a unique "fingerprint" for a given material. This method allows for the determination of the sample's polymorphs, crystallinity, and bulk purity. The data obtained through powder X-ray diffraction can be compared with diffraction patterns from various sources in the scientific community, including the International Centre for Diffraction Data. Such comparisons play a crucial role in confirming the identity and purity of materials, ensuring consistency and reliability in scientific research and various industrial applications (214).

2.7.6: Filtration, washing and drying

The filtration, washing, and drying steps play a crucial role in isolating active pharmaceutical ingredients (API). These challenges include achieving high purity, controlling crystal size and morphology, and avoiding crystal breakage or agglomeration. However, researchers have implemented various techniques, such as sonocrystallisation, to address these issues and improve the overall efficiency of the process (215).

Filtration involves separating a solid phase from a liquid (filtrate) using a porous medium (filter medium). As the filtrate passes through the filter medium, particles of the solid phase are captured on its surface through a process known as 'bridging'. The particles form layers over the medium's pores, creating a 'filter cake', which acts as an additional filter medium. This buildup of the particle bed in the filter cake leads to an increase in the cake's resistance to flow, resulting in a reduction in flow rate over time when filtration is conducted at a constant driving force (216). Numerous factors can influence the filtration process, such as particle size distribution, crystal habit (changes in habit can affect filtration behaviour, e.g., plate-like to needle-like) and the viscosity of the feed suspension. Ultrasonic-assisted filtration has enhanced particle separation and improved filtration rates, resulting in a higher-quality product (128).

The crucial role of the interaction between particles and the wash solvent in the filtration process has been well established (217-219). Selecting an appropriate wash solvent ensures its compatibility and ability to mix with the crystallisation solvent. In

the specific case of the bulk ultrasonic experiments detailed in this thesis, ethanol served as the crystallisation solvent, while n-heptane was chosen as the wash solvent. Various physical and chemical properties of the wash solvent, such as density, viscosity, solubility of both the product and known impurities, miscibility, and surface tension all must be carefully considered (220, 221).

Through the utilisation of ultrasonic-assisted washing, the permeation of the wash solvent into the filter cake experiences a significant enhancement, resulting in a more efficient removal of impurities, as stated by Ottoboni (222). The research paper revolves around the creation and assessment of a continuous filter dryer prototype unit, known as CFD20, designed for small-scale pharmaceutical manufacturing processes. The primary objective of this unit is to transition from traditional batch filtration to continuous processing, providing real-time data logging and improved API isolation. The test compound used in the study was paracetamol, CFD20 demonstrated a filtration and washing performance comparable to manual best practices, successfully eliminating impurities and achieving a similar cake purity. Significantly, the study's focus was confined to paracetamol, and further validation using other compounds is necessary. Additionally, there is a need to investigate the potential for particle agglomeration during washing and drying, and to conduct a toxicity assessment of the continuous process. Furthermore, scaling up the technology and examining broader aspects, such as energy efficiency and cost-effectiveness, will be imperative for its successful integration into commercial pharmaceutical manufacturing processes.

The significance of effective washing cannot be overstated, as it plays a crucial role in eliminating impurities and any residual dissolved solute that may be present in the filter cake after crystallisation. Inadequate washing could result in the incorporation of impurities and dissolved solutes into the final product during the drying process, leading to undesirable granulation and modification of the overall crystal size distribution (223).

To address these challenges, sonication has proven to enhance mass transfer, promote nucleation, and enable better control of crystal size and morphology. Consequently, sonocrystallisation has been applied to enhance filtration rates, improve washing efficiency, prevent granulation during washing, and ensure the desired crystal size during drying (128, 222).

2.7.7: MODDE (MODeling and DEsign)

MODDE Pro is a software tool used in this thesis to implement the design of experiments (DoE) approach. The program facilitates the generation and evaluation of statistical experimental designs. DoE is a statistical technique that enables the execution of multivariate experiments to extract maximum information from a minimal number of experiments. A mathematical model establishes the relationship between these factors and the measured responses by simultaneously varying all selected factors across several planned experiments. This model is then employed to interpret the data, predict optimal operating regions, optimise processes, and identify a design space, resulting in significant time and material savings during hypothesis development and verification (224).

The experimental design cycle in MODDE Pro comprises of three main stages:

1. Design: Users select the experimental factors to investigate, determine the ranges (high and low levels) for each factor, and decide which responses will be measured to align with the overall objective. Based on this information, a worksheet of the experimental design (DoE) is created.
2. Analysis: After the experimental phase is completed, the raw data is input into the results table and analysed using various tools provided by MODDE Pro. This includes data fitting, plotting, and checking the validity of the experiments.
3. Prediction: The fitted model can be employed to predict outcomes anywhere within the investigated experimental space, allowing the identification of optimum conditions for the desired process outcome.

In this thesis, DoE was employed to assess bulk suspension crystallisation with and without ultrasonic intervention. The variables identified for investigation were ultrasonic power at 100%, 50% and 0% power, and the quantity of two impurities, metacetamol and acetanilide, with selected levels of 4, 2 and 0 mol%. A factorial correlation was applied to determine the number of individual experiments to be conducted, represented by the formula:

$$N = 2^k$$

<div align="right">**Equation 16**</div>

$$\therefore N = 2^3 \Rightarrow 8$$

<div align="right">**Equation 17**</div>

Where *N* is the number of experiments and *k* is the number of variables. Leardi (225) indicated that the interactions between three variables can be graphically represented, as shown in Figure 25, where eight experiments are represented by the eight corners of a cube. Additionally, a centre-point experiment is replicated to assess any curvature in the response to any factor and to evaluate experiment reproducibility.
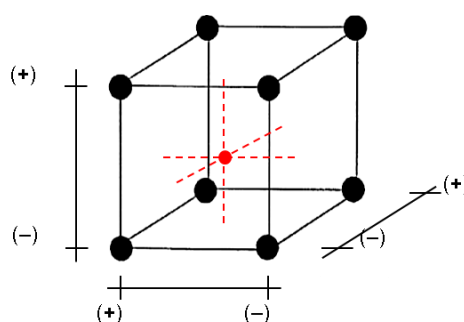
Figure 25: Graphical representation of a 2^3 factorial design (+) high range and (-) low range (225).

Chapter 3:

Experimental, Materials and Methods

3.0: Materials section

The following materials were used in all experiments:

Paracetamol (BioXtra grade, purity ≥ 99.0%, Lot number 637515L263) was obtained from Sigma-Aldrich (St. Louis, MO, USA). Acetanilide 99.0%, Lot number STBD0193V, and metacetamol 97.0%, Lot number MKBX4643V, were also sourced from Sigma-Aldrich. The selected solvents, ethanol (puriss. p.a., ACS reagent, absolute alcohol, ≥99.8%) and isoamyl alcohol (3-methyl-1-butanol) (ACS reagent, ≥98.5% (Riedel-de Haën)), were likewise supplied by Sigma-Aldrich.

In addition, for the bulk suspension crystallisation experiments, N-Heptane (99%) from Ward Hill, MA, USA, was used to wash the filtered cake. HPLC grade water and methanol, used for HPLC analysis, were purchased from Alfa Aesar.

3.1: Methodology

3.1.1: MODDE

A design of experiments (DoE) framework was established using MODDE (Umetrics Modde, Version 11, MKS Instruments, Umeå, Sweden). This software played a crucial role in analysing the data gathered from the single crystal growth experiments. Additionally, in the bulk suspension crystallisation experiments, the DoE approach was implemented with the aim of minimising the quantity of required experiments. This strategy ensured an adequate distribution of data while concurrently decreasing the total number of experiments, particularly in comparison to multiple factorial problems.

3.1.2: Paracetamol solubility (Including MODDE)

3.1.2a Preparation of saturated solutions

Saturated paracetamol solutions were prepared with specific impurity concentrations relative to the amount of dissolved paracetamol. To determine the quantity of selected impurities, their known solubility in the chosen pure solvents at the selected measurement temperatures was considered. The method for calculating this solubility and accurately dispensing the required impurities is detailed in Appendix A, Sections, 2.0, 2.1 and 2.2, accordingly. 1, 2, and 4% mass of the chosen impurities were added to create a stock solution, based on the expected solubility of paracetamol in the given volume of solvent used in the equilibration experiments. A 50 mL volume of this stock solution was prepared, ensuring an accurate measurement of the impurity mass.

This method involved dissolving the impurities in the specified pure solvent prior to adding paracetamol. It ensured that the paracetamol was introduced into a solution already containing the dissolved impurities, with their concentrations maintained below their solubility limits. This approach minimised the likelihood of impurities crystallising during the equilibration process, aimed at saturating the solution with paracetamol.
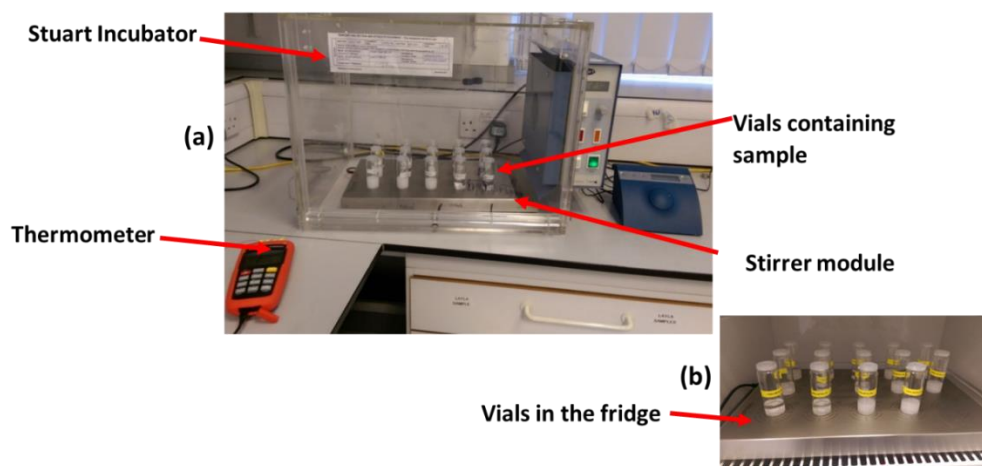
Figure 26: Depicting (a) Stuart incubator set up with a magnetic stirrer plate and thermocouple to measure the temperature of the solution in the incubator. (b) The corresponding equilibration set up in the laboratory fridge.

Equilibration measurements above ambient temperature was conducted in a Stuart SI60D Incubator (Stuart, Staffordshire, UK), covering a temperature range from 19 to 50 °C. To further reduce the temperature, a fridge was used, achieving a measurement temperature of 13.7 °C. This was recorded in the Royal College Solous Lab, as illustrated in Figure 26. The experimental procedure involved adding an excess of paracetamol to a vial, followed by a stock solution containing pre-dissolved impurities, thus creating an undersaturated solution. These labelled vials were then placed on a Thermo Scientific Submersible Telesystem 15.20 magnetic stirrer plate (Thermo Fisher Scientific, Waltham, MA, USA) and maintained isothermally at the selected equilibration temperature, agitating at 190 rpm for 24 hours. The temperature was kept within ± 0.2°C of the desired level and monitored using a calibrated Omega precision thermocouple (Omega, Manchester, UK). After confirming equilibration within 24 hours (see Appendix A, Section 1.0), the excess solid paracetamol was allowed to settle for 1 hour without agitation.

For analysis, a sample of the solution was subjected to evaporation until it was dry. This involved pipetting 2 mL of the clear, saturated solution into a pre-labelled and weighed vial. The vial with the solution was then promptly weighed. The samples were left uncovered in a fume hood to evaporate for seven days. Subsequently, they were placed in a Memmert GmbH vacuum oven V0200 (Memmert GmbH + Co. KG, Schwabach, Germany) set at 70°C for an additional 48 hours to ensure complete drying. The mass loss from solvent evaporation was determined, and from this, the mass of impurities in the stock solution was calculated. This impurity mass was then subtracted from the dry residue mass to ascertain the final paracetamol mass, as outlined in Appendix A, Sections 2.1 and 2.2.

The presence of impurities was found to influence paracetamol solubility compared to pure solutions, resulting in deviations from the targeted 1, 2, and 4% mass impurity loadings. These deviations were accounted for in the gravimetric calculations. The method used facilitated accurate determination of paracetamol concentration and precise measurement of the relative mass percentage concentration of the impurity.

3.1.3: Single crystal growth (Including MODDE)

3.1.3a Face indexing

SC-XRD was used to assign faces to paracetamol crystals. However, the inability to extract the measured single crystals from the experimental setup meant that SC-XRD could not be performed on every grown crystal. Instead, individual crystals were prepared using the method outlined in Section 4.1.3c. This process involved assigning faces based on geometric similarity and measuring interfacial angles using a protractor graticule in the eyepiece of an optical microscope, along with the angle measurement tool in ImageJ. The dominant faces of the growing paracetamol crystals were identified by comparing predicted and experimental morphologies as well as referencing data reported in the literature (124, 162, 226-229).

It was observed that the habits of individual paracetamol crystals often varied, even under identical conditions, posing challenges in face assignment. This contrasted with systems like ibuprofen, where differences between individual crystals were less pronounced (1). Nevertheless, the growth rates of pairs of faces parallel to the dominant face were measured in crystals exhibiting diamond and needle-like habits. However, for truncated, equant, and multi-faceted crystals, pairs of faces were not parallel due to variations in structural orientation caused by molecular arrangement within the lattice. Consequently, unambiguous indexing was not feasible for two habits, although identifiable faces have been noted.

In each instance, efforts were made to index the crystals, with the results presented in Table 9. Initially, the faces of these crystals were labelled as A and B (as shown in Figure 27) and this labelling was carried over to the face indexing table. Details of the face assignment process are available in Appendix B, Section 1.0. Including information on the chosen crystal habit, assigned faces, and the orientation for single crystal X-ray diffraction. The indexed results were compared against the BFDH model of paracetamol to verify if the faces and corresponding parallel indexed faces matched the predicted ones. This comparison showed a generally consistent agreement, identifying the main face and side facets of each habit.
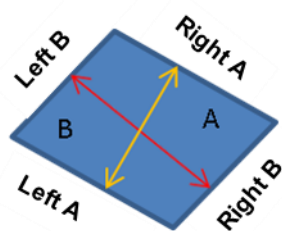
Figure 27: Labelling of faces A and B before indexing was possible.

3.1.3b Image analysis

To determine the crystal growth rate, each sequence of captured images was analysed using ImageJ. Initially, a pair of perpendicular crystal faces were selected. Two diagonal lines were then drawn across these faces, forming a 90° angle. Measurements were taken along the line extending at 90° from one perpendicular face to the other, as illustrated in Figure 28. This process was repeated for each pair of parallel faces of the crystal, assuming that the crystal remained stationary during image capture (a fact verified from the series of images). In instances where the crystal faces were not parallel, the lines were plotted as described, and any anomalies encountered were noted and discussed.
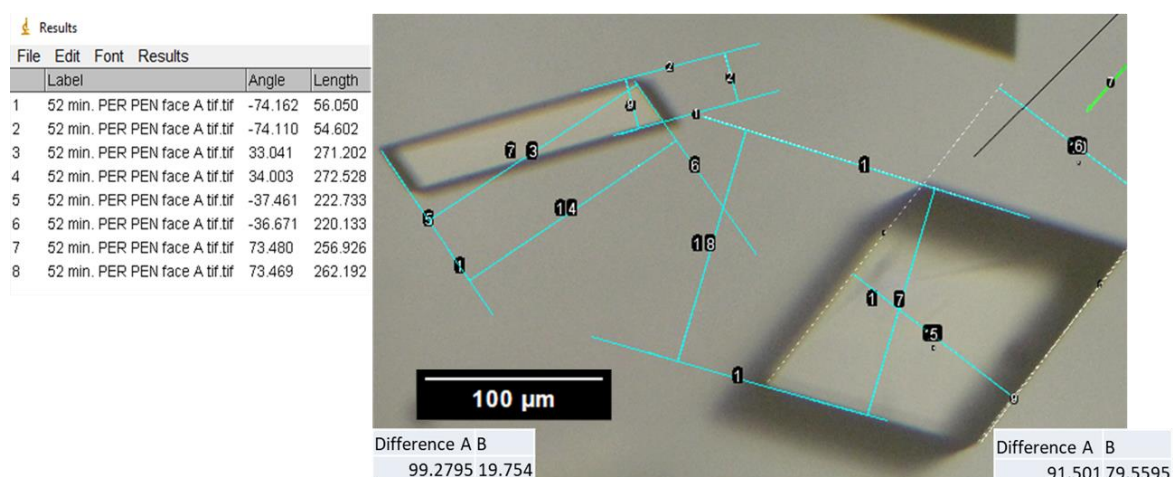
Figure 28: ImageJ crystal measurements and examples of perpendicular faces.

3.1.3c Preparation of paracetamol single crystals for X-ray diffraction indexing and analysis

The method used for growing single crystals for X-ray diffraction was similar to that employed in the single crystal growth experiments. The following steps were undertaken to grow single crystals:

1. The necessary mass of material and solution was weighed and placed into a vial. This vial was then set on a hot block to initiate nucleation, replicating conditions of the stagnant cell.

2. Once nucleation occurred and a few single crystals began to grow, the vial contents were gently tipped onto tissue paper.

3. From the yielded crystals, those that were optically clear, unfractured, and without noticeable imperfections, were carefully selected. These were then placed on a glass slide and examined under a microscope. The ideal size for single crystal X-ray diffraction (SC-XRD) analysis was approximately 150-250 microns.

4. Several crystals that met these criteria were selected for further analysis and characterisation.

3.1.3d Single crystal X-ray diffraction (SC-XRD)

Samples were sent to the CMAC X-ray facility for single crystal X-ray diffraction measurements and unit cell determination, along with face indexing. The diffraction data were collected using a Bruker D8 Venture single crystal diffractometer (GX001015) with the following setup: IμS Microfocus Source, Point Focused. Cu Kα1 source radiation: 1.540596 Å, operating at room temperature (295 K), with a voltage of 50 kV and a current of 1 mA. A Photon II CCD detector with a frame size of 1024 x 1024 was used. A total of 780 scans were collected, each with a scan image width of 0.5° in omega.

To mount the crystal, a single crystal of appropriate size (approximately 150-250 microns) was carefully chosen and inspected under a microscope to ensure it was free of noticeable imperfections, optically clear, and unfractured. The crystal was then mounted onto the tip of a thin glass fibre rod using epoxy resin adhesive. The fibre with the crystal was subsequently attached to a brass mounting pin with a small amount of super glue. The pin, bearing the mounted crystal, was placed onto the diffractometer, which was centred using a live video viewing microscope. The X, Y, and Z axes were adjusted until the crosshairs were centred for all crystal orientations, ensuring precise centring within the X-ray beam.

Once the crystal was accurately aligned with the X-ray beam, the machine performed a quick frame of X-rays to verify that the material was crystalline. This was followed by recording blank frames for background readings. After this step, the machine began collecting diffraction data while rotating the crystal. The gathered data was then processed and analysed using a structural analysis program, facilitating the determination of the crystal's structure and the indexing of its faces.

3.1.3e MODDE

A representation of the qualitative and quantitative factors considered in the analysis of single crystal growth rates is detailed in Table 4. A full factorial design (mixed) was chosen for data analysis, resulting in fifteen experiments. The software employed a multiple linear regression (MLR) method to assess the impact of three factors: impurity concentrations of acetanilide and metacetamol at 0, 2, and 4% by mass; temperature settings of 15, 20, and 30 °C; and supersaturation levels of 1.25, 1.5, and 1.75. The measured responses were the growth rates of face A and face B.

Table 4: Design of Experiment (DoE) factors and responses selected to investigate in this study.

Factors				
Name	Abbreviation	Units	Type	Settings
Impurity	Imp	%	Multilevel	0, 2, 4
Temperature	Temp	°C	Qualitative	15, 20, 30
Supersaturation	Sup		Qualitative	1.25, 1.5, 1.75
	Response			
Name (abbreviation)		Units		
Growth rate in A direction (grA)		µm		
Growth rate in B direction (grB)		µm		

3.1.4: Bulk suspension crystallisation (Including MODDE)

3.1.4a MODDE design of experiments

Table 5 presents the qualitative and quantitative factors considered in the bulk suspension crystallisation analysis. For data analysis, a full factorial design with two levels was chosen, resulting in twenty-two experiments. Each experiment was conducted in triplicate, amounting to a total of sixty-six experiments. The software used a multiple linear regression (MLR) method to assess the effects of three factors: ultrasonic power levels at 0, 50, and 100% in the ultrasonic bath, with corresponding intensities of 0.34 ± 0.13 mW cm^{-2} and 4.11 ± 0.84 mW cm^{-2}, respectively (further details are discussed later in this section) and impurity concentrations of acetanilide and metacetamol at 0, 2, and 4% mol.

The measured responses included the nucleation temperature, particle size distribution (PSD) formed during crystallisation (in-situ characterisation of suspended crystals) using the Mettler Toledo FBRM probe (G400 series) and isolated dry product PSD using Sympatec QICPIC. Additionally, several parameters were measured: filtration duration and rate, filter cake resistance, yield, and the percentage of impurity found within the product, all determined using HPLC.

Table 5: Design of experiment (DoE) factors and responses selected to investigate in this study.

Factors				
Name	Abbreviation	Units	Type	Settings
Ultrasonic power	Ult	%	Qualitative	0, 50,100
Acetanilide impurity	Ace	Mol%	Multilevel	0, 2, 4
Metacetamol impurity	Met	Mol%	Multilevel	0, 2, 4
Response				
Name		Units		
Yield		g		
Nucleation temperature		°C		
PSD FBRM		µm		
Filtration time		s		
Filtration rate		mL s^{-1}		
Cake resistance		m kg^{-1}		
Metacetamol impurity in powder		%		
Metacetamol impurity in mother liquor		%		
Metacetamol impurity in wash 1		%		
Metacetamol impurity in wash 2		%		
Acetanilide impurity in powder		%		
Acetanilide impurity in mother liquor		%		
Acetanilide impurity in wash 1		%		
Acetanilide impurity in wash 2		%		
PSD Lasentec x50		µm		

3.1.4b Ultrasonic intensity measurements

The acoustic intensity of the XUB25 ultrasonic bath was evaluated using an NH4000 PVDF needle hydrophone (Precision Acoustics Ltd., Dorset, UK), as depicted in Figure 29. To align the needle hydrophone with the central axis and position it 25 mm from the base of the Celstir vessel, a custom-made PVC plug was used to replace the vessel's lid. The hydrophone measured the acoustic intensity inside the vessel and the time domain waveform was recorded using an Agilent Technologies InfinniVision

X2024-A digital oscilloscope (Agilent Technologies, South Queensferry, UK). To ensure precise timing for measurements, a submersible piezoelectric transducer was situated on the stirrer plate surface within the ultrasonic bath, tuned to the bath's operating frequency.

Before measurements, the needle hydrophone was immersed in deionised water for an hour. To overcome the hydrophone tip's incompatibility with organic solvents, a latex rubber sheath with an 8 mm diameter was employed to encase the hydrophone. The sheath, filled with deionised water, safeguarded the hydrophone tip during the acoustic intensity measurements.

For the actual measurements, the Celstir vessel was filled with a sample of the crystallisation solvent. The hydrophone, encased in the latex rubber sheath, was then inserted into the vessel (Figure 29). The vessel was placed at predefined locations on the stirrer plate to measure the ultrasonic intensity, with these measurements being replicated at each position at 30 °C. The peak intensity of the acoustic waveforms was ascertained at both 50% and 100% power settings of the ultrasonic bath (128).

Figure 29: Needle hydrophone arrangement within the Celstir vessel, omitting the latex rubber sheath for clarity.

3.1.4c Sonocrystallisation analysis.

The samples were prepared as follows: A 150 mL solution, containing 36.93 g of paracetamol, was mixed with the required amount of metacetamol or acetanilide or both, to achieve a target concentration of 2 or 4 mol% of the selected impurity. This mixture was then dissolved in 99 g of ethanol. Each solution was prepared in a Celstir® 125 mL cell culture flask, equipped with an overhead magnetic agitator blade mounted in the lid. The paracetamol suspension in ethanol, with or without impurities, was placed in an ultrasonic bath and sonicated at a frequency of 35 ± 3 kHz.

The solution in the flasks was continuously stirred at approximately 150 rpm using a Thermo Scientific Submersible Telesystem 15.20. The solutions were heated to 65 °C and maintained at this temperature for 20 minutes to ensure complete dissolution, confirmed by visual inspection. The solutions were then gradually cooled to 15 °C over a period of 2 hours using the programmable cooling function of an IKA circulator attached to the ultrasonic bath. The cooling ramp was linear, with heat removed by circulating liquid from the ultrasonic bath through a pair of external chillers, as illustrated in Figure 30.

During the cooling crystallisation process, the time and temperature of solution nucleation were documented. Once the temperature reached 20 °C, the crystal size distribution was monitored in-situ for approximately 15 minutes using the Mettler Toledo FBRM probe (G400 series) coupled with iC FBRM 4.4 software. This enabled the determination of the mean chord length distribution of the crystals.
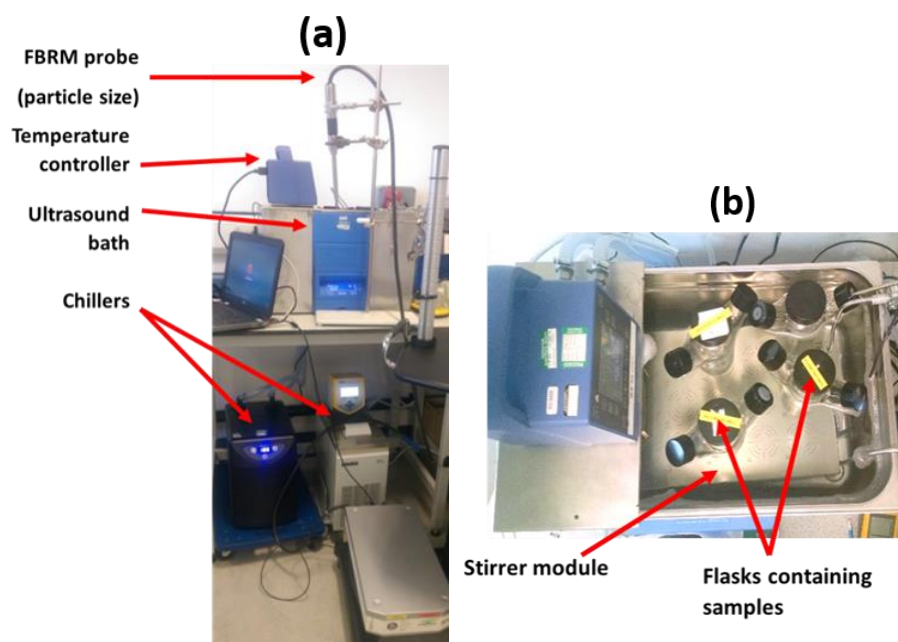
Figure 30: (a) Experimental setup for bulk suspension crystallisation consists of a Grant ultrasonic bath XUB25 operating at 35 ± 3 KHz, maximum ultrasonic power 400 W, 16 W.L^{-1}. Particle size is measured using a Mettler Toledo FBRM probe (G400 series) used with iC FBRM 4.4 software. The crystallisation temperature was controlled using an IKA ICC Control heater circulator. Cooling was provided using a Lauder ECO RE 420G heating/cooling thermostat, and where required, additional cooling was provided by a stainless-steel coil connected to a Hailea HC-150 flow chiller. (b) Depicts a submersible Telesystem 15.20 from Thermo Scientific used to stir the Wheaton cell culture flasks with double-sided arms, Celstir® 125 mL.

3.1.4d Filtration, washing and drying

The product crystals were transferred to a modified Biotage VacMaster 10 system (Biotage Ltd., Uppsala, Sweden) for separation from the mother liquors and washing. This system comprised a VacMaster vessel and lid with a modified rack capable of holding four shortened 50 mL graduated cylinders, as depicted in Figure 31. A Buchi V850 vacuum controller controlled the pressure driving force of 200 mbar. The chamber lid was equipped with a pair of PTFE valves; one valve was used on the filter tube to prevent leakage during weighing and transferring for solution/wash steps, while the other valve prevented air influx into the vacuum chamber upon removal of the filter tube.

For the isolation, conducted in triplicate for each suspension, three equal 50 mL sub-samples of the crystal suspension were measured into a measuring cylinder. These sub-samples were then poured into a pre-weighed 70 mL Biotage ISOLUTE single filter tube, fitted with a polyethylene filter with a 10 μm pore size (Biotage Ltd., Uppsala, Sweden). The PTFE valves were opened to allow the filtrate to pass through the medium into the measuring cylinders. The time taken to collect specific volumes of filtrate (e.g., 5, 10, and 15 mL, etc). was recorded. Filtration was stopped at dryland, which is when the filter cake surface first appeared above the mother liquors, to keep the filter cake fully saturated and prevent cake cracking. The filter tube and upper PTFE valve were then carefully weighed to record the mass of the tube, filter cake, and filter cake thickness.

Next, the sample was moved to the next valve on the filter chamber for washing with n-heptane. The volume of n-heptane used was based on the cake height (mm), considering the internal diameter of the filter and measuring cylinder at 27 mm. This allowed the measurement of the cake height and corresponding dispensation of the wash liquor. N-heptane, selected due to its miscibility with ethanol and negligible solubility of paracetamol, was carefully added, running down the walls of the filter tube with a disposable pipette to avoid disturbing the saturated filter cake. Filtration time was noted, and the process was halted at dryland. The reweighed filter cake was returned to the VacMaster for the final wash. The procedure was repeated, and in the final step, the cake was fully deliquored before a final weighing. This enabled the segregation of the collected filtrate and wash liquors for weighing and assay sampling. Utilising this data, along with the dry solid mass, allowed for the completion of a mass balance. The washed crystals were then dried in-situ in the solute filter tubes at room temperature, with their dry mass recorded.
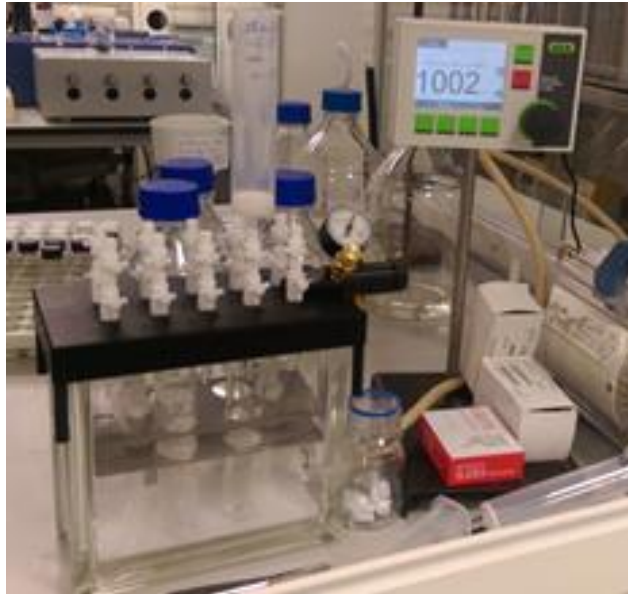
Figure 31: Modified Biotage VacMaster 10 with a Buchi V850 vacuum controller and vacuum valve. The filters used had a 70 mL capacity and were equipped with 10 µm PE frits. Shortened 50 mL measuring cylinders from Fisher Scientific were used to collect the filtrate samples.

Using the measured filtration rate data, Darcy's equation, which describes the flow of fluid through a porous medium, was used to calculate both the filtration rate and filter cake resistance (230).

$$\frac{dt}{dV} = \frac{\mu \alpha C}{\Delta P A^2} V + \frac{\mu R_m}{A \Delta P}$$

Equation 18

Where: t is time (s); V is filtrate volume (m³); α is the cake resistance relating to cake filterability (m.kg⁻¹); μ is the mother liquor viscosity (Ns m⁻²); ΔP is pressure difference along the filter axis (Pa); C is the concentration of solids (kg m⁻³); A is the filtrate area of cake (m²); and R_m is the resistance of the filter medium (m⁻¹).

In this study, filtration was conducted at a constant pressure difference of ΔP = 200 mbar. Integrating Darcy's equation gives:

$$\frac{t}{V} = \frac{\mu \alpha C}{2 \Delta P A^2} V + \frac{\mu R_m}{A \Delta P}$$

Equation 19

Where the cake resistance α and the medium resistance R_m can be determined from a t/V versus V plot, α corresponds to the gradient and R_m to the intercept (231). Further information on the isolation parameters used to calculate the filtration flow rate, cake resistance, and filtration time can be found in Appendix C, Section 1.3.

3.2. Crystal and solution analysis

3.2.1: DSC/VanHoff plot

The onset temperature of melting for paracetamol, metacetamol, and acetanilide was determined using differential scanning calorimetry (DSC) analysis. Additionally, the enthalpy and entropy of paracetamol dissolution in ethanol and isoamyl alcohol were calculated.

For each analysis, 2-4 mg of the substance was accurately weighed into an aluminium pan with a pierced lid. The samples were then heated from 30 to 200 °C at a rate of 10 °C min^{-1} under a helium purge gas flow of 40 mL min^{-1}. These DSC measurements were conducted using a Netzsch DSC214 Polyma instrument, as shown in Figure 32. A blank measurement with an empty pan was performed prior to analysing the samples. Each sample was prepared and analysed three times to ensure accuracy. The analysis was conducted using the Netzsch Proteus Analysis Software v7.0.1. The first melting peak was integrated (using a sigmoidal baseline) to determine the enthalpy value (J g^{-1}). For an example of Vant Hoff Calculations, see Appendix A, Section 2.3.

Figure 32: Netzsch DSC214 Polyma instrument.

The concept of ideal solubility is defined as 'the solubility of a solute in a perfect solvent, where there is no energy penalty associated with the dissolution process' (232). It is important to note that this definition does not account for chemical reactions such as ionic effects or acid-base chemistry. If the enthalpy of fusion and melting point of a substance are known, its ideal solubility can be predicted using the Van't Hoff equation:

$$\ln x = \frac{\Delta Hf}{R}\left[\frac{1}{Tf} - \frac{1}{T}\right]$$

Equation 20

In this equation, x represents the mole fraction of the solute in the solution. ΔH_f denotes the molar enthalpy of fusion of the solute in joules per mole (J mol $^{-1}$). R is the gas constant (8.314 mol^{-1} K^{-1}). T_f is the fusion temperature (melting point) of the solute, and T is the temperature of the solution. Calculating this across various temperatures allows for the creation of an ideal solubility curve. However, it is crucial to acknowledge that Equation 20 does not apply to non-ideal solutions. For an example of ideal solubility prediction, see Appendix A, Section 2.4.

3.2.2: XRPD

Powder X-ray diffraction (XRPD) was used to assess the solid-state properties of paracetamol equilibrated in the presence of 1, 2, and 4% mass of metacetamol and acetanilide. The aim was to confirm that the polymorphic state of paracetamol remained unchanged. This investigation was motivated by a separate study (161), where the addition of metacetamol to a continuous crystallisation system resulted in the identification of paracetamol form II. To facilitate comparison, diffraction patterns of pure paracetamol reported in the literature were considered.

The XRPD data were collected using a Bruker D8 Advance II diffractometer (GX002103- Priscilla) operating at ambient temperature (293 K) with a Cu source radiation of 1.540596 Å.

3.2.3: Crystal imaging

3.2.3a Growth rate measurement in a stagnant cell using microscopy

The growth rates of single crystal faces were examined in relation to various factors such as: the chosen solvent, temperature, supersaturation, impurity loading, and the presence or absence of sonication delivered by an ultrasonic toothbrush.

To determine the ratio of solute *mg* to solvent *g*, the supersaturation ratio *S* was calculated according to Equation 8.
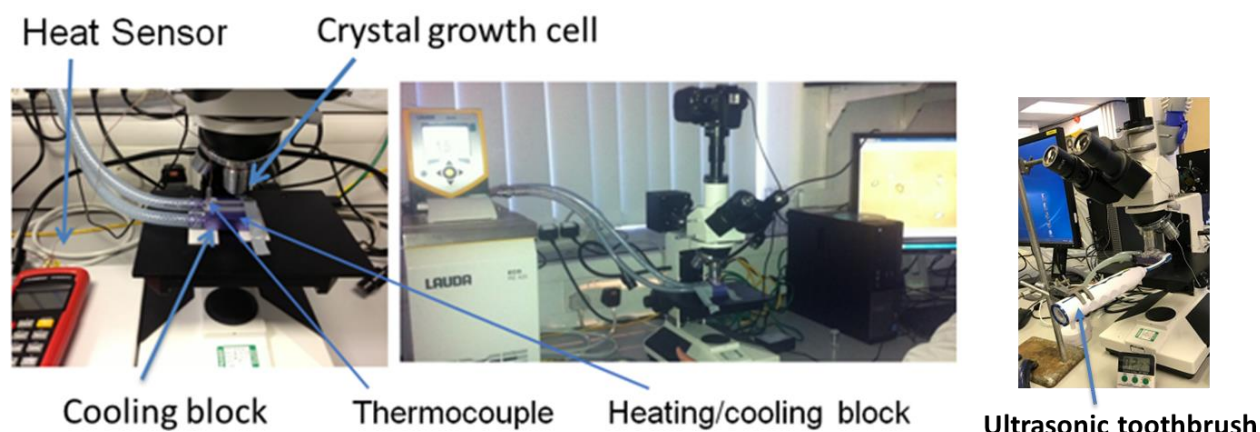
Figure 33: Crystal growth setup comprising of: Brunel SP-200XM microscope, Canon EOS 4100 D camera and the attachment of an ultrasonic toothbrush (1.6 MHz). The cooling block is connected to a circulator and has positioning rods to hold the single crystal stagnant cell.

The experimental setup employed for growing single crystals and recording their growth rates is depicted in Figure 33. Precise amounts of materials and solvent were placed into pre-labelled and pre-weighed vials, along with a stirrer bar. The vials were then positioned on an IKA RET control-visc hotplate stirrer IP42 model RET CV (Staufen im Breisgau, Germany). The vials were heated and stirred to dissolve the crystalline input. After complete dissolution, the material was transferred to a preheated stagnant cell 48/G/2 (the crystal stagnant growth cell) from Starna Scientific Ltd. (Ilford, UK) using an Eppendorf pipette and a pre-warmed pipette tip.

The filled crystal stagnant cell was promptly positioned onto the ZFE aluminium water-cooled heatsink block from Amazon (Seattle, Washington, U.S.), which was securely fastened to the microscope stage. Two aluminium bars were used to fix the cell in place. Efficient heat transfer was facilitated by applying a thin film of oil to the block's surface. The target temperature was set using a water bath ECO RE 420G with a gold controller from Lauda (Lauda Brinkmann, NJ, USA), allowing the aluminium block to reach the desired temperature. Observations were made using a Brunel SP-200-XM metallurgical microscope (Chippenham, Wiltshire, UK) equipped with a Canon EOS 4100 D camera (Canon Japan). Two identical setups were prepared to run two experiments concurrently.

A multi-channel logging thermometer HH806AU from Omega Engineering (Norwalk, Connecticut, U.S.) was used, with thermocouples inserted into the solution in the flow cells to measure the supersaturated solution's temperature. For specific experiments, an ultrasonic toothbrush operating at a frequency of 1.6 MHz per second (Emmident, Mörfelden-Walldorf, Germany) was occasionally used and placed beside the stagnant cell.

The solution in the stagnant cell was allowed to cool to the desired temperature to achieve the target level of supersaturation. The solution was periodically examined under the microscope to select a suitable small crystal for monitoring. Reflected white light illumination with a 10x objective lens was used. Upon identifying an appropriate crystal, the camera's interval timer was set to capture images every four minutes. The focus was regularly checked and adjusted as necessary during the crystal growth phase. Crystal growth was observed for up to sixty minutes, with images saved to the network drive for later measurement using ImageJ. Each experiment was conducted twice to confirm the reproducibility of the data.

3.2.3b Brunel SP350P microscope

The size and morphology of the isolated paracetamol crystals were examined using a Brunel SP350P microscope, equipped with transmitted light illumination and various objective lenses: x5, x10, x20 and x50. Images of the crystals were captured using a Canon camera.

3.2.3c Sympatec QICPIC

To determine the particle size distribution of the isolated and dried product, the Sympatec QICPIC system was used. This instrument utilises image-based particle sizing and image analysis. During the drying process, the dry paracetamol crystals tended to form agglomerates. To ascertain the primary particle size, these agglomerates were gently broken apart using a spatula before being introduced into the instrument via the charging funnel and vibratory feeder.

The instrument parameters were established as follows: measuring range = 1.00 to 63.0 mm - M7, trigger conditions = 175 Hz, with measurements commencing always and ceasing at 120 s. The operating pressure was maintained at 0.5 bar, the feed rate was set at 40% and the gap width was adjusted to 0.5 mm.

3.2.4: HPLC

The chemical purity analysis of the isolated product was performed using an Agilent 1260 Infinity II HPLC system. This system is comprised of an online degasser, quaternary pump, automatic injector, thermostated autosampler and column compartment. It was equipped with a photodiode array detector, covering a wavelength range from 190 to 950 nm, and a refractive index detector. The chromatography data system used for analysis was OpenLAB Chemstation.

For the separation of analytes, a 4.6 x 100 mm Agilent Poroshell 120 EC-C18 column with a particle size of 4 µm was used. The pump operated at a flow rate of 1 mL min^{-1}, employing a mobile phase of 80% water and 20% methanol in isocratic mode. The column temperature was set at 40 °C. The optimal wavelength for detecting the analytes was established at 243 nm, selected for its alignment with the maximum absorbance of both paracetamol and metacetamol (233) and its proximity to the λ max of acetanilide at 242 nm (234).
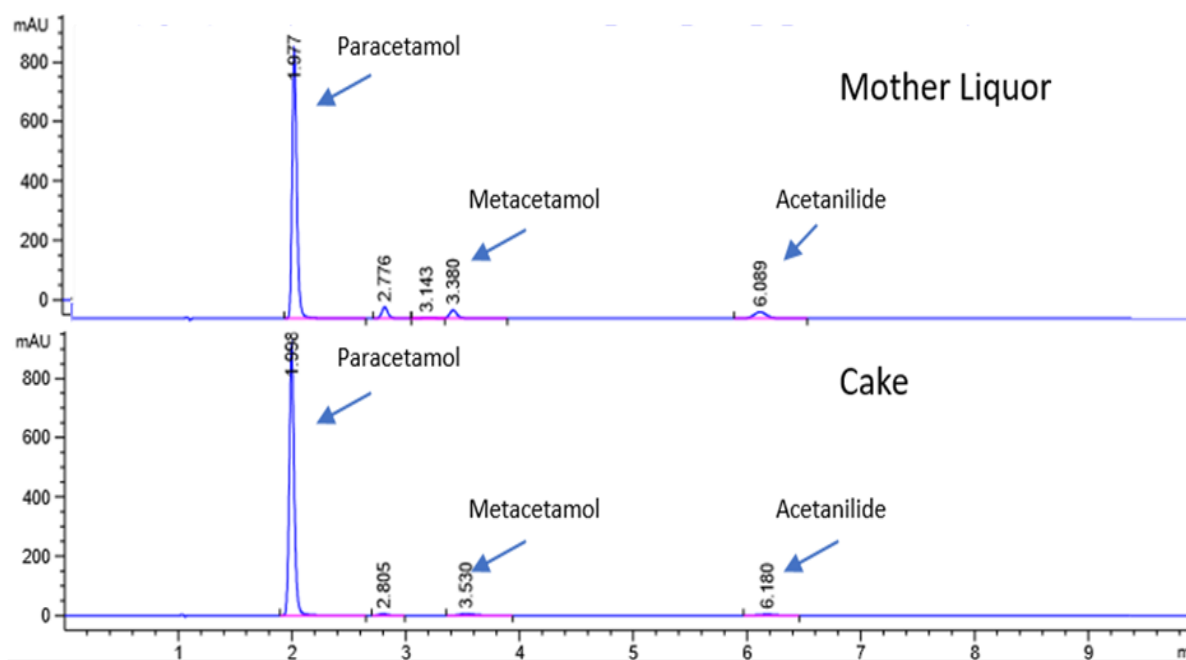
Figure 34: HPLC chromatograms for isolated paracetamol product and mother liquor peaks corresponding to metacetamol and acetanilide.

Calibration curves were prepared for paracetamol, metacetamol, and acetanilide using the specified column elution conditions. To assess the purity of the product crystals, individual 'cake' samples were created by accurately weighing around 15 mg of the product. These were diluted in a 100 mL volumetric flask with a mixture of 5% methanol and 95% water, which fell within the instrument's calibration concentration range. The flasks were then placed in an ultrasonic cleaning bath for five minutes to ensure complete dissolution.

Analytical samples of the mother liquor were also prepared. For this, 1 mL of the mother liquor was transferred into a 100 mL volumetric flask, diluted as described previously, and then further diluted with a 10 mL volumetric flask using the 5% methanol and 95% water mixture. Subsequently, 1 mL of this solution was transferred to an HPLC vial for analysis. Similar procedures were followed for wash samples 1 and 2 to determine the impurity concentration relative to paracetamol in the mother liquors, wash samples, and isolated product, allowing for the calculation of segregation coefficients for each component.

For mother liquor samples, the preparation involved evaporating the sample to dryness, after which the crystals were dissolved in 1500 µL of methanol. From this, 7.5 µL of the solution was taken and mixed with 1492.5 µL of water in a HPLC vial to achieve an appropriate analyte concentration for analysis.

However, the presence of heptane in the wash liquor samples prevented direct analysis due to the potential for damaging the HPLC column packing material. Instead, a 30 µL sample of the first wash was placed into a HPLC vial and left to evaporate for 7 days to remove heptane residue. Afterwards, the sample was diluted in a manner similar to the mother liquor samples and then analysed by HPLC.

As the analyte concentration in the second wash was expected to be much lower, a 1000 µL sample of wash 2 was transferred to an HPLC vial and left to evaporate for one week. The dry residue was then dissolved in 1000 µL of methanol, and 50 µL of the solution was transferred to a HPLC vial, followed by the addition of 950 µL of water to achieve an appropriate analyte concentration for analysis. If the concentration was not suitable, further dilutions were made to ensure the analyte concentration fell within the calibrated HPLC range.

Chapter 4:
Solubility of Paracetamol and Structurally Related Impurities

Summary:

This chapter presents the measured solubility of paracetamol with the addition of structurally related impurities; metacetamol and acetanilide. The temperature range studied was from 8.7 to 30 °C in ethanol and 20 to 40 °C in isoamyl alcohol. The dataset in isoamyl alcohol has been published in 'The Effect of Ultrasound on the Crystallisation of Paracetamol in the Presence of Structurally Similar Impurities' by Thai T. H. Nguyen, Azeem Khan, Layla M. Bruce, Clarissa Forbes, Richard L. O'Leary, and Chris J. Price (DOI:10.3390/cryst7100294). The impact of these impurities on paracetamol's solubility was investigated using the gravimetric method, and the results were expressed as a function of additive concentration. It was observed that a small quantity of metacetamol and acetanilide (2-4% mass) led to an increase in solubility as the temperature rose.

4.0: Introduction

The study of solubility holds significant importance in optimising crystallisation processes, particularly in pharmaceutical applications where high crystal purity and adherence to stringent quality standards are of utmost significance. However, a comprehensive review of the existing literature reveals a considerable lack of information regarding the influence of impurities on solubility. Despite the abundance of studies on solubility, few reports have delved into the solubility data specifically concerning the effects of impurities, particularly those that are structurally related to the target compound, such as paracetamol, metacetamol, and acetanilide. This research gap underscores the need for a more thorough understanding of the solubility behaviour of these impurities (235).

Understanding the behaviour of impurities is critical, as they can have a profound impact on the crystallisation process. Impurities can incorporate into growing crystal structures, disrupt crystal growth, or induce various effects like agglomeration and inclusion, especially when their solubilities are comparable to or lower than those of the desired product. Such phenomena can significantly influence the yield, purity, and properties of the final crystals (235).

Impurities, even in small quantities, have been found to exert significant implications on downstream crystallisation processes and crystal forms. Agnew (161) exemplified this phenomenon through the production of paracetamol form II using a multicomponent templating approach during cooling crystallisation. By harnessing the differing solubilities of the templating molecules, namely metacetamol and 4-fluorobenzoic acid, in the chosen solvent system, Agnew achieved higher concentrations of the templating material, enabling successful scale-up of the process to yield over 100 g of paracetamol form II in an 800 mL volume. This innovative approach was particularly advantageous, as paracetamol form II is known for its higher solubility and excellent compressibility, making it ideal for tablet production (236).

Furthermore, real-world examples serve as stark reminders of the criticality of studying impurities and their effects on solubility in pharmaceutical products. A notable case is the recall of Ranitidine, a commonly used medication for heartburn, by the US Food and Drug Administration. The recall was prompted by the discovery of N-nitrosodimethylamine (NDMA), a known carcinogen, as an impurity in the drug. This incident highlighted the potential risks associated with impurities and their significant implications for patient safety and product quality (237, 238).

Suppose the solubility of an impurity is similar to or lower than that of the product. In that case, it is less likely to be eliminated during the crystallisation process than a more soluble impurity. Hendriksen (11) stated that impurities can modify the solubility of the solute and thus affect the crystallisation process that delivers the solute into a solid. However, the study did not focus on the impact of impurities on solubility but instead on the impacts on nucleation, incorporation, and growth. Keshavarz (80) discovered a slight increase in paracetamols solubility with the addition of impurities 4-nitrophenol and 4'chloroacetanilide. However, they stated that the impurities did not have a significant effect on the solubility of paracetamol.

This study has presented the results of solubility measurements conducted through isothermal equilibration and gravimetric analysis. The main objective was to assess the effect of structurally related impurities on the solubility of paracetamol within the temperature range of 8.7 to 55 °C. The impurity concentrations were varied up to 4% by mass of the individual impurities in both ethanol and isoamyl alcohol. Ethanol and isoamyl alcohol were chosen as suitable crystallisation solvents for paracetamol, considering their respective advantages. Ethanol, being a relatively inexpensive solvent, lacked sufficient data on paracetamol recrystallisation. Crystal samples obtained from ethanol exhibited well-formed structures, but the presence of diverse crystal habits within the same conditions complicated the analysis of single crystal growth rates. Isoamyl alcohol, commonly used in the production of synthetic flavours, boasted a low eco-toxic profile, and demonstrated a favourable solubility relationship with temperature for paracetamol. Nonetheless, scarce literature data on the use of isoamyl alcohol as a crystallisation solvent prompted its consideration for further investigations in this study (239).

The findings from this chapter have underscored the significant impact of impurities on solubility, nucleation, and crystal growth rates. It has demonstrated the vital importance of determining solubility in crystallisation experiments and revealed how even fractional changes in impurity composition can alter the overall outcome. Notably, the specific influence of impurities on paracetamol solubility in isoamyl alcohol remains largely unexplored in existing literature. Therefore, the outcomes of this study are expected to serve as a valuable guide for future investigations into the impact of impurities and the acquisition of essential solubility data in isoamyl alcohol as a crystallisation solvent.

By addressing this research gap and gaining a more comprehensive understanding of impurity effects on solubility, we can significantly enhance the optimisation of crystallisation processes, particularly in pharmaceutical applications. This knowledge is crucial for achieving high crystal purity, ensuring adherence to stringent quality standards, and ultimately improving patient safety and product quality in the pharmaceutical industry.

4.1: Results and discussion.

4.1.1: Differential Scanning Calorimetry (DSC)

Differential scanning calorimetry measurements of paracetamol, metacetamol, and acetanilide were conducted in order to confirm the melting peak and ΔH_{fus}, the enthalpy values were reported in J g^{-1} for the melting endotherm of each sample, which were all measured in triplicate, the average of which is summarised in

Table **6** and displayed in Figure 35. The units were converted from J g^{-1} to KJ mol^{-1}. The resultant melting peak and enthalpy of fusion decreased in the following order: paracetamol>metacetamol>acetanilide (

Table **6**).

Table 6: DSC data: onset of melting point and enthalpy of fusion.

Material	Molecular weight (g mol^{-1})	Melting peak (°C)	ΔH_{fus} (KJ mol^{-1})
Paracetamol	151.16	170.8 $\pm$ 0.3	29.83 $\pm$ 0.9
Paracetamol (79)			27.1 $\pm$ 0.2
Paracetamol (240)			26
Paracetamol (241)			30.2
Metacetamol	151.16	144.5 $\pm$ 0.2	26.88 $\pm$ 1.5
Metacetamol (242)			23 KJ mol^{-1} (242)
Acetanilide	135.17	113.1 $\pm$ 0.2	23.30 $\pm$ 1.8
Acetanilide (243)			21.7 KJ mol^{-1} (243)
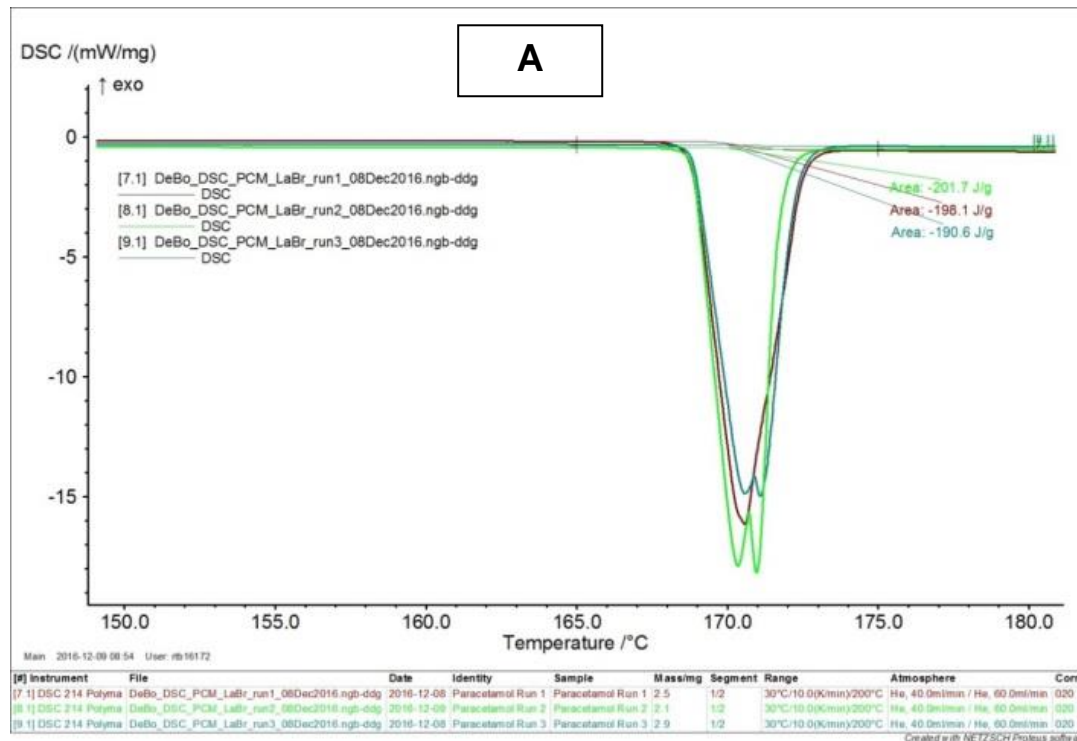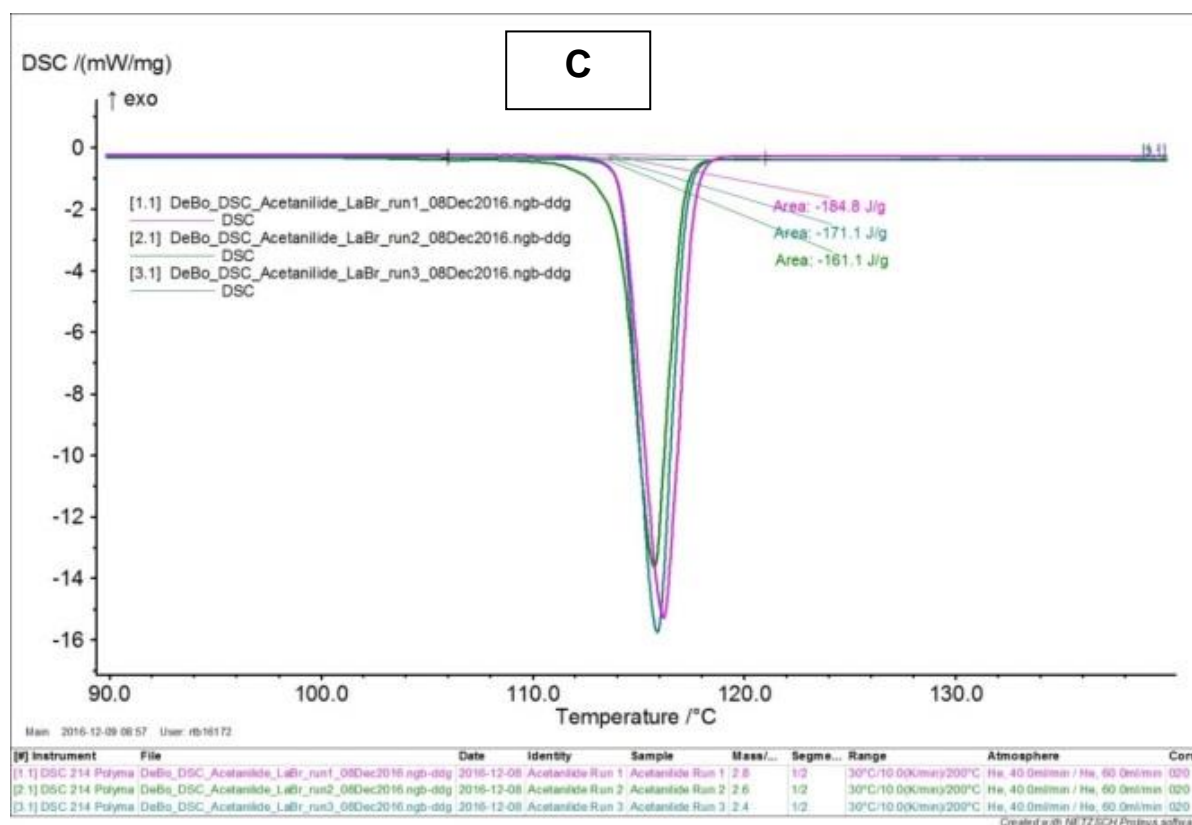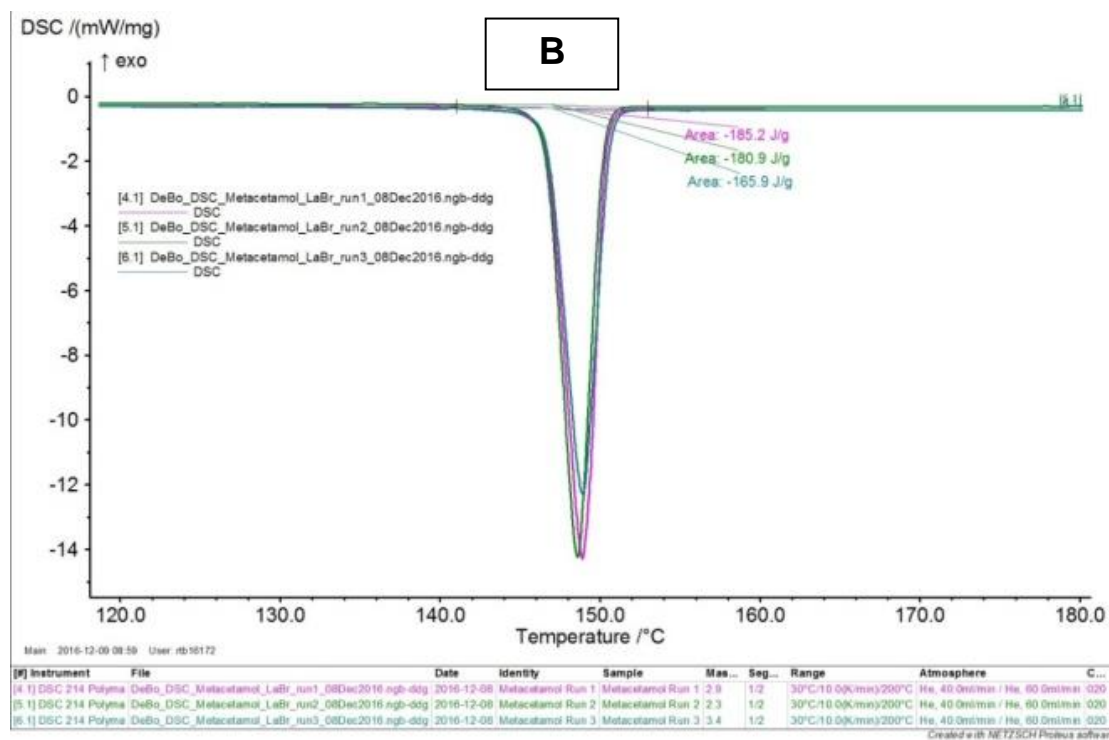
Figure 35: DSC of (a) Paracetamol, (b) Metacetamol and (c) Acetanilide raw material, measured in triplicate showing resultant melting points and enthalpy of fusion.

In literature, the enthalpy of fusion varies depending on the purity of the material. For pure paracetamol. Considering batches and material purity, the results obtained are in good agreement with the literature stated values found in

Table **6**; these values were then used to calculate the theoretical solubility.

4.1.2: Van't Hoff prediction vs experimental results

The theoretical solubility of paracetamol, metacetamol and acetanilide was measured in ethanol and isoamyl alcohol. These were calculated using the Van't Hoff equation, assuming the solution behaviour was ideal. The enthalpy of fusion and melting temperature were taken from the DSC measurements above and compared against equilibration experimental results shown in Figure 36.
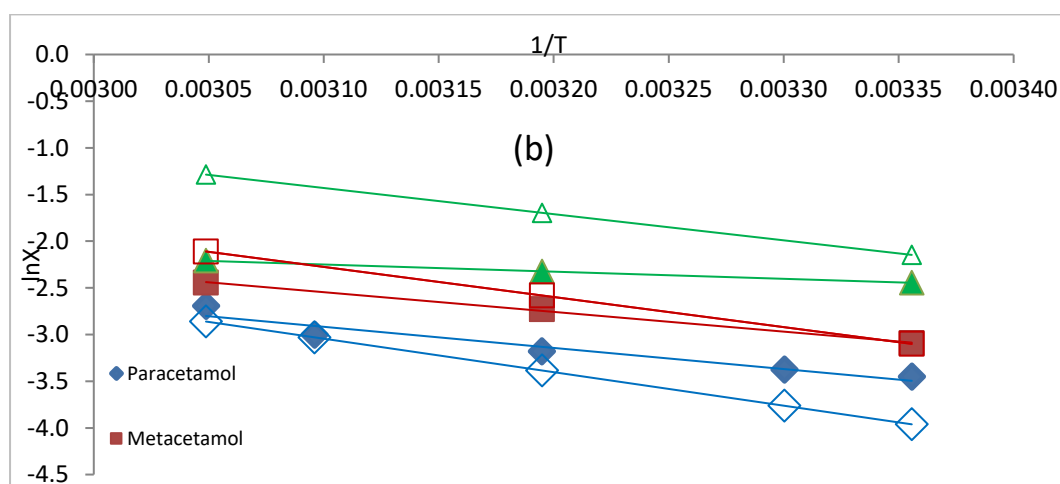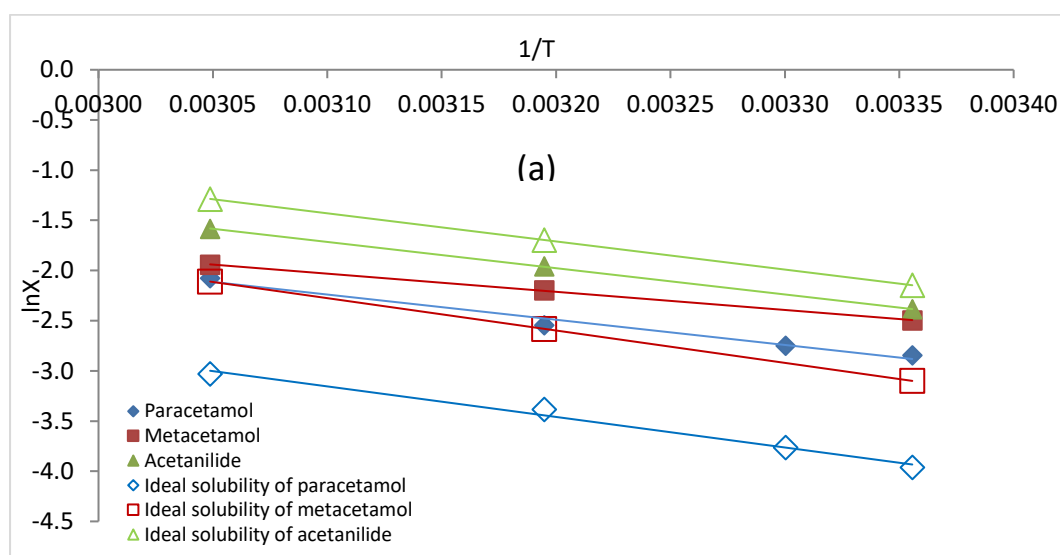
Figure 36: Plot of 1/T vs lnX of Ideal solubility vs experimental solubility of paracetamol, metacetamol, and acetanilide in (a) ethanol and (b) isoamyl alcohol.

The solubility of paracetamol shown in Figure 36 (a), ethanol, exceeds the ideal value; the same applies to metacetamol, though to a lesser extent. In the case of acetanilide, the situation is reversed; the solubility was less than the ideal value. In Figure 36 (b), isoamyl alcohol, the solubility of paracetamol also exceeds the ideal value, though it is much closer to the ideal solubility than in ethanol. Metacetamol is less soluble than the ideal value; however, one point is found to be equal to the ideal solubility, and acetanilide was found to be even less than ethanol. The solubility of all three solutes is notably lower in isoamyl alcohol than in ethanol; this is consistent with the reduced strength of hydrogen bonds formed between solute and solvent. The lower solubility of acetanilide relative to paracetamol and metacetamol is consistent with acetanilide's lack of a hydroxyl group on the benzene ring, reducing the available hydrogen bonding opportunities.

To some degree, all solutions can be classified as non-ideal due to the solute-solute and solute-solvent interactions being different. Suppose the experimental solubility curve is below the ideal solubility curve. In that case, the solution will exhibit less than ideal behaviour as the intermolecular interactions between the solute-solute and solvent-solvent are stronger than the interactions between the solute-solvent molecules, resulting in the solute having a lower solubility in the solvent when it's less than favourable (1). In the case of no enthalpy of mixing, or it equalling to 0, there is no net change in energy when the solute and solvent molecules interact. This mixing is known as ideal; the enthalpy of the solution is only dependent on the enthalpy of fusion of the dissolving solid. The solubility is independent of the chemical composition of the solvent. If mixing is favourable, the experimental solubility would be above ideal (244).

4.1.3: PXRD of paracetamol with the addition of impurities

There are three known polymorphic forms of paracetamol, two of which are generally mentioned in the literature: form I monoclinic (18), form II orthorhombic (19) and form III which is highly metastable. Form I and II are found to have similar crystallographic structures, which vary with the organisation of hydrogen bonds. The melting temperatures of form I and II lie in the range of 166.8 to 171.8 °C and 153.8 to 159.8 °C respectively (20). Grant (241) reported that the orthorhombic to monoclinic transformation temperature was around 87 °C. This is substantially above the temperature range used in the present work, indicating that it is unlikely for the paracetamol to undergo any polymorphic transitions during the equilibration experiments used to determine solubility.

Paracetamol with 4% Acetanilide in ethanol at 40°C

(f)

Paracetamol with 2% Acetanilide in isoamyl alcohol at 40°C

(e)

(d) Form III

(c) Form III

(b) Form II

(a) Form I

2-Theta - Scale
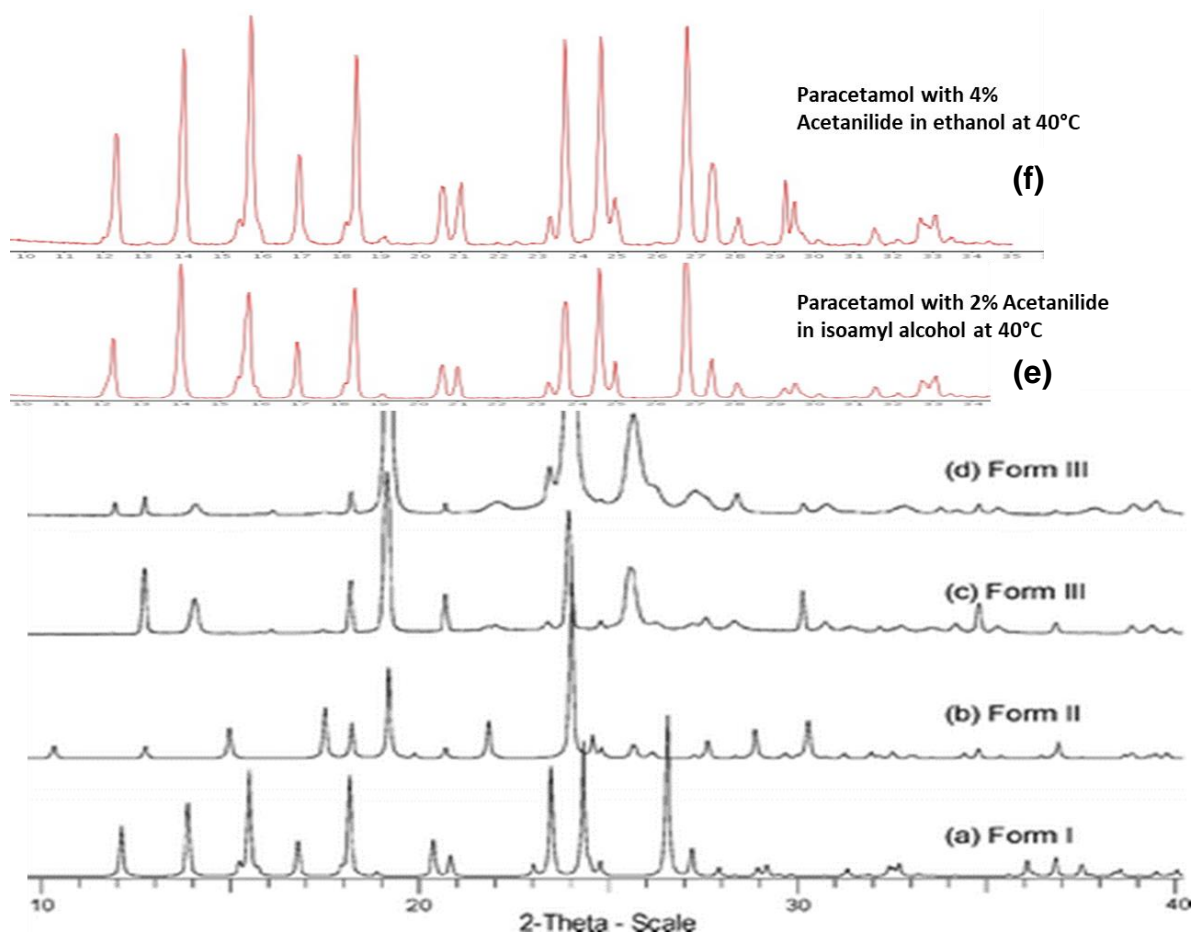
Figure 37: XRPD pattern of paracetamol obtained at room temperature (a) Form I, (b) Form II, (c) Form III rotating sealed capillary, using transmission (Debye–Scherrer geometry) and (d) Form III TTK-450 camera, using reflection (Bragg–Brentano parafocusing geometry), (e) and (f) are XPRD patterns of paracetamol with impurities from this study (226).

Similar data sets taken from the solubility analysis at 4% metacetamol and acetanilide evaporated to dryness can be found in Appendix A, Section 1.1. The PXRD was run in triplicate for the recovered material from the solubility measurement experiments with 4% impurity to determine the polymorphic form of paracetamol which remained. The same was true with the addition of impurity loading; the replicate patterns were all consistent. The results were compared against Perrin (226), where the crystal structure of paracetamol form III was determined and compared against form I and II , it was concluded that the addition of impurities, regardless of impurity and strength, did not change the form of paracetamol, remaining as form I.

4.1.4: Solubility of paracetamol, metacetamol and acetanilide in ethanol and isoamyl alcohol

The solubility of paracetamol, metacetamol and acetanilide increases with an increase in temperature. The least soluble component is paracetamol, with the most soluble being acetanilide in both ethanol and isoamyl alcohol (Figure 38).

The approach to equilibrium was measured see Appendix A, Section 1.0. In both selected solvents at 25 °C over a period of 0, 1, 2, 4, 24 and 48 hours. This confirmed that the sample had fully equilibrated after 24 hours when sampling had begun.
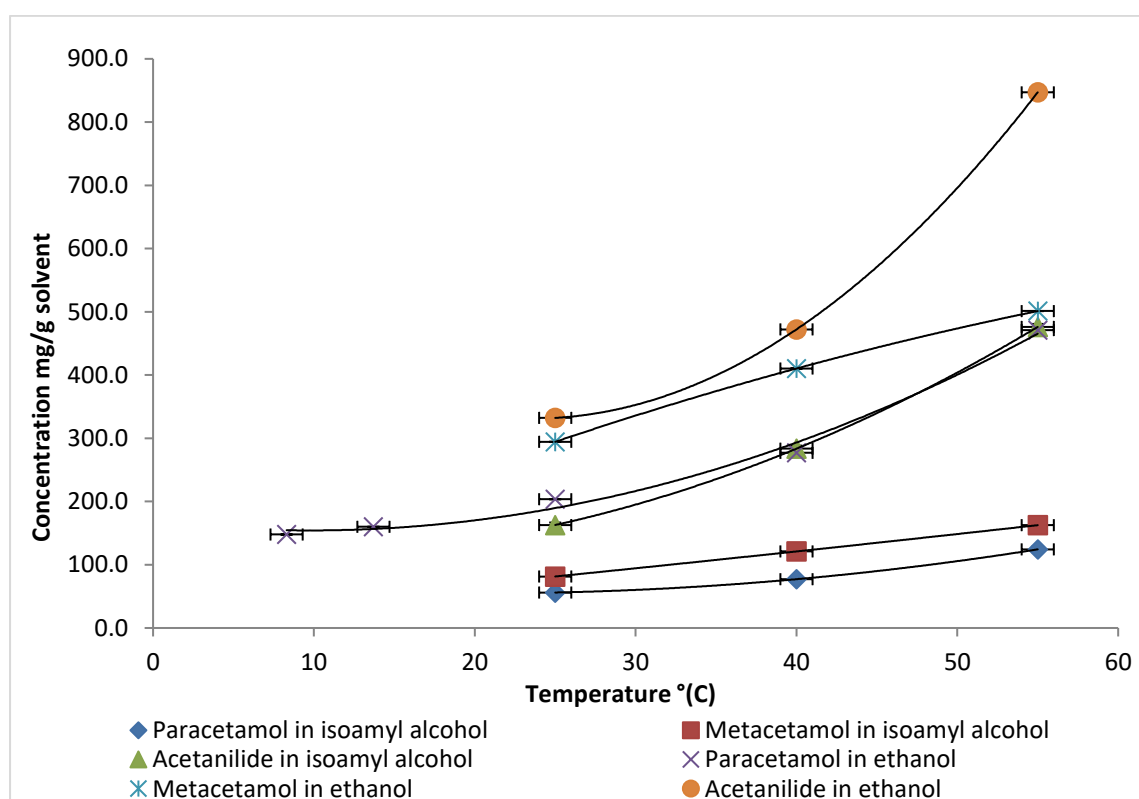
Figure 38: Solubility of paracetamol, metacetamol and acetanilide in ethanol and isoamyl alcohol.

Table 7: Solubility, C_s, given in mg of paracetamol and impurity % g^{-1} of solvent (ethanol), with different concentrations at temperatures between 8.3 and 30 °C with the corresponding standard deviation (s.d) and number of samples (n).

Ethanol	8.3 °C			13.7 °C		
Solute	Cs	$s.d$	n	Cs	$s.d$	n
Paracetamol	147.8	0.0	2	160.0	0.0	2
Metacetamol	-	-	-	-	-	-
Acetanilide	-	-	-	-	-	-
1% Metacetamol	146.4	0.8	2	158.8	0.3	2
2% Metacetamol	146.2	0.2	2	158.4	0.6	2
4% Metacetamol	147.0	0.3	2	158.0	0.1	2
1% Acetanilide	147.0	1.3	2	158.6	1.1	2
2% Acetanilide	147.3	0.3	2	159.2	0.7	2
4% Acetanilide	146.7	0.3	2	159.2	0.9	2

Ethanol	25 °C			40 °C			55 °C		
Solute	Cs	$s.d$	n	Cs	$s.d$	n	Cs	$s.d$	n
Paracetamol	203.6	0.0	5	276.9	0.0	3	471.2	0.0	3
Metacetamol	294.4	0.0	3	410.3	0.0	3	501.1	0.0	3
Acetanilide	332.2	3.10	5	472.2	0.1	6	847.0	0.0	3
1% Metacetamol	201.5	0.4	3	273.5	0.6	3	444.0	2.6	3
2% Metacetamol	200.6	0.3	3	291.8	0.9	3	488.0	6.8	3
4% Metacetamol	202.8	0.5	3	300.9	1.1	3	482.8	5.5	3
1% Acetanilide	198.2	0.8	3	279.8	0.3	3	394.5	15.3	5
2% Acetanilide	201.2	0.6	3	301.3	0.8	3	420.6	10.6	6
4% Acetanilide	202.8	0.4	3	305.2	0.6	3	459.2	9.5	3
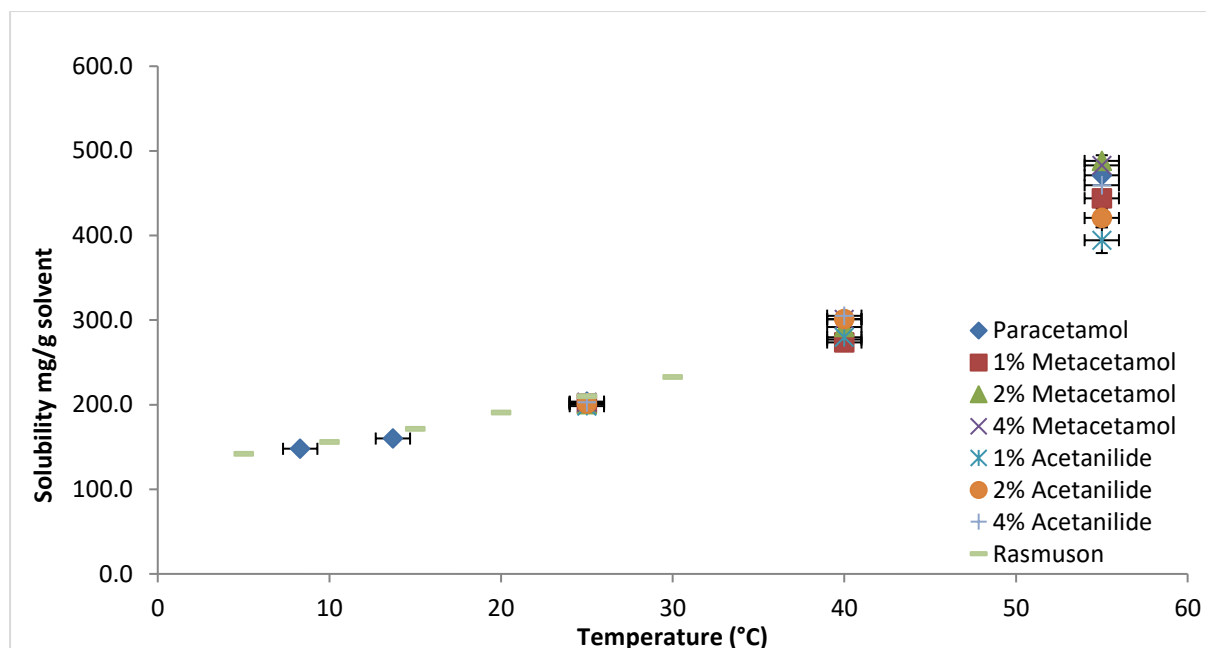
Figure 39: Solubility plot of paracetamol and impurity concentrations in ethanol at several temperatures compared with Granberg and Rasmuson (79).

There are several factors to consider when analysing the solubility of a crystalline organic material, such as the selected solvent, the morphology of the crystal, melting point, and molecular weight. The results of the solubility in ethanol (8.3-55 °C) are in good agreement with the literature stated values reported by Granberg (79) (Figure 39); Granberg investigated paracetamol solubility in different solvents, including ethanol. In this study, the solubility of paracetamol in ethanol at 25 °C was found to be Cs = 202.4 mg g^{-1}; this is less than the reported values by Granberg (Cs = 209.9 mg g^{-1}), showing a 7% decrease and higher than the reported values by Romero (240) (Cs = 187.9 mg g^{-1}).

The differences found between the various publications are notable and exceed what could be expected due to the different companies from which the material and selected solvent were purchased, as well as the purity of the material. The selected materials (paracetamol and impurities) were shown to have a dependence on temperature, where the solubility increased with an increase in temperature, which allows for more solute molecules that are held by intermolecular bonds to be effectively broken apart.
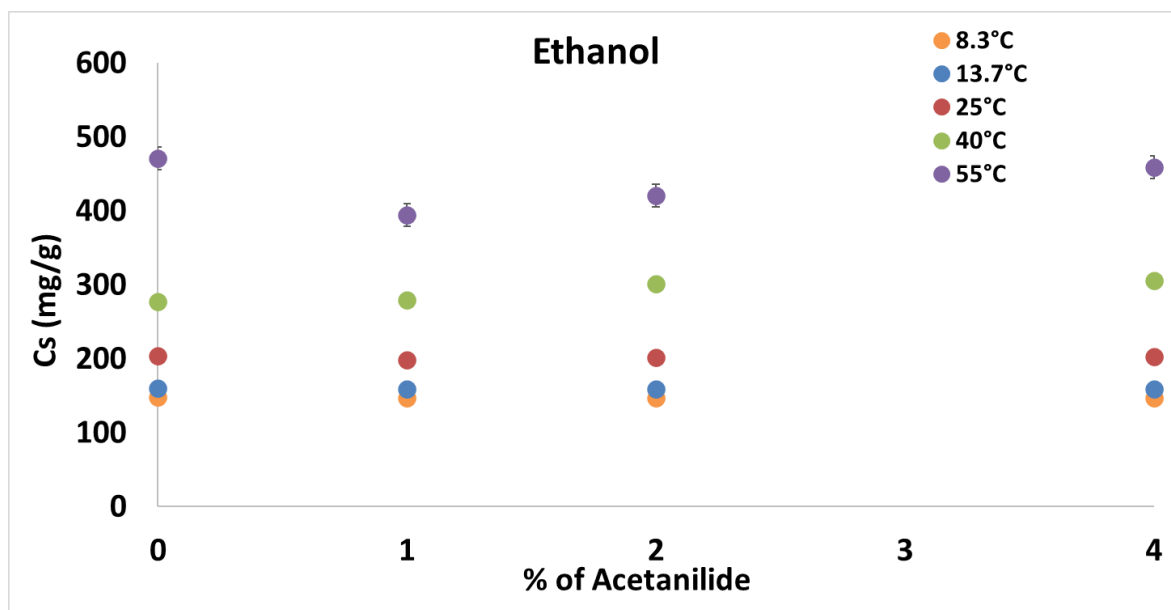
Figure 40: Solubility plot of paracetamol and % of acetanilide concentrations in ethanol at several temperatures.
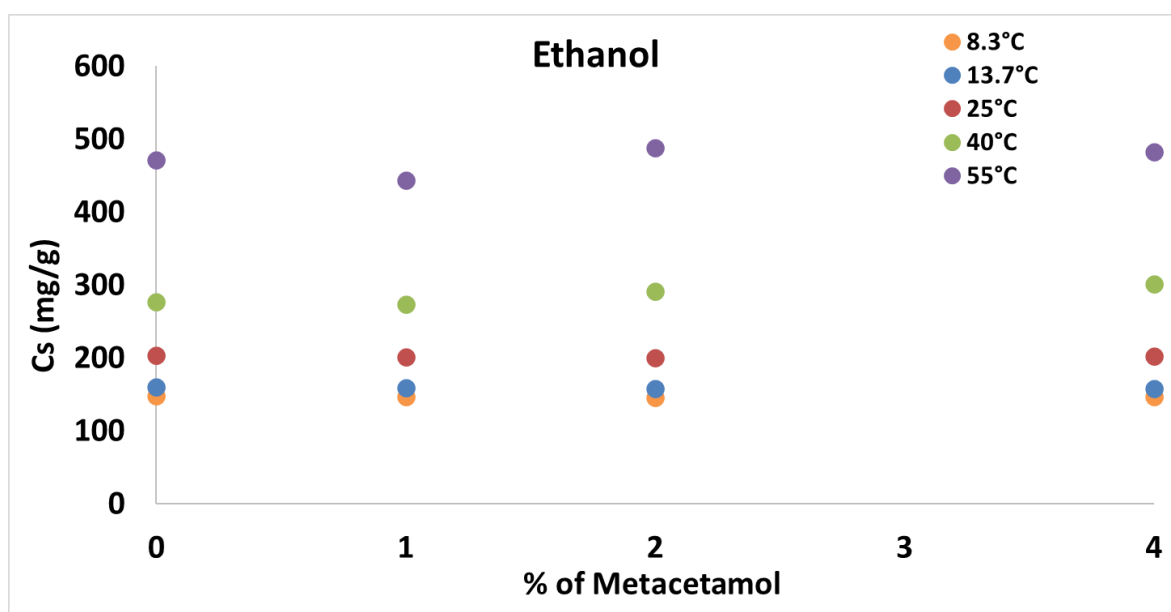
Figure 41: Solubility plot of paracetamol and % of metacetamol concentrations in ethanol at several temperatures.

Impurities were found to have varying effects on the solubility of paracetamol. Looking at Figure 40-Figure 41, as the temperature increases, the solubility of paracetamol also increases. When impurities are added to the system, this has varying impacts on the solubility, depending on the concentrations of impurities. For example, 1% of impurities

151

have a slightly decreasing effect on solubility. As the percentage of impurity increased to 2%, there was a slight increase in its effect on reducing the solubility. Little effect can be seen at the lower range of temperatures 8.3 °C and 13.7 °C. The addition of 2% metacetamol and 4% metacetamol, respectively, decreased the solubility fractionally. At 25 °C and 55 °C, 1% acetanilide decreased the solubility more than metacetamol; however, at 40 °C, 1% metacetamol decreased the solubility more than acetanilide. Interestingly, 2% metacetamol had a decreasing effect at 8.3 °C but also had an increasing effect at 55 °C.

Moving further up in temperature, the difference between replicate samples begins to increase slightly with the exception of the addition of impurities at 55 °C, 1, 2 and 4% acetanilide showing the biggest variance; this could be due to acetanilide being the most soluble component in ethanol. The experimental challenge of accurately sampling a saturated solution with a high concentration (around 400mg paracetamol per gram of solvent) in a relatively volatile solvent just 15 °C below the solvent boiling point, will likely contribute to this scatter amongst the data. The experimental procedure involved the impurities being dissolved into the solution, then paracetamol being added; this will have changed the solvent composition as the acetanilide occupied some of the solvation opportunity, which means paracetamol would have less opportunity to solvate; this is likely down to the bonding arrangement of acetanilide. Acetanilide lacks a hydroxyl group in the para-position of the aromatic ring, therefore lacking a proton donor, with hydrogen bonding being the primary feature of paracetamol crystal structure; this results in the formation of hydrogen-bonded chains of molecules that pack in a herringbone confirmation; similarly, metacetamol is also bound together by this network of hydrogen bonding interactions.

Interestingly, in

Table **6**, the melting peak and delta heat of fusion decrease in the following order: paracetamol> metacetamol> acetanilide. For acetanilide, the lack of a hydroxyl group results in an overall less stable crystal lattice, which is bound by weaker forces when compared with paracetamol and metacetamol. This is evidenced by the lower melting point of acetanilide, which results in a reduction in the opportunity for a stable hydrogen-bonded network, which then relates back to acetanilide occupying more of

the solvation opportunity than paracetamol. The greater spread of the experimental data that occurs with an increase in temperature to 55 °C and with the addition of impurities could simply be down to the impurity's ability to occupy more of the solvation opportunity when competing with paracetamol; the possibility is that slightly more or slightly less will dissolve; however, this is all dependent on intermolecular interactions within the solution. Keshavarz (126) discovered that an impurity concentration of 5 mol% 4-nitrophenol and 4'chloroacetanilide only slightly increased the solubility of paracetamol in 2-propanol across a temperature range of 5 to 55 °C; they noted that 4'chloroacetanilide incorporated into the solid phase of paracetamol, whereas 4-nitrophenol was found to remain within the solution and not affect paracetamol's solid phase (80).

The solubility of paracetamol and the corresponding impurity concentrations in ethanol were investigated at temperatures of 25, 40, and 55 °C to provide a more detailed representation of the data points and their associated error bars.

Isoamyl alcohol	25 °C			40 °C			55 °C		
Solute	Cs	$s.d$	n	Cs	$s.d$	n	Cs	$s.d$	n
Paracetamol	56.1	1.9	6	77.2	2.10	4	124.3	5.1	3
Metacetamol	81.4	3.7	6	121.1	0.9	3	162.6	4.8	3
Acetanilide	162.8	3.9	6	283.5	4.9	4	476.1	4.8	3
1% Metacetamol	56.8	0.1	3	86.9	0.9	3	118.4	3.8	3
2% Metacetamol	57.0	0.1	3	85.3	1.8	3	126.2	2.7	3
4% Metacetamol	59.9	5.2	3	85.7	1.8	3	115.5	15.9	3
1% Acetanilide	53.2	5.9	3	80.5	0.4	3	105.4	3.7	3
2% Acetanilide	57.0	0.7	3	82.8	0.8	3	102.0	3.4	3
4% Acetanilide	55.3	1.7	3	85.9	3.5	3	112.7	2.9	3

Table 8: Solubility, Cs, of paracetamol in isoamyl alcohol reported in mg of paracetamol and impurity % / g of solvent, with different impurity concentrations at temperatures between 8.3 and 55 °C with the corresponding standard deviation (s.d) and number of samples (n).
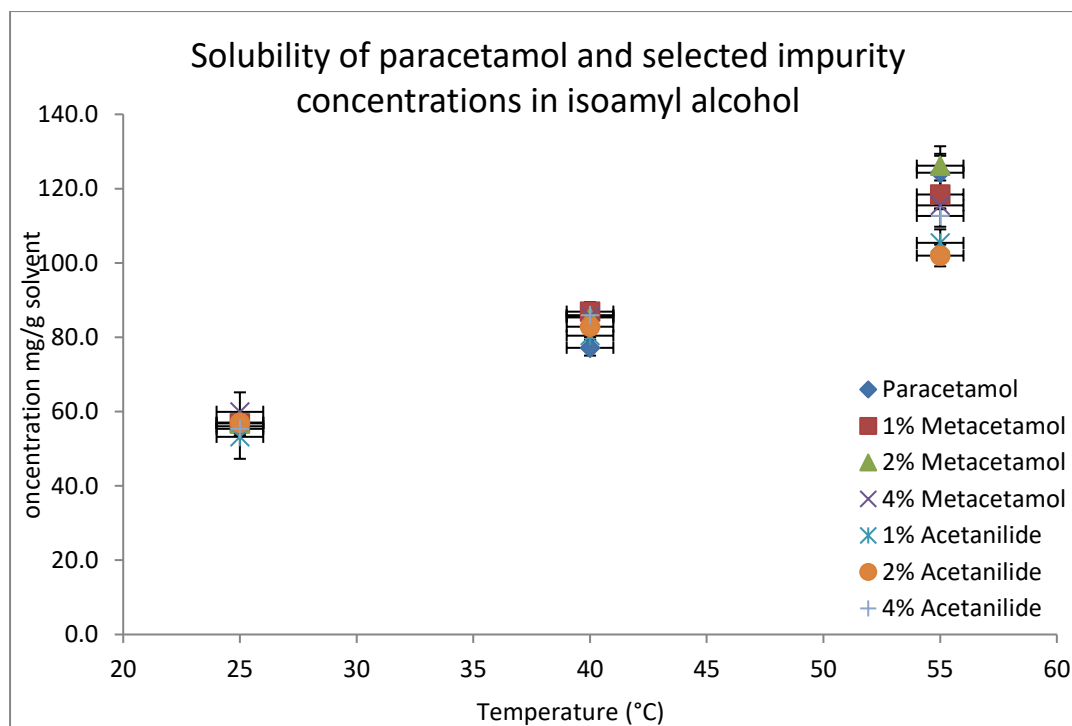
Figure 42: Solubility of paracetamol and impurity concentrations in isoamyl alcohol.

Paracetamol, metacetamol, and acetanilide exhibit higher solubility in isoamyl alcohol compared to ethanol (refer to Figure 42 and Table 8). Although the solvent has changed, the underlying behaviour of these molecules and their ability to occupy solvation sites remain consistent, as discussed earlier. Moreover, consistent with our previous publication by Nguyen (128), the solubility of these compounds is observed to increase with rising temperatures.
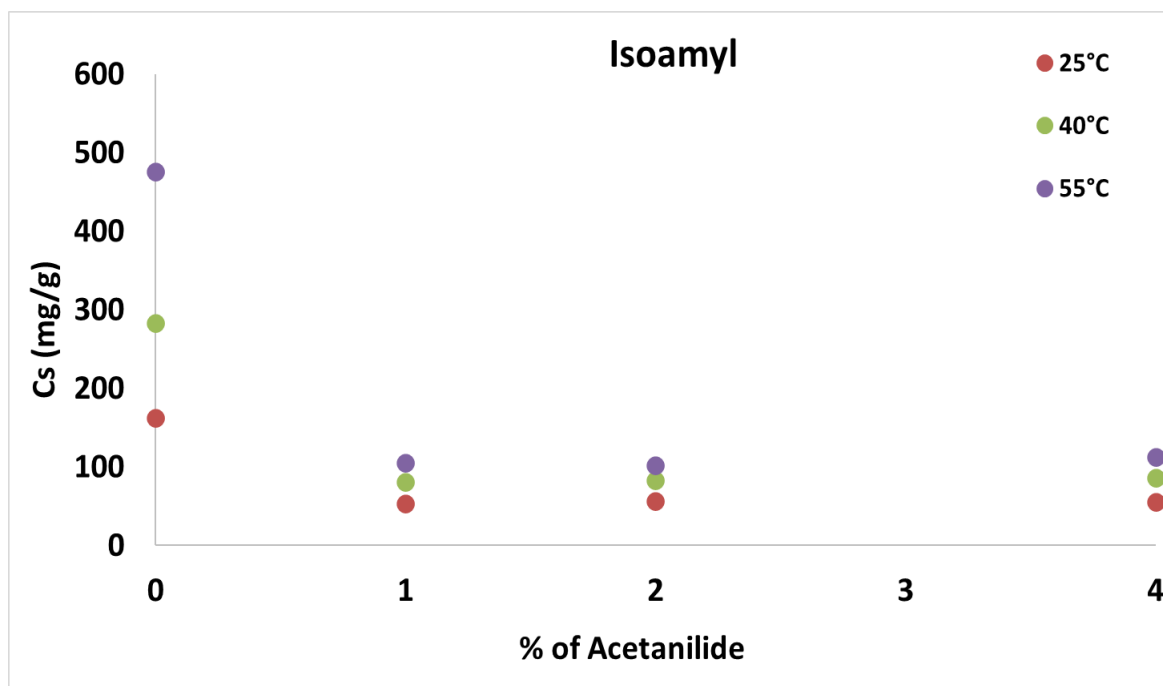
Figure 43: Percentage of acetanilide solubility at 25, 40, and 55 °C.
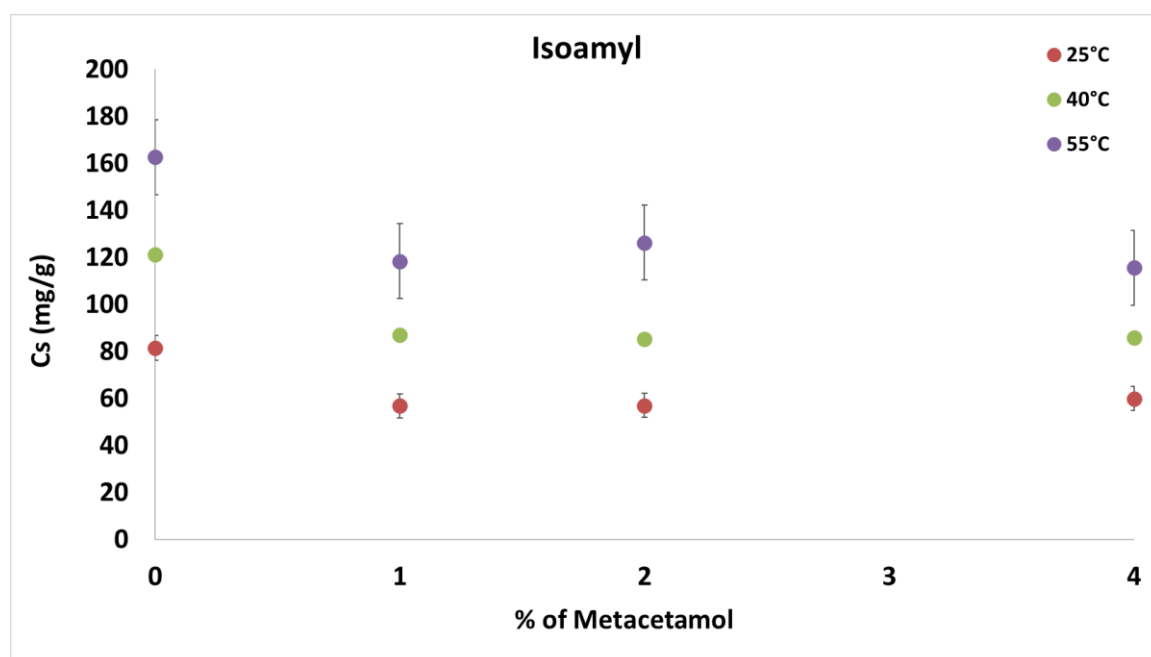
Figure 44: Percentage of metacetamol solubility at 25, 40, and 55 °C.

The findings depicted in Figure 42 suggest that the inclusion of impurity loadings ranging from 1% to 4% has a minimal effect on the solubility of paracetamol. Specifically, at 25 °C, the solubility is slightly decreased by 1% and 4% acetanilide, while the other impurities cause a marginal increase in solubility. It is important to note that these observations are based on a limited range of scattered data, where the

155

solubility difference between 1% acetanilide and 4% metacetamol is 6.7 mg g^{-1}. As the temperature is raised to 40 °C, the addition of impurities enhances the solubility, albeit with a slightly increased variation in concentration, resulting in a solubility difference of 9.7 mg g^{-1}. Finally, at 55 °C, the presence of impurities, except for 2% metacetamol, led to a decrease in solubility. Notably, the data for 2% metacetamol indicates a 1.9 mg g^{-1} increase in solubility.

In general, impurities in isoamyl alcohol have a decreasing effect on the solubility of paracetamol. For instance, acetanilide (Figure 43) decreased the solubility at 25 °C with 1% impurity loading and at 55 °C with 2% impurity loading. On the other hand, metacetamol (Figure 44) increased the solubility at 25 °C with 4% impurity loading, 40 °C with 1% impurity loading, and 55 °C with 2% impurity loading.

Detailed information regarding the solubility of paracetamol and impurity concentrations in isoamyl alcohol at 25, 40, and 55 °C, along with individual data points and associated error bars, can be found in Appendix A, Section 2.5a and b.

The difference in solubility with these impurity loadings is relatively small in ethanol and isoamyl alcohol. Although some degree of noise is present when examining the finer details of the data, overall, the results remain relatively consistent. For individualised solubility graphs of paracetamol and impurity concentrations at 25, 40, and 55 °C, see Appendix A, Sections 2.5a and 2.5b.

4.2: Conclusion

This chapter focused on investigating the solubility of paracetamol in both ethanol and isoamyl alcohol and the impact of two structurally related impurities, metacetamol and acetanilide, on crystal incorporation. Valuable insights were gained through equilibration and gravimetric analysis methods.

The solubility data of paracetamol in ethanol showed good agreement with the literature values. However, due to the lack of available literature data, a direct comparison of paracetamol solubility in isoamyl alcohol was not possible.

Chapter 4: Solubility of Paracetamol and Structurally Related Impurities

The inclusion of structurally related impurities, metacetamol and acetanilide, at various concentrations and temperatures did not exhibit a discernible trend. Their effects on solubility varied depending on temperature, concentration, supersaturation, and the selected solvent. Therefore, it can be concluded that these impurities are likely to have a small impact on the growth of paracetamol crystals, depending on their strength and the specific experimental conditions. Further analysis and determination of their effects will be conducted in subsequent chapters. X-ray powder diffraction (XRPD) analysis confirmed that the investigated impurity concentrations did not alter the crystal form I of paracetamol.

Overall, this chapter provides valuable insights into the solubility of paracetamol and highlights the significant impact of structurally related impurities on its solubility. It explores the intricate relationship between impurities and solubility, revealing how impurities can alter the solubility behaviour of paracetamol. By elucidating the effects of impurities on solubility, this research contributes to a deeper understanding of the complex dynamics involved in crystallisation processes. It emphasises the importance of considering impurity effects for optimising crystal purities and ensuring high-quality pharmaceutical products.

Chapter 5:

Single Crystal Growth with and without Ultrasonic Intervention

Summary:

In this chapter, Single Crystal Growth (SCG) experiments were conducted to investigate face-specific growth rates of paracetamol crystals with the addition of structurally related impurities (metacetamol and acetanilide). The effect of ultrasound was also investigated, along with supersaturation and temperature. The influence of these factors on growth rates was studied in two solvents: ethanol and isoamyl alcohol. The relative growth rates of sets of perpendicular faces and the effect on the crystal habit of monoclinic paracetamol were observed in-situ using optical microscopy. This revealed that in a non-sonicated system, the face growth rates increased with an increase in supersaturation and temperature; as the impurity concentration increased, the growth rate of the faces affected by the impurities decreased. A characteristic of paracetamol crystal growth under the conditions examined was the wide range of crystal habits observed among individual crystals grown under identical conditions. The two different solvents were also found to influence the paracetamol crystal habits. The application of ultrasound to these systems caused the growth rates to increase; this altered the overall habit of the crystals, making it challenging to index the crystal faces.

5.0: Introduction

The growth of single crystals plays a crucial role in the development of pharmaceuticals and the design of drug formulations. It offers valuable insights into crystal structures, influencing essential properties such as solubility, stability, and bioavailability. Through the cultivation of single crystals and the exploration of growth conditions, a deeper understanding of drug properties can be achieved, enhancing their effectiveness. Ultimately, this knowledge drives the optimisation of drug formulations, leading to improved efficiency and better patient outcomes.

Single crystals can be cultivated using a variety of vessels, including crystallisers (245) and flasks (246), to collect the resulting crystal products. The growth process of both large and small single crystals typically involves solution-based methods, wherein specific temperature conditions and gradual cooling rates are employed. This facilitates the retrieval of the final crystals within a specific timeframe, ranging from ten hours to a few days, depending on equipment and experimental conditions (112, 236, 237). When researching single crystal growth, the scope encompasses a wide range of factors, including the influence of temperatures and supersaturations (247), the effects of impurities (8, 125, 248), the impact of mixing conditions (245) and even the cultivation of different crystal forms (161, 236).

A limited amount of research is available that examines in-situ face-specific growth rates over time. Additionally, no existing studies have specifically investigated the impact of impurities, such as acetanilide and metacetamol, on the in-situ face-specific growth rates of paracetamol. While similar studies have been conducted by other researchers, they used different experimental setups, including flow cells (249), stagnant cells, and different drug products like RS-ibuprofen (129, 247).

The choice of cell type plays a crucial role in these measurements. Stagnant cells offer several advantages over flow cells, providing a controlled and stable growth environment by eliminating flow-induced hydrodynamic effects such as convection and shear forces (249). This simplifies the experimental setup, reduces contamination risks, and enables higher spatial resolution for precise measurements and analysis of

specific crystal faces or regions of interest. Stagnant cells also offer better stability for long-term measurements, making them suitable for prolonged observation. However, flow cells have their own merits as they allow for rapid mixing of solutions, induce supersaturation, and facilitate the observation of nucleation and subsequent growth of single crystals (74, 78, 247).

First, the perpendicular faces were initially labelled as face A or face B, and measurements were recorded. While this labelling would have been sufficient, it was also vital to determine the indexing of the crystal faces. Indexing plays a significant role in classifying and characterising each crystal, providing valuable information about its internal structure and symmetry. This indexing enables a better understanding of how atoms, ions, or molecules are arranged within the crystal lattice. In the case of paracetamol crystals in form I, their shape varies from thick plates to needle-like structures, depending on the specific crystallisation conditions. A BFDH model was generated using the CCDC habit tool to visualise the crystal structure, which allowed us to gain insights into the primary faces and exposed functional groups. Figure 20 illustrates the primary facet, identified as (001).

Impurities play a multifaceted role in crystallisation environments, as they can act as hindrances or catalysts, leading to changes in systems and altering crystal habits and drug properties. These effects can have positive or negative implications for upstream processes, such as solubility, stability, and bioavailability. The literature has extensively examined several structurally related impurities and their impact on the nucleation and growth of paracetamol crystals, resulting in variations in crystallisation kinetics and morphology. Notable impurities studied include p-acetoxyacetanilide (PAA), metacetamol, acetanilide, orthocetamol, methylparaben, and p-acetoxybenzoic acid (18, 250-252).

When crystallisation conditions are altered, different crystal habits can be formed. For example, Parasad (18) observed a transformation in the morphology of paracetamol single crystals from columnar to plate-like shapes in a pure system as supersaturation increased. However, with the addition of the impurity p-acetoxyacetanilide (PAA), columnar crystals were observed, and the growth was inhibited, resulting in decreased

yield with higher PAA levels. However, there was a lack of discussion regarding specific techniques used for impurity analysis and characterisation and no explicit mention of limitations in the study, such as the chosen impurity concentration or suggestions for future research.

Thompson (8) also observed a similar crystal habit and growth change when introducing structurally related impurities. They used atomic force microscopy (AFM) to investigate the growth of paracetamol crystals. They found that metacetamol incorporation onto the (001) face led to steps interspersed with holes, indicating disruption of the hydrogen bonding network on the crystal surface. On the other hand, acetanilide resulted in hole formation that potentially originated from defects. These holes deepened over time, suggesting dissolution reaching into the crystal core. It should be noted that these effects did not occur in all crystals, as some grew under these conditions without disruption.

Interestingly, previous studies discussing crystal growth at various supersaturation levels often reported the presence of only one crystal habit at each supersaturation (8, 227, 253). In contrast, the current work has observed the occurrence of more than one crystal habit under the same conditions of supersaturation and temperature, with some habits growing simultaneously.

Using ultrasound in crystallisation has been a subject of research and application for several decades. This chapter focused on investigating the impact of structurally related impurities on single crystal growth and exploring a novel aspect of incorporating ultrasound in a single crystal stagnant cell that has yet to be previously reported. This chapter presents the findings of studying the effects of metacetamol and acetanilide impurities on paracetamol crystals, with loadings of 2 and 4% by mass. Additionally, it examines the influence of sonication on a spontaneously nucleated single paracetamol crystal, considering factors such as the solvent used (ethanol 99.8% and isoamyl alcohol 98.5%), temperature (15, 20, or 30 °C) and relative supersaturation, σ, ranging from 1.25 to 1.75 in ethanol and 1.75 to 2.25 in isoamyl alcohol.
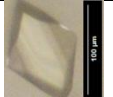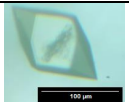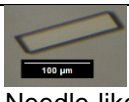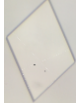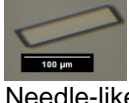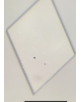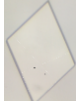
5.1: Results and discussion
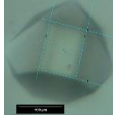
5.1.1: Face indexing

To gain insights into the impact of external conditions on specific crystal faces, it is crucial to assign faces whenever possible in crystallisation studies. Although there is no standardised naming system, it was feasible to correlate crystal faces with commonly observed paracetamol crystal faces using the Mercury BFDH model. Ristic (132) documented that monoclinic paracetamol crystals grown from pure aqueous solutions displayed prominent {110} faces at lower supersaturations, while {001} faces became increasingly significant as supersaturation levels rose, leading to a change in crystal habit from columnar to plate-like. However, at both lower and higher supersaturation levels, this study cannot assert the dominance of a specific assigned face due to the influence of exhibited habits. Table 9 presents the assigned faces observed under each condition, offering a more refined identification of individual faces and their corresponding growth rates. This new assignment replaces the previous labelling of faces in the A growth direction and B growth direction, allowing for a more precise characterisation of crystal faces. However, it is crucial to acknowledge that this representation only covers a limited area of the stagnant cell. As a result, the crystal face distribution and variation observed in Table 9 may not fully capture the complete picture.

Table 9: Assigned face indexing from SC-XRD at each condition along with the associated habit(s) found in pure non-sonicated systems. There is no universally agreed-upon naming system for crystal habits; therefore, the habits found in this study were described as diamond, needle-like, truncated, equant and multi-faceted.

Condition	Main Face	Right A	Left A	Right B	Left B	Habit
Temperature- 15 °C Supersaturation- 1.25	$(10\bar{1})$	$(0\bar{1}\bar{1})$	(011)	$(0\bar{1}1)$	$(01\bar{1})$	Truncated
	$(10\bar{1})$	(110)	Not indexed	Not indexed	$(01\bar{1})$	Multi-faceted
Temperature- 15 °C Supersaturation- 1.75	$(10\bar{1})$	$(0\bar{1}\bar{1})$	(011)	$(0\bar{1}1)$	$(01\bar{1})$	Truncated
	$(0\bar{1}1)$	$(1\bar{1}0)$	$(\bar{1}01)$	$(0\bar{1}\bar{1})$	(001)	Needle-like
	$(10\bar{1})$	(110)	$(0\bar{1}\bar{1})$	$(01\bar{1})$	$(0\bar{1}1)$	Diamond
Temperature- 20 °C Supersaturation- 1.25	$(10\bar{1})$	$(0\bar{1}\bar{1})$	(011)	$(0\bar{1}1)$	$(01\bar{1})$	Truncated
	$(10\bar{1})$	(110)	Not indexed	Not indexed	$(01\bar{1})$	Multi-faceted
Temperature- 20 °C Supersaturation- 1.75	$(0\bar{1}1)$	$(1\bar{1}0)$	$(\bar{1}01)$	$(0\bar{1}\bar{1})$	(001)	Needle-like
	$(10\bar{1})$	(110)	$(0\bar{1}\bar{1})$	$(01\bar{1})$	$(0\bar{1}1)$	Diamond
Temperature- 30 °C Supersaturation- 1.25	$(10\bar{1})$	(110)	$(0\bar{1}\bar{1})$	$(01\bar{1})$	$(0\bar{1}1)$	Diamond

	$(0\bar{1}1)$	(001)	$(0\bar{1}0)$	$(\bar{1}\bar{1}1)$	Not indexed	Equant
Temperature- 30 °C Supersaturation- 1.75	$(10\bar{1})$	$(0\bar{1}\bar{1})$	(011)	$(0\bar{1}1)$	$(01\bar{1})$	Truncated
	$(10\bar{1})$	(110)	Not indexed	Not indexed	$(01\bar{1})$	Multi-faceted

In the study conducted by Ristic (132), it was observed that monoclinic paracetamol crystals cultivated from pure aqueous solutions displayed prominent {110} faces under lower supersaturation conditions. However, as the level of supersaturation increased, the significance of {001} faces escalated, leading to a transition in crystal morphology from columnar to plate-like structures. Within the scope of this study, the prevailing face was identified as {$10\bar{1}$}, although variations were noted, specifically a shift to {$0\bar{1}1$} as the dominant face, which depended on the shape of the crystals rather than the degree of supersaturation. This shift was particularly evident in crystals with a need-like or equant shape. Sudha (228) conducted a study examining the influence of solvent polarity on the modification of monoclinic paracetamol's crystal habit using various solvents. Single crystals were grown through a slow evaporation process. In the case of ethanol, the main face index observed was {$00\bar{1}$}, accompanied by corresponding faces such as {$1\bar{1}0$}, {$01\bar{1}$}, {$1\bar{1}0$} and {$0\bar{1}1$}. The crystal shape in ethanol closely resembled the equant habit described in Table 9, which displayed a dominant {$1\bar{1}0$} face. However, unlike the equant crystal images presented in Table 9, the ethanol grown crystals did not exhibit any perpendicular faces.

5.1.2: Habit analysis

Given that the internal structure of the crystal lattice remains the same, the external appearance (crystal habit) is influenced by factors such as: solvent, temperature, supersaturation and the presence of impurities (137). In literature, it is commonplace to find mention of one crystal habit being associated with specific conditions (8, 124, 132, 228, 254); however, this study has found examples of at least two or three

separate habits of paracetamol forming in the same experiment or in the replicates, as observed in Figure 45Figure **46**. This appears to be a particular characteristic of paracetamol. It is more common to find variations of habits in systems that contain impurities or are subject to some other intervention, for example, ultrasonic agitation resulting in particle breakage. However, this phenomenon occurred without these interventions and was reproducible, as illustrated in Figure 45 and Table 10. This could arise due to variations in supersaturation levels, solvent properties, or nucleation sites.
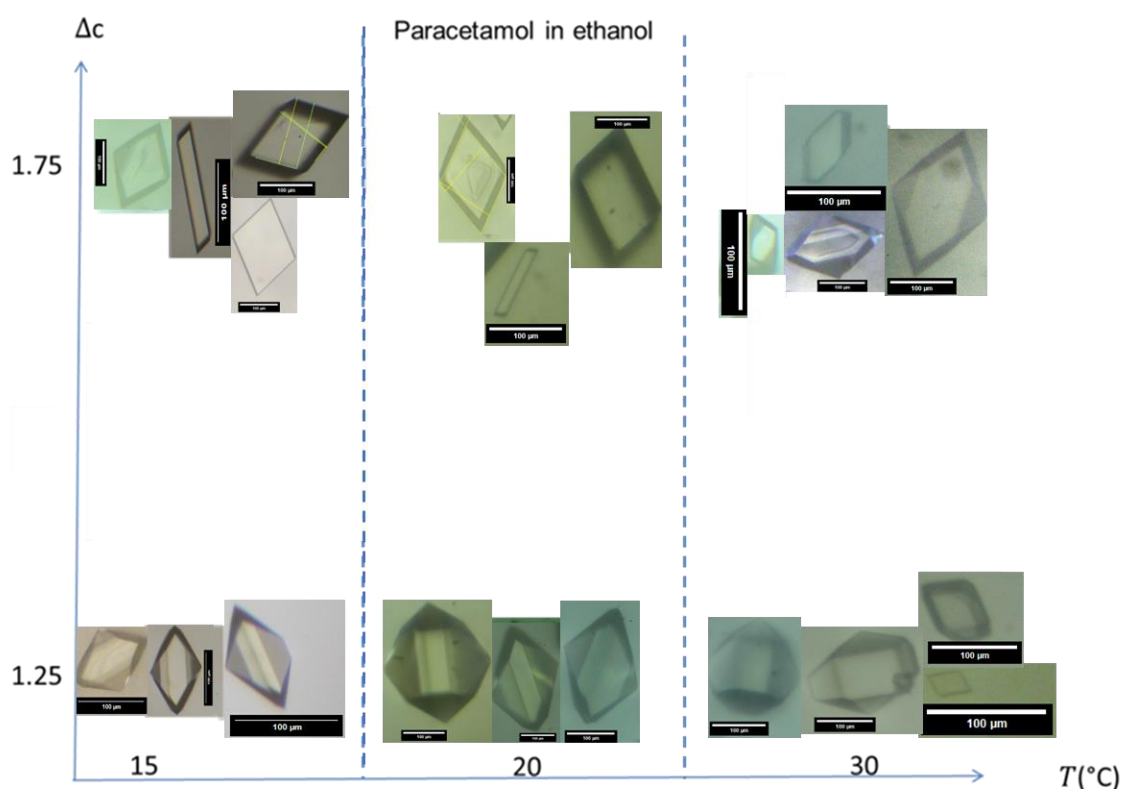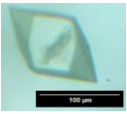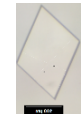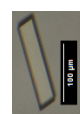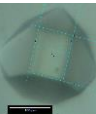
Figure 45: Paracetamol in ethanol habit analysis at σ= 1.25 and 1.75 and temperatures of 15, 20, and 30 °C.

Table 10: The estimated count of observed habits from single crystal growth rate images, regardless of crystal clarity, if it was measurable or what it was next to.

Temperature (°C) and Supersaturation (σ)	Condition parameters	Estimate count of observed habits from images obtained.				
		Multifaceted e.g.,	Truncated e.g.,	Diamond e.g.,	Needle e.g.,	Equant e.g.,
°C = 15 σ = 1.25	Pure no ultrasound	1	6	0	0	0
	Impurities no ultrasound	24	1	0	*1*	0
	Pure with ultrasound	3	1	0	0	*1*
	Impurities with ultrasound	17	0	0	>50	0
°C = 15 σ = 1.5	Pure no ultrasound	16	17	14	2	4
	Impurities no ultrasound	32	23	*10*	*1*	0
	Pure with ultrasound	No data	No data	No data	No data	No data
	Impurities with ultrasound	12	0	>50	0	0
°C = 15 σ = 1.75	Pure no ultrasound	0	4	2	9	0
	Impurities no ultrasound	0	8	9	>40	0
	Pure with ultrasound	0	0	0	>30	0
	Impurities with ultrasound	0	*5*	6	>50	0
°C = 20 σ = 1.25	Pure no ultrasound	*6*	8	0	0	0
	Impurities no ultrasound	*4*	*4*	18	>40	0
	Pure with ultrasound	12	6	0	0	0
	Impurities with ultrasound	>40	*5*	0	>50	0
°C = 20 σ = 1.75	Pure no ultrasound	0	0	12	9	0
	Impurities no ultrasound	0	*2*	18	*15*	0
	Pure with ultrasound	*5*	*2*	*10*	>50	*3*

	Impurities with ultrasound	2	0	1	13	0
°C = 30 **σ = 1.25**	**Pure no ultrasound**	0	0	2	0	12
	Impurities no ultrasound	0	0	4	>60	0
	Pure with ultrasound	0	0	0	0	11
	Impurities with ultrasound	0	0	0	30	0
°C = 30 **σ = 1.75**	**Pure no ultrasound**	2	5	3	*0*	0
	Impurities no ultrasound	1	1	14	8	0
	Pure with ultrasound	3	3	*8*	24	0
	Impurities with ultrasound	4	0	0	15	0

A comprehensive analysis was conducted using experimental data images to estimate the occurrence of different crystal habits under various conditions. The objective was to gain a comprehensive understanding of the breadth of habits observed. Table 10 presents the results of this analysis, with red-highlighted numbers indicating habits that were identified but could not be measured accurately due to factors such as limited measurable images or crystals growing in close proximity to each other.

The estimation primarily focuses on specific areas within the stagnant cell where the growth was concentrated on one or two crystals. However, in cases where more than one hundred crystals exhibited different habits, obtaining a definitive count through visual inspection alone was not feasible. Nevertheless, the table provides valuable insights and reaffirms the observation of diverse habits across different systems. It underscores the complexity and variability of crystal habits, highlighting the need for further investigation and analysis to fully comprehend their characteristics and underlying factors.

Determining the exact reason for the observed variations in crystal habits is challenging. Paracetamol contains both polar and nonpolar functional groups, including hydroxyl, carbonyl, amide groups, and C-H bonds. Ethanol, a polar protic

solvent with a hydroxyl group, exhibits strong intermolecular interactions through hydrogen bonding, enabling the dissolution of positively and negatively charged species (228). These changes in crystal habit are uncommon at low temperatures and supersaturation levels. The observed variations may be influenced by kinetic and thermodynamic factors that become prominent at higher temperatures and supersaturation levels, Gibbs (255) also noted this phenomenon.

The presence of different crystal habits in various locations within the stagnant cell can be attributed to local variations in supersaturation. As crystals nucleate and grow, the concentration of solute near the crystals may deplete, leading to a locally lower supersaturation. This depletion of supersaturation can occur if the rate of supersaturation depletion surpasses the rate of diffusion. Another related phenomenon is growth rate dispersion (GRD), where crystals of similar size exhibit different growth rates despite seemingly identical crystallisation conditions in terms of temperature, supersaturation, and hydrodynamics (1, 243). Three models have been proposed to explain these fluctuations: the Constant Crystal Growth model, the Random Fluctuation model, and the 'fast-growers' and 'slow-growers' model. Among these, the random fluctuation model proposed by Randolph and White (256) is particularly relevant to this discussion. This model suggests that crystal growth rates fluctuate around an average constant growth rate, which can be caused by changes in surface structure over time, resulting in deviations in growth rates on specific crystal surfaces (1, 244).

The crystal habit of a substance is influenced by molecular scale factors and bulk phenomena. At the molecular level, impurity molecules can attach to specific crystal faces at specific locations, affecting habit. Bulk phenomena such as supersaturation and temperature, which are external to individual crystals, play a role in determining crystal habit. The impact of these bulk phenomena becomes evident at higher supersaturation levels and temperatures.

It is uncommon for paracetamol crystals to exhibit different habits under identical conditions; variations in factors such as: nucleation sites, growth rates, the possibility of polymorphism, and micro-environmental effects can contribute to the formation of crystals with distinct habits. These variations arise due to differences in the crystal growth process, leading to diverse crystal habits even under seemingly identical conditions.

5.1.2a Habit analysis: impact of impurities
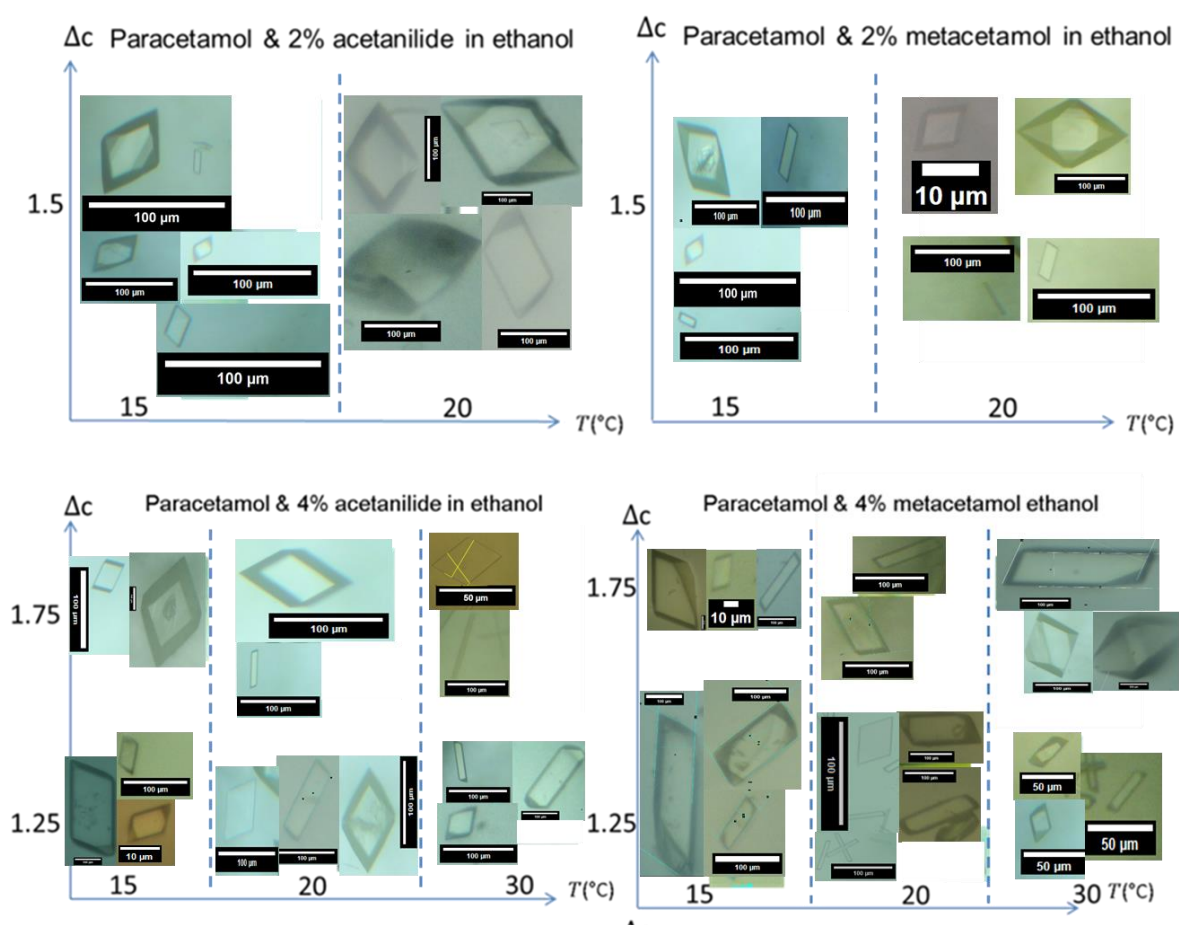
Figure 46: Example paracetamol crystals grown in the presence of 2 and 4% acetanilide and metacetamol in ethanol, habit analysis at σ= 1.25, 1.5 and 1.75 and temperatures = 15, 20, and 30 °C.

In the case of measured crystals, when 2% acetanilide was added to the solution at a supersaturation of 1.5 and a temperature of 15 °C, faceted and truncated crystal habits were found to be favoured. As the temperature increased to 20 °C, the presence of needles and diamonds became more apparent. The overall effect of the 2%

acetanilide addition was clearly visible, as more crystal faces and edges were observed, resulting in multi-faceted habits. On the other hand, the addition of 2% metacetamol led to a mixture of crystal habits. However, as the temperature was further increased, more crystals with truncated and multi-faceted habits were observed.

In other studies that investigated the effects of metacetamol and acetanilide on paracetamol crystallisation in 2-propanol, it was found that the crystal morphology was modified to a more columnar shape, somewhat equant, as opposed to the truncated habits observed in the current study (244).

5.1.2b Habit analysis: impact of ultrasound

As previously discussed in Chapter 3 ultrasonic intervention is known to have a variety of effects on crystallisation processes.
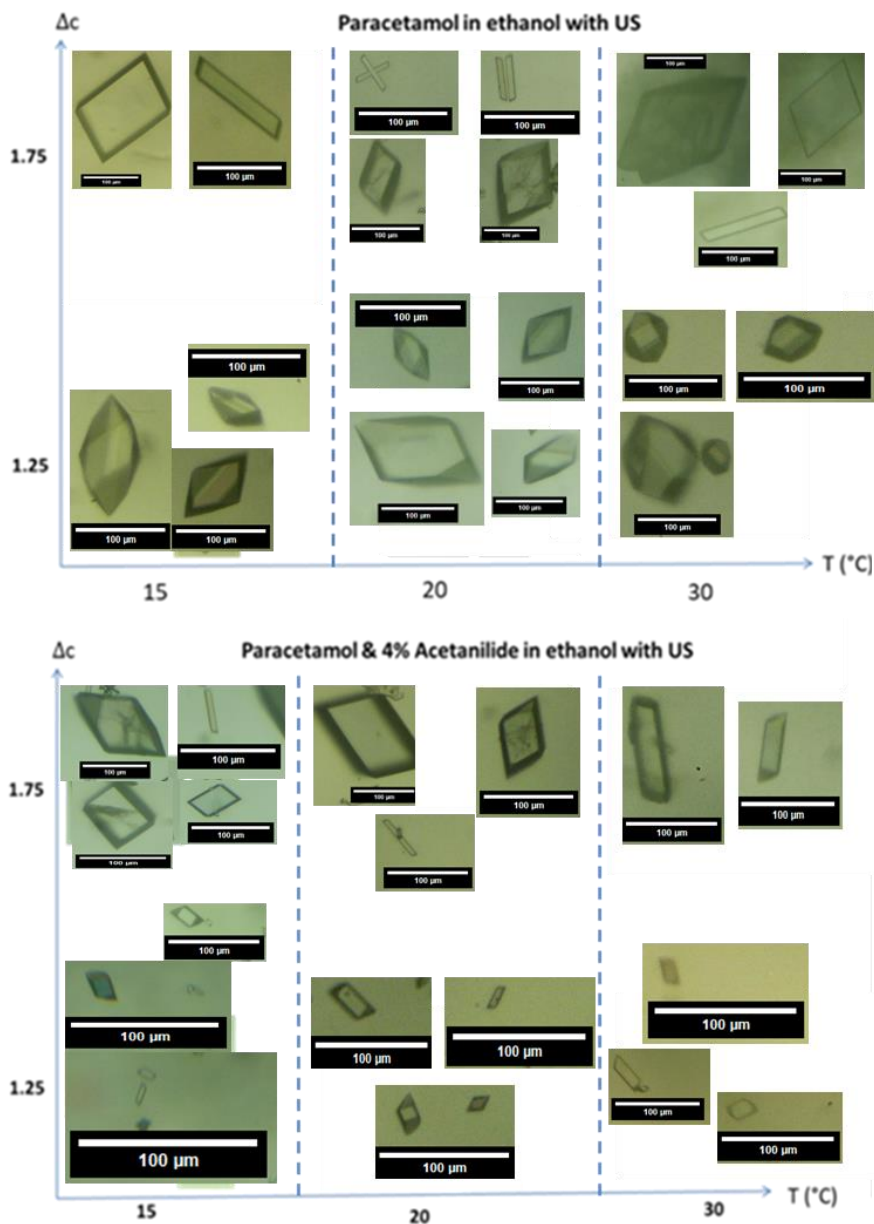
Figure 47: Paracetamol 4% acetanilide in ethanol, habit analysis at σ= 1.25 and 1.75 and temperatures of 15, 20, and 30 °C with the addition of an ultrasonic toothbrush.
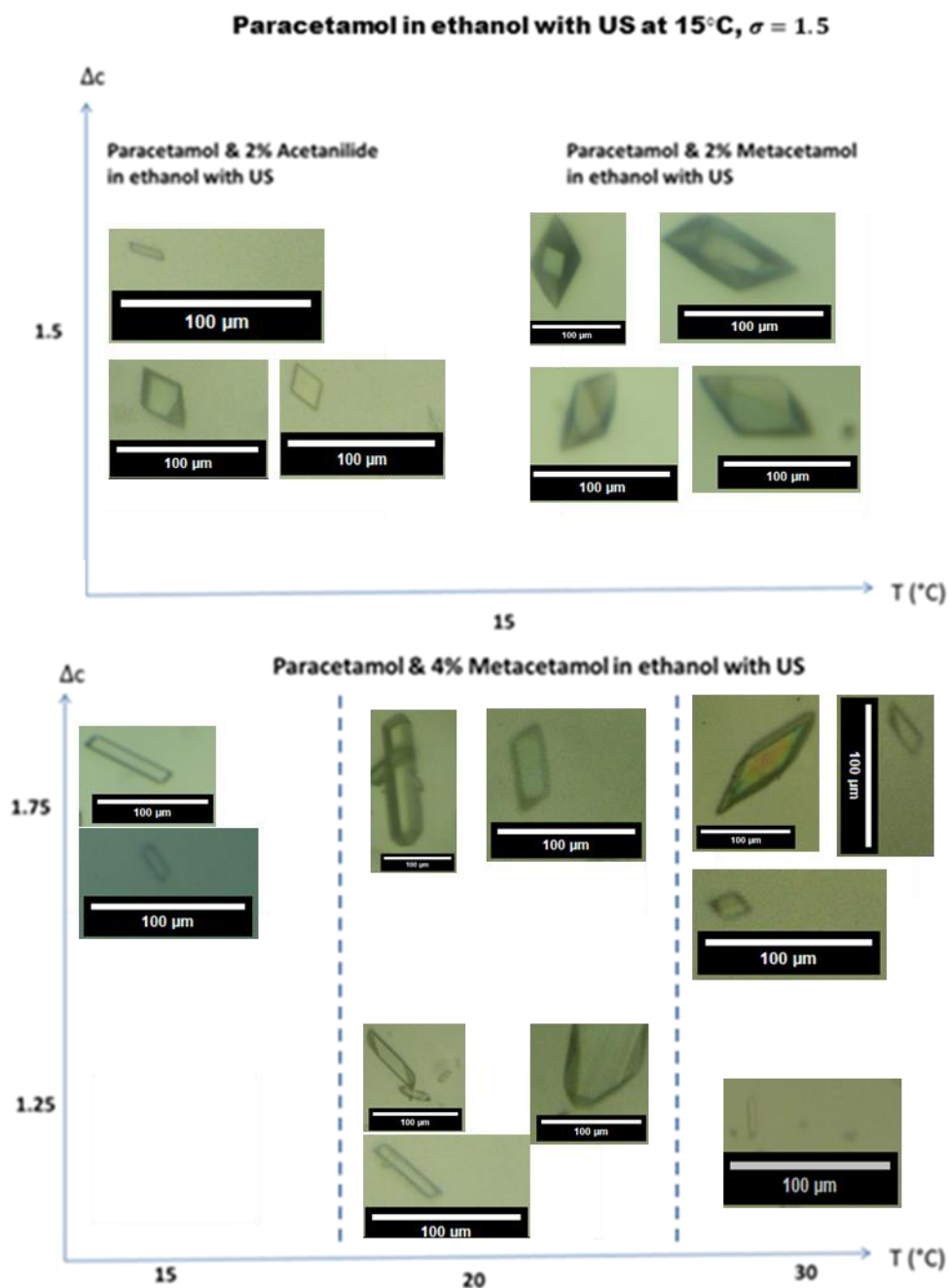
Figure 48: Paracetamol with 2 and 4% acetanilide and metacetamol in ethanol, habit analysis at σ= 1.25, 1.5, and 1.75 and temperatures 15, 20, and 30 °C with the addition of an ultrasonic toothbrush.

Figure 47-Figure 48 exhibit a combination of crystal habits that were grown under identical conditions, contrasting with the non-sonicated data depicted in Figure 45-Figure **46**. These figures demonstrate the noticeable impact of ultrasound on the resulting crystal habits. For a more comprehensive comparison of the observed habits, refer to Table 10.

Figure 48 reveals the presence of needle-like crystal habits in all conditions when 4% metacetamol and acetanilide were added. However, needles were not observed at low supersaturation levels across the temperature ranges in the paracetamol conditions. This suggests that the impurities influence the crystal habit by modifying the growth rates.

According to Zeiger (184) and Gielen (186), ultrasound-induced modification of crystal habit is attributed to the collapse of cavitation bubbles. The symmetric collapse of bubbles in the bulk solution within the stagnant cell leads to a reduction in the boundary layer, enhancing the mass transfer rate of molecules to the crystal surface. In contrast, the asymmetric collapse of cavitation bubbles near the crystal surface results in microjets of solution striking the surface, causing pitting, erosion, and potential fragmentation of the crystal.

Comparing the images of pure paracetamol crystals grown without ultrasound in Figure 45 and those grown in the presence of ultrasound in Figure 48, it is evident that the habits formed are relatively similar within each condition. Some overgrowth on specific faces was observed (e.g., ultrasound addition at 20 and 30 °C with 4% metacetamol). Additionally, needle-like habits were found with ultrasound at 30 °C and a supersaturation level of 1.75, both with and without impurities present.

5.1.3: Growth rate determination

As previously discussed, the single crystal growth rate experiments were conducted to investigate face-specific growth rates. Carefully selected conditions of supersaturation and temperature were analysed. The impacts of impurity concentrations were also determined. The associated habit change was analysed as discussed in Section 5.2.2. The growth rate was measured using the method described in Section 5.1.3. Each family of images was captured at four-minute intervals, as seen in Figure 49 below.
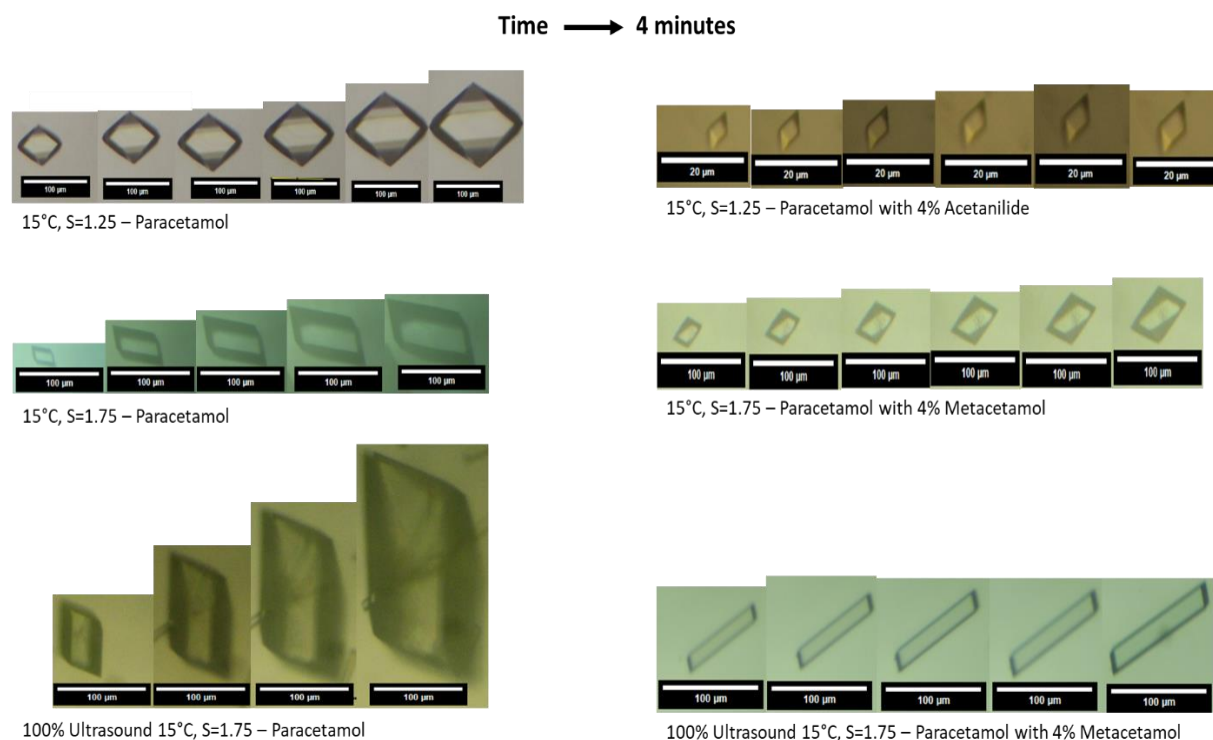
Figure 49: In-situ crystal growth sequenced images, collected at four-minute intervals. For a temperature of 15 °C in ethanol. Showcasing a variety of habits, depending on supersaturation, impurity, and ultrasound addition.

There are several approaches to measuring and expressing the growth rates of crystals; the image-based approach taken here allows the dependency on several factors: supersaturation, temperature, habit, and size to be measured. Other researchers have also taken similar approaches (7, 257). The image-based approach is built on assuming the face identity by observation of interfacial angles, as it is impractical to subject every crystal studied to single crystal x-ray diffraction to assign the faces unambiguously. With this method, faces were assigned as A (face A) or B (face B), as described in Section 5.2.1. The growth rates for each face measured under each experimental condition were then plotted in a combined graph, taking no account of differences in habit, or starting size at the point when measurements began.

For example, paracetamol single crystals grown in ethanol at 15 °C, at supersaturation 1.75, with no added impurities and without ultrasound are shown in Figure 50-Figure **51**.
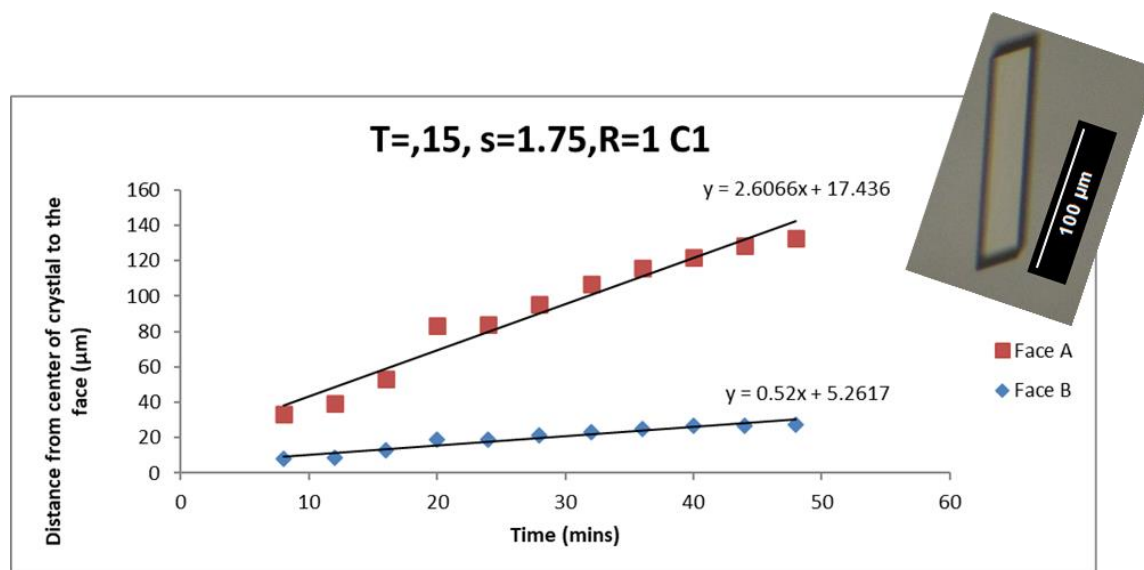
Figure 50: Single crystal growth rate measurements of paracetamol at 15 °C, supersaturation 1.75. run 1 crystal 1.
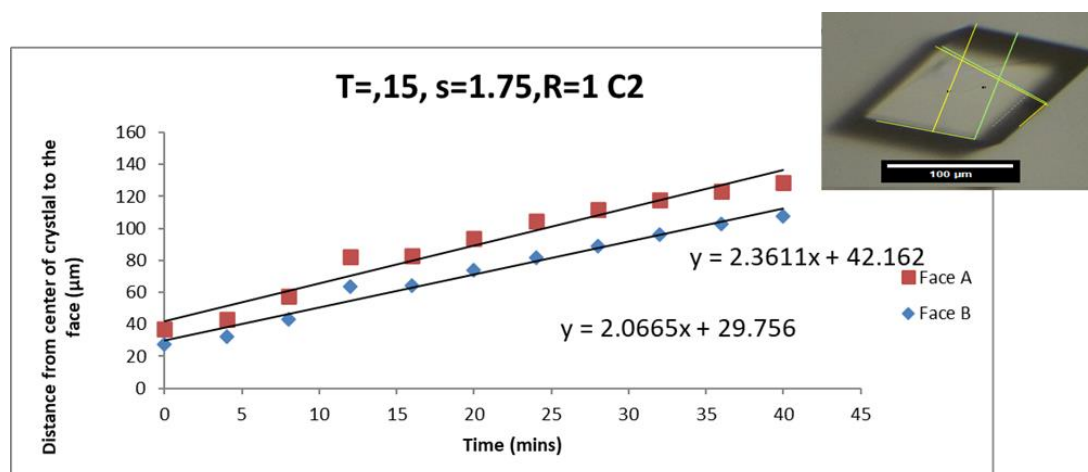
Figure 51: Single crystal growth rate measurement of paracetamol at 15 °C, supersaturation 1.75. run 1 crystal 2.

Face growth rate measurements were obtained by calculating the gradient of the plotted lines. In Figure 50, crystal 1 exhibited a growth rate of 2.61 µm min^{-1} for face A and 0.52 µm min^{-1} for face B. The subsequent crystal, depicted in Figure 51, had a diamond shape, and showed a growth rate of 2.36 µm min^{-1} for face A and 2.07 µm min^{-1} for face B. Two additional crystals, one diamond-shaped and one truncated (refer to Table 9 for habit descriptors), were included in the growth rate data presented in Figure 52-Figure 53. The growth rates of all faces (A and B) were plotted separately in the respective graphs.
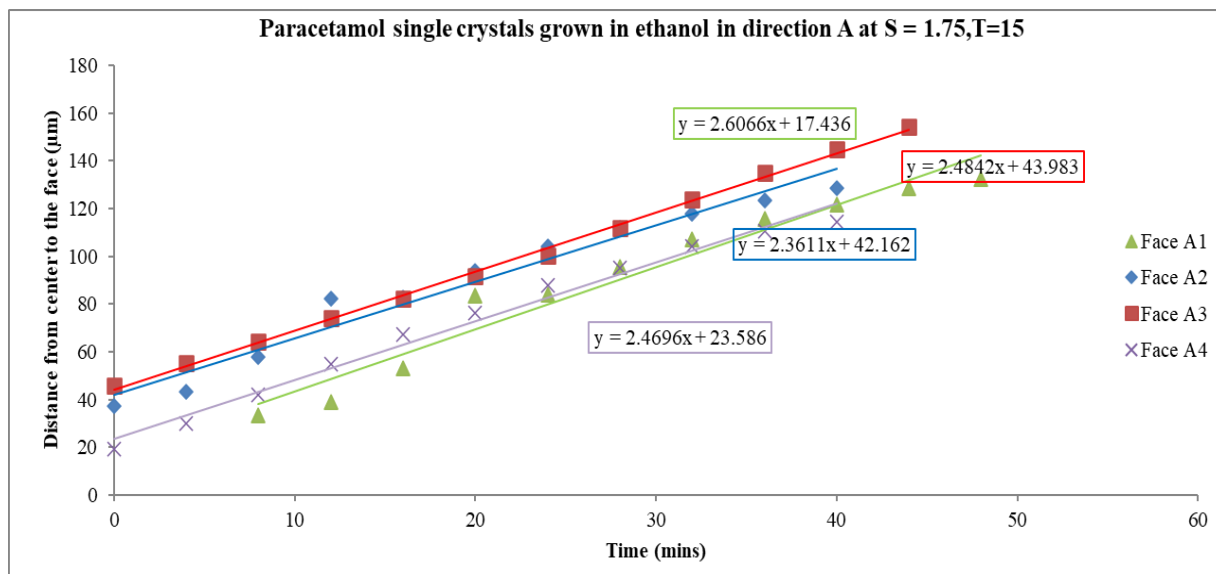
Figure 52: Single crystal growth rate measurement of paracetamol at 15 °C, supersaturation 1.75. Direction A.
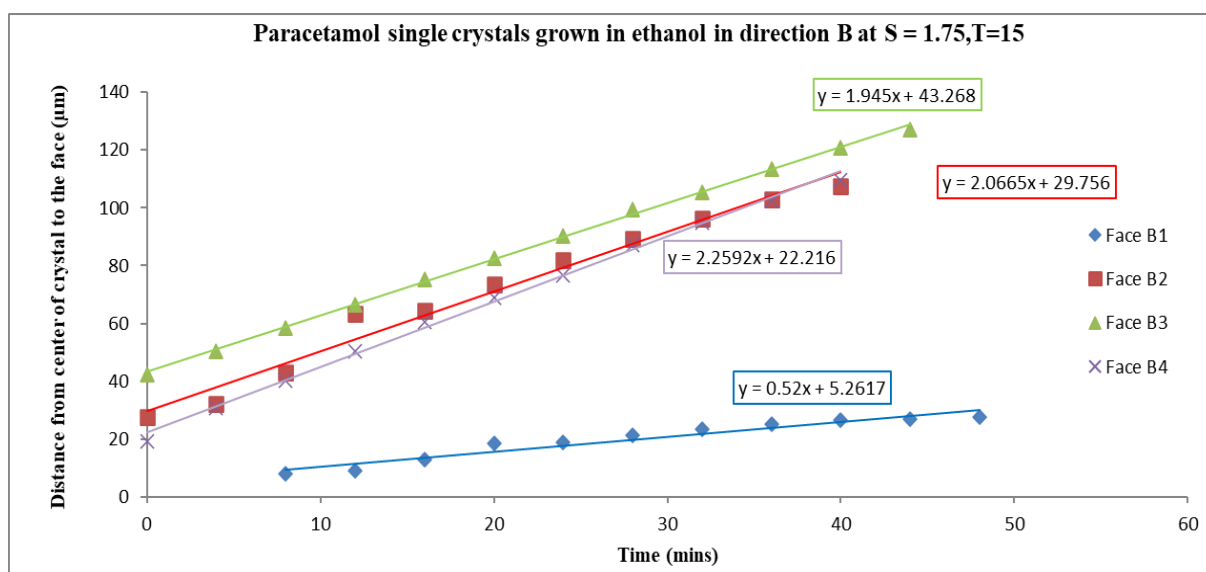
Figure 53: Single crystal growth rate measurement of paracetamol at 15 °C, supersaturation 1.75. Direction B.

The mean growth rate and standard deviation were calculated. Despite the small amount of crystal growth during the measurement period, the concentration remained nearly constant, resulting in a negligible impact on supersaturation. The depletion of supersaturation was insignificant as the crystals grew. By collecting growth rate data

176

from multiple crystals, the variation in growth rates could be expressed within certain confidence limits. In Figure 53, a significantly lower growth rate is observed in the B direction compared to the other measured crystals. This difference can be attributed to the variations in crystal habits and the assignment of faces as A and B directions. Average growth rates for single crystals measured in both the A and B directions are provided in Table 11.

Table 11: Average single crystal growth rate measured for pairs of faces A and B in ethanol at various temperatures, supersaturations, impurities, and impurity concentration.

	Temperature (°C)	Supersaturation (σ)	Growth in Ethanol – Displacement of face A (µm/min)		Growth in Ethanol - Displacement of face B (µm/min)	
			No US	With US	No US	With US
Pure paracetamol	15	1.25 1.75	0.90 ± 0.26 2.48 ± 0.10	0.48 ± 0.08 0.18	0.88 ± 0.20 1.70 ± 0.80	0.42 ± 0.09 0.97
Pure paracetamol	20	1.25 1.75	0.45 ± 0.08 0.84 ± 0.29	0.63 ± 0.08 0.23	0.39 ± 0.02 0.61 ± 0.45	0.69 ± 0.02 1.20
Pure paracetamol	30	1.25 1.75	0.18 ± 0.10 0.31 ± 0.41	0.73 2.48 ± 1.37	0.22 ± 0.17 0.20 ± 0.25	0.83 4.49 ± 0.76
Paracetamol with 2% Acetanilide	15	1.5	0.51 ± 0.63	0.48	0.42 ± 0.51	0.51
Paracetamol with 4% Acetanilide	15	1.25 1.75	0.21 ± 0.19 0.59 ± 0.16	1.04 0.75 ± 0.94	0.12 ± 0.12 0.44 ± 0.04	0.91 0.75 ± 0.41
Paracetamol with 4% Acetanilide	20	1.25 1.75	0.16 ± 0.14 1.22 ± 0.29	0.26 0.90 ± 1.17	0.02 ± 0.01 0.94 ± 0.08	0.16 0.76 ± 0.28
Paracetamol with 4% Acetanilide	30	1.25 1.75	0.37 ± 0.24 0.29 ± 0.30	0.15 0.17	0.07 ± 0.05 0.17 ± 0.12	0.47 0.52
Paracetamol with 2% Metacetamol	15	1.5	1.32 ± 0.19	2.88	1.06 ± 0.24	2.59
Paracetamol with 4% Metacetamol	15	1.25 1.75	0.20 ± 0.08 0.31 ± 0.25	0.04 0.14	0.03 ± 0.01 0.08 ± 0.06	0.56 0.72
Paracetamol with 4% Metacetamol	20	1.25 1.75	0.85 ± 1.06 1.80 ± 0.27	0.01 0.25 ± 0.11	0.54 ± 0.90 1.36 ± 0.10	0.14 0.38 ± 0.17
Paracetamol with 4% Metacetamol	30	1.25 1.75	0.07 ± 0.01 1.09 ± 0.79	0.03 0.19	0.04 ± 0.02 0.33 ± 0.27	0.05 0.27

The information presented in Table 11 indicates that, in the absence of ultrasound, the growth rate of face A is generally larger than that of face B. However, when ultrasound is introduced, more variability is observed, with four out of fifteen cases showing a higher growth rate in the A direction. The standard deviation among the replicates varies significantly, likely due to the observed variations in crystal habits, which consequently lead to larger standard deviations.

As the level of supersaturation increases, the growth rate of crystals also tends to increase. Supersaturation serves as the driving force behind crystal nucleation and growth, ultimately influencing the final size and habit of the crystals. Typically, higher supersaturation is associated with an elevated nucleation rate, growth rate and a decrease in overall crystal size. At lower supersaturation levels, crystals have the opportunity to grow faster than the rate of nucleation, leading to the formation of larger crystals. However, at higher supersaturation levels, crystal nucleation becomes a more dominant process, resulting in a larger population of smaller crystals competing for growth within the same system (258). Results from this dataset are portrayed in the graphs below (Figure 54-Figure **57**), illustrating the correlation between the growth rate (y-axis) and temperature (x-axis). This visualisation highlights the influence of temperature on growth rates, especially at elevated impurity concentrations, observed at both high and low supersaturation levels on faces A and B. It is crucial to emphasise that some data points were excluded from the plots because either standard deviation information was unavailable or there were insufficient data points for meaningful comparisons, resulting from the MODDE sweet spot data generation process.
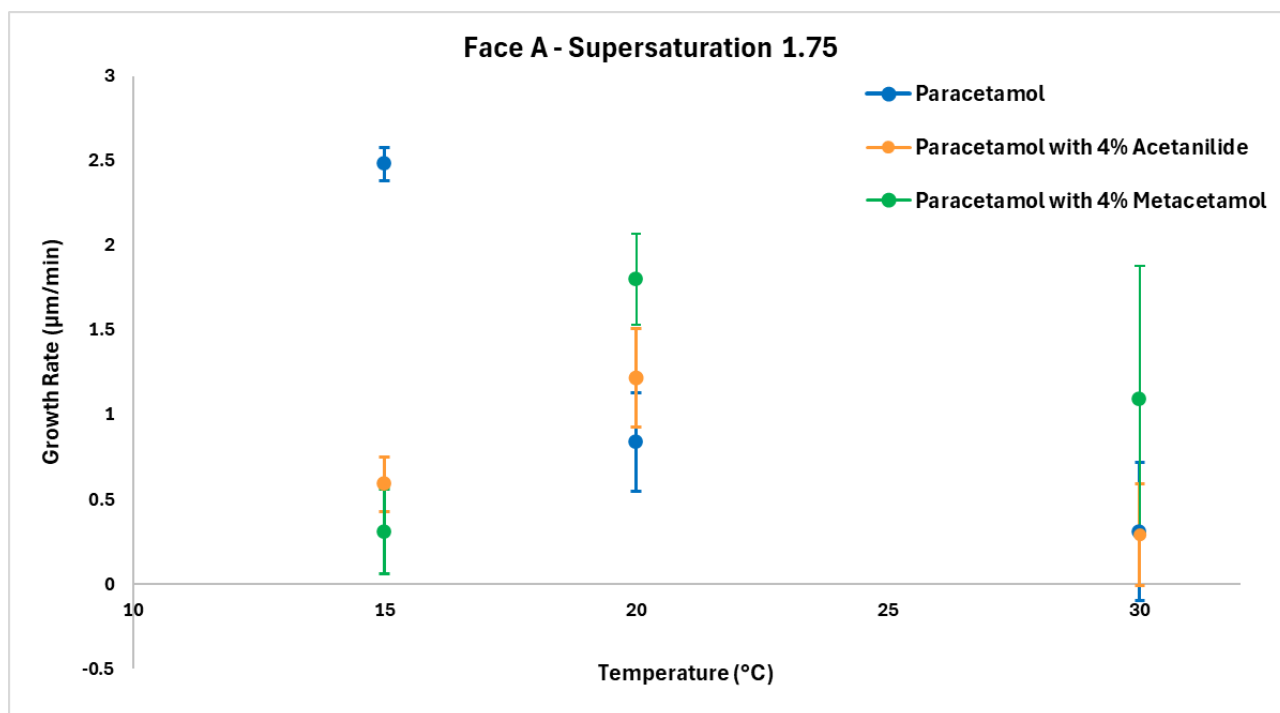
Figure 54: Face A at supersaturation 1.75: Growth rate (µm min^{-1}) vs temperature (°C) for various impurity concentrations.
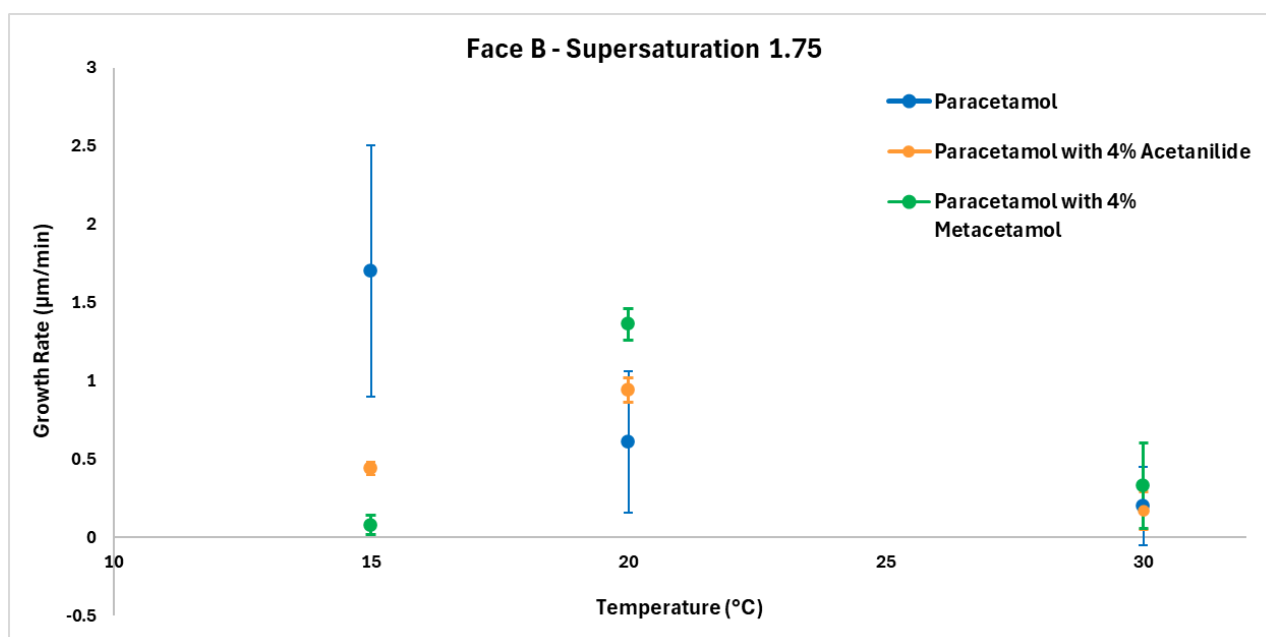
Figure 55: Face B at supersaturation 1.75: Growth rate (µm min^{-1}) vs temperature (°C) for various impurity concentrations.
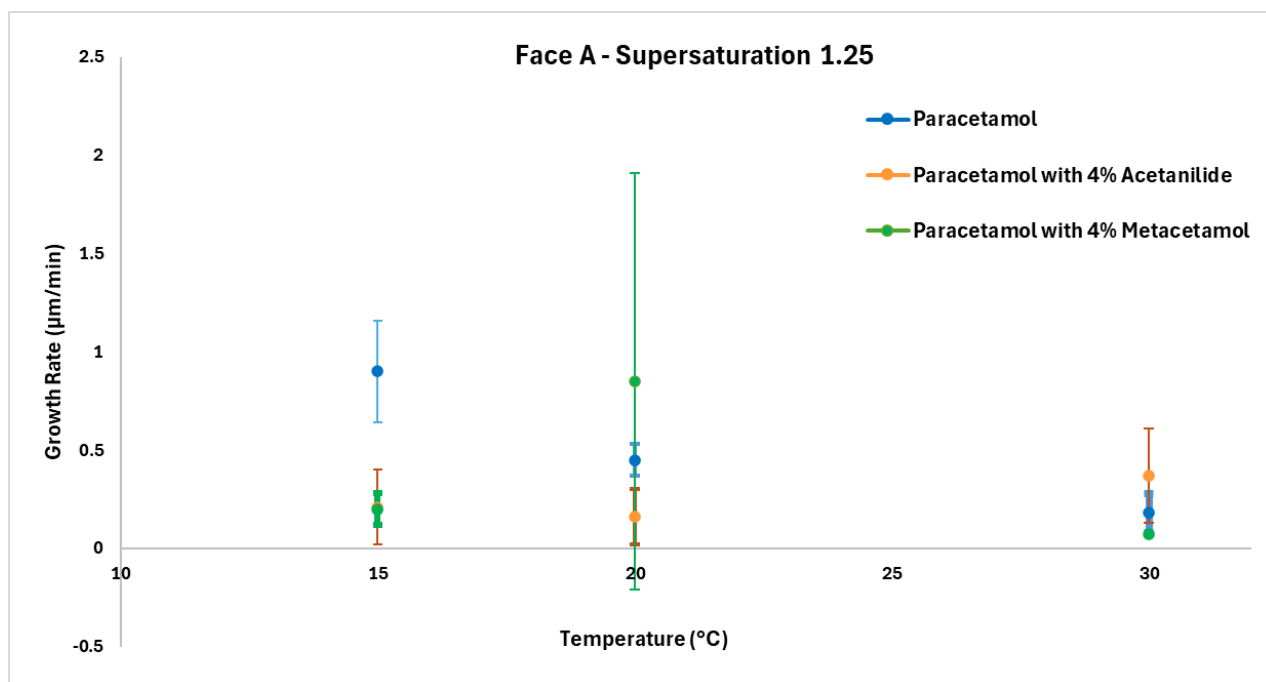
Figure 56: Face A at supersaturation 1.25: Growth rate (μm min^{-1}) vs temperature (°C) for various impurity concentrations.
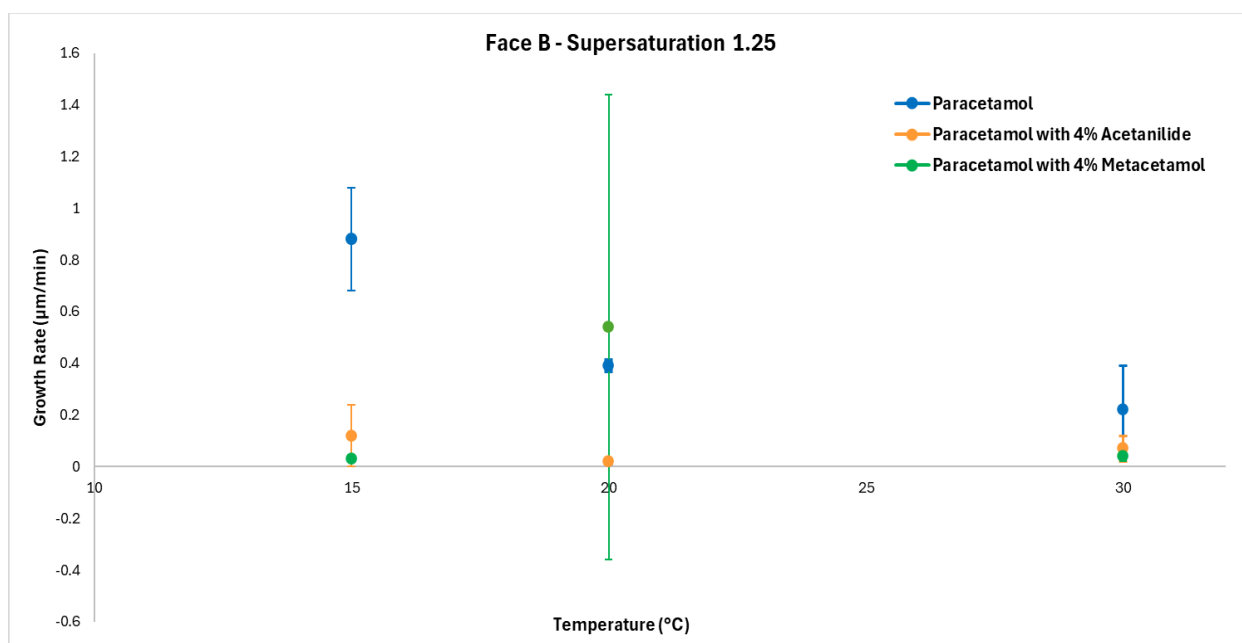
Figure 57: Face B at supersaturation 1.25: Growth rate (μm min^{-1}) vs temperature (°C) for various impurity concentrations.

Chapter 5: Single Crystal Growth with and without Ultrasonic Intervention

In the context of the compiled data, this pattern was not consistently observed in all cases. This discrepancy can be attributed to the presence of different crystal habits that were measured together, which may have influenced the observed growth rates and deviated from the expected trends. Therefore, Table 12 was compiled based on crystal habit and the indexing of assigned faces.

When comparing systems with and without impurities, it was observed that impurities generally decelerated the growth rate in both face directions. Across various temperatures and supersaturation levels, the growth rates consistently decreased, except for the case of 4% acetanilide at S = 1.25 and 30 °C, where face A exhibited a growth rate of 0.38 ± 0.24 μm min^{-1}, compared to 0.16 ± 0.12 μm min^{-1} in the condition without impurity addition. The crystal habits for both conditions were similar, with elongated needle-like shapes, as depicted in Figure 45-Figure **46**.

A rise in growth rate was additionally noted at 20 °C, with supersaturations 1.25 and 1.75 for both pairs of faces in a system containing 4% metacetamol. The crystal habits exhibit significant differences when comparing paracetamol with and without the impurity addition, suggesting that the presence of the impurity has a considerable impact on the growth rate. At a supersaturation of 1.25, a more equant shape is observed, whereas the addition of the impurity results in the presence of elongated crystals along with some equant-shaped ones. Similarly, at a supersaturation of 1.75, the presence of needles and diamond-shaped crystals is observed. With the addition of impurities, diamond-shaped crystals are more prominent, while the needle-like shapes, which contribute to a smaller size distribution, are absent. At 30 °C and a supersaturation of 1.75, with 4% metacetamol, an increase in crystal size is observed for both pairs of faces compared to crystals without impurity addition. When comparing the effects of impurities, it was found that metacetamol had the most significant impact on reducing growth rates at 15 and 30 °C, whereas acetanilide showed greater dominance at 20 °C. For a more detailed analysis of Table 11, refer to Appendix B, Section 1.1.

5.1.4: MODDE: growth rate correlations and predictions

Using the MODDE DoE software, scaled and centred coefficient plots were generated. Three individual factors were considered, denoted by the labels Sup (supersaturation), Temp (temperature) and Imp (impurity), along with three combinations: Sup*Temp (supersaturation and temperature), Sup*Imp (supersaturation and impurity) and Temp*Imp (temperature and impurity). The measured responses of face A and face B were analysed and presented in Figure 58. The error bars in the figure represent 95% confidence intervals, indicating the uncertainty associated with each coefficient. The data is represented using vertical error bars.

When examining the individual impact of these factors on face A, it becomes evident that supersaturation has the most significant influence, resulting in an approximate increase of 0.5 µm per minute in the growth rate. Conversely, altering the temperature has a notable effect on reducing the growth rate by around 0.35 µm per minute. For face B, increasing supersaturation leads to an increase in the growth rate, while elevating the impurity concentration and temperature both result in a decrease in the growth rate. Combining supersaturation and temperature is predicted to result in a growth rate increase of approximately 0.1 µm per minute (Figure 58). These observations regarding the role of temperature are unexpected, as it is generally presumed that crystal growth rates increase with increasing temperature (7). However, two additional factors should be considered the alteration in crystal habit (refer to Figure 45-Figure **46**) and the initial size of the monitored crystal.
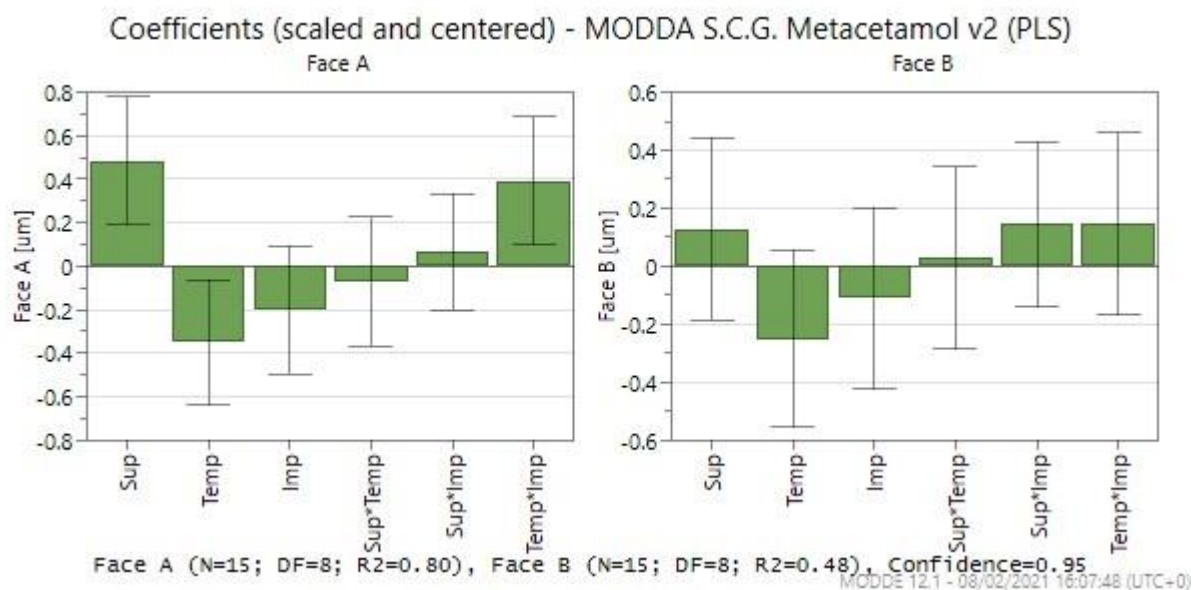
Figure 58: Coefficient plots prepared using DOE, showing six factors (Sup- supersaturation, Temp- temperature, Imp- impurity, Supt*Temp- supersaturation and temperature, Sup*Imp-supersaturation and impurity, Temp*Imp- temperature and impurity).

MODDE enables the visualisation of data through a 4-D response contour plot. An example of such a plot for faces A and B can be found in Figure 59, which displays the predicted response values based on the selected factors. These graphs reveal that for face A, in the absence of impurities, the growth rate increases with higher supersaturation and lower temperature. For example, a 2 µm min^{-1} growth rate is predicted for a supersaturation of 1.64 and a temperature of 15.8 °C, with a 2% impurity present.

The MODDE model predicts an average increase in crystal size of at least 0.5 µm per minute in all cases. Similarly, a decrease in temperature and an increase in supersaturation are associated with higher growth rates. For instance, growth rates of 1.5 µm can be achieved at temperatures around 17 °C and a supersaturation level of 1.65. However, when 4% impurity is added, reduced growth is predicted, with only 1 µm of growth expected at temperatures near 18 °C and a supersaturation of 1.6. In the case of face B, the growth rates display more variability. Without impurity addition, the greatest growth of 1 µm is observed at lower temperatures (<16 °C) and supersaturation levels (<1.28). When 2% impurity is introduced, the largest growth

183

rate of 0.7 µm is observed with increased supersaturation (>1.68) and a temperature decrease to approximately <17 °C. With 4% impurity addition, the growth rates appear to level off around 22 °C, with the largest growth rate observed at a supersaturation level greater than 1.6.
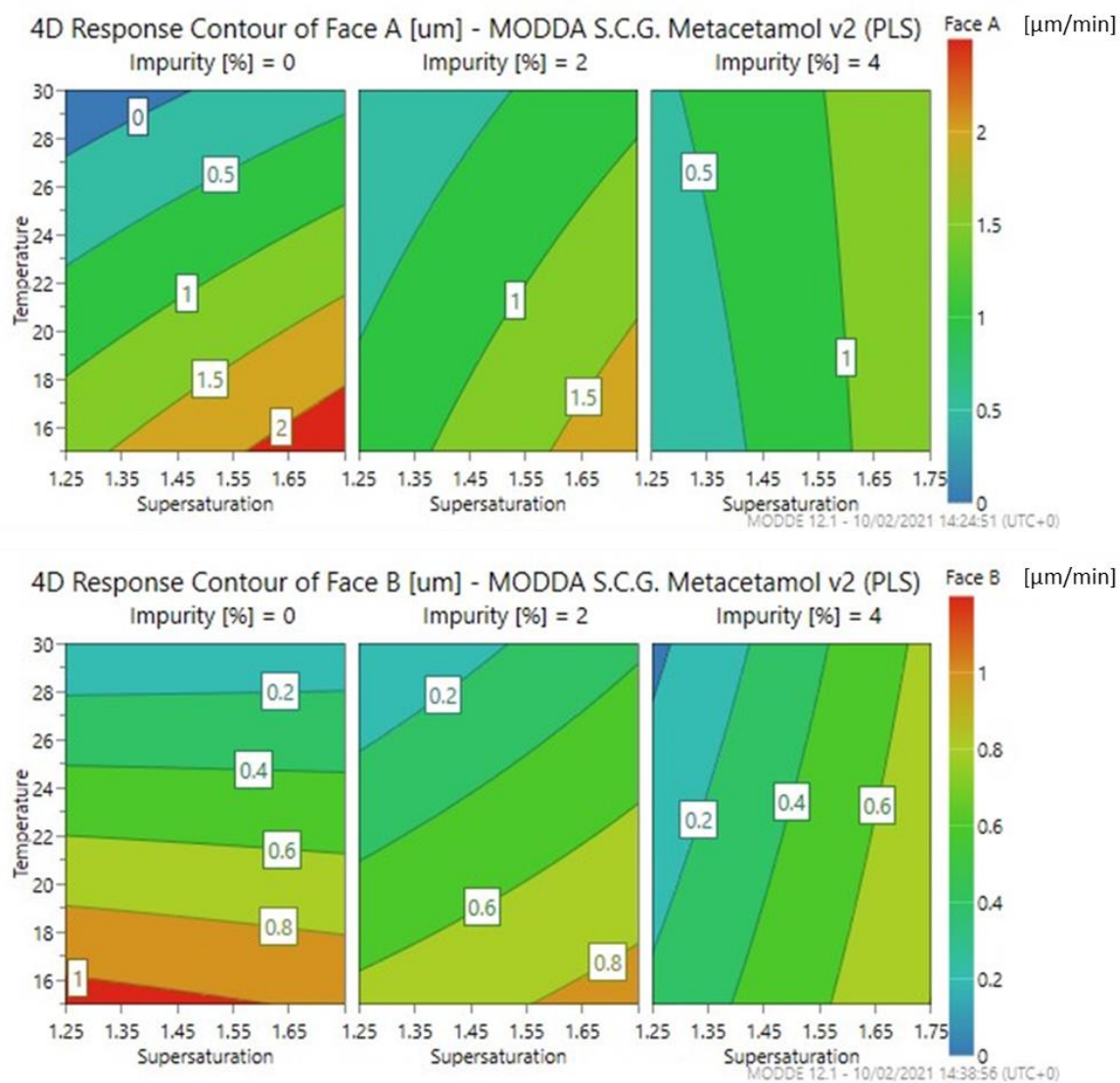
Figure 59: MODDE predicted growth rates in ethanol as a function of impurity, temperature, and supersaturation.
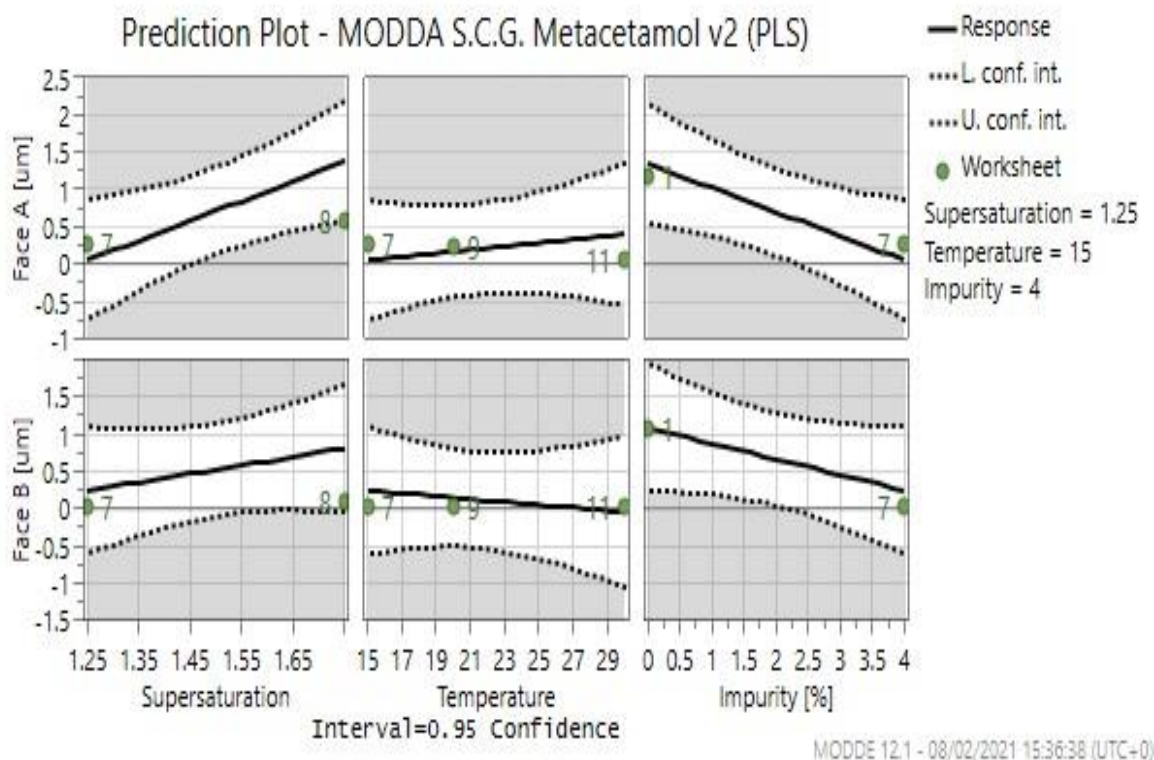
Figure 60: MODDE predicted plot vs observed data of paracetamol in ethanol at supersaturation 1.25, temperature 15 °C and impurity 4% metacetamol.

MODDE can be used for predictive purposes based on the input factors and responses provided   to   the   software. Figure 60 demonstrates MODDE's predictions for both face A and face B, indicating a slight increase in growth rate with higher supersaturation. However, when examining the green-numbered dots representing experimental data, it becomes apparent that there is a slight growth increase observed for face B, while face A exhibits a slight decrease. Moving to the following columns, MODDE predicts a marginal growth rate increase with higher temperature for face A and a slight decrease for face B. Once again, the green data points indicate a slight deviation from the predictions. Although the data points align closely with the predictions, they exhibit a decrease in growth rate.

When reviewing the data above, which follows the conventional method of discussing and analysing single crystal growth rate data, it became evident that there were additional factors requiring further investigation. As a result, an alternative analysis

approach was employed, taking into account factors such as crystal habit, index of the dominant face, indices of face pairs, total measurement time for the crystals, initial size of crystals measured in the A and B directions, final size of crystals measured in the A and B directions, and the percentage growth rate in the A and B directions. This analysis is presented in Table 12.

5.1.5: Single crystal growth habit and indexing

The information provided in Table 12 presents the measurements of single crystal growth rates obtained from multiple crystals under identical conditions. The data encompasses various temperatures, supersaturations, and impurity concentrations, including cases involving a single impurity and the simultaneous presence of two impurities. Additionally, the data includes conditions with and without the application of ultrasound achieved through the vibrations generated by an ultrasonic toothbrush.

The determination of the intensity output from the ultrasonic toothbrush within the stagnant cell was not conducted, as it operates in the MHz region associated with medical ultrasound. The available needle hydrophone technology suitable for the stagnant cell only covered the 20-100 kHz range typically used for sonochemistry. The toothbrush manufacturer confirmed that the sound frequency of the toothbrush is 1.65 MHz per second. Consequently, mapping the ultrasound field within the stagnant cell was not feasible, limiting the investigation to a phenomenological rather than quantitative approach. In conditions involving the addition of ultrasound, overall, there are fewer variations in habits, even under the same conditions, with a preference for truncated habits.

Table 12: The percentage growth rate of pairs of parallel faces of paracetamol crystals with the addition of 2 and 4% metacetamol and acetanilide, individually and as mixtures, at σ= 1.25, 1.5, and 1.75 and at temperatures of 15, 20, and 30 °C, along with associated habits and indexing of pairs of faces, in no ultrasound (No US) and with ultrasound (US).

Material	Temperature (°C)	Supersaturation (σ)	Habit	Index of dominant face	Index of pair of faces in A and B direction respectively	Growth rate of pairs of faces parallel to dominant face in A and B direction (μm min⁻¹)
Paracetamol (No US)	15	1.25	Truncated	$(10\bar{1})$	(011) and $(0\bar{1}\bar{1})$	0.52
					$(0\bar{1}1)$ and $(01\bar{1})$	0.54
		1.75	Truncated	$(10\bar{1})$	(011) and $(0\bar{1}\bar{1})$	1.06
					$(0\bar{1}1)$ and $(01\bar{1})$	1.12
			Needle	$(0\bar{1}1)$	$(1\bar{1}0)$ and $(\bar{1}01)$	0.24
					$(0\bar{1}\bar{1})$ and (011)	1.10
			Diamond	$(10\bar{1})$	(011) and $(0\bar{1}\bar{1})$	1.35
					$(01\bar{1})$ and $(0\bar{1}1)$	1.41
	20	1.25	Truncated	$(10\bar{1})$	(011) and $(0\bar{1}\bar{1})$	0.24
					$(0\bar{1}1)$ and $(01\bar{1})$	0.23
		1.75	Needle	$(0\bar{1}1)$	$(1\bar{1}0)$ and $(\bar{1}01)$	0.07
					$(0\bar{1}\bar{1})$ and (011)	0.29
			Diamond	$(10\bar{1})$	(011) and $(0\bar{1}\bar{1})$	1.56
					$(01\bar{1})$ and $(0\bar{1}1)$	1.95
	30	1.25	Diamond	$(10\bar{1})$	(011) and $(0\bar{1}\bar{1})$	0.01
					$(01\bar{1})$ and $(0\bar{1}1)$	0.03
			Equant	$(0\bar{1}1)$	(011) and $(0\bar{1}0)$	0.09
					$(\bar{1}\bar{1}1)$	0.11
		1.75	Truncated	$(10\bar{1})$	(011) and $(0\bar{1}\bar{1})$	5.69
					$(0\bar{1}1)$ and $(01\bar{1})$	5.47
			Diamond	$(10\bar{1})$	(011) and $(0\bar{1}\bar{1})$	0.24
					$(01\bar{1})$ and $(0\bar{1}1)$	0.13
			Multi-faceted	$(10\bar{1})$	(110)	2.04
					$(01\bar{1})$	2.15
Paracetamol and 2% acetanilide (No US)	15	1.5	Truncated	$(10\bar{1})$	(011) and $(0\bar{1}\bar{1})$	0.59
					$(0\bar{1}1)$ and $(01\bar{1})$	0.56
			Multi-faceted	$(10\bar{1})$	(110)	0.08
					$(01\bar{1})$	0.10
Paracetamol and 4% acetanilide (No US)	15	1.25	Multi-faceted	$(10\bar{1})$	(110)	0.04
					$(01\bar{1})$	0.03
		1.75	Diamond	$(10\bar{1})$	(011) and $(0\bar{1}\bar{1})$	1.36
					$(01\bar{1})$ and $(0\bar{1}1)$	1.54
	20	1.25	Diamond	$(10\bar{1})$	(011) and $(0\bar{1}\bar{1})$	0.91
					$(01\bar{1})$ and $(0\bar{1}1)$	0.61
			Needle	$(0\bar{1}1)$	$(1\bar{1}0)$ and $(\bar{1}01)$	0.07
					$(0\bar{1}\bar{1})$ and (011)	0.78
		1.75	Diamond	$(10\bar{1})$	(011) and $(0\bar{1}\bar{1})$	3.24
					$(01\bar{1})$ and $(0\bar{1}1)$	3.01
	30	1.25	Needle	$(0\bar{1}1)$	$(1\bar{1}0)$ and $(\bar{1}01)$	0.04
					$(0\bar{1}\bar{1})$ and (011)	0.26
		1.75	Diamond	$(10\bar{1})$	(011) and $(0\bar{1}\bar{1})$	0.34

					$(01\bar{1})$ and $(0\bar{1}1)$	0.28
			Needle	$(0\bar{1}1)$	$(1\bar{1}0)$ and $(\bar{1}01)$	0.03
					$(0\bar{1}\bar{1})$ and (011)	0.06
			Multi-faceted	$(10\bar{1})$	(110)	1.64
					$(01\bar{1})$	3.86
Paracetamol and 2% metacetamol (No US)	15	1.5	Truncated	$(10\bar{1})$	(011) and $(0\bar{1}\bar{1})$	0.69
					$(0\bar{1}1)$ and $(01\bar{1})$	0.64
Paracetamol and 4% metacetamol (No US)	15	1.25	Truncated	$(10\bar{1})$	(011) and $(0\bar{1}\bar{1})$	0.30
					$(0\bar{1}1)$ and $(01\bar{1})$	0.22
			Multi-faceted	$(10\bar{1})$	(110)	0.01
					$(01\bar{1})$	0.02
		1.75	Truncated	$(10\bar{1})$	(011) and $(0\bar{1}\bar{1})$	0.95
					$(0\bar{1}1)$ and $(01\bar{1})$	2.28
			Needle	$(0\bar{1}1)$	$(1\bar{1}0)$ and $(\bar{1}01)$	0.42
					$(0\bar{1}\bar{1})$ and (011)	2.54
	20	1.25	Diamond	$(10\bar{1})$	(011) and $(0\bar{1}\bar{1})$	0.64
					$(01\bar{1})$ and $(0\bar{1}1)$	1.09
			Needle	$(0\bar{1}1)$	$(1\bar{1}0)$ and $(\bar{1}01)$	0.07
					$(0\bar{1}\bar{1})$ and (011)	0.45
		1.75	Diamond	$(10\bar{1})$	(011) and $(0\bar{1}\bar{1})$	0.77
					$(01\bar{1})$ and $(0\bar{1}1)$	1.02
	30	1.25	Needle	$(0\bar{1}1)$	$(1\bar{1}0)$ and $(\bar{1}01)$	0.25
					$(0\bar{1}\bar{1})$ and (011)	0.68
			Diamond	$(10\bar{1})$	(011) and $(0\bar{1}\bar{1})$	0.32
					$(01\bar{1})$ and $(0\bar{1}1)$	0.55
		1.75	Needle	$(0\bar{1}1)$	$(1\bar{1}0)$ and $(\bar{1}01)$	3.80
					$(0\bar{1}\bar{1})$ and (011)	12.99
			Truncated	$(10\bar{1})$	(011) and $(0\bar{1}\bar{1})$	0.95
					$(0\bar{1}1)$ and $(01\bar{1})$	0.89
			Multi-faceted	$(10\bar{1})$	(110)	9.19
					$(01\bar{1})$	14.41
Paracetamol (US)	15	1.25	Multi-faceted	$(10\bar{1})$	(110)	0.54
					$(01\bar{1})$	0.48
			Truncated	$(10\bar{1})$	(011) and $(0\bar{1}\bar{1})$	0.42
					$(0\bar{1}1)$ and $(01\bar{1})$	0.35
		1.75	Needle	$(0\bar{1}1)$	$(1\bar{1}0)$ and $(\bar{1}01)$	0.18
					$(0\bar{1}\bar{1})$ and (011)	0.97
	20	1.25	Multi-faceted	$(10\bar{1})$	(110)	0.57
					$(01\bar{1})$	0.67
			Truncated	$(10\bar{1})$	(011) and $(0\bar{1}\bar{1})$	0.68
					$(0\bar{1}1)$ and $(01\bar{1})$	0.70
		1.75	Needle	$(0\bar{1}1)$	$(1\bar{1}0)$ and $(\bar{1}01)$	0.23
					$(0\bar{1}\bar{1})$ and (011)	1.20
	30	1.25	Equant	$(0\bar{1}1)$	(011) and $(0\bar{1}0)$	0.73
					$(\bar{1}\bar{1}1)$	0.83
		1.75	Multi-faceted	$(10\bar{1})$	(110)	3.01
					$(01\bar{1})$	5.12
			Truncated	$(10\bar{1})$	(011) and $(0\bar{1}\bar{1})$	3.51
					$(0\bar{1}1)$ and $(01\bar{1})$	3.64
			Needle	$(0\bar{1}1)$	$(1\bar{1}0)$ and $(\bar{1}01)$	0.93
					$(0\bar{1}\bar{1})$ and (011)	4.71

Sample	Temp	Supersat.	Habit	Direction	Faces	Growth rate
Paracetamol and 2% acetanilide (US)	15	1.5	Diamond	(10$\bar{1}$)	(011) and (0$\bar{1}\bar{1}$)	0.48
					(01$\bar{1}$) and (0$\bar{1}$1)	0.51
Paracetamol and 4% acetanilide (US)	15	1.25	Multi-faceted	(10$\bar{1}$)	(110)	1.04
					(01$\bar{1}$)	0.91
		1.75	Diamond	(10$\bar{1}$)	(011) and (0$\bar{1}\bar{1}$)	1.41
					(01$\bar{1}$) and (0$\bar{1}$1)	1.07
			Needle	(0$\bar{1}$1)	(1$\bar{1}$0) and ($\bar{1}$01)	0.08
					(0$\bar{1}\bar{1}$) and (011)	0.49
	20	1.25	Multi-faceted	(10$\bar{1}$)	(110)	0.26
					(01$\bar{1}$)	0.16
		1.75	Diamond	(10$\bar{1}$)	(011) and (0$\bar{1}\bar{1}$)	1.72
					(01$\bar{1}$) and (0$\bar{1}$1)	0.96
			Needle	(0$\bar{1}$1)	(1$\bar{1}$0) and ($\bar{1}$01)	0.07
					(0$\bar{1}\bar{1}$) and (011)	0.56
	30	1.25	Needle	(0$\bar{1}$1)	(1$\bar{1}$0) and ($\bar{1}$01)	0.15
					(0$\bar{1}\bar{1}$) and (011)	0.47
		1.75	Needle	(0$\bar{1}$1)	(1$\bar{1}$0) and ($\bar{1}$01)	0.17
					(0$\bar{1}\bar{1}$) and (011)	0.52
Paracetamol and 2% metacetamol (US)	15	1.25	Needle	(0$\bar{1}$1)	(1$\bar{1}$0) and ($\bar{1}$01)	0.04
					(0$\bar{1}\bar{1}$) and (011)	0.56
		1.5	Multi-faceted	(10$\bar{1}$)	(110)	2.88
					(01$\bar{1}$)	2.59
		1.75	Needle	(0$\bar{1}$1)	(1$\bar{1}$0) and ($\bar{1}$01)	0.14
					(0$\bar{1}\bar{1}$) and (011)	0.72
Paracetamol and 4% metacetamol (US)	20	1.25	Needle	(0$\bar{1}$1)	(1$\bar{1}$0) and ($\bar{1}$01)	0.01
					(0$\bar{1}\bar{1}$) and (011)	0.04
		1.75	Multi-faceted	(10$\bar{1}$)	(110)	0.17
					(01$\bar{1}$)	0.26
			Needle	(0$\bar{1}$1)	(1$\bar{1}$0) and ($\bar{1}$01)	0.33
					(0$\bar{1}\bar{1}$) and (011)	0.50
	30	1.25	Needle	(0$\bar{1}$1)	(1$\bar{1}$0) and ($\bar{1}$01)	0.03
					(0$\bar{1}\bar{1}$) and (011)	0.05
		1.75	Multi-faceted	(10$\bar{1}$)	(110)	0.19
					(01$\bar{1}$)	0.27

As observed in Table 12, segmenting the data according to individual habits results in a significant expansion of the table. This underscores the significance of avoiding averaging growth rates, especially when different habits are present. However, drawing meaningful comparisons becomes more challenging when compared with Table 11, as the data set becomes more fragmented and consistent habits are not found across all conditions. This makes drawing conclusive insights more difficult.
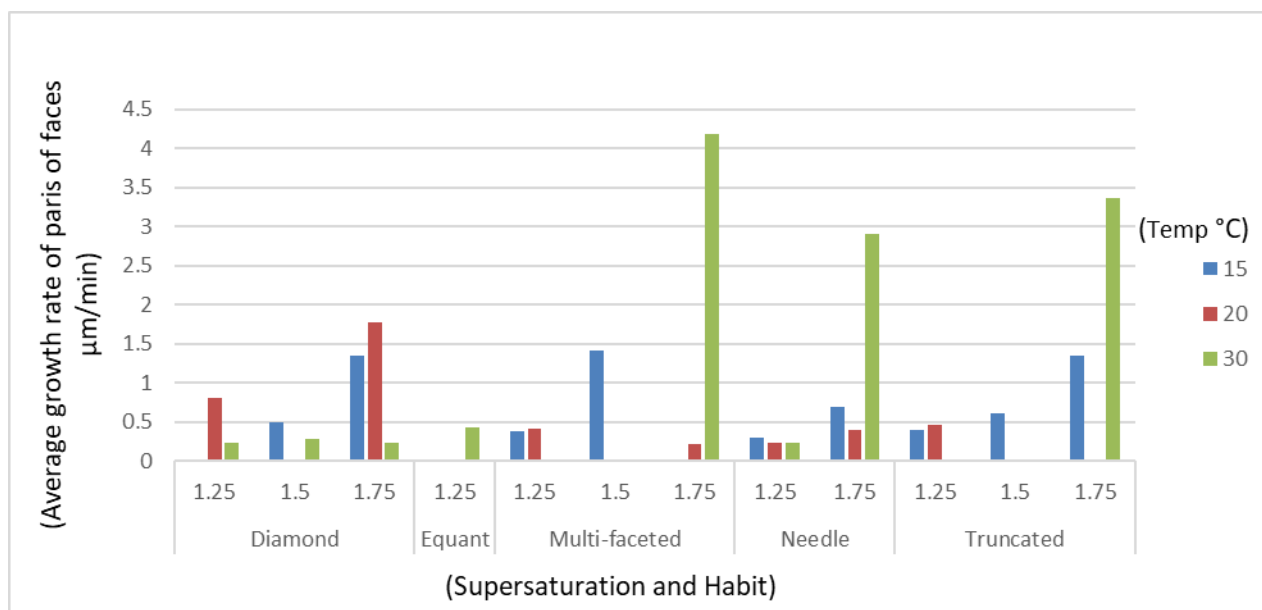
Figure 61: Average growth rate of pairs of faces (µm min⁻¹) vs supersaturation, habit, and temperature.

As anticipated, Figure 61 shows that when habits are distinguished, the average growth rate and supersaturation increases alongside rising temperatures. However, it should be noted that there are a few minor outliers. These deviations could initially be attributed to variations in initial size or the absence of replicates, which would affect the analysis of the data in Figure 61.
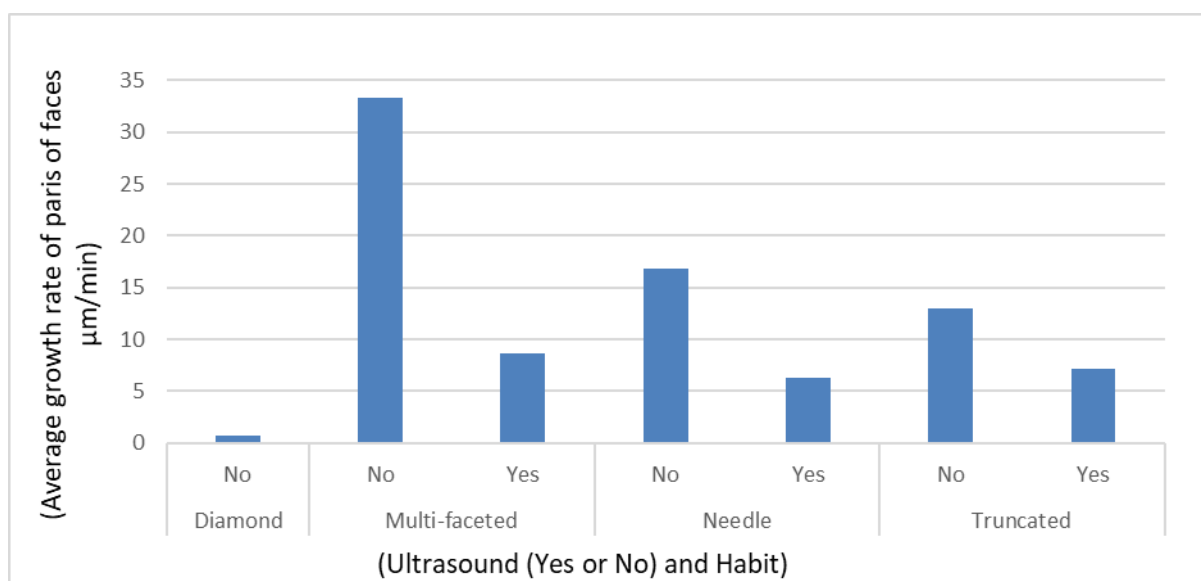
Figure 62: Average growth rate of pairs of faces (µm min⁻¹) vs the addition of ultrasound (Yes or No) and habits at S = 1.75 and 30 °C.

Based on Figure 62, it is evident that ultrasound does not exert a positive influence on the average growth rate of face pairs. Looking closer at individual results, at a temperature of 15 °C and a supersaturation of 1.75, the growth rate of the needle habit in the $(1\bar{1}0)$ and $(\bar{1}01)$ direction was 0.18 µm min^{-1} and 0.97 µm min^{-1}, respectively, while in the $(0\bar{1}\bar{1})$ and (011) direction, it was 0.24 µm min^{-1} and 1.10 µm min^{-1} without the presence of ultrasound. The application of ultrasound has the potential to improve mass transfer by disrupting the boundary layer surrounding crystals. This disruption facilitates an increased nutrient supply, resulting in higher growth rates. However, it is important to note that there are instances where the presence of ultrasound induces acoustic streaming or turbulence, which can adversely affect the growth process and impede overall crystal growth. This phenomenon is discussed in greater detail in Chapter 8.
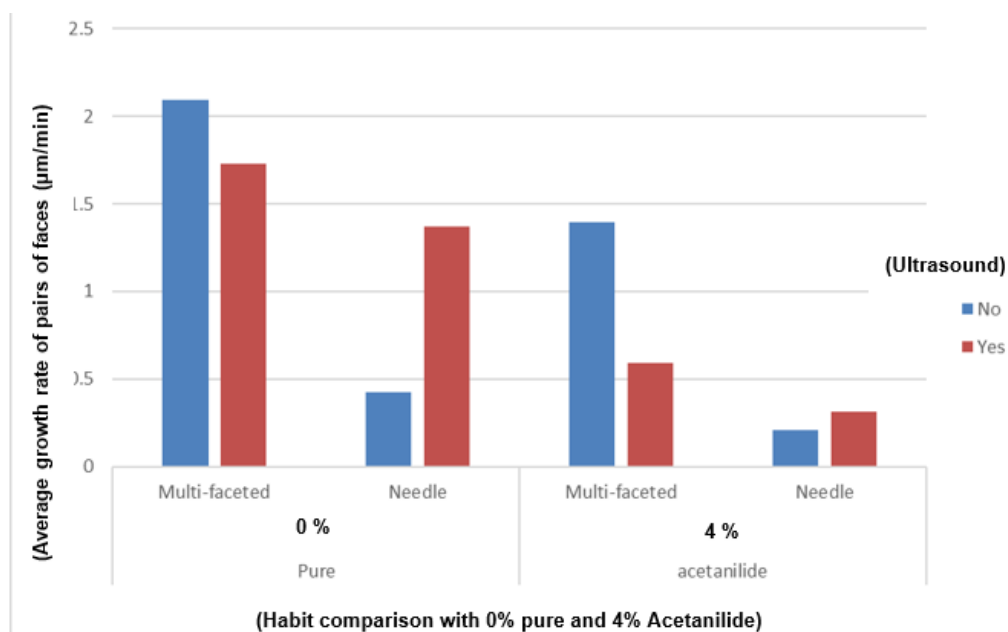
Figure 63: Average growth rate of pairs of faces (µm min^{-1}) vs habit comparison with 0 and 4% acetanilide and ultrasound addition (Yes or No).

In Figure 63, a comparison is presented regarding the influence of ultrasound on the average growth rates of crystal habits under different conditions (pure and 4% acetanilide). The results indicate that ultrasound was effective in boosting the growth rate of needle-like habits, both in pure conditions and in the presence of 4%

acetanilide. However, it did not lead to improvements in the growth rates of multi-faceted faces. It should be noted that not all crystal habits could be analysed, as there were no corresponding comparisons with the addition of ultrasound.
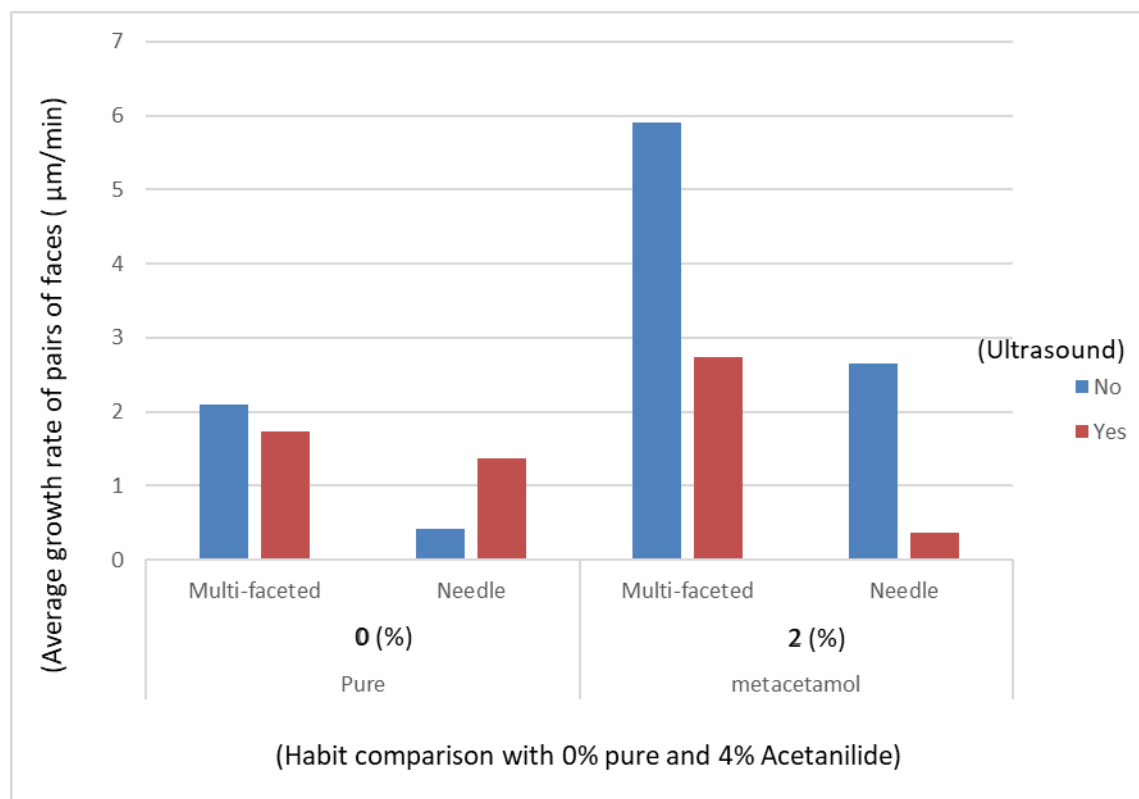
Figure 64: Average growth rate of pairs of faces (μm min^{-1}) vs habit comparison with 0 and 2% metacetamol and ultrasound addition (Yes or No).

Likewise, Figure 64 shows a marginal enhancement in the average growth rates of needle habits when ultrasound is introduced to paracetamol. However, when compared to the addition of 2% metacetamol, it was discovered that ultrasound hindered the growth. Interestingly, the average growth rate for both observed habits was found to increase with the addition of 2% metacetamol. This phenomenon could be attributed to the structural similarity between metacetamol and paracetamol, wherein metacetamol readily integrates into the developing crystal lattice, thus aiding the growth process. Furthermore, metacetamol has the potential to modify the surrounding solvent environment, influencing the solubility and supersaturation levels near the growing crystals.

5.2: Conclusions

This chapter has comprehensively analysed single crystal growth rates for paracetamol crystals, focusing on the influences of: temperature, supersaturation, impurities, and ultrasound. Key findings include a significant deviation in crystal habits from those outlined in existing literature, presenting new research directions. The analysis of growth rates across different crystal faces has revealed variable patterns and complex habits.

An unexpected correlation was observed where an increase in temperature is associated with a decrease in average growth rate across all crystal habits. However, when considering individual habits, growth rates actually increase with temperature, highlighting the necessity of habit-specific analysis.

The study also explored the impact of impurities. Metacetamol at a 4% concentration typically reduces growth rates, especially under certain conditions, but at 2%, it positively influences individual habits. Acetanilide affects crystal habits at higher supersaturations, producing results similar to those in purer systems.

Higher supersaturation levels have been linked to more consistent crystal habits and increased growth rates for individual habits. Temperature variations were found to affect crystal thickness, with lower temperatures resulting in thicker crystals and higher temperatures leading to truncated corners and lower growth ratios.

Furthermore, the application of ultrasound, through an ultrasonic toothbrush, was found to induce nucleation and affect crystal habits. This technique predominantly promotes needle-like habits and introduces new habits not observed in pure or impurity added conditions. Specifically, with 4% acetanilide, ultrasound was shown to enhance the growth rate of needle-like habits.

Overall, this chapter highlights the crucial role of various external factors in determining crystal habits and growth rates. It emphasises the complex nature of crystal growth and the importance of understanding specific growth conditions for accurate and efficient crystallisation processes.

Chapter 6:

Bulk Suspension Crystallisation with and Without Ultrasonic Intervention

Summary:

In this chapter, the effects of ultrasonic intervention in controlling: nucleation, crystal growth, morphology, crystal size distribution, yield, and product purity on bulk suspension crystallisation are described. The model system is paracetamol in ethanol with and without the addition of structurally related impurities, acetanilide and metacetamol, at 2 and 4 mol%. This experimental method and data analysis approach were also applied to crystallisation of paracetamol from isoamyl alcohol and the results have been published: "The Effect of Ultrasound on the Crystallisation of Paracetamol in the Presence of Structurally Related Impurities", Thai, T. H. Nguyen, Azeem Khan, Layla M. Bruce, Clarissa Forbes, Richard L. O'Leary and Chris J. Price, Crystals (DOI: 10.3390/cryst7100294). In both cases, the ultrasonic frequency investigated was 35 ± 3 kHz. The results indicate ultrasonic intervention; initiates nucleation at lower supersaturation, increases the nucleation rate, and hence decreases crystal size and size distribution. Agglomeration is also significantly reduced. Some changes in crystal morphology are observed. Ultrasound intervention was also found to increase the yield and improve product purity. These findings for crystallisation from ethanol are consistent with those reported for crystallisation from iso-amyl alcohol.

6.0: Introduction

In recent years, there has been a growing focus on optimising crystallisation processes through various methods and techniques (259-261). Sonocrystallisation, which involves the application of ultrasound in the crystallisation process (262), has a long history dating back to 1927, when Richard and Loomis investigated its effects on the properties of liquids and solids (263). Subsequent studies on ultrasound in crystallisation were conducted during the 1950s, 60s, and 70s (264-266).

Recent research has highlighted the potential of sonocrystallisation to induce and accelerate nucleation (49, 166, 168, 189, 195, 267-269), leading to reduced processing time and improved particle size distribution (PSD). It also has an impact on mean crystal size, agglomeration, and crystal habit (19, 49, 50, 172, 189, 196, 270). As a result, sonocrystallisation has attracted growing attention in different industries and processes, particularly in the enhancement of crystallisation processes. There is a pressing need to better understand and control these processes, driving the exploration of ultrasound applications. However, the documentation of the effects of sonocrystallisation on product purity, filtration properties, and crystal habits in the development of industrial processes remains limited.

The presence of impurities in a drug substance directly impacts the safety of the final drug product. Therefore, it is crucial to identify, quantify, and effectively control impurities throughout the crystallisation processes. In industrial settings, feed streams often contain impurities at concentrations of several mole percent, leading to unfavourable outcomes. These impurities can cause reductions in crystal growth (271), changes in crystal habits (272), prolonged processing time, and hinder the approach to equilibrium. In some cases, the resulting products are so impure that re-crystallisation is necessary to meet the required product specifications (128). Ruecroft (273) presents a study on the application of sonocrystallisation technology to remove impurities, specifically sodium oxalate, from the caustic process stream in the Bayer process. The results from laboratory experiments, pilot trials, and full-scale trials demonstrate the effectiveness of sonocrystallisation in reducing impurity concentrations and improving alumina productivity. The technology enhances crystal

formation and yield of sodium salts, resulting in increased efficiency and reduced operational costs. However, the paper lacks detailed information on the specific mechanisms and process parameters involved in sonocrystallisation. Additionally, the study primarily focuses on sodium oxalate and further research is needed to assess the technology's effectiveness in removing other impurities. Despite these limitations, the findings highlight the potential of sonocrystallisation to optimise the Bayer process by reducing impurities, increasing productivity, and minimising environmental impact.

In another report, Evrad (274) explored the use of sonocrystallisation by applying ultrasound during the crystallisation of coordination compound powders. The findings demonstrate that sonocrystallisation effectively controls the size, morphology, and purity of the powders. It reduces crystal size distribution, improves morphology, and maintains chemical integrity and magnetic behaviour. The technique enhances purity through efficient micromixing and can be applied to different coordination compounds. However, the study's limitations include its focus on a specific compound and the need for further research on generalisability and underlying mechanisms. Overall, sonocrystallisation shows promise for producing controlled and pure coordination compound powders.

Nguyen (128) investigated the effects of metacetamol and acetanilide on paracetamol crystallisation in isoamyl alcohol. Results from cooling crystallisation experiments, conducted with and without ultrasound, showed faster nucleation, changes in crystal size distribution, higher yields, and enhanced purity of the product crystals. Yet, the precise mechanisms driving these outcomes remain unclear. To date, this research appears to be the only one examining the impact of high-power ultrasound on paracetamol crystallisation with structurally similar impurities like metacetamol and acetanilide. Building on this, the following chapter will explore the potential of sonocrystallisation for enhancing crystal purity in ethanol solutions. It will also investigate sonocrystallisation's effects on yield, filtration, washing, and drying processes, as well as crystal habits, extending the research presented in Chapter 6 on single crystal growth. Moreover, the study will delve into established research areas, including nucleation point, rate of nucleation, control of crystal size distribution, and the degree of agglomeration. The comprehensive analyses aim to deepen the understanding of ultrasound's effects and benefits in crystallisation processes.

6.1: Results and discussion

6.1.1: Ultrasonic intensity profiling

Table 13: The ultrasonic intensity in ethanol, measured at four positions within the ultrasonic bath.

Positions on the stirrer plate at the bottom of the ultrasonic bath	Ultrasonic Intensity (mW cm^{-2})	
	50% Ultrasonic Power	100% Ultrasonic Power
1	1.11 +/- 0.93	3.77 + /- 2.44
2	0.30 +/- 0.18	4.43 +/- 3.74
3	0.49 + /- 0.17	3.16 +/- 2.36
4	0.25 +/- 0.12	4.74 +/- 5.88
Average values	**0.54 +/- 0.40**	**4.03 +/- 0.71**

The ultrasonic intensity was measured by Clarissa Forbes (164, 261). The volume of the bath was 25 L, and ultrasound was delivered using an 8-transducer array, which resulted in a non-uniform field. This is evident from the intensity measurements noted in Table 13. At 50% ultrasonic power, the intensities ranged from 0.25 mW cm^{-2} to 1.11 mW cm^{-2} and from 3.16 mW cm^{-2} to 4.74 mW cm^{-2} at 100% power. This data shows no linear descriptor between the percentage of ultrasonic powers. The crystallisation experiments were conducted at positions 2, 3, and 4. A blank flask was placed at position one, which contained ethanol and a thermometer. During these experiments, the intensity applied was: low and set at 50% ultrasonic power (0.34 ± 0.13 mW cm^{-2}), high intensity was set at 100% ultrasonic power (4.11 ± 0.84 mW cm^{-2}).

6.1.2: Nucleation temeprature, and time

Table 14: Summary of recorded nucleation temperatures with and without ultrasound during the crystallisation of paracetamol in the presence and absence of 2 and 4 mol% acetanilide and metacetamol.

Sample	Nucleation Temperature (°C)		
	Ultrasonic power 0%	Ultrasonic power 50%	Ultrasonic power 100%
Pure paracetamol	29.87 ± 0.36		42.15 ± 1.64
2% Acetanilide	29.20 ± 0.50		39.79 ± 4.0
2% Metacetamol	23.16 ± 11.19		41.17 ± 0.48
2% Acetanilide and 2% Metacetamol	25.54 ± 9.72	32.72 ± 2.56	33.62 ± 1.28
4% Acetanilide	23.75 ± 7.55		35.70 ± 3.23
4% Metacetamol	25.56 ± 8.50		30.74 ± 1.43
2% Acetanilide and 4% Metacetamol	18.03 ± 0.21		34.34 ± 3.11
4% Acetanilide and 2% Metacetamol	26.01 ± 7.85		31.79 ± 0.10
4% Acetanilide and 4% Metacetamol	22.91 ± 0.69		32.23 ± 3.11

Table 14 and Figure 65 present a summary of the nucleation temperature data obtained during the crystallisation of paracetamol in the presence and absence of 2 and 4 mol% acetanilide and metacetamol, with and without ultrasound. While some degree of variation in the data is expected, it is evident that the nucleation process is induced by the addition of ultrasound, leading to a significant increase in the number of nuclei. The exact nature of these nuclei, whether primary or secondary, is unclear. Nguyen (128) discussed how ultrasonic waves can cause fragmentation within the vessel, potentially resulting in secondary nucleation. Observations of particle growth and fragmentation in the samples support this possibility. Chow (39) noted that ultrasound can raise the nucleation temperature by 1 to 3 °C and observed an increase in cavitation events. They proposed that pre-existing ice crystals could be fragmented, leaving a population of crystal nuclei. Secondary nucleation may be caused by cavitation bubbles or high shear flows near cavitation sites.

Chapter 6: Bulk Suspension Crystallisation with and without Ultrasonic Intervention

As an example, in the crystallisation experiment with 2 mol% acetanilide and 2 mol% metacetamol, nucleation was observed at a temperature of 17.48 °C. When 100% ultrasonic power was introduced, nucleation occurred at 32.49 °C. In contrast, the system without impurities or ultrasound exhibited nucleation at approximately 29.87 °C. Although the temperature with 100% ultrasound (42.15 °C) was higher, it was lower than the system with impurity additions.

Similarly, Guo (189) found that ultrasound had a significant effect on the reduction of the induction time, the order of nucleation changed slightly, however the nucleation rate constant (k_N) showed a larger increase, as well as an improvement in the quality of the nuclei when compared with seeds by grinding. There are also many other examples in literature of a decrease in induction time being reported (50, 88, 168, 169, 196, 275, 276).
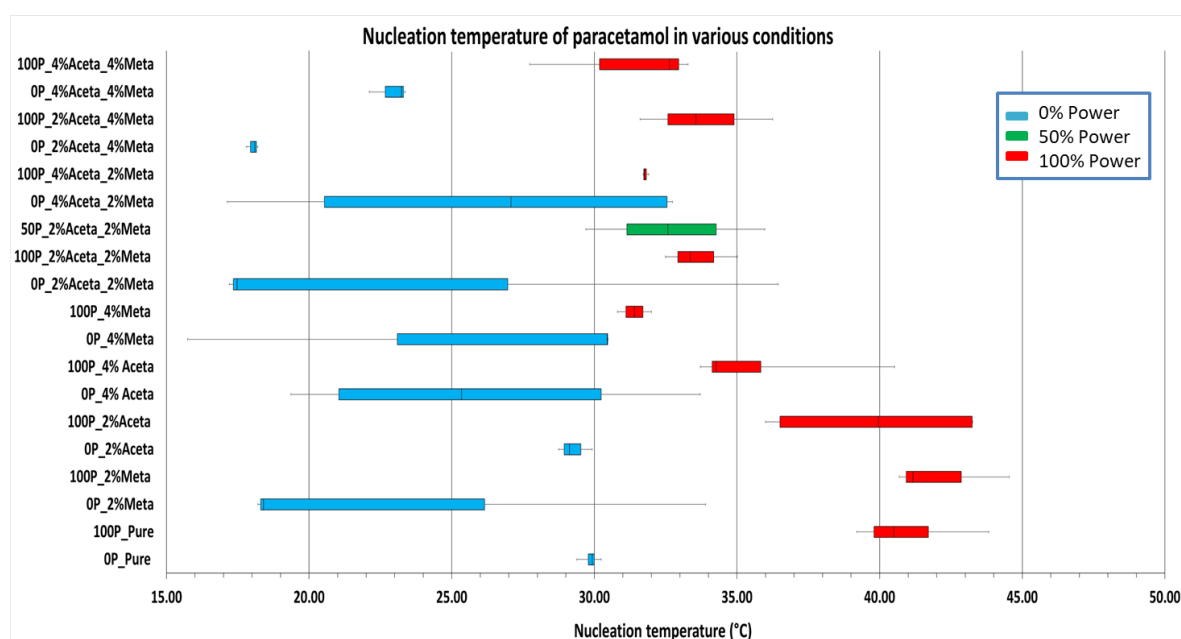
Figure 65: Bulk suspension cooling crystallisation data on nucleation temperature, recorded in triplicate with and without the addition of structurally related impurities, with a non-sonicated control sample compared against 50 and 100% ultrasonic power levels.

Figure 65 provides a visual representation of the distribution of nucleation data. In the non-sonicated samples, nucleation occurs later and at lower temperatures (higher supersaturations) compared to samples crystallised at 50 and 100% ultrasonic power. The presence of impurities further inhibits nucleation in all cases. A similar study

conducted by Keshavarz (80) investigated the impact of 4'chloroacetanilide or 4-nitrophenol impurities on the crystallisation of paracetamol in ethanol and 2-propanol. They observed a reduction in the nucleation rate of paracetamol by a factor of 1.9 or 2.6 due to the presence of 1 mol% impurity of 4'chloroacetanilide or 4-nitrophenol. They noted that 4-nitrophenol exhibited a more efficient inhibition of the nucleation rate compared to 4'chloroacetanilide. Both impurities hindered the formation of paracetamol clusters, resulting in longer growth times.

In the earlier publication by Nguyen (128), comparable results were noted with isoamyl alcohol, highlighting that ultrasound application raised the nucleation temperature. The study, however, did not delve into how various impurities affect the extent of the increase in the metastable zone width (MZW). On the other hand, Kim (19) mentioned that ultrasound irradiation of a solution results in a decrease in MZW. The impact of ultrasound on the MZW during the cooling crystallisation of paracetamol was examined by Jordens (2014), using a wide frequency range of 41-1140 kHz in a single reactor configuration. Minor variations in the MZW were observed among different transducers, while the power within the reactor was maintained constant through calorimetry. A reduction in MZW was identified across all ultrasonic frequencies, displaying an almost linear trend. The maximum reduction of 17 °C was observed at 41 kHz, with the reduction diminishing as the frequency increased (192).

The addition of ultrasound has been recognised as a promoter of primary and secondary nucleation, regardless of the system setup, frequencies and corresponding intensities. There is ample evidence to support the notion that sonication promotes nucleation even at low supersaturation levels and in solutions that are ostensibly particle-free (16, 128, 178, 197). Despite this understanding, the exact mechanism behind ultrasound-induced nucleation remains unknown (277).

Two classical mechanisms of secondary nucleation can be associated with this experiment. Firstly, collision breeding involves collisions between: crystal-crystal, crystal-wall vessel/internal, and crystal-stirrer (278). Secondly, fluid shear stress is another possibility wherein an ordered surface layer is disrupted. However, this mechanism would require a combination of high supersaturation and high shear levels. High shear levels have been observed in boiling processes during evaporative

crystallisation experiments, where bubble rupturing generates significant shear stress (279). This concept could also apply to cavitation bubbles, which have been theorised to act as nucleation centres. As the cavitation bubble grows to its critical size, it eventually collapses, leading to various effects such as regions of extreme excitation, the release of shockwaves, highly localised temperature increases (up to 5000 K), pressures of approximately 1000 bar, microjets, and improved mixing. These effects may contribute to the system's ability to overcome energy barriers associated with nucleation (19, 38, 45). However, such extreme temperatures are likely to degrade the solute and are far above the melting point of paracetamol.

Sanchez-garcia (187) investigated the effects of different ultrasonic frequencies and powers on lactose nucleation. They proposed that the increase in k-values (coefficient) and the reduction in induction time at low ultrasonic frequencies (20-44 kHz) could be attributed to transient cavitation, which is associated with a higher energy release from the large growth and more violent collapse of bubbles. They postulated that bubble collapse could provide enough energy to overcome the critical energy of nucleation, resulting in an acceleration of nucleation and a further decrease in induction time. If the bubble in the transient cavitation phase collapses on or near a growing crystal surface, it would result in shear stress, potentially breaking fragments from the surface, increasing supersaturation levels, and creating an opportunity for secondary nucleation (39-42, 280).

Similarly, Kim (173) found that cavitation bubbles acted as foreign bodies, creating opportunities for heterogeneous nucleation, especially when polyvinylpyrrolidone (PVP) was added. They stated that the kinetic prefactor of nucleation kinetics increased significantly due to PVP's inhibitory effect on bubble coalescence. PVP acts as a surface-active solute in hydrophilic solvents, thereby prolonging the lifetime of cavitation bubbles through absorption onto their surfaces.

Wan, Feng and Haar (2017) proposed that acoustic frequency plays a crucial role in determining cavitation bubble lifetime, size distribution, and collapse velocity. At higher frequencies, bubbles have less time to expand, resulting in smaller bubble sizes (281). Interestingly, it was found that 50% intensity was as effective as 100% intensity in terms of nucleation temperature (Figure 65). Low-frequency ultrasound can lead to

larger bubbles with smaller contact angles, which in turn become more effective in initiating nucleation (192). Similar results were reported by Kordylla (282) in a simulation of ultrasound-induced nucleation, where a reduction in contact angle correlated with an increase in the nucleation rate. Based on this observation, it can be presumed that larger foreign particles involved in nucleation result in smaller contact angles between the foreign surface and clusters, thereby reducing the activation energy required for nucleation.

Figure 66: Coefficient plots prepared using DoE and showing how the six factors (ult-ultrasound, Ace-acetanilide, Met-metacetamol, Ult*Ace-ultrasound and acetanilide, Ult*Met-ultrasound and metacetamol, Ace*Met- acetanilide and metacetamol) influenced nucleation temperature.

When examining the coefficient plots generated by MODDE DOE for nucleation temperature in Figure 66, it becomes clear that ultrasound plays a dominant role in initiating nucleation at higher temperatures, resulting in a 5 °C increase in nucleation temperature. Metacetamol and acetanilide, impede nucleation causing a decrease in the nucleation temperature. The inhibitory effect of metacetamol (approximately 2.2 °C reduction) is more pronounced than that of acetanilide (approximately 1.2 °C reduction). However, the introduction of ultrasound alleviates the inhibitory effects of the impurities, leading to a slight increase in nucleation temperature of about 0.15 and 0.25 °C for metacetamol and acetanilide samples with ultrasound, respectively.

Interestingly, when both impurities are simultaneously added, there is an unexpected increase in nucleation temperature by approximately 1 °C, contrary to what would be anticipated based on the behaviour of individual impurities. The underlying reason for this phenomenon remains unknown.
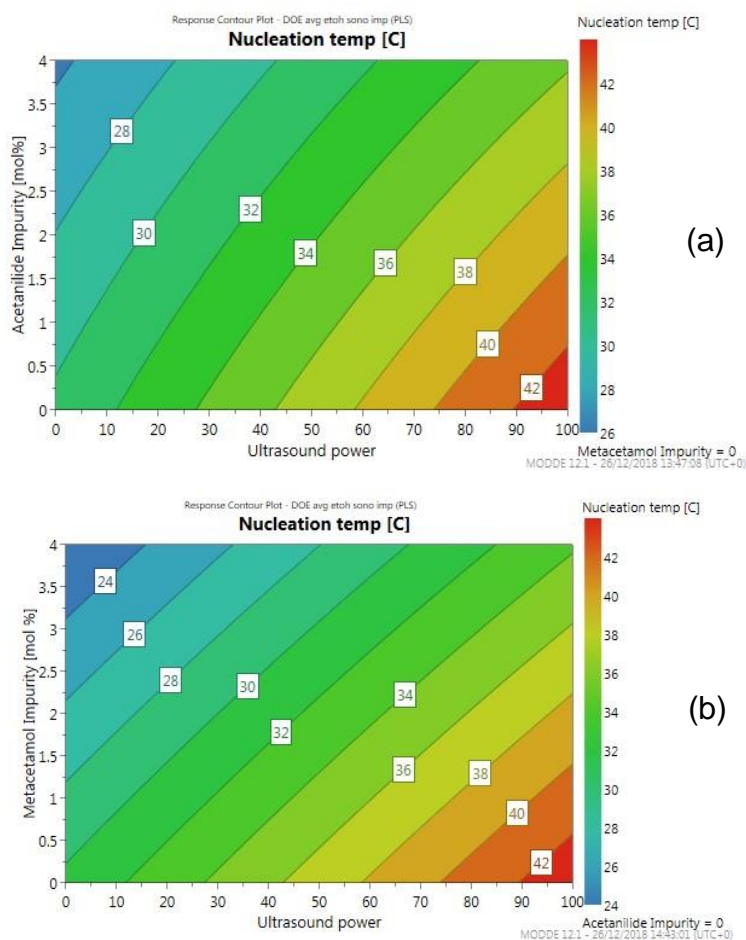
Figure 67: Response contour plot depicting the effect of ultrasonic power (ranging from 0 to 100%) has on (a) Nucleation temperature with the addition of acetanilide and (b) Nucleation temperature with the addition of metacetamol.

When examining Figure 67, the response contour plot generated by MODDE revealed that the nucleation temperature was elevated with the introduction of ultrasound power. This temperature increase was more pronounced in the presence of acetanilide (a) when compared with metacetamol (b). Furthermore, the addition of impurity mol% had a greater impact on impeding the decrease in nucleation temperature, particularly in the case of metacetamol.

6.1.3: Filtration (particle isolation)

The separation of mother liquors and subsequent washes after crystallisation was achieved through filtration. Due to the total volume of the crystallisation vessel, the slurry was divided into approximately equal suspensions for filtration. However, obtaining similar filtration results proved challenging, as it was difficult to separate the suspension into portions with the same solid loading, even when the volumes were matched. This highlights the difficulties that can arise in performing wet solids handling operations on a small scale.

For comparison, the last filtrate of each sample, which typically had the highest particle concentration, was graphically plotted in Figure 68 (a). The graph depicts the volume of collected filtrate (m^3) against time (s), providing information on filtration duration and the filtration rate of both sonicated and non-sonicated samples with and without the addition of impurity mixtures. Additionally, Figure 68 (b) presents the elapsed time/cumulative volume of filtrate ($t\,v^{-1}$) against the volume of collected filtrate (v), showing the results for sonicated and non-sonicated samples with and without impurity mixtures.

To provide a representative measurement of the filtration data collected, Table 15 summarises the averages across all three suspensions and replicates. The table includes information on filtration rate, filtration duration, and filter cake resistance.

(a)

(b)
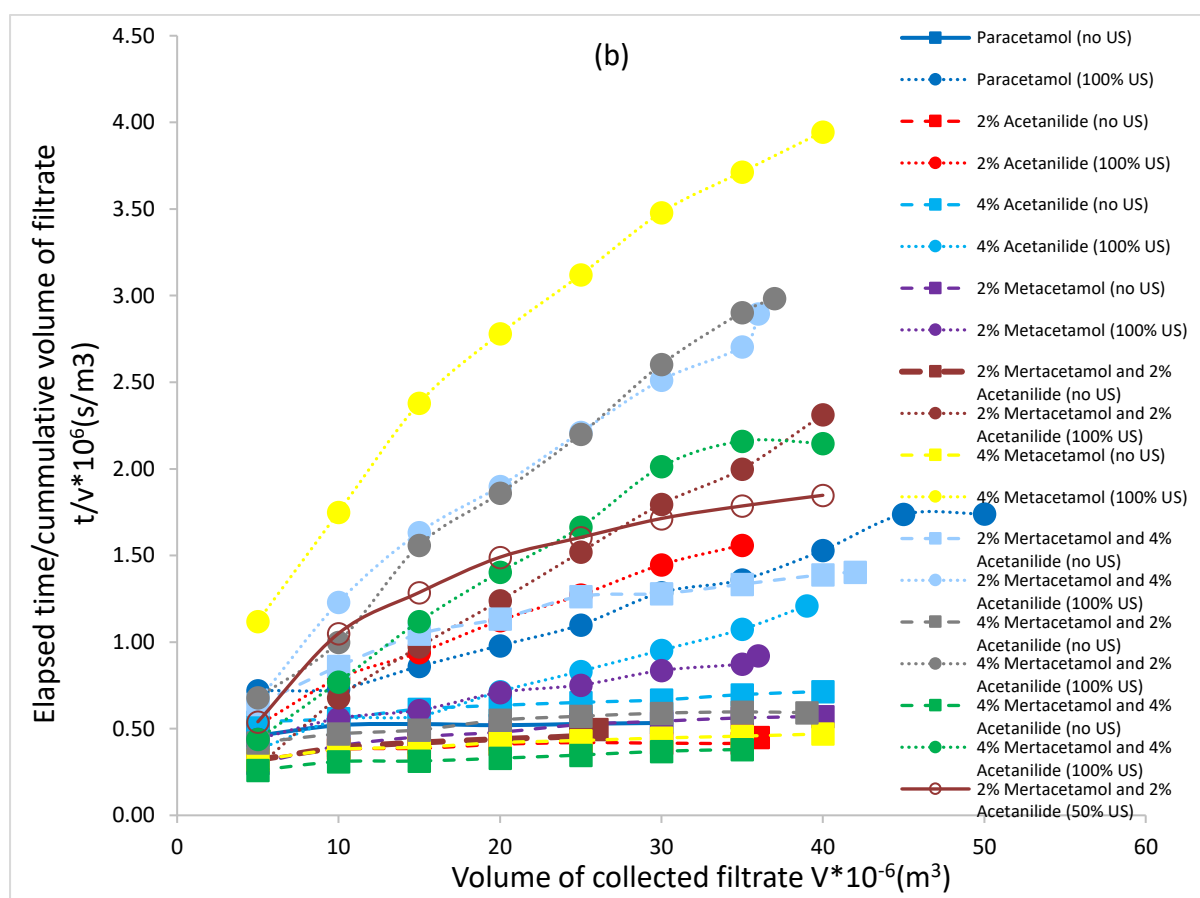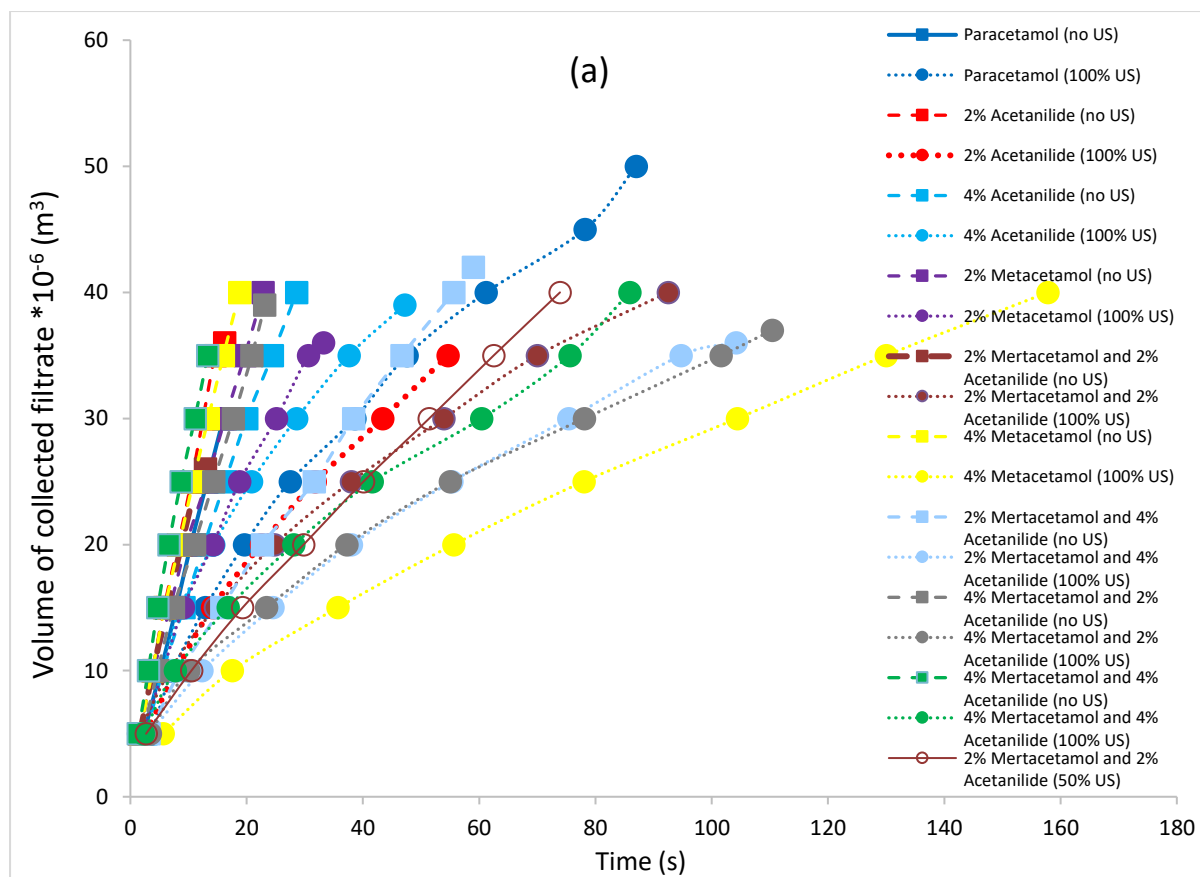
Figure 68: (a) A graphical representation of the volume of collected filtrate (m^3) versus time (s), showing the filtration duration and rate of filtration of sonicated and non-sonicated samples with and without the addition of impurity mixtures and (b) The elapsed time/ cumulative volume of filtrate ($t\,v^{-1}$) versus volume of collected filtrate (v), showing results for sonicated and non-sonicated samples with and without the addition of impurity mixtures.

Table 15: Summary of the average across all three suspensions and replicates to provide a representative measurement of the filtration rate, filtration duration, and filter cake resistance of pure and impure samples with and without ultrasonic intervention.

Sample	Filtration time (s)	Filtration rate ($m^3\,s^{-1}$)	Cake resistance ($m\,kg^{-1}$)
Paracetamol (no ultrasound)	24.2 ± 11.0	2.01x10^{-6}	1.15x10^8
Paracetamol (100% ultrasound)	67.5 ± 17.9	6.11x10^{-7}	1.14 x10^9
2% Aceta (no ultrasound)	22.8 ± 0.6	1.89x10^{-6}	1.31 x10^8
2% Aceta (100% ultrasound)	86.0 ± 24.8	5.00x10^{-7}	1.72 x10^9
2%Meta (no ultrasound)	25.1 ± 4.3	1.67 x10^{-6}	2.58 x10^8
2% Meta (100% ultrasound)	71.7 ± 54.8	6.42 x10^{-7}	1.51 x10^9
2% Aceta and 2%Meta (no ultrasound)	27.9 ± 5.8	1.56 x10^{-6}	3.37 x10^8
2% Aceta and 2%Meta (100% ultrasound)	97.9 ± 25.0	3.67 x10^{-7}	2.95 x10^9
2% Aceta_2%Metac (50% ultrasound)	66.4 ± 33.0	6.34 x10^{-7}	1.69 x10^9
4% Aceta (no ultrasound)	25.6 ± 6.1	1.98 x10^{-6}	2.11 x10^8
4% Aceta (100% ultrasound)	53.4 ± 14.7	6.45 x10^{-7}	1.34 x10^9
4% Meta (no ultrasound)	41.0 ± 19.3	1.25 x10^{-6}	8.65 x10^8
4% Meta (100% ultrasound)	128.4 ± 13.3	2.67 x10^{-7}	3.32 x10^9
2% Aceta and 4% Meta (no ultrasound)	24.7 ± 5.5	1.67 x10^{-6}	2.94 x10^8
2% Aceta and 4% Meta (100% ultrasound)	102.3 ± 13.6	3.22 x10^{-7}	3.22 x10^9
4% Aceta and 2% Meta (no ultrasound)	32.3 ± 10.1	1.52 x10^{-6}	7.76 x10^8
4% Aceta and 2% Meta (100% ultrasound)	106.4 ± 4.7	3.11 x10^{-7}	2.93 x10^9
4% Aceta and 4% Meta (no ultrasound)	29.0 ± 9.7	1.32 x10^{-6}	7.15 x10^8
4% Aceta and 4% Meta (100% ultrasound)	95.3 ± 13.7	3.67 x10^{-7}	2.51 x10^9

When comparing the effect of ultrasound on filtration performance (Table 15), it is evident that the presence of ultrasound increases the filtration duration for all samples analysed. For instance, the filtration duration for paracetamol without ultrasound was 24.2s, while the addition of ultrasound extended the filtration duration to 67.5s. This observation holds true for all samples, also aligning with the smaller crystal size observed in sonicated materials. The introduction of impurities had a significant impact

on filtration performance. For instance, the addition of 4% acetanilide increased the filtration duration to 128s. As there is a change in particle habit and a reduction in size with the sonicated samples (supported by data in microscopy and FBRM analysis) this will, in turn, alter the compaction behaviour within the filtration cake as the solvent moves through narrower pore sizes between the crystals during filtration, therefore affecting the filtration time and filtration rate.

The cake resistance, as indicated by the data in Figure 68 and Table 15, also demonstrates an increase. For paracetamol without ultrasound, the cake resistance ranged from 1.15×10^8 kg m^{-1}. With the addition of 50 and 100% ultrasound, as well as both impurities, the corresponding resistance values were 1.69×10^9 and 2.95×10^9 kg m^{-1}, respectively. The gradients in Figure 68 (b) are much steeper for the non-sonicated samples compared to the sonicated samples, and Figure 68 (a) shows that the filtration duration for non-sonicated samples is significantly shorter. Notably, the addition of 4% metacetamol with 100% ultrasound power has the most pronounced effect on filtration performance, which could be attributed to the ability of metacetamol to incorporate into paracetamol crystals.

Overall, ultrasound reduces particle size, resulting in increased filtration duration, decreased filtration rate, and increased filtration resistance. The decrease in particle size is also associated with an increase in yield. Therefore, if the quantity of material in the system to be filtered increases, the overall time and resistance to filtration will be further heightened. For example, the yield of paracetamol without ultrasound was 44%, which slightly increased to 45% with the addition of ultrasound. Conversely, the addition of 4% metacetamol resulted in yields of 36% without ultrasound and 49% with ultrasound.

To apply Darcy's equation for cake resistance, the viscosity of the mother liquor was measured using a GV500 viscometer (Hydramotion, Malton, UK). The viscosity measurements were performed on the following solutions: pure ethanol, an ethanol-paracetamol mixture, and a sonicated solution of paracetamol in ethanol with the addition of 4% metacetamol and 4% acetanilide. A comparison of viscosity values is shown in Figure 69.

The results indicated that the addition of paracetamol to ethanol increased the viscosity, while there was not much difference in viscosity between the sonicated and non-sonicated samples. Both mother liquors recorded a consistent viscosity value of 0.0022 Pa·s at the desired temperature of 15 °C.
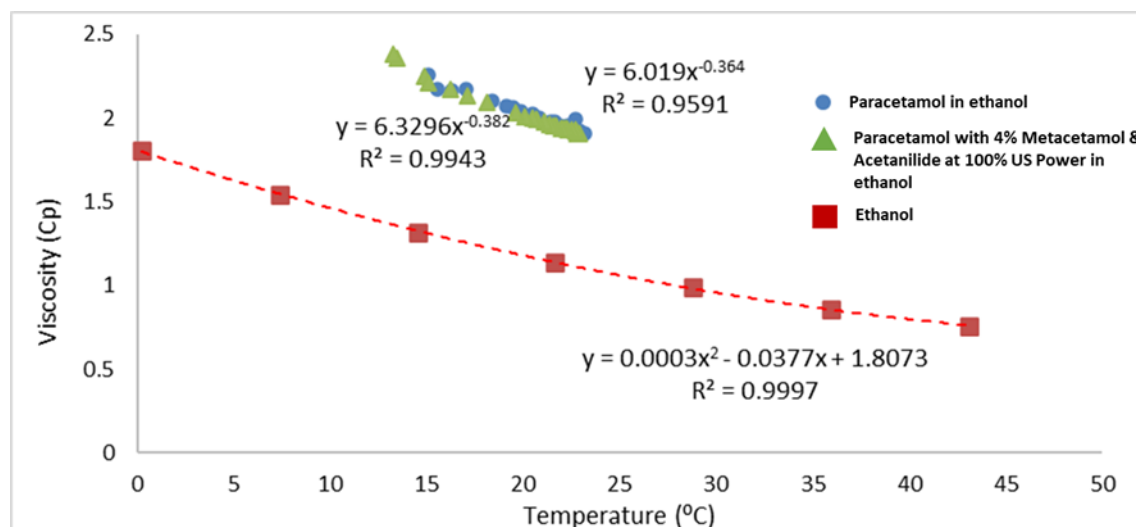
Figure 69: Viscosity of the mother liquor of paracetamol in ethanol, pure ethanol, and paracetamol with 4% acetanilide and 4% metacetamol in ethanol with the addition of 100% ultrasonic power.

6.1.4: Crystal size distribution

The data presented in Table 16 demonstrates that ultrasound intervention leads to a reduction in the distribution of crystal sizes. The wet particle size distribution (measured using FBRM) is smaller than the dry particle size distribution (measured using SYMPATEC). This discrepancy arises from the ability of particles to agglomerate during filtration, washing, and drying steps. The addition of impurities significantly inhibits crystal growth. For instance, the FBRM data for pure paracetamol without ultrasound (0% power) exhibits a mean square rate (chord length) of 108.6 µm. However, with the addition of 2% acetanilide, the mean square rate reduces to 92.5 µm. Further reduction is observed when 4% acetanilide and 4% metacetamol are added, resulting in a mean square rate of 58 µm. When the acetanilide concentration is increased to 4%, the mean square rate increases to 98 µm, likely due to increased agglomeration, as depicted in Figure 73-Figure 77. Comparatively, paracetamol grown

in the presence of metacetamol shows a significantly lower mean square rate compared to the effect of acetanilide as a dissolved impurity, as shown in the impurity percentage within the HPLC cake analysis presented in Table 16. This difference can be attributed to metacetamol's ability to effectively attach to the crystal surface and become incorporated within the crystal lattice without impeding the arrival of other molecules. Furthermore, metacetamol's disruptive properties are found to inhibit the nucleation process (251).

A comparison of the wet (108.6 $\pm$ 5.1 µm) and dry (125.3 $\pm$ 35.4 µm) data obtained from Sympatec and FBRM reveals notable differences. For instance, at 0% power, the dry particle data exhibits more scattering, and the overall particle size is greater. This could be attributed to particles clumping together during the drying process. In the case of the Sympatec analysis, the non-sonicated cake required breaking apart before analysis, whereas the sonicated cake did not. This is evident from the decrease in size observed in the wet analysis. However, the particle sizes in the dry analysis are still slightly larger than those in the cake analysis, with higher standard deviations that align with the wet samples.

Table 16: Comparison of FBRM (Wet) and SYMPATEC (dry) PSD, with and without ultrasonic intervention and with the addition of impurities. Samples were measured in triplicate, with the error shown.

Sample	Ultrasonic power 0%	Ultrasonic power 50%	Ultrasonic power 100%
Paracetamol Wet (µm)	108.6 ± 5.1		69.6 ± 9.4
2% Acetanilide Wet (µm)	92.5 ± 1.7		48.1 ± 6.1
2% Metacetamol Wet (µm)	74.5 ± 11.8		43.5 ± 1.4
2% Acetanilide and 2% Metacetamol Wet (µm)	79.2 ± 18.1	40.2 ± 4.6	41.1 ± 0.6
4% Acetanilide Wet (µm)	98.0 ± 1.5		44.1 ± 3.5
4% Metacetamol Wet (µm)	66.8 ± 22.0		30.1 ± 0.6
4% Acetanilide and 2% Metacetamol Wet (µm)	61.1 ± 31.7		32.4 ± 0.3
2% Acetanilide and 4% Metacetamol Wet (µm)	74.5 ± 4.7		30.6 ± 0.9
4% Acetanilide and 4% Metacetamol Wet (µm)	58.0 ± 9.0		32.5 ± 0.4
Paracetamol Dry (µm, x50)	125.3 ± 35.4		74.3 ± 12.0
2% Acetanilide Dry (µm, x50)	175.3 ± 11.7		51.8 ± 14.6
2% Metacetamol Dry (µm, x50)	133.3 ± 68.0		93.6 ± 33.7
2% Acetanilide and 2% Metacetamol Dry (µm, x50)	114.6 ± 28.8	84.7 ± 78.1	74.8 ± 32.8
4% Acetanilide Dry (µm, x50)	104.4 ± 20.2		56.1 ± 21.2
4% Metacetamol Dry (µm, x50)	123.0 ± 67.3		36.7 ± 3.2
4% Acetanilide and 2% Metacetamol Dry (µm, x50)	109.9 ± 50.9		39.2 ± 4.0
2% Acetanilide and 4% Metacetamol Dry (µm, x50)	133.0 ± 22.4		35.1 ± 2.6
4% Acetanilide and 4% Metacetamol Dry (µm, x50)	108.1 ± 65.3		34.7 ± 0.9
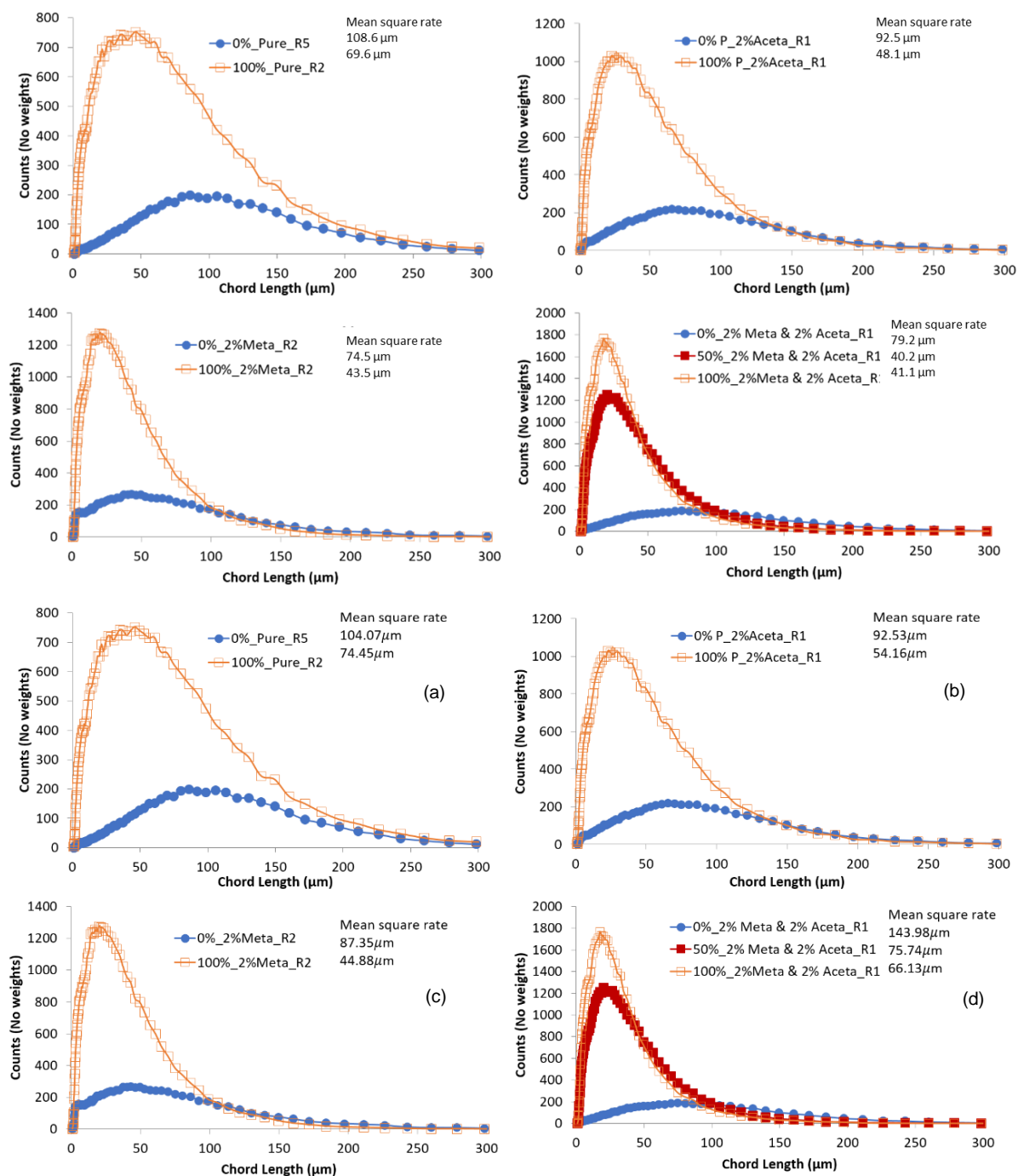
Figure 70: FBRM particle size distribution of (a) Pure paracetamol, (b) The addition of 2% acetanilide, (c) The addition of 2% metacetamol and (d) The addition of 2% acetanilide and 2% metacetamol with and without the addition of ultrasound at 50% and 100% power.

Ultrasound has been associated with crystal breakage and fragmentation (178, 200). The proximity of agglomerate breakage to cavitation bubble collapse has been theorised (202) and this was experimentally confirmed by Guo (203). The implosions of cavitation bubbles, as well as the vibrations and collisions of crystals, resulted in

de-agglomeration. If the formation of agglomerates is similarly reduced, as observed when adding 50% power, the introduction of impurities in a non-sonicated system will result in a decrease in particle size distribution. This reduction in overall particle size can be explained by the theory that ultrasound intervention promotes the growth of secondary nuclei, thereby reducing the growth rate of crystals within the solution. Figure 70 illustrates a pure system with the addition of impurities, both separately and as mixtures, with 50% ultrasonic power (0.34 ± 0.13 mW cm^{-2}) and 100% ultrasonic power (4.11 ± 0.84 mW cm^{-2}). The mean square rate (crystal size) decreased, with 50% power having a lesser effect on particle size compared to 100%, as expected.

Similarly, in a study on the use of ultrasound to enhance industrial crystallisation, it was found that the crystal size distribution (CSD) could be tailored by adjusting the duration of ultrasound power input into the system. A short burst of ultrasound-induced nucleation at lower supersaturation levels, allowed for the growth of larger crystals. On the other hand, continuous or extended bursts of ultrasound resulted in higher nucleation rates, increasing the number of particles at the expense of crystal growth. Pulsed or intermittent application of ultrasound produced intermediate effects (16). Assuming that pulsed application is similar to 50% ultrasonic power, this aligns with the findings of this study.

In another study focusing on the cooling crystallisation of paracetamol, pulsed ultrasound was used, resulting in a nearly 70% reduction in particle size. It was suggested that as the crystal passed through sonicated and silent regimes, the particle size decreased due to breakage and secondary nucleation. This reduction in particle size was correlated with the intensity of ultrasound, where the time spent in the ultrasonic zone determined the final crystal size (186). This observation is also evident in the current study when comparing continuous 100% ultrasonic power with pulsed 50% ultrasonic power.

Regarding particle breakage, various theories have been mentioned in the literature. One theory involves the production of microjets from asymmetric bubble collapse, which primarily affects particles larger than 200 μm. Another significant contributor to particle breakage and reduction in size (184) is the direct interaction of shockwaves produced by the expansion and rapid collapse of cavities, leading to high local

temperatures and pressures that generate pressure shockwaves. These shockwaves cause interparticle collisions, damaging nearby objects and contributing to a reduction in average particle size and size distribution.
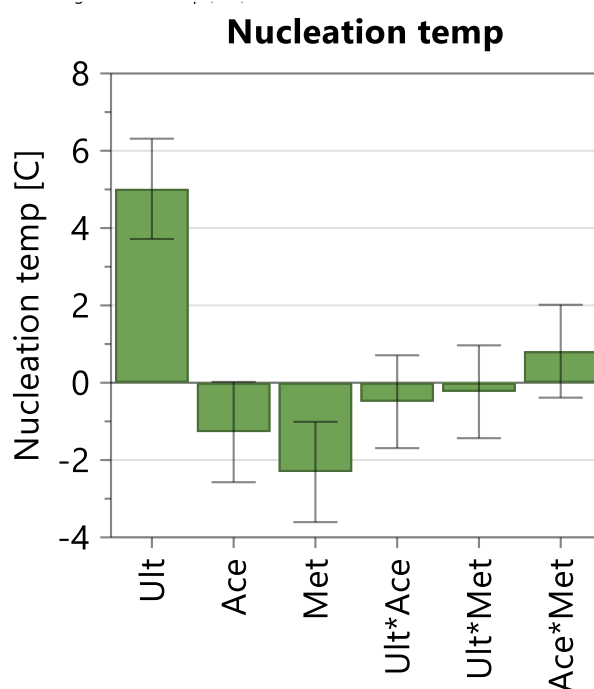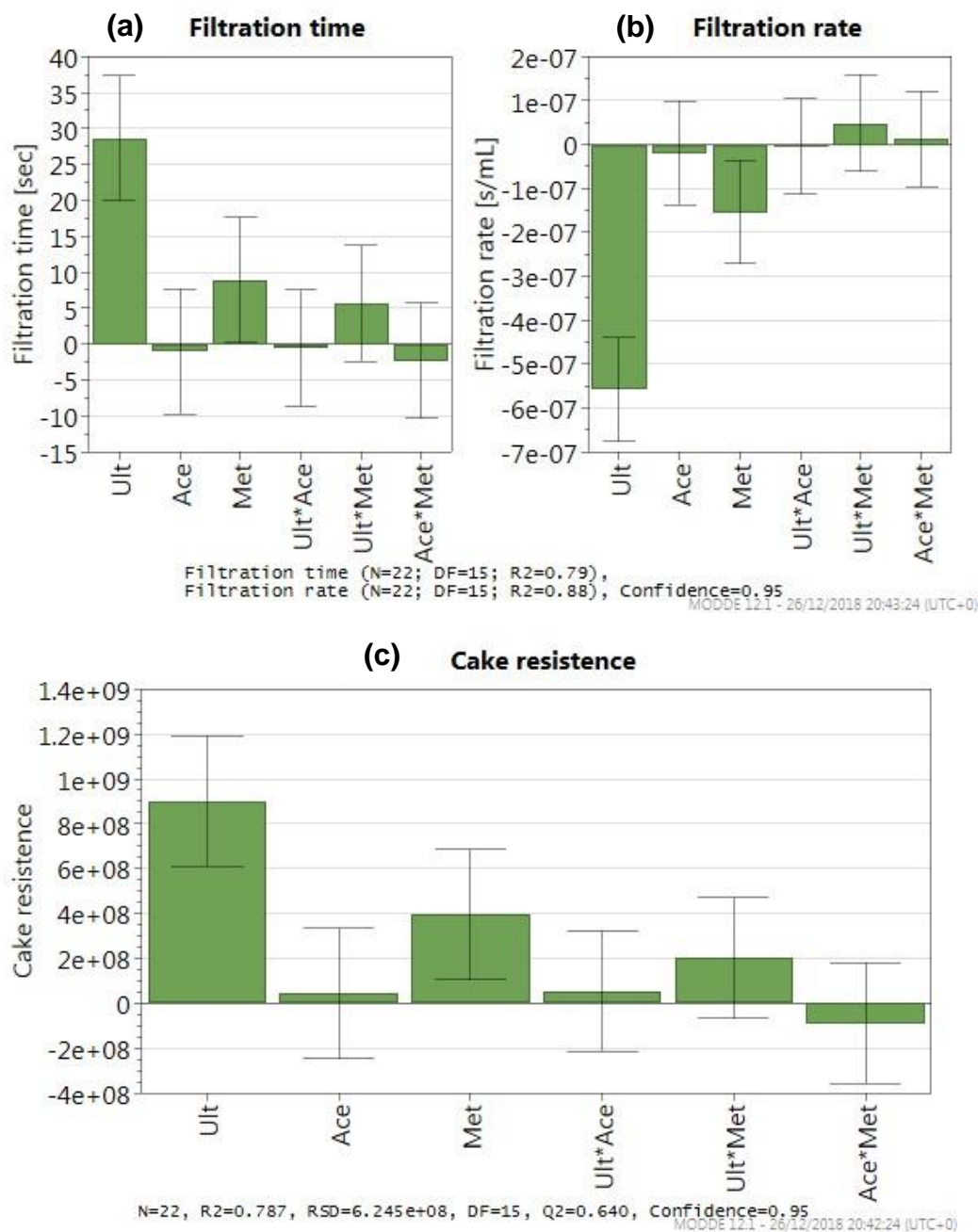

Figure 71: Coefficient plots prepared using DoE and showing how the six factors (ult-ultrasound, Ace-acetanilide, Met-metacetamol, Ult*Ace- ultrasound and acetanilide, Ult*Met-ultrasound and metacetamol, Ace*Met- acetanilide and metacetamol) influence the following responses (a) Filtration time (b) Filtration rate (c) Cake resistance.

When examining the filtration time, rate, and cake resistance in Figure 71 (a, b, and c), ultrasound was found to have the most significant impact, increasing the filtration time by approximately 27.5 seconds, reducing the filtration rate, and resulting in the highest cake resistance. This is likely attributed to the changes in particle size distribution (PSD). Metacetamol also played a larger role compared to acetanilide, increasing the filtration time by around 7.5 seconds, decreasing the filtration rate, and increasing cake resistance. The other factors, namely acetanilide, acetanilide with ultrasound, and 2% acetanilide with 2% metacetamol, showed modest effects on the filtration data. They had a slightly negative effect on filtration time, a small increase in filtration rate of approximately 0.1 s mL^{-1}and a further decrease in cake resistance.

In Figure 72 (a and b), a comparison between systems with acetanilide and metacetamol impurities demonstrated that ultrasound once again played a more dominant role in the acetanilide system. The filtration time, rate, and cake resistance were all faster in the case of acetanilide compared to metacetamol. For instance, with a 3 mol% impurity loading, the filtration time at 90% ultrasonic power was approximately 65 seconds for acetanilide and 90 seconds for metacetamol. The mol% of acetanilide had little effect on the filtration rate, whereas the addition of ultrasound power resulted in a steady decrease at 4 mol% of metacetamol. Overall, the filtration properties were found to be faster in the presence of acetanilide and slower when metacetamol was present.
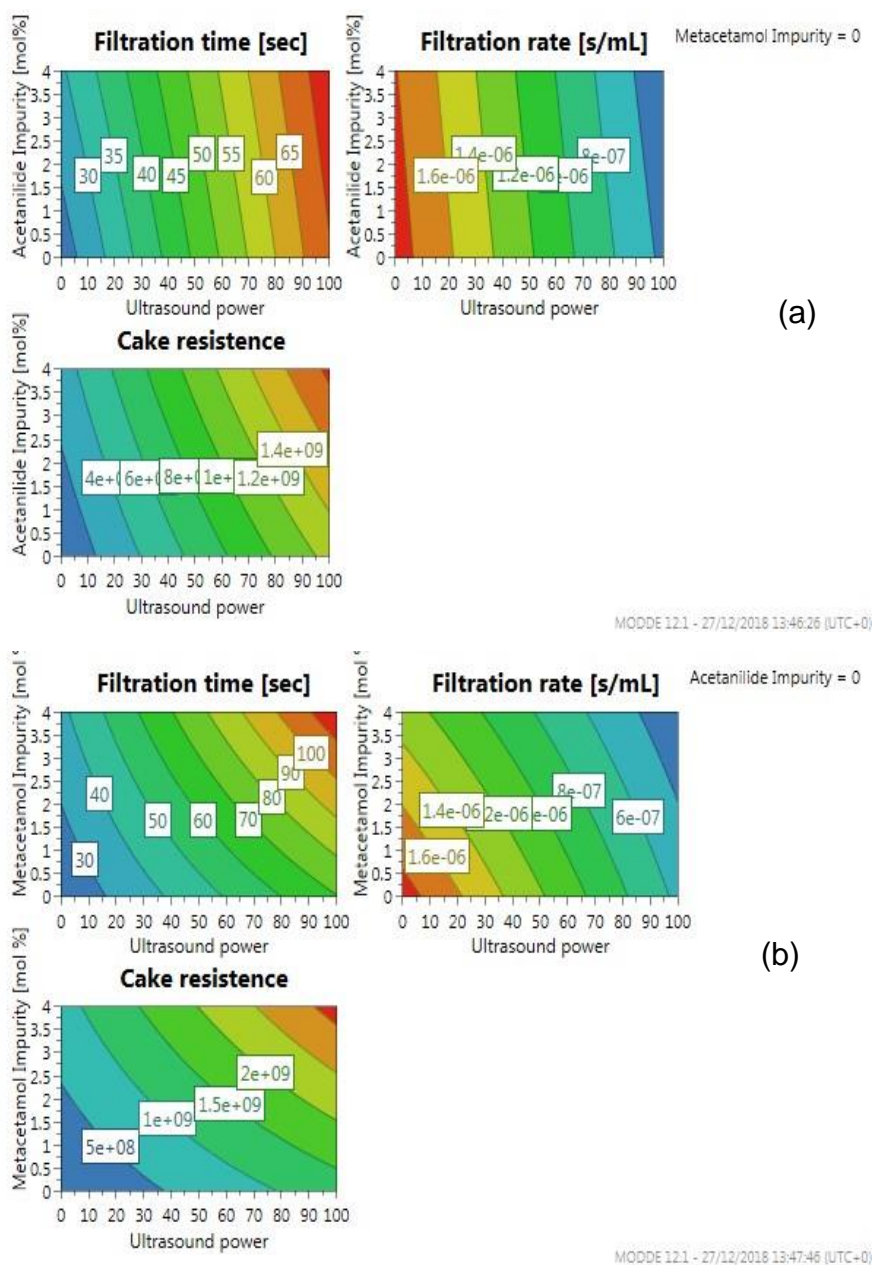
Figure 72: Response contour plot depicting the effect that ultrasonic power ranging from 0 to 100% has on (a) Filtration properties with the addition of acetanilide impurity and (b) Filtration properties with the addition of metacetamol impurity to the system.

6.1.5: Crystal habit
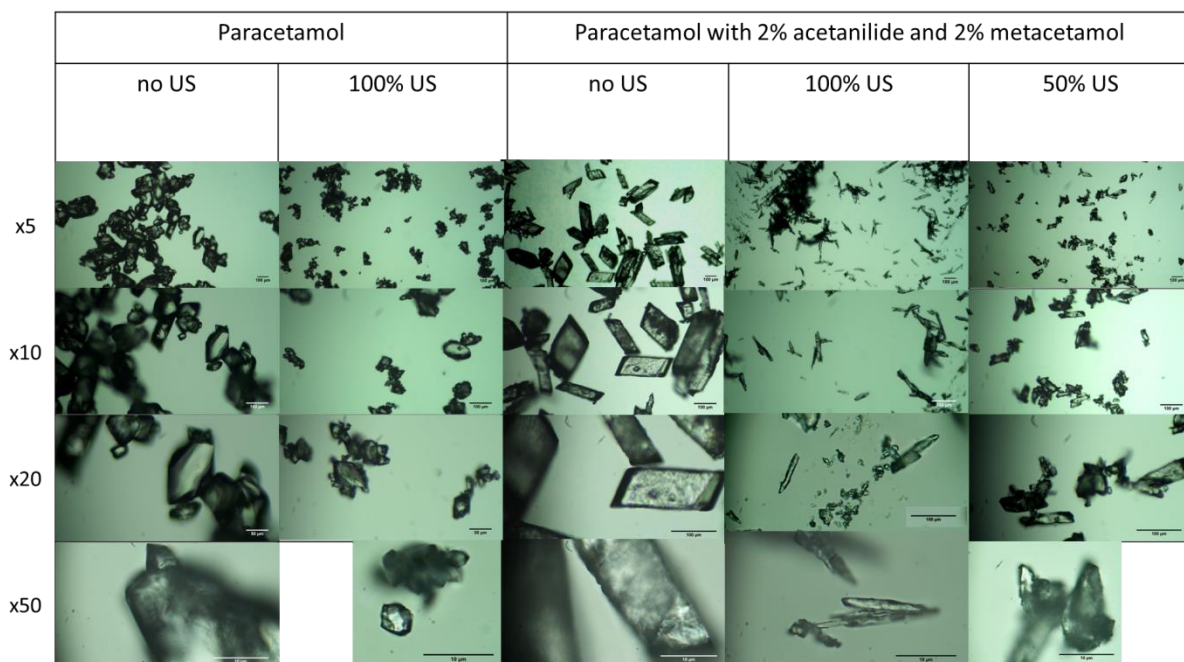
Figure 73: Optical microscopy images of recrystallised paracetamol crystal habits grown in ethanol (from left to right) for a system with paracetamol and no ultrasound (US), paracetamol with 100% US, paracetamol with 2% acetanilide and 2% metacetamol and no US, paracetamol with 2% acetanilide and 2% metacetamol with 100% US, and paracetamol with 2% acetanilide and 2% metacetamol with 50% US. Images range from 5x to 50x magnifications. Scale bar is set to100 µm.
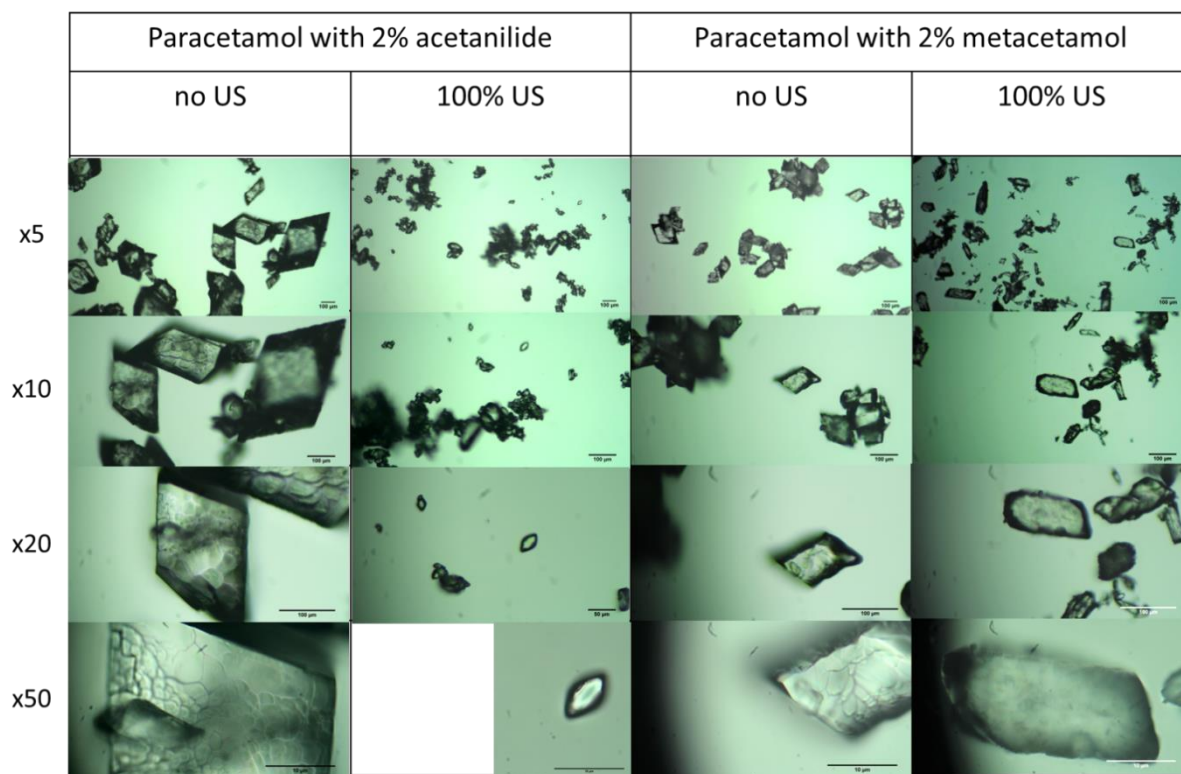
Figure 74: Optical microscopy images of recrystallised paracetamol crystal habits grown in ethanol (from left to right) for a system of paracetamol with 2% acetanilide and no ultrasound (US), paracetamol with 2% acetanilide and 100% US, paracetamol with 2% metacetamol and no US, and paracetamol with 2% metacetamol and 100% US. Images range from 5x to 50x magnifications. Scale bar is set to 100 µm.
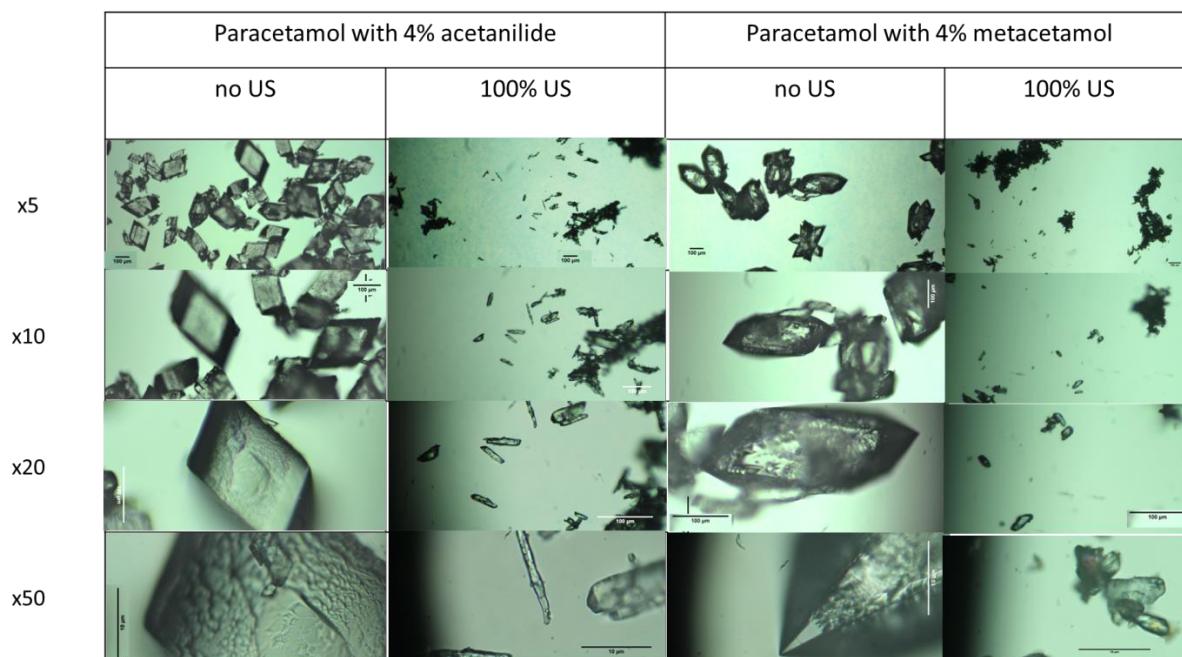
Figure 75: Optical microscopy images of recrystallised paracetamol crystal habits grown in ethanol (from left to right) for a system of paracetamol with 4% acetanilide and no ultrasound (US), paracetamol with 4% acetanilide and 100% US, paracetamol with 4% metacetamol and no US, and paracetamol with 4% metacetamol and 100% US. Images range from 5x to 50x magnifications. Scale bar is set to 100 µm.
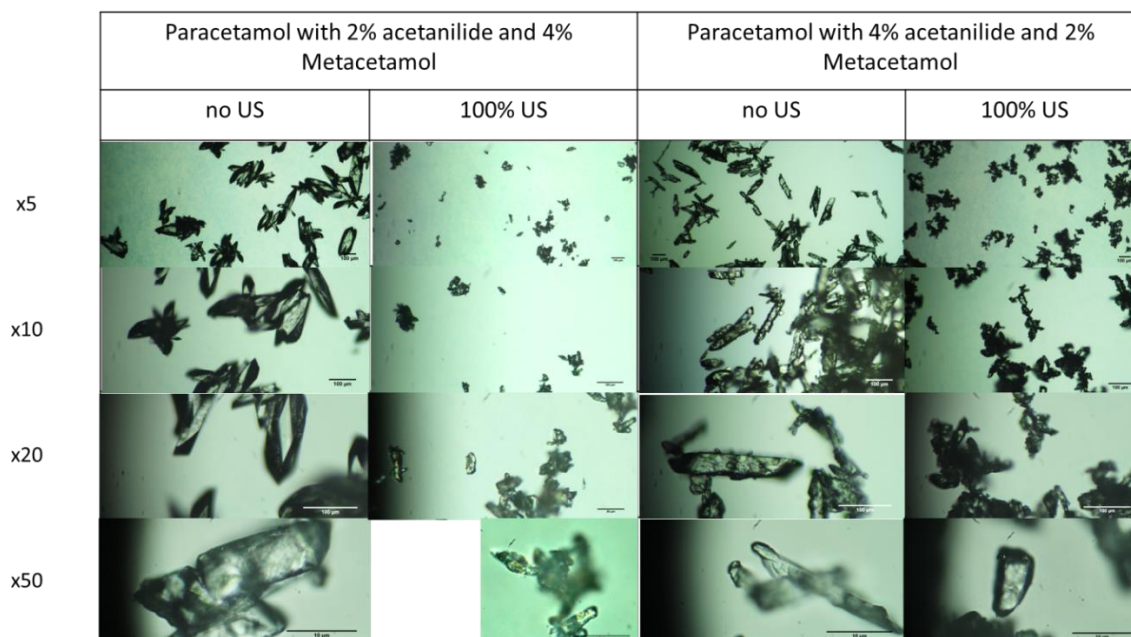
Figure 76: Optical microscopy images of recrystallised paracetamol crystal habits grown in ethanol (from left to right) for a system of paracetamol with 2% acetanilide and 4% metacetamol and no ultrasound (US), paracetamol with 4% acetanilide and 2% metacetamol and no US, paracetamol with 2% acetanilide and 4% metacetamol and 100% US, paracetamol with 4% acetanilide and 2% metacetamol and 100% US. Images range from 5x to 50x magnifications. Scale bar is set to 100 μm.
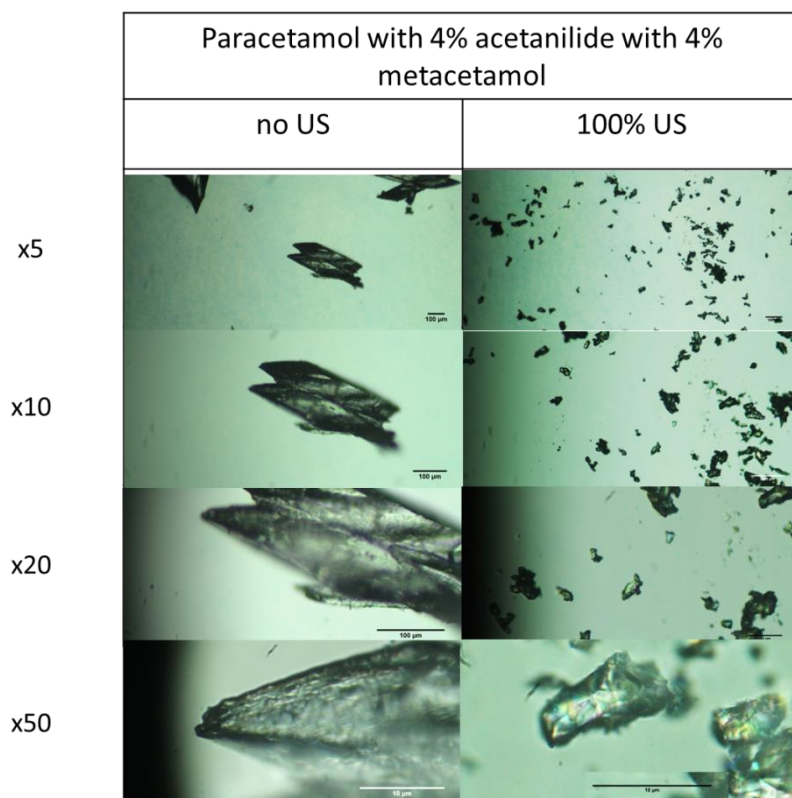
Figure 77: Optical microscopy images of recrystallised paracetamol crystal habits grown in ethanol (from left to right) for a system of paracetamol with 4% acetanilide and 4% metacetamol and no ultrasound (US), and paracetamol with 4% acetanilide and 4% metacetamol and 100% US. Images range from 5x to 50x magnifications. Scale bar is set to 100 μm.

The crystal habit plays a crucial role in downstream processes, as it directly impacts various factors such as: filterability, washing time, flowability, compressibility, and drying time. These parameters are essential considerations in formulation processes (6, 283).

A collection of images captured using a polarised light microscope showcased the isolated dry filter cake samples. These images, ranging from Figure 73-Figure 77, provide visual representations at magnifications of 5x to 50x. They depict the crystal habit of paracetamol under different conditions, including the presence of impurities and the application of ultrasound. The observed crystal habits align with the findings from the analysis of single crystal growth rates in Chapter 6.

For instance, Figure 73 illustrates the crystallisation of paracetamol without ultrasonic power, resulting in well-developed truncated crystal habits. Upon adding 2% of each impurity, the crystal habits transformed into a more elongated and diamond shaped crystals. The introduction of ultrasound at 100 and 50% power leads to an overall reduction in the growth rate, consistent with the PSD data and the increased nucleation rate.

The impact of ultrasound on crystal shape and size is further elucidated in the images obtained at different ultrasound intensities and impurity concentrations. At 100% ultrasound power, crystal facets display more signs of breakage and damage. In contrast, 50% ultrasound power in a system with 2% of each impurity, produces crystal shapes similar to the non-sonicated system but smaller in size. The presence of more crystals, in this case, correlates with the discussed ultrasound intensity data in Section 6.4.1. However, these findings contrast with the single crystal growth rate data presented in Table 12, where the addition of ultrasound did not disturb the crystal growth, even with the use of an ultrasonic toothbrush at frequencies in the MHz range. The absence of disturbance in the crystal growth can be attributed to the stagnant solution and the absence of particle collision, allowing the crystals to grow undisturbed.

In a bulk suspension crystallisation system, ultrasound enhances mixing at a molecular scale through acoustic microstreams, which generate shear forces from collapsing cavitation bubbles (50). The variation in particle size distribution is evident in both wet and dry filter cakes when ultrasound is applied, resulting in a significant reduction in particle size. This reduction is also reflected in the differences observed in the crystal habits of the dry cakes. Sonicated samples exhibit smaller and more consistent crystal habits, potentially attributed to the asymmetric collapse of cavitation bubbles. When crystals are in close proximity to the bubble, symmetrical collapse is prevented, and microjets are generated in the direction of the solids. These microjets cause erosion, pitting, and shear force, contributing to particle fragmentation observed in the images captured under ultrasound at 50 and 100% power (186, 284).

Chapter 6: Bulk Suspension Crystallisation with and without Ultrasonic Intervention

Previous research has used sonication to minimise agglomeration and attain preferred crystal forms (285), aligning with the findings in this study. Nevertheless, crystals that were continuously sonicated displayed a heightened propensity for agglomeration. This may be due to their small, needle-like shape, which tends to cluster at 100% power; a reduction in agglomeration at 50% power was similarly observed in this study's images. Intriguingly, Kim (173) posited that agitation, rather than sonication, promotes agglomeration, asserting that sonication mitigates it when considering size reduction and dissolution properties.

Exploring a direct comparison between continuously agitating the solution, with and without ultrasound, presents an interesting potential research path, as it was not addressed in the current study.

Gielen (286) investigated the effect of ultrasound on agglomeration during the crystallisation of an API in an ethanol mixture denatured with methyl ethyl ketone. Their findings indicated that agglomeration could be minimised by reducing the stirring rate and employing a seed loading of 1 mass % or greater. These conditions resulted in non-agglomerated monocrystals with the application of ultrasound using a 30 kHz sonotrode operating at 10 W. Gielen's study examined post-treatment ultrasound application, where continuous ultrasound was applied for sixty minutes once the solution cooled to 15 °C. This approach led to the removal of smaller particles that attached and grew on the surface of larger crystals but did not break the agglomerates. Additionally, they investigated ultrasonic treatment throughout the entire cooling process, utilising pulsed mode sonication. They discovered that pulsed ultrasound could prevent agglomerate formation without requiring further adjustments in the crystallisation process for both seeded and non-seeded solutions. They concluded that sonication during the initial stages of crystallisation inhibits agglomeration if sufficient exposure time is provided, specifically until FBRM and IR signal counts reach a steady state, indicating complete desupersaturation of solutes at the seeding temperature. With ultrasound enhancing the degree of macromixing and increasing the number of particles and particle collisions, agglomerate formation can be disrupted at the aggregate stage before they become firmly cemented together.

This could be a valuable direction for future research, where the impact of pulsed ultrasound treatment on samples could be explored in relation to impurity uptake. The results of this study demonstrated that the application of ultrasound significantly reduced the particle size distribution in both wet and dry cakes. This effect was particularly evident when comparing the characteristics of sonicated and non-sonicated dry cakes, which exhibited distinct variations in morphologies. Sonicated samples showed smaller and more consistent habits, which could be attributed to the asymmetric collapse of cavitation bubbles. The collapse of these bubbles near the crystals generated microjets that exerted erosion, pitting, and shear forces, ultimately leading to particle fragmentation. These findings suggest that ultrasound plays a crucial role in modifying particle size and morphology through its impact on cavitation-induced effects (186, 284).
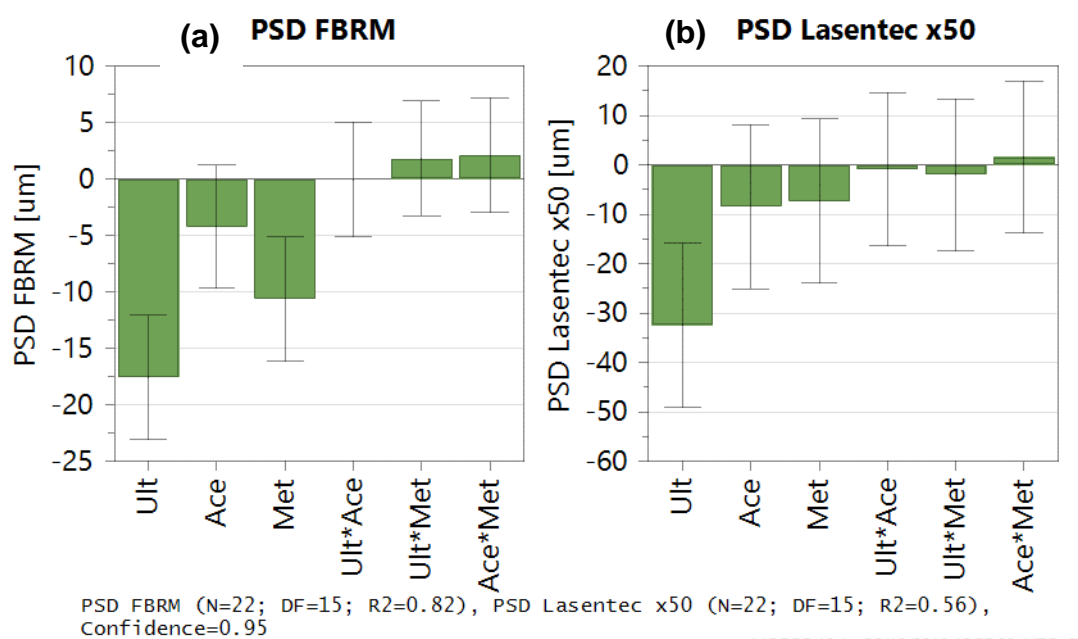
Figure 78: Coefficient plots prepared using DoE and showing how the six factors (ult-ultrasound, Ace-acetanilide, Met-metacetamol, Ult*Ace-ultrasound and acetanilide, Ult*Met-ultrasound and metacetamol, Ace*Met- acetanilide and metacetamol) influence the following responses (a) PSD FBRM and (b) PSD Lasentec.

When examining the coefficient plots using the Design of Experiments (DoE) in Figure 78, it was observed that ultrasound had a significant impact on reducing particle size in both wet and dry materials. In the FBRM analysis, ultrasound led to a reduction of approximately 17 μm in particle size, whilst in the Lasentec analysis, the reduction was

around 33 µm. Interestingly, metacetamol had a greater effect on reducing particle size in the FBRM analysis, with a reduction of approximately 10.5 µm, compared to a reduction of about 5 µm in the Lasentec analysis. On the other hand, the effect of acetanilide on particle size reduction was relatively smaller, with reductions of approximately 4 µm in the FBRM analysis and 6 µm in the Lasentec analysis.

In the FBRM analysis, the addition of ultrasound to the impurities had a minimal effect on acetanilide, resulting in a reduction of less than 0.2 µm. However, when ultrasound was applied to a metacetamol mixture, a more significant reduction in particle size of approximately 2 µm was observed. In the Lasentec analysis, adding ultrasound to the impurities resulted in a reduction in particle size of approximately 1 µm for acetanilide and 3 µm for metacetamol.

Moreover, introducing 2% metacetamol and 2% acetanilide to the system increased the particle size distribution (PSD) by approximately 4 µm in the FBRM analysis and 2 µm in the Lasentec analysis.
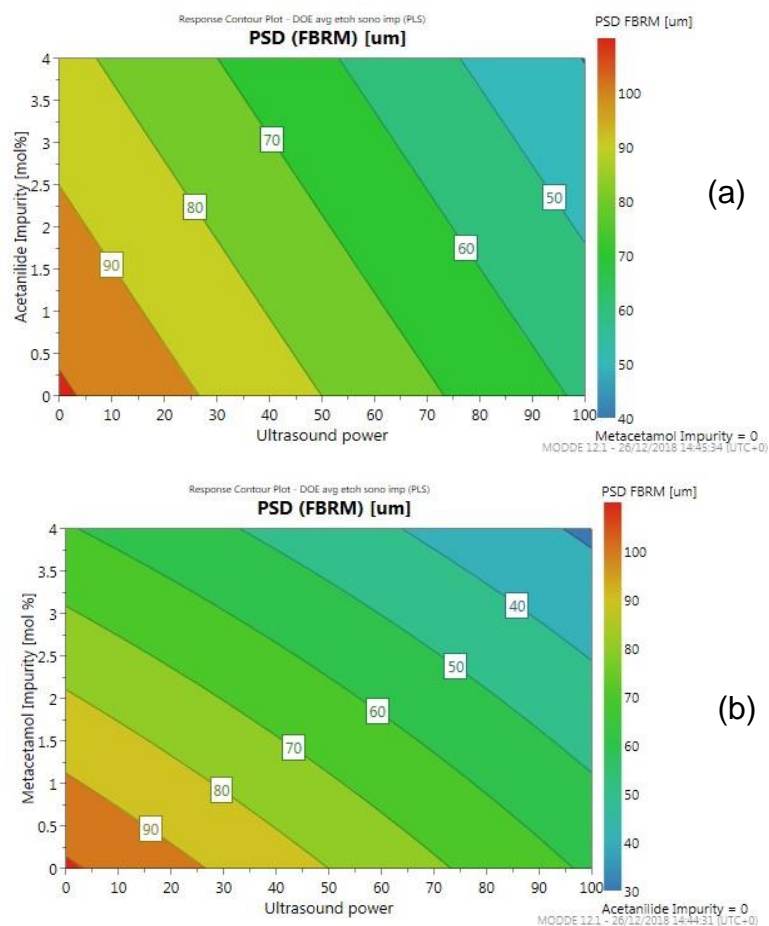
Figure 79: Response contour plot depicting the effect of ultrasonic power ranging from 0 to 100% on (a) PSD-(FBRM) with the addition of acetanilide and (b) PSD-(FBRM) with the addition of metacetamol.

The contour plot depicting the response of ultrasound power on particle size distribution (PSD) in Figure 79 revealed a clear linear relationship between impurity concentration and the increase in ultrasonic power. As ultrasonic power increased, there was a corresponding decrease in PSD.

For acetanilide (a), particles with an estimated size of 90 µm remained present even at an impurity concentration of 2.5 mol% and slightly over 25% ultrasonic power. In contrast, metacetamol (b) exhibited particles of 90 µm in size only at a slightly higher impurity concentration of just over 1 mol% with a similar power level.

When comparing the effects of impurities at a concentration of 4 mol% and 100% ultrasonic power, the particle size was estimated to be around 50 µm for both acetanilide and metacetamol. This observation suggests that metacetamol possesses a greater ability to incorporate into the crystal lattice and inhibit growth compared to acetanilide.

6.1.6: Yield

The crystallisation yield was determined by calculating the percentage of the mass of the recovered crystal product after filtration, washing, and drying relative to the overall mass of the input materials. An example of the calculation for maximum yield output with 99g of solvent can be found in Appendix C, Section 1.2. This calculation assumes that no dissolution of crystals occurred during the washing of the cake, which is supported by the low solubility of paracetamol and the miscibility of ethanol with the selected wash solvent, n-heptane.

It is important to note that there are inevitable losses of product during the transfer of materials and residues left behind on vessel walls and in the cylinder, among other factors. A product loss of approximately 5% is typically expected in small-scale filtration and washing processes due to material handling losses.
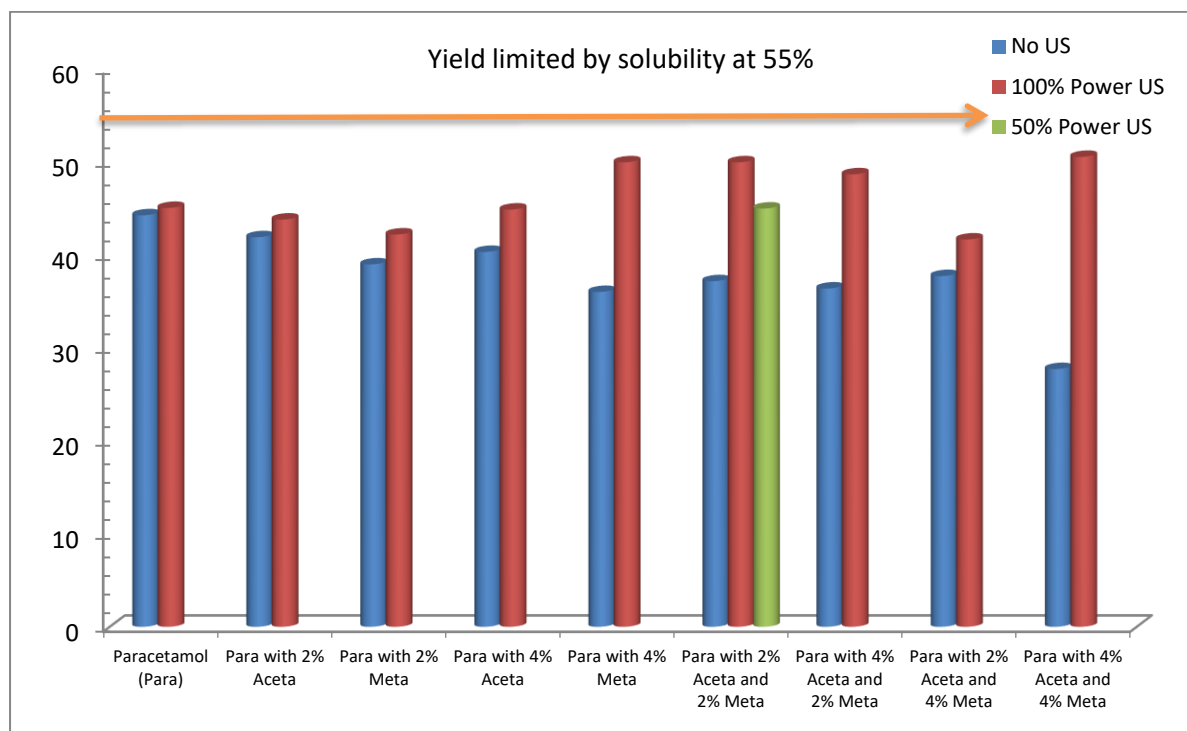
Figure 80: Calculated yield of products with and without ultrasonic intervention.

The maximum thermodynamic yield at the isolation temperature, based on the solubility of a pure system, is determined to be 55.23% (Figure 80). This demonstrates the highly effective nature of ultrasonic intervention in increasing the product yield towards the maximum thermodynamic equilibrium solubility. However, the presence of impurities has a noticeable impact on reducing the overall yield, with metacetamol having the most significant effect on reducing the yield. The largest reduction occurs when both 4% acetanilide and 4% metacetamol are added, resulting in a yield of 27.8%.

Similar results were reported by Nguyen (128) in a system involving paracetamol, metacetamol, acetanilide, and isoamyl alcohol, where ultrasonic intervention improved the average product yield by 50.7% compared to non-treated samples, which had an average yield of 45.2%. Similarly, Guo (195) observed that rapid and efficient mixing techniques employed in precipitation, anti-solvent, and reaction crystallisation processes result in higher product yields. Another study focused on the nucleation and growth rates of lactose and found that the application of ultrasound increased the yield (287). This finding further supports the notion that ultrasound can be utilised to achieve a faster and more efficient crystallisation process.

The impact on yield can be primarily attributed to changes in nucleation behaviour. The introduction of ultrasound to the system leads to a reduction in the width of the metastable zone, indicating that the Gibbs free energy for nucleation becomes available earlier in the presence of ultrasound. Additionally, there is an increase in the rate of secondary nucleation, resulting in a higher number of nuclei throughout the crystallisation process. This, in turn, provides a significantly larger crystal surface area for the deposition of material.

In non-sonicated samples, the nucleation rate is slower, leading to the formation of a smaller number of larger crystals with less surface area available for growth. Consequently, the solution has limited opportunities to fully desupersaturate, hindering the overall yield.
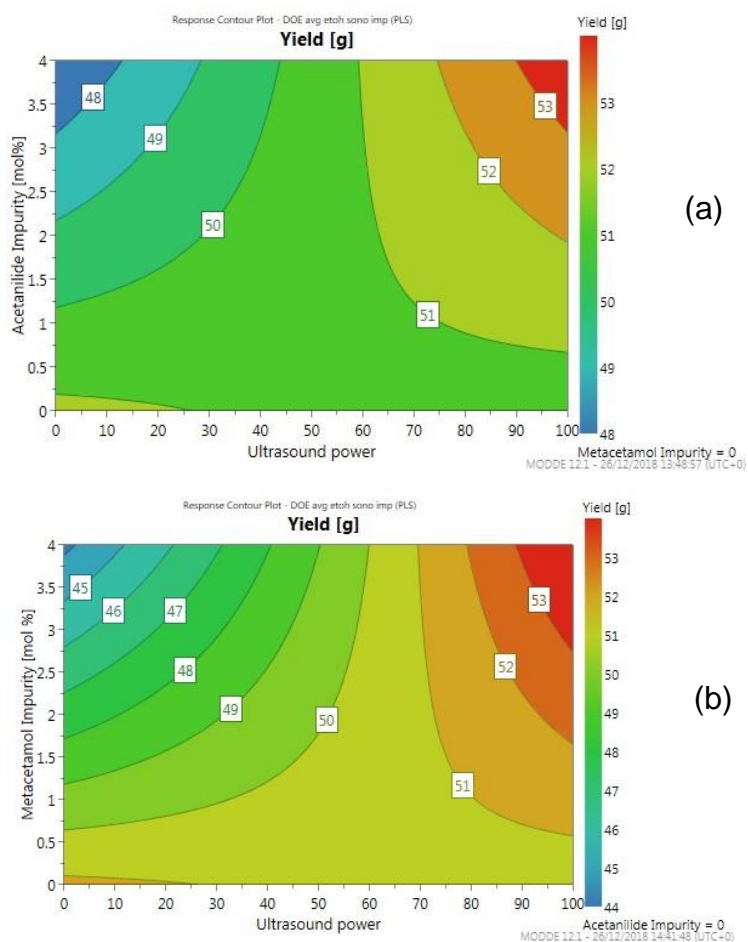
Figure 81: Response contour plot depicting the effect of ultrasonic power ranging from 0 to 100% on (a) Yield with the addition of acetanilide and (b) Yield with the addition of metacetamol.

When utilising MODDE for generating response contour plots, Figure 81 demonstrated that at a 4% impurity concentration, metacetamol (b) exhibited a greater reduction in yield (estimated at 45g) compared to acetanilide (a) (estimated at 48g) in the absence of ultrasound. However, as the ultrasound power was increased, there was a substantial increase in yield observed for both cases when 4 mol% impurity was added as an example.

6.1.7: Impurity analysis using High-performance liquid chromatography (HPLC)

When analysing a crystallisation process, product purity is a critical factor to consider. To assess the purity, each cake, mother liquor, wash 1 and wash 2 were subjected to analysis by HPLC (High-performance liquid chromatography).

Cake (a)	Substance	Retention time	UV Peak area	Peak area (%)	Metacetamol fraction
0% ultrasound	Paracetamol	1.987	2593.86	95.19	0.49%
	Metacetamol	2.79	12.68	0.46	
100% ultrasound	Paracetamol	1.994	3030.54	97.54	0.33%
	Metacetamol	2.802	10.0619	0.32	

Mother Liquor (b)	Substance	Retention time	UV Peak area	Peak area (%)	Metacetamol fraction
0% ultrasound	Paracetamol	1.947	2606.73	92.48	3.07%
	Metacetamol	2.714	82.66	2.93	
100% ultrasound	Paracetamol	1.98	2338.69	91.83	3.30%
	Metacetamol	2.774	79.82	3.13	

Figure 82: Example of HPLC peak analysis (a) Filter cake from an experiment starting with paracetamol with 2% added metacetamol, with and without the application of ultrasound power and (b) The corresponding mother liquor extraction.

Figure 82 depicts the cake analysis, indicating a decrease in the metacetamol fraction within the final crystal product for the 100% power ultrasound sample compared to the 0% power ultrasound sample. The concentration is measured by the UV peak area. In the case of the mother liquors (b) under the 100% ultrasound condition, a higher concentration of metacetamol is observed in comparison to the 0% power sample. This finding suggests that there is an elevated impurity concentration in the filtrate, resulting in a reduced metacetamol concentration within the final cake product.

Table 17: Summary of the impurity percentage of each compound in the isolated filter cake, the mother liquor, and washes 1 and 2.

Conditions	Compounds	Percentage of Compounds in Cake (%)			Percentage of Compounds in Mother Liquor (%)		
		No US	50% US	100% US	No US	50% US	100% US
Paracetamol	Paracetamol	100		100	100		100
	Metacetamol	0		0	0		0
	Acetanilide	0		0	0		0
Paracetamol with 2% Acetanilide	Paracetamol	99.54		99.63	96.17		95.94
	Acetanilide	0.46		0.37	3.83		4.06
Paracetamol with 2% Metacetamol	Paracetamol	99.51		99.62	96.86		97.33
	Metacetamol	0.49		0.38	3.14		2.67
Paracetamol with 4% Acetanilide	Paracetamol	99.26		99.23	93.38		91.84
	Acetanilide	0.74		0.77	6.62		8.16
Paracetamol with 4% Metacetamol	Paracetamol	98.55		98.36	93.95		92.74
	Metacetamol	1.45		1.64	6.05		7.26
Paracetamol with 2% Metacetamol and 2% Acetanilide	Paracetamol	98.93	98.78	98.65	93.41	92.65	92.86
	Metacetamol	0.62	0.65	0.66	3.55	3.93	4.10
	Acetanilide	0.45	0.57	0.70	3.06	3.42	3.04
Paracetamol with 2% Metacetamol and 4% Acetanilide	Paracetamol	98.61		98.76	89.91		88.89
	Metacetamol	0.82		0.46	3.75		4.04
	Acetanilide	0.57		0.78	6.34		7.07
Paracetamol with 4% Metacetamol and 2% Acetanilide	Paracetamol	98.12		98.11	89.91		88.89
	Metacetamol	1.34		1.20	3.75		4.04
	Acetanilide	0.54		0.69	6.34		7.07
Paracetamol with 4% Metacetamol and 4% Acetanilide	Paracetamol	97.11		98.13	87.08		84.20
	Metacetamol	1.63		0.83	6.97		9.16
	Acetanilide	1.26		1.04	5.95		6.64

Conditions	Compounds	Percentage of Compounds in Wash 1 (%)			Percentage of Compounds in Wash 2 (%)		
		No US	50% US	100% US	No US	50% US	100% US
Paracetamol	Paracetamol	100		100	100		100
	Metacetamol	0		0	0		0
	Acetanilide	0		0	0		0
Paracetamol with 2% Acetanilide	Paracetamol	96.40		95.97	95.09		96.21
	Acetanilide	3.60		4.03	4.91		3.79
	Paracetamol	96.42		96.68	96.70		96.48

System	Compound						
Paracetamol with 2% Metacetamol	Metacetamol	3.58		3.32	3.30		3.52
Paracetamol with 4% Acetanilide	Paracetamol	93.48		92.35	94.82		92.21
	Acetanilide	6.52		7.65	5.18		7.79
Paracetamol with 4% Metacetamol	Paracetamol	93.77		92.92	93.65		98.89
	Metacetamol	6.23		7.08	6.35		1.11
Paracetamol with 2% Metacetamol and 2% Acetanilide	Paracetamol	93.05	92.86	92.57	93.11	92.56	92.51
	Metacetamol	3.26	3.33	3.47	5.74	3.47	3.51
	Acetanilide	3.69	3.81	3.96	1.15	3.97	3.98
Paracetamol with 2% Metacetamol and 4% Acetanilide	Paracetamol	90.30		88.43	86.31		88.31
	Metacetamol	3.13		3.63	4.05		3.65
	Acetanilide	6.57		7.94	9.61		8.04
Paracetamol with 4% Metacetamol and 2% Acetanilide	Paracetamol	90.23		89.28	90.08		88.14
	Metacetamol	6.14		6.83	6.23		7.53
	Acetanilide	3.63		3.89	3.69		4.33
Paracetamol with 4% Metacetamol and 4% Acetanilide	Paracetamol	88.66		84.36	80.11		84.62
	Metacetamol	5.23		6.64	9.10		6.44
	Acetanilide	6.11		9.00	10.79		8.94

For a visual representation and further discussion on each system, refer to Appendix C, Section 1.4. Analysing the data in Table 17, it is evident that the impurities generally lead to a reduction in the percentage of paracetamol in the cake, regardless of the ultrasound condition. However, the percentages of metacetamol and acetanilide in the cake increase with the addition of impurities and ultrasound power. This effect is more pronounced for metacetamol compared to acetanilide. In this specific context, ultrasound does not seem to have a significant impact on reducing the percentages of metacetamol and acetanilide in the cake.

Turning to the compounds' percentages in the mother liquor, a similar trend is observed in comparison to the cake. Impurities generally result in higher percentages of metacetamol and acetanilide in the mother liquor. The increase in impurity percentages is more significant with higher ultrasound power, particularly for metacetamol.

Regarding the compounds' percentages in wash 1 and wash 2, the percentage of impurities generally increases with the addition of impurities and ultrasound power. However, the percentage of paracetamol remains relatively high in both washes, indicating the effectiveness filtration and the selected wash solvent in removing impurities.

Overall, these trends indicate that the presence of impurities and the application of ultrasound power influence the distribution of compounds between the cake, mother liquor, and washes. The impact of impurities on the product composition is more pronounced when higher ultrasound power is used.

Based on the provided data, it does not appear that ultrasound consistently increases the amount of impurity in the cake. The percentages of metacetamol and acetanilide in the cake vary depending on the specific conditions and impurity concentrations. While there are cases where the addition of ultrasound results in higher impurity percentages in the cake, there are also instances where the percentages remain relatively low or show only slight increases with ultrasound.

Therefore, it would be inaccurate to make a general statement that ultrasound universally increases the amount of impurity in the cake. The effect of ultrasound on the impurity content of the cake appears to be dependent on various factors, including specific conditions and impurity concentrations. Further analysis and experimentation are needed to gain a more comprehensive understanding of the effects of ultrasound on impurity levels in the cake.

In the analysis with isoamyl alcohol (128), it was observed that ultrasound treatment resulted in product crystals with reduced impurity content compared to non-sonicated samples. The impurity concentration in the paracetamol product decreased from 1.88% to 1.52% in the presence of ultrasound. Similarly, the uptake of acetanilide was reduced from 0.85% to 0.35% in the ultrasound-treated samples.

The analysis of the filtrate showed that more impurities remained in solution in the ultrasound-treated samples. This effect was more pronounced when considering the difference in particle size between the treated and non-treated samples. The ultrasound-treated products consisted of smaller particles with a larger combined surface area, providing more sites for impurity retention and presenting a greater challenge for washing due to the finer pore structure and increased contact area between particles.

Furthermore, the study observed that the reduction in particle size was more significant when the impurity loading in the crystallisation solution was higher, such as in the case of a 2% metacetamol and 2% acetanilide.

Overall, the data suggests that ultrasound treatment can effectively reduce impurity content in product crystals and influence impurity distribution between the crystals and the mother liquor. The particle size reduction achieved through ultrasound treatment played a crucial role in enhancing impurity retention and impacting subsequent washing processes.
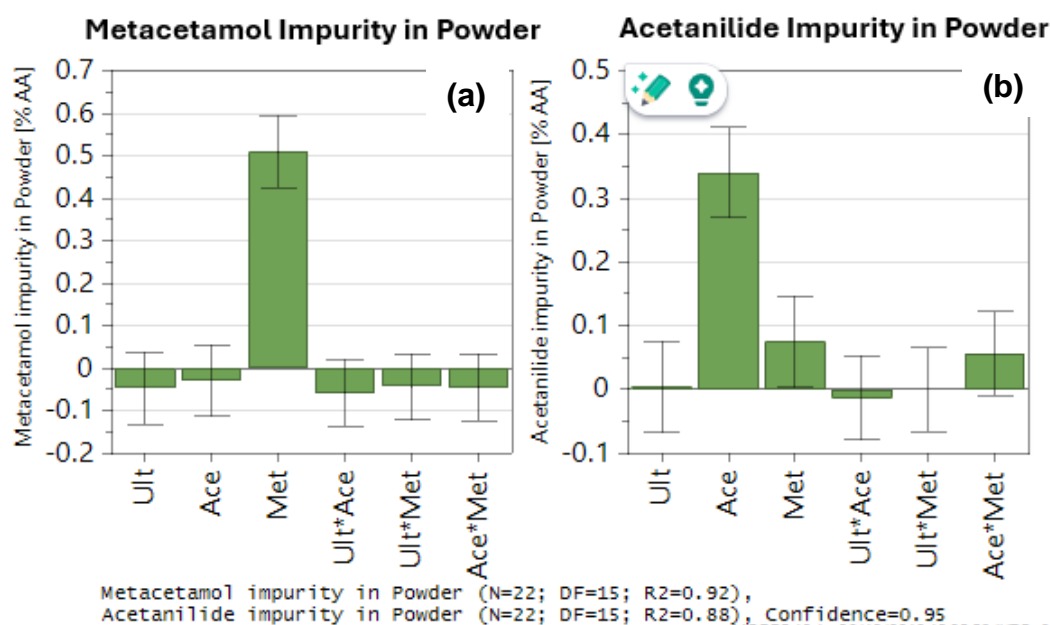
Figure 83: Coefficient plots prepared using DoE and showing how the six factors (ult-ultrasound, Ace-acetanilide, Met-metacetamol, Ult*Ace-ultrasound and acetanilide, Ult*Met-ultrasound and metacetamol, Ace*Met- acetanilide and metacetamol) influence the following responses: (a) Percentage of metacetamol impurity in cake (powder) and (b) Percentage of acetanilide impurity in cake (powder).

The MODDE coefficient plots, prepared using DOE, provide insights into the principal factors influencing the amount of impurity in the powder. Observing Figure 83, It is clear that the impurity concentration added to the system plays a significant role. Metacetamol (a) and acetanilide (b) are the main factors influencing the impurity amount, with concentrations of 0.5% and 0.35%, respectively. Other factors in Figure 83 (a) show minimal positive influence on the impurity amount.

According to Figure 83 (b), acetanilide is the primary factor affecting the impurity amount. However, metacetamol also has a small influence of approximately 0.55%. Although not intentionally added, this could be attributed to metacetamol crystallising out during the crystallisation process.

Impurity mixtures also exhibit an influence in Figure 83 (b), accounting for approximately 0.5% of the total effect. Again, this could be attributed to the minor influence that metacetamol has when competing with acetanilide. The segregation coefficient further supports this observation, with a value of 0.25 for metacetamol and 0.11 for acetanilide (265).

The coefficient plots generated by MODDE through DOE analysis shed light on the key factors impacting the impurity content in the powder, with impurity concentration, specific impurities (metacetamol and acetanilide) and impurity mixtures all playing a role.
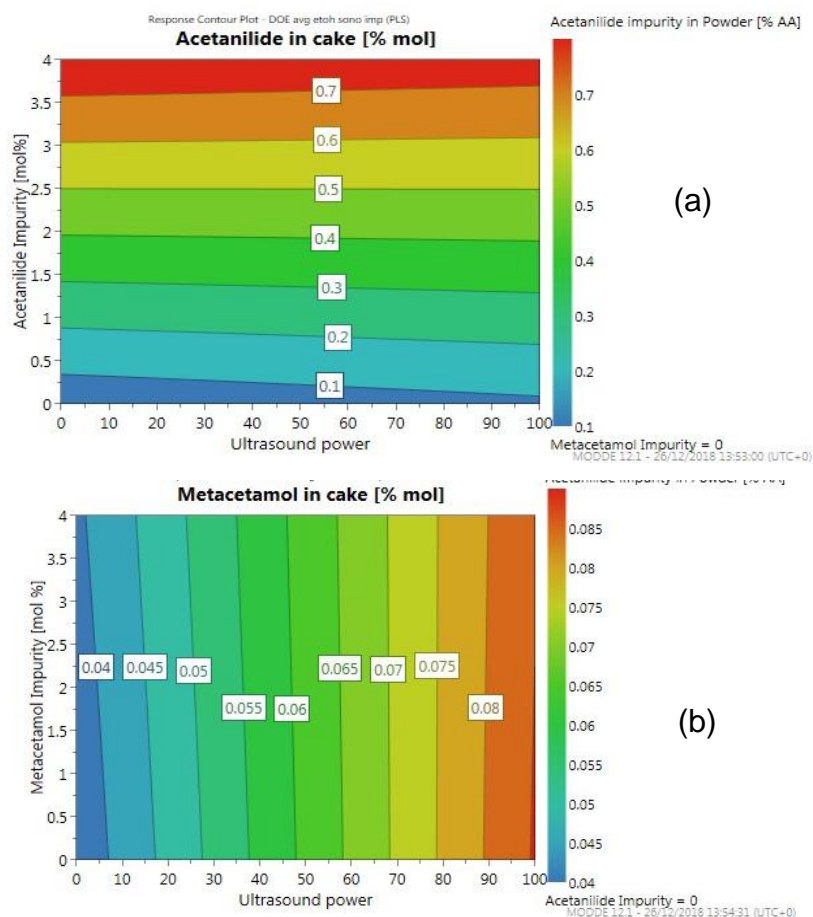
Figure 84: Response contour plot depicting the effect of ultrasonic power ranging from 0 to 100% power on (a) Percentage of acetanilide found in the cake and (b) Percentage of metacetamol found in the cake.

The response contour plots in Figure 84, generated using MODDE, provide insights into the impact of ultrasound power on the amount of acetanilide and metacetamol in the product.

In the case of acetanilide, the response contour plot indicates that ultrasound power has a minimal effect on its presence in the product. However, for metacetamol, it is evident that the addition of ultrasound, along with an increase in power, leads to a significant improvement in product purity. This effect is observed regardless of the mol% of impurity present.

The response contour plots highlight the beneficial impact of ultrasound and increased power, specifically on the product purity of metacetamol. The findings suggest that ultrasound intervention can effectively enhance the purity of the final product, while the influence on acetanilide is comparatively limited.

6.2: Conclusion

This chapter explored the effects of sono-crystallisation on the bulk suspension crystallisation of paracetamol in an ethanol system, along with two structurally related impurities, metacetamol and acetanilide. The findings confirmed the well-documented advantages of ultrasound reported in previous studies, such as accelerating nucleation, reducing crystal size and size distribution, minimizing agglomeration, and increasing product yield.

The study provides valuable insights into the impact of ultrasound treatment on impurity incorporation and crystallisation processes. Metacetamol emerged as the most challenging impurity, affecting nucleation, growth, and crystal morphology. The increased variability in nucleation points in the presence of metacetamol indicates its disruptive influence. Ultrasound intervention, by inducing nucleation earlier and at higher temperatures, resulted in increased secondary nucleation and a significant reduction in particle size. Microscopic analysis revealed particle breakage and a shift towards needle-like crystal shapes, particularly when applying 100% ultrasonic power.

Ultrasound treatment had a negative impact on filtration properties, leading to an increased filtration time and an increase in cake resistance due to the smaller particle size. The wash solvent, heptane, demonstrated its effectiveness in removing impurities from the solution. However, it should be noted that dried sonicated cake samples exhibited agglomeration due to the reduced particle size, which could potentially impact downstream processes.

The study aimed to investigate the reduction of impurity incorporation into the final product through ultrasound intervention. While 100% ultrasonic power showed a modest improvement in product yield across a range of impurities analysed, the

outcomes varied in other cases. Further investigations are required to gain a comprehensive understanding of the underlying mechanisms driving these effects. The proposed theoretical mechanisms include ultrasound-induced nucleation at lower supersaturation levels, disruption of impurity attachment through shockwaves, and increased availability of host molecules for crystal growth. However, these mechanisms necessitate additional experimental analysis for validation.

In summary, this research highlights the benefits of ultrasound application in enhancing crystallisation properties and downstream processes. The findings underscore the potential of ultrasound technology to reduce impurity content and enhance product quality. Further studies exploring the mechanisms underlying these effects will contribute to the development of more efficient and controlled crystallisation processes in various industrial applications.

Chapter 7: Conclusions and Future Work

Chapter 7: Conclusions and Future Work

This study aimed to examine the influence of structurally related impurities on the solubility of paracetamol in ethanol and their impact on the growth rates of single crystals. The selected growth conditions for single crystals were then scaled up to bulk suspensions. Additionally, the potential benefits of incorporating ultrasound into the crystallisation process were evaluated in terms of improving the yield and purity of the final product.

Traditional approaches to industrial crystallisation process development typically rely on the average growth rates of the crystal population. In contrast, this study employed an in-situ, real-time investigation of crystal morphology and growth rates at the individual crystal face level. This enabled the tracking of crystal growth rates and changes in crystal habits as individual crystals developed.

Sonocrystallisation, through the induction of nucleation at moderate supersaturation levels, has been shown to reduce process times and facilitate control over particle size (16, 128, 168, 178, 182, 186, 288). However, limited data regarding its effectiveness in reducing the uptake of structurally related impurities in a drug substance is available.

The research question underlying this PhD was:

"What are the implications of structurally related impurities in crystallisation systems, and to what extent do they affect solubility, crystal growth, and habit formation? Can sonocrystallisation effectively mitigate these impacts by preventing impurity incorporation, on the crystal surface during growth, thereby preserving the overall growth process?"

This question was answered using the following:

- Determined the overall effect selected impurities have on the solubility of the model compound, paracetamol, in ethanol.
- Analysed the impact of structurally related impurities (metacetamol and acetanilide) on individual crystal face growth rates and habits in the presence

and absence of ultrasound as a function of supersaturation and impurity loading in a single crystal stagnant cell.

- Scaled up the single crystal stagnant cell quantities to simulate batch production in the industry (bulk suspension crystallisation). Utilising an ultrasonic bath during cooling crystallisation to examine the effects of ultrasonic intervention on product purity, crystal habit, yield, and degree of crystal perfection.

Chapter 4 focused on analysing the solubility of paracetamol, metacetamol, and acetanilide in ethanol and isoamyl alcohol, considering the impact of impurities. The obtained solubility data provided valuable additions to the existing literature, highlighting the need to consider impurity effects rather than relying solely on solubility measurements of pure substances or fixed impurity compositions.

The results demonstrated that solubility increased with temperature for all components in both ethanol and isoamyl alcohol. Paracetamol exhibited the lowest solubility, while acetanilide had the highest. The presence of impurities at different concentrations caused varying effects on solubility at different temperatures. For example, 2% metacetamol decreased solubility at lower temperatures but increased it at higher temperatures. Similarly, impurities affected solubility in isoamyl alcohol, with metacetamol consistently increasing solubility at all concentrations and temperatures.

The impact of impurity loading on solubility was relatively modest, especially with 1-4% metacetamol or acetanilide. However, variability in the data was observed at elevated temperatures due to experimental challenges in sampling saturated suspensions close to the solvent's boiling point. Nonetheless, the overall data showed consistency.

The complex relationship between impurity loading and solubility highlights the limitations of simple models in predicting the effects of impurities on solubility. Experimental measurements of solubility in the presence of impurities are crucial for precise crystallisation process designs.

Chapter 7: Conclusions and Future Work

The obtained data can be used to support researchers in developing solubility prediction tools that account for the influence of impurities. Such tools have the potential to save time and resources in experimentation and benefit future industrial crystallisation research, particularly in systems with impurities. Given that crystallisation is commonly employed for purification purposes in organic systems, this research holds significant importance.

Chapter 5 of the study examined the single crystal growth rates and habits of paracetamol crystals in the presence and absence of structurally related impurities (metacetamol and acetanilide). The experiments were conducted in ethanol and isoamyl alcohol at different temperatures and supersaturations, with the additional investigation of ultrasound using an ultrasonic toothbrush.

Key findings included the observation of crystals with different habits growing simultaneously, which is a novel phenomenon for paracetamol. This variation in habits can impact downstream processes such as solubility, stability, and bioavailability in patients. The experiments involved continuous monitoring of nucleation and growth whilst also considering external factors that could influence crystal behaviour.

Changes in habits were typically associated with increased temperature and supersaturation, but the experiments were conducted isothermally to maintain constant supersaturation. Introducing impurities resulted in various habits, regardless of temperature and supersaturation. Impurities influenced habits by attaching to specific crystal faces, often leading to needle-like shapes. Additionally, the presence of impurities could cause low supersaturation in local areas.

Analysis of the average growth rates of different crystal faces revealed that face A consistently exhibited the fastest growth. Variations in growth rates were more pronounced at higher supersaturations, potentially due to changes in habits. Temperature also influenced crystal habits, with a wider range observed at 30 °C compared to 15 and 20 °C. The average growth rate decreased with increasing temperature, attributed to the variety of habits present. When growth rates were analysed for indexed faces, it was found that the growth rate increased with temperature.

Impurities, particularly 4% acetanilide and 4% metacetamol, had different effects on single crystals. Metacetamol significantly reduced the overall growth rate, especially under specific temperature and supersaturation conditions. However, at a concentration of 2%, metacetamol positively impacted growth for certain crystal habits.

Various analysis methods were employed, including face indexing and tracking the growth rates of specific habits. Challenges were encountered in assigning faces to crystals due to habit variability and the inability to remove crystals from the cell. Introducing ultrasound through an ultrasonic toothbrush induced nucleation and predominantly led to needle-like habits. The use of ultrasound also resulted in the formation of rapidly growing but poorly faceted crystals not observed without ultrasound.

Additionally, ultrasound influenced crystal habits by inducing nucleation and promoting the growth of needle-like habits. Cavitation bubbles and hot spots were believed to play a role in facilitating nucleation and secondary nucleation processes, thereby enhancing crystal formation. Ultrasound showed a positive effect on the growth rate of needle-like habits in the presence of 4% acetanilide, while other crystal habits did not experience significant improvement.

Future research could focus on understanding the simultaneous occurrence of multiple habits under the same growth conditions, investigating the relationship between habit changes, and decreasing growth rates with increasing temperature, developing methods for recovering and analysing individual crystals, and improving ultrasound mapping in the stagnant cell.

Overall, this chapter provides valuable insights into the challenges of observing and understanding the effects of growth conditions on single crystals, contributing to the planning of larger-scale crystallisation processes.

Chapter 7: Conclusions and Future Work

Chapter 6 of the study examined the effects of sonocrystallisation on the bulk suspension crystallisation of paracetamol in ethanol with the addition of metacetamol and acetanilide impurities. The results were consistent with previous literature, showing that ultrasound accelerated nucleation, reduced crystal size and size distribution, minimised agglomeration at 50% power addition, and increased product yield.

Metacetamol was the most problematic impurity, significantly affecting nucleation, growth, and crystal habit. This aligns with the findings in Chapter 5 regarding single crystal growth. The presence of metacetamol resulted in variable induction times for nucleation.

Using ultrasound in the crystallisation process increased the filtration time and cake resistance while decreasing the filtration rate. This was attributed to the smaller particle size and increased compaction, making it more challenging for the solution to pass through. Heptane was effective as a wash solvent, removing impurities from the cake. However, the sonicated samples exhibited agglomeration after drying, resulting in compacted particles.

100 and 50% ultrasonic power produced an average improvement of 44% in product yield. This improvement was attributed to changes in nucleation behaviour induced by ultrasound. The reduced metastable zone width allowed for earlier crystal growth initiation, while the increased secondary nucleation rate provided a larger crystal surface area for material deposition.

100% ultrasonic power improved product purity in four out of eight samples. However, for a sample with 2% acetanilide and 2% metacetamol, 50% ultrasonic power produced higher purities compared to 100% power, although the non-sonicated condition yielded the highest purity. Overall, there were mixed results, but an improvement in purity was observed.

The filtration and washing steps effectively removed impurities, as indicated by the consistently higher percentage of impurities in the filtrate compared to the cake product.

Chapter 7: Conclusions and Future Work

The findings underscore the overall benefits of ultrasound in a bulk suspension system, addressing issues related to nucleation, yield, impurity incorporation, and crystal habits. Implementing similar techniques in other applications can enhance control over the crystallisation process, save time, and contribute to environmental friendliness.

Future work should investigate the effects of 50% ultrasonic power, which showed less drastic effects on individual crystals, reduced agglomeration and changes in habit, and demonstrated improved impurity removal compared to 100% ultrasonic power. Exploring the contact time with the wash solvent could also be beneficial, as could observing the yields of leftover products with increased contact time.

Appendix A: Solubility of Paracetamol and Structurally Related Impurities

Appendix A: Solubility of Paracetamol and Structurally Related Impurities

1.0: Approach to equilibrium
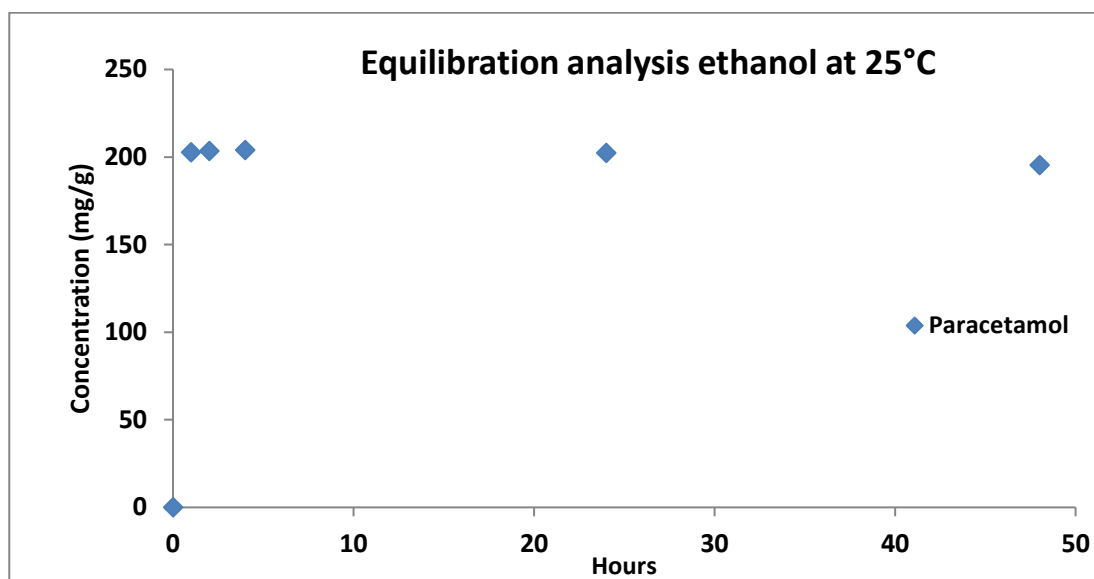
Figure 85: Gravimetric analysis of the approach to equilibrium in ethanol looking at the concentration over hours.
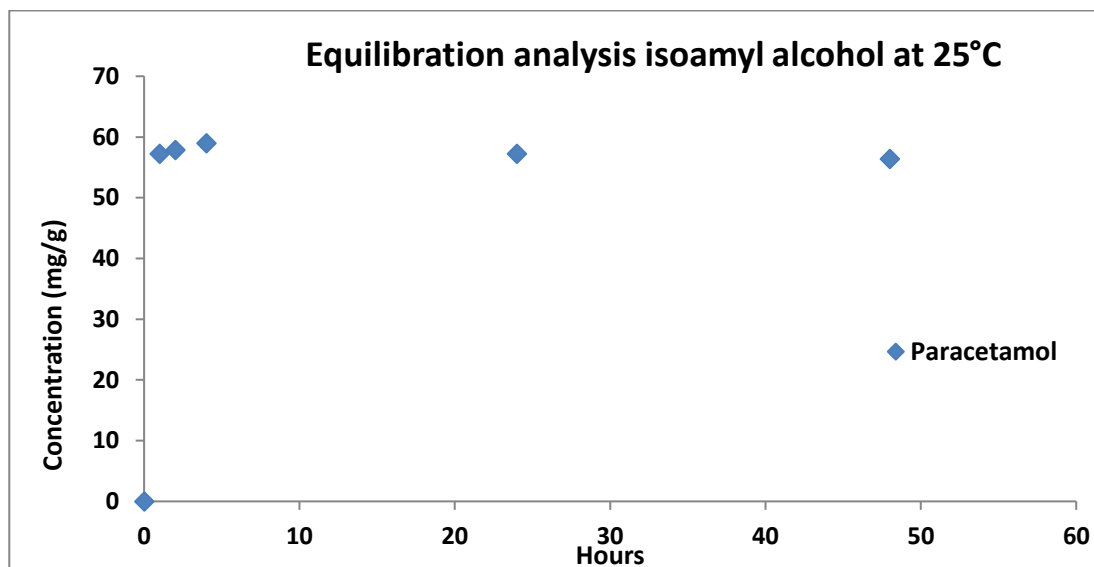
Figure 86: Gravimetric analysis of the approach to equilibrium in isoamyl alcohol looking at the concentration over hours.

1.1: Raw data report from XRPD analysis
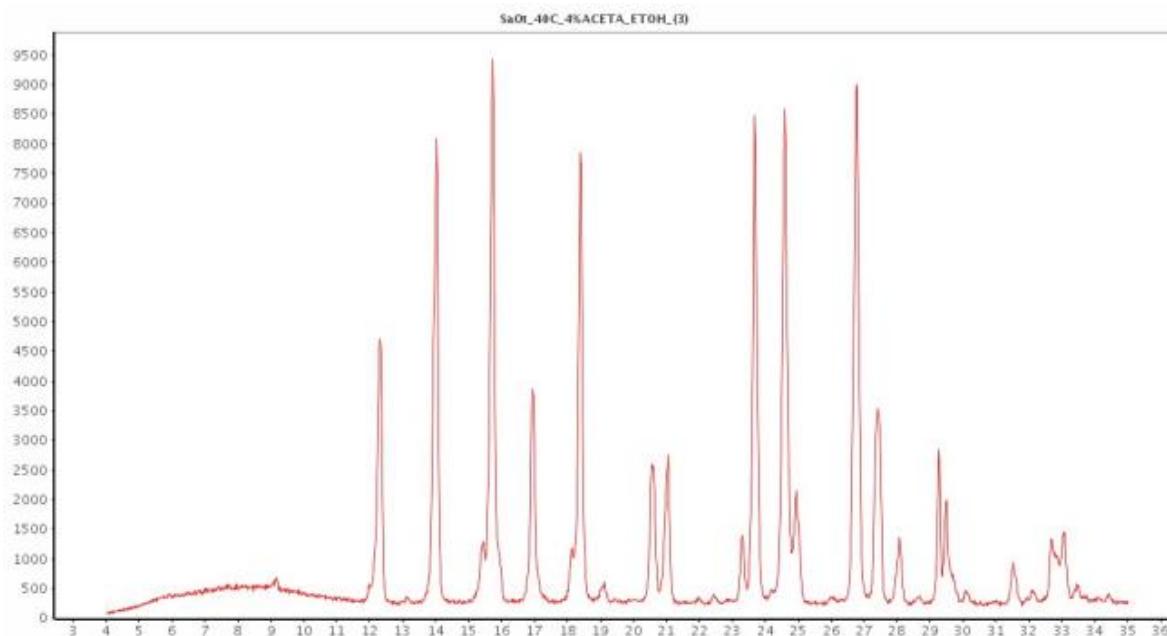
Figure 87: XRPD data report of 4% acetanilide in ethanol at 40 °C.
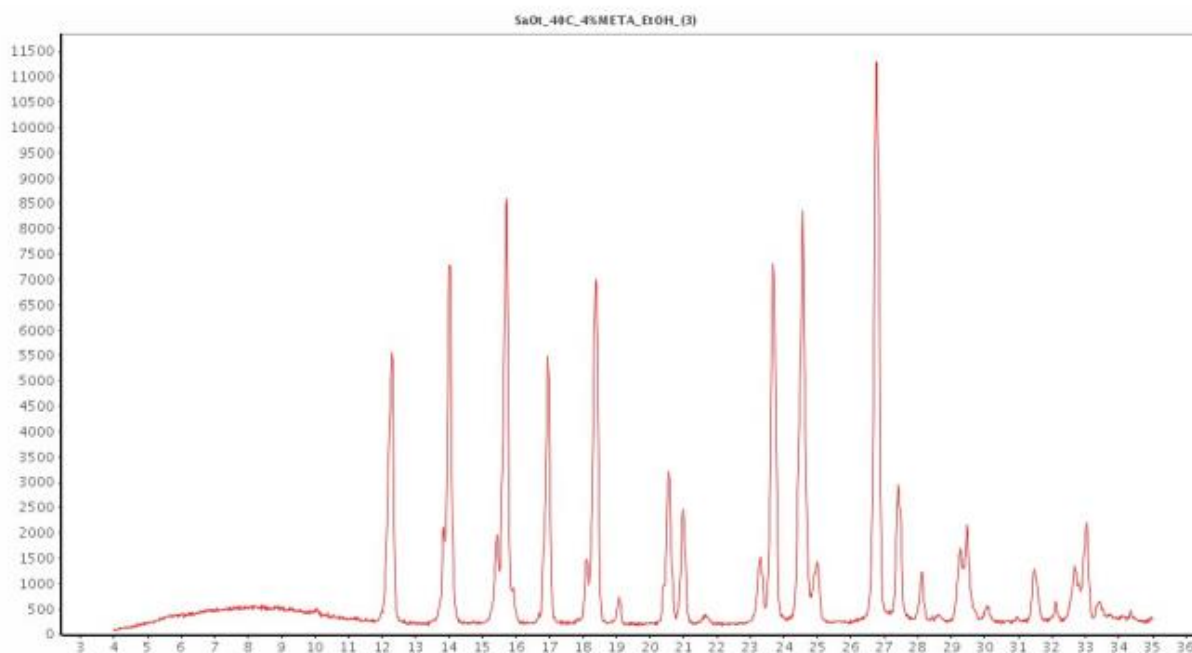
Figure 88: XRPD data report of 4% metacetamol in ethanol at 40 °C.

Figure 89: XRPD data report of paracetamol in isoamyl alcohol at 40 °C.
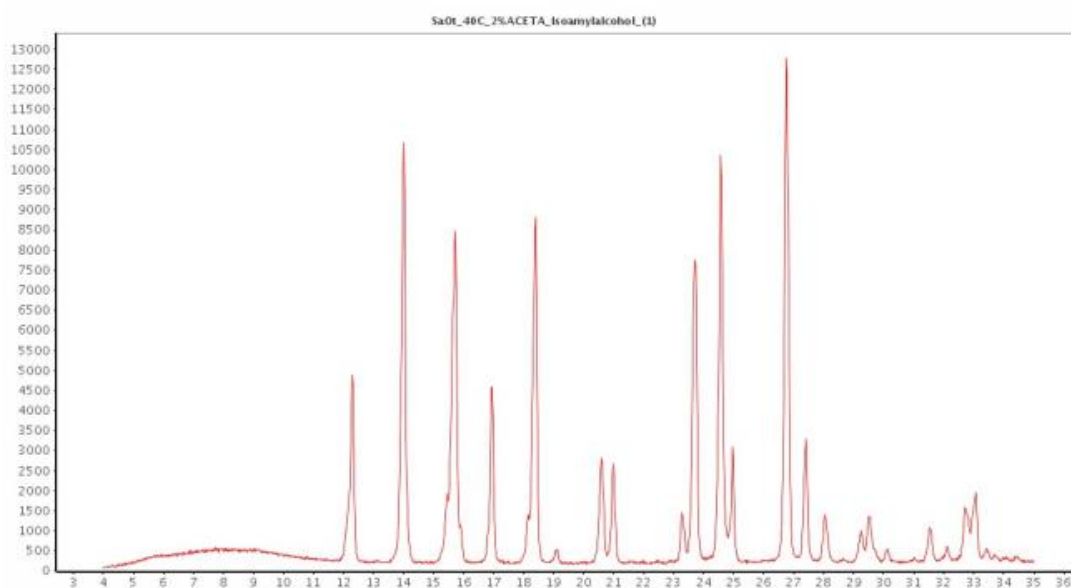
Figure 90: XRPD data report of 2% acetanilide in isoamyl alcohol at 40 °C.

Appendix A: Solubility of Paracetamol and Structurally Related Impurities
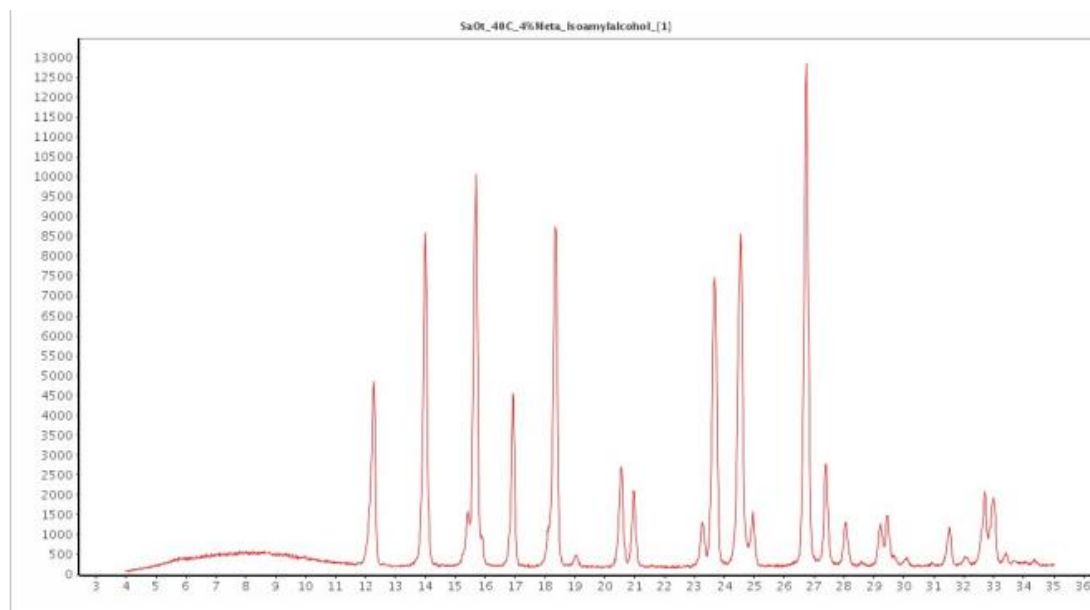
Figure 91: XRPD data report of 4% metacetamol in isoamyl alcohol at 40 °C.

2.0: Example of the amount of impurities and paracetamol weighed

<u>Calculation for 8.7° cells.</u>

Mass paracetamol (mg) to add to 5 mL (3.945g of solvent) = 147.8*3.945 = 583.2.

Mass (mg) of impurity to reach 1% impurity by mass = 583.2*0.01 = 5.8.

Mass (mg) of impurity to reach 2% impurity by mass = 583.2*0.02 = 11.7.

Mass (mg) of impurity to reach 4% impurity by mass = 583.2*0.04 = 23.3.

Mass of paracetamol (mg) was added to 7.5 mL (5.918g of solvent containing impurities from stock solution) = 147.8*3.945*1.5 = 874.8.

Mass in mg to reach 1% impurity by mass in a 50 mL volumetric flask = (874.8*0.01)*50/7.5 = 58.3.

Mass in mg to reach 2% impurity by mass in a 50 mL volumetric flask = (874.8*0.02)*50/7.5 = 116.6.

Mass in mg to reach 4% impurity by mass in a 50 mL volumetric flask = (874.8*0.04)*50/7.5 = 233.3.

A 30% excess of paracetamol was then added, total to add in mg to individual containers to which 7.5 mL of stock solution is then added = 874.8*1.3 = 1137.2.

2.1: Example of the impurity in the solution

Temp	mass 1%	Volume	conc g mL^{-1}	1% estd mass/density*vol
8.7	58.3	50	1.16638659	1.47831
13.7	63.1	50	1.26232899	1.59991
25	81.1	50	1.62256272	2.05648
40	103.0	50	2.05929	2.61
55	125.5	50	2.50902	3.18

Mass 1% = Mass in mg to reach 1% impurity by mass in a 50 mL volumetric flask.

Volume = volumetric flask used.

Conc g mL^{-1} = 58.3/50 = 1.16638659

1% estd mass/density = 58.3/(0.789*50) = 1.47831

2.2: Solubility calculations

Mass of Vial (g)	Mass of vial with solvent (g)	Dry mass of vial + dry residual solid (g)
10.0389	11.6675	10.3145
10.1134	11.7535	10.3902
9.9669	11.6205	10.2467

Appendix A: Solubility of Paracetamol and Structurally Related Impurities

Residual solid (g) = Dry mass of vial + dry residual solid (g) - Mass of Vial (g)

$$= 10.3145 - 10.0389$$

$$= 0.2756$$

Solution mass (g) = Mass of vial with solvent (g) - Mass of Vial (g)

$$= 11.6675 - 10.0389$$

$$= 1.6286$$

Concentration (g/solution) = Residual solid (g) / Solution mass (g)

$$= 0.2756 / 1.6286$$

$$= 0.169225101$$

Solvent mass (g) = Mass of vial with solvent (g) - Dry mass of vial + dry residual solid (g)

$$= 11.6675 - 10.3145$$

$$= 1.353$$

Concentration (g/g solvent) = Residual solid (g) - Solvent mass (g)

$$= 0.2756/1.353$$
$$= 0.203695492$$

Appendix A: Solubility of Paracetamol and Structurally Related Impurities

Impurity in solution sample (g) = Solution mass (g)* 25 °C con g mL^{-1}

$$= 1.6286 * 0.001622563$$

$$= 0.002642506$$

Corrected dry solid mass (para only) (g) = Residual solid (g) - Impurity in the solution sample (g).

$$= 0.2756 – 0.002642506$$

$$= 0.272957494$$

Solubility of paracetamol g/g solution = Corrected dry solid mass (para only) (g) / Solution mass (g).

$$= 0.272957494 – 1.6286$$

$$= 0.167602539$$

Solubility of paracetamol g/g solvent = Corrected dry solid mass (para only) (g)/ Solvent mass (g).

$$= 0.272957494 / 1.353$$

$$= 0.20174242$$

Solubility of paracetamol mg/g solvent = Solubility of paracetamol g/g solvent*1000

$$= 201.7424201$$

Actual impurity loading % = 100* Impurity in solution sample (g)/ corrected dry solid mass (para only) (g).

$$= 100*0.002642506/0.272957494$$

$$= 0.968$$

2.3: Van't Hoff calculations

2.3.1: DSC measurements of enthalpy of fusion and melting point of paracetamol, metacetamol, and acetanilide

Material	Area (J g^{-1})	Temperature (°C)
Paracetamol	-201.7	170.5
	-198.1	170.8
	-190.6	171
Average	-196.8	170.8
Standard deviation	5.7	0.3

Conversion from J g^{-1} to KJ mol^{-1}

The molecular weight of paracetamol = 151.6

= -196.8*151.6/1000

= -29.83 KJ mol^{-1}

Appendix A: Solubility of Paracetamol and Structurally Related Impurities

Material	Area (J g^{-1})	Temperature (°C)
Metacetamol	-185.2	144.3
	-180.9	144.5
	-165.9	144.6
Average	-177.3	144.5
Standard deviation	10.1	0.2

Conversion from J g^{-1} to KJ mol^{-1}

The molecular weight of metacetamol = 151.6

= -177.3*151.6/1000

= -26.88 KJ mol^{-1}

Material	Area (J g^{-1})	Temperature (°C)
Acetanilide	-184.8	113
	-171.1	113.3
	-161.1	113
Average	-172.3	113.1
Standard deviation	11.9	0.2

Conversion from J g^{-1} to KJ mol^{-1}

The molecular weight of acetanilide = 135.2

= -172.3*135.2/1000

= -23.30 KJ mol^{-1}

2.3.2: Van't Hoff plot results/calculations example

	Molecular weigh of solvents	Paracetamol	{g solute/g solvent}					
Ethanol	46.068 Mw		151.163					
Temperature ©		8.3	13.7	20	25	30	40	55
Run 1		0.147442993	0.159597097	0.179553265	0.202630786	0.22184511	0.278759714	0.471424855
Run 2		0.14821883	0.160385697	0.185548189	0.202260559	0.220658729	0.285386029	0.460166986
Run 3				0.18556556	0.20200662	0.227457098	0.274263496	0.481852206
Run 4				0.185896537	0.202486679	0.228553732		
Run 5								
Run 6								
Average		0.147830911	0.159991397	0.184140888	0.202346161	0.224628667	0.279469746	0.471148016
Mol fraction of solute in solution {X}		0.04311	0.04649	0.05314	0.05808	0.06407	0.07849	0.12556
lnX		-3.14399	-3.06848	-2.93489	-2.84586	-2.74776	-2.54484	-2.07499
1/T		0.00355	0.00349	0.00341	0.00336	0.00330	0.00319	0.00305
Ideal Sol								
TM	444.15							
kJ/mol	29.83							
lnX		-4.676614776	-4.436377957	-4.167293589	-3.96183261	-3.763152521	-3.384835164	-3.02994303
		67.22797587	69.16639028	70.4268699	71.83179097	73.01756908		

Figure 92: Example of Van't Hoff plot results and calculations.

Mol fraction of solute in solution X = (Average/molecular weight of paracetamol)/((Average/ molecular weight of paracetamol)+(1/molecular weight of solvent)

Mol fraction of solute in solution X = ((0.147830911/151.163)/((0.147830911/151.163)+(1/46.068))

$\underline{= 0.04311}$

lnX = LN(mol fraction of solute in solution (X))
lnX = LN(0.04311)

$\underline{= -3.14399}$

1/T = 1/(273+temperature)
1/T = 1/(273/8.3)

$\underline{=0.00355}$

2.4: Ideal solubility prediction

TM = (melting point+273.15)

 TM = (171+273.15)

   = <u>444.15</u>

KJ mol^{-1} = enthalpy of fusion

   = 29.83

InX = (KJ mol^{-1} * 1000/8.314)*(1/TM-1/T)

   = (29.83*1000/8.3214)*(1/444.15)

   = -4.676614776

   = (InX experimental / InX Ideal solubility*100)

   = (-3.14399 / -4.676614776 *100)

   = 67.22797587

2.5a Solubility of paracetamol and impurity concentrations in ethanol individualised at 25, 40, and 55 °C
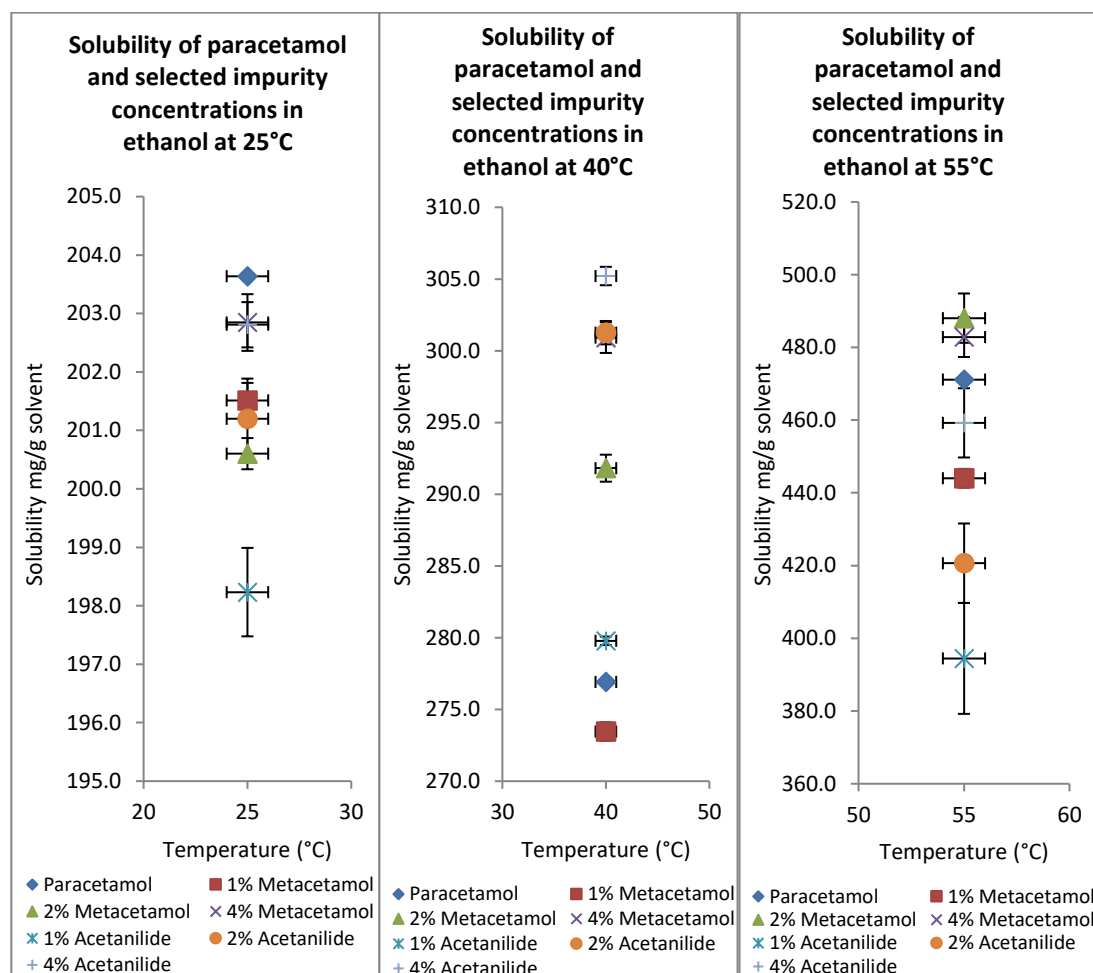
Figure 93: Solubility plot of paracetamol and impurity concentrations in ethanol at 25, 40 and 55 °C to allow for a better representation of individual points and associated error bars.

2.5b Solubility of paracetamol and impurity concentrations in isoamyl alcohol individualised at 25, 40, and 55 °C
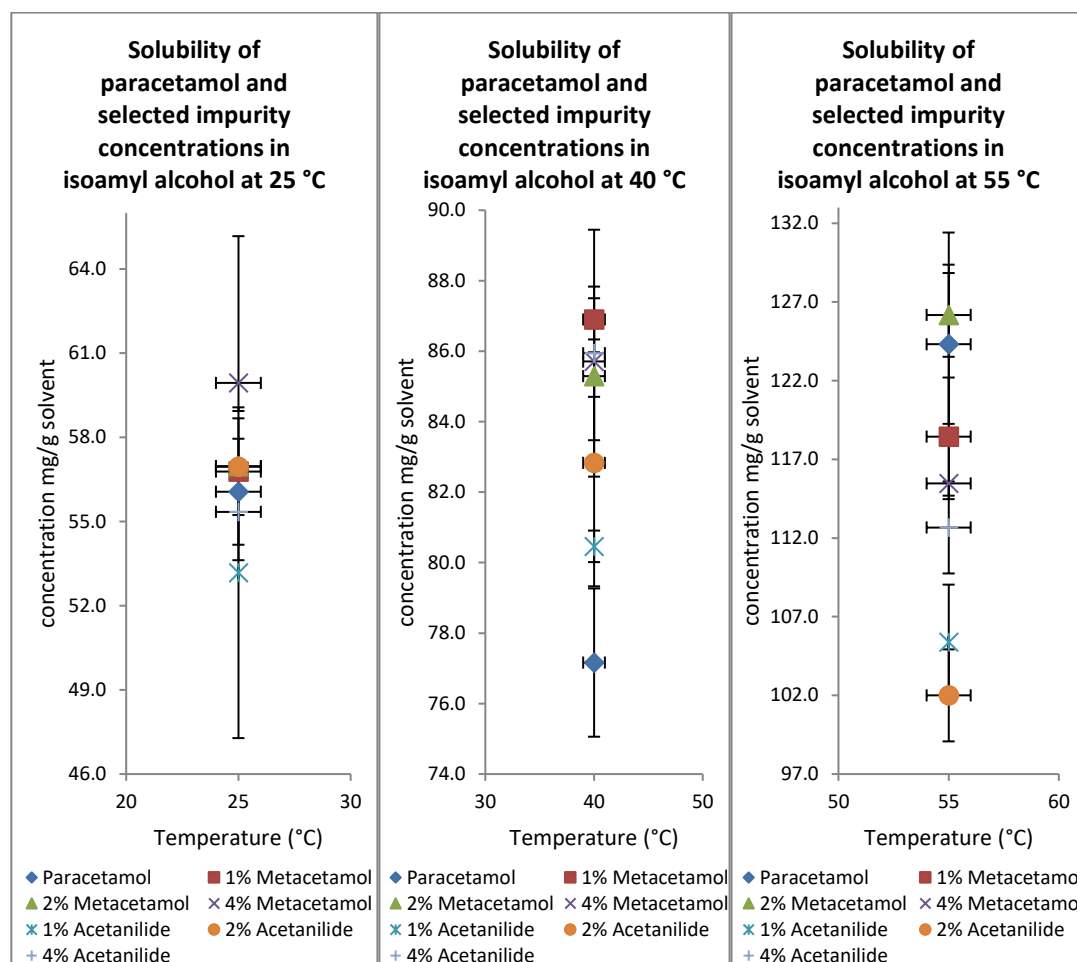
Figure 94: Solubility of paracetamol and impurity concentrations in isoamyl alcohol individualised at 25, 40, and 55 °C to allow for a better representation of the individual points and associated error bars.

APPENDIX B:

Single Crystal Growth with and without Ultrasonic Intervention

1.0: Face indexing and habit analysis
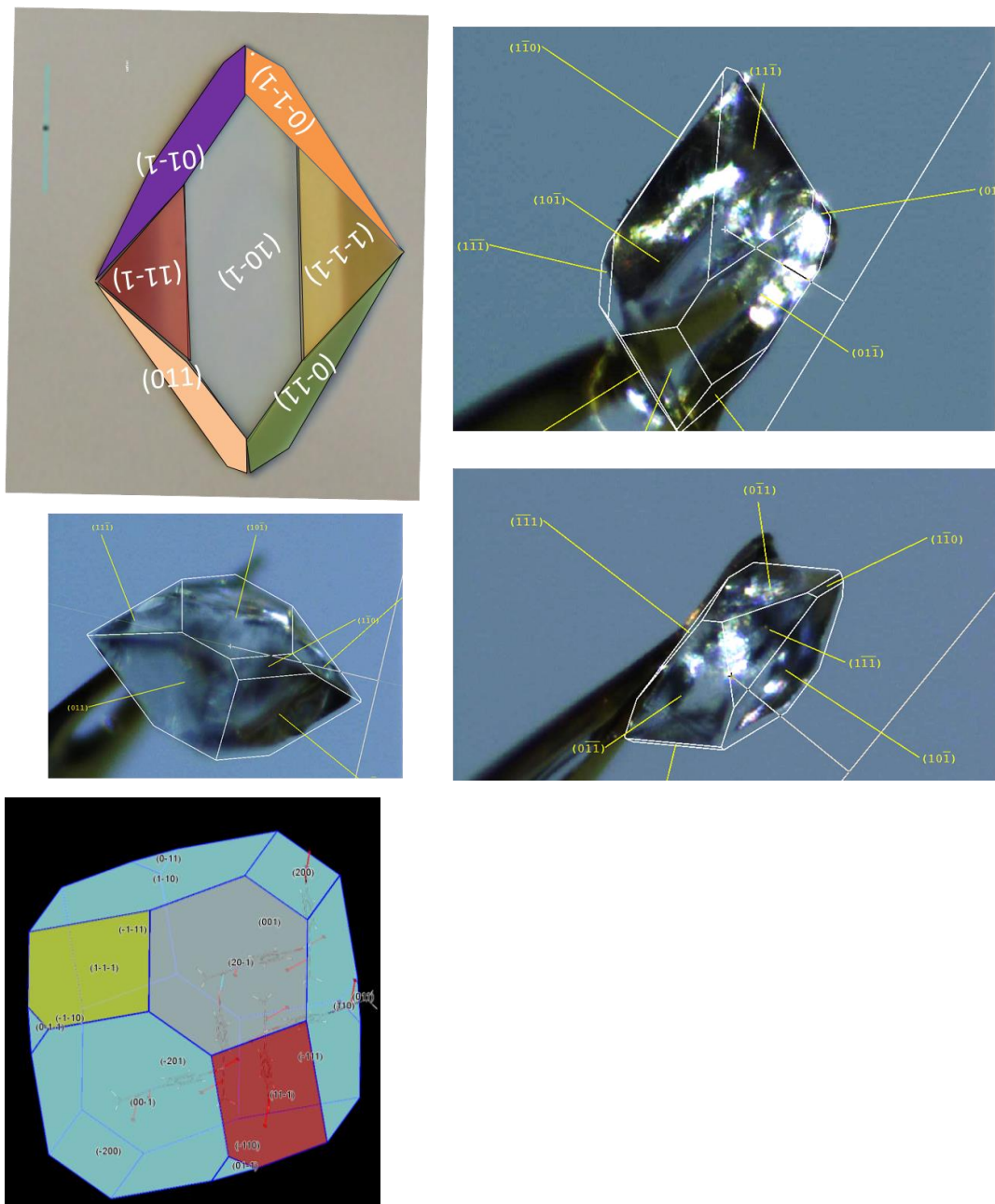
Figure 95: Truncated habit of a paracetamol single crystal grown in ethanol in this study, face assignment based on single crystal x-ray diffraction of typical crystals and attempting to match these with the BFDH model of paracetamol using Mercury With acknowledgement of support from Dr Alan Martin (Crystallographer at the University of Strathclyde).

Figure 96: Multi-faceted habit of a paracetamol single crystal grown in ethanol in this study, face assignment based on single crystal x-ray diffraction of typical crystals and attempting to match these with the BFDH model of paracetamol using Mercury With acknowledgement of support from Dr Alan Martin (Crystallographer at the University of Strathclyde).

Figure 97: Diamond habit of a paracetamol single crystal grown in ethanol in this study, face assignment based on single crystal x-ray diffraction of typical crystals and attempting to match these with the BFDH model of paracetamol using Mercury With acknowledgement of support from Dr Alan Martin (Crystallographer at the University of Strathclyde).

Figure 98: Needle-like habit of a paracetamol single crystal grown in ethanol in this study, face assignment based on single crystal x-ray diffraction of typical crystals and attempting to match these with the BFDH model of paracetamol using Mercury With acknowledgement of support from Dr Alan Martin (Crystallographer at the University of Strathclyde).

Appendix B: Single Crystal Growth with and without Ultrasound Intervention

1.1: In-depth analysis of single crystal growth rate data

1.1a Effect of supersaturation

For the experimental conditions T = 15 °C, S = 1.25, and impurity % = 0, growth rates for faces A and B were obtained on three crystals:

Table 18: Single crystal growth rate measurements for pairs of faces A and B at T = 15 °C, S = 1.25, and impurity % = 0.

Crystal	Face A	Face B
1	1.16	1.06
2	0.87	0.67
3	0.66	0.90

Figure 99: Images of single crystal habits for the first image at 0 mins, last image at 44 mins and final image of surroundings. For conditions, T = 15 °C, S = 1.25 and impurity % = 0, a 100µm scale bar is also present.

Looking at the crystal's habits (Figure 99), there is an evident similarity between them and whilst the growth rates differ to some extent (Table 18), the relationship between the growth rates for faces A and B is similar; the ratios between growth rates for faces A and B are 1.09, 0.97, and 0.97 respectively, for crystals 1, 2, and 3. The difference in measured growth rates is more marked; for face A, the average growth rate is 0.9 ±

Appendix B: Single Crystal Growth with and without Ultrasound Intervention

0.26 μm min^{-1}and for face B it is 0.88 ± 0.2 μm min^{-1}. The difference in rates affects the ultimate crystal size reached, but the similarity in the ratio between the faces leads to consistent habits. The images found in Figure 99 show the expected growth progress between the starting and end sizes of the selected crystals. Interestingly, the final image of crystal 1 shows a crystal in the top right, which is larger in size and displays evidence of pitting on the surface.

For the experimental conditions T = 15 °C, S = 1.75, and impurity % = 0, single crystal face growth rates were obtained on four crystals. The corresponding growth rates are:

Table 19: Single crystal growth rate measurements for pairs of faces A and B at T = 15 °C, S = 1.75, and impurity % = 0.

Crystal	Face A	Face B
1	2.61	0.52
2	2.36	2.07
3	2.48	1.95
4	2.47	2.26
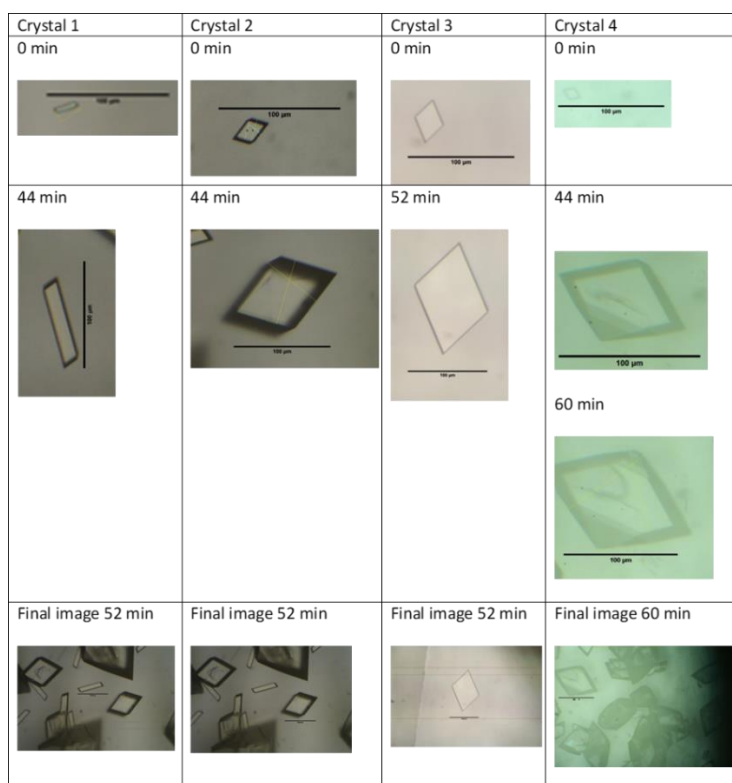
Figure 100: Images of single crystal habits for the first image at 0 mins, the last image at 44 mins and the final image of surroundings. For conditions, T = 15 °C, S = 1.75 and impurity % = 0, a 100μm scale bar is also present.

Appendix B: Single Crystal Growth with and without Ultrasound Intervention

The most striking observation is the habit difference between the crystals (Figure 100); the crystal thickness and the size of faces A and B are noticeably different. Crystal 1 has a much lower growth rate for face B than the other crystals (Table 19); this is consistent with the observed habit. Crystal 2 (Figure 100) shows evidence of growth in all three directions; based on the shadows, it is the thickest crystal in the group, i.e., there has been significant growth in the Z direction. Crystal 3 appears quite thin, indicating inhibited growth in the Z direction, along with a similar diamond habit. Crystal 4 has a more complex habit, consistent with those seen under the growth conditions at the same temperature but at lower supersaturation (15 °C and S = 1.25, Figure 99).

Interestingly, the truncation of the corner can only be seen on one side of the crystal. Crystals 1 and 2 were observed simultaneously growing in the same solution, but the difference in habit is very significant. In the final images of crystals 1 and 2, a variety of thin needle-like crystals are observed, along with some thicker diamond habits and the presence of similar truncated-like habits as observed in crystal 4's final images. For crystal 3, no crystals were observed around the selected measured crystal. For the final image of crystal 4, a variety of habits were observed.

Similarly, in crystals 1 and 2, the crystals have started to cluster together, and there is a noticeable growth in the z direction, with a clear thickness of crystal observed from shadows. For some crystals, it is difficult to determine where the faces are, as they have a rounder appearance. Some crystals also have clear, favourable faces, growing quicker than others.

The four measured growth rates for face A are relatively consistent (Table 19); the ratios between growth rates for faces A and B were 5.01, 1.14, 1.28, and 1.09, respectively, for crystals 1, 2, 3, and 4 the ratios correspond as expected with the habits observed. The mean growth rate is 2.48 ± 0.1 µm min^{-1} for face A, and the corresponding values for face B are 1.7 ± 0.8 µm min^{-1}, indicating a slightly bigger variance, which is due to the needle-like habit of crystal 1. By eliminating the growth rate measured for crystal 1, the mean growth rate of face A is 2.44 ± 0.07 µm min^{-1} and face B is 2.09 ± 0.16 µm min^{-1}, resulting in a decrease in error and an increase in growth rate for face B.

Appendix B: Single Crystal Growth with and without Ultrasound Intervention

Considering the effect of supersaturation, all face A growth rates are faster at supersaturation 1.75 compared with 1.25 and are relatively consistent despite the noticeable habit differences in the z dimension (not measured).

For T = 30 °C, S = 1.25 and impurity % = 0. There are growth rates for faces A and B on four crystals:

Table 20: Single crystal growth rate measurements for pairs of faces A and B at T = 30 °C, S = 1.25, and impurity % = 0.

Crystal	Face A	Face B
1	0.14	0.13
2	0.28	0.24
3	0.06	0.05
4	0.24	0.45
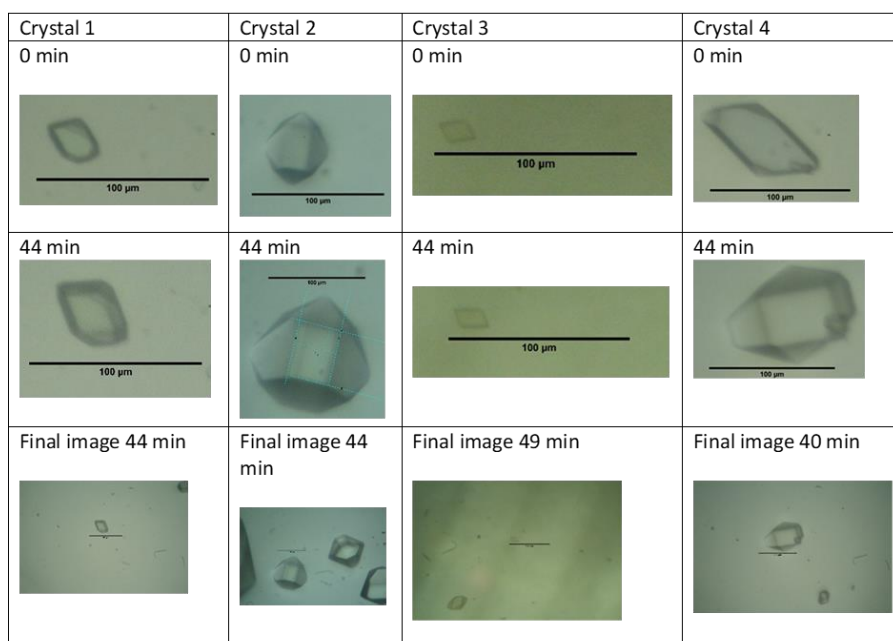
Figure 101: Images of single crystal habits for the first image (e.g., 0 mins) and last image (e.g., 44 mins) and final image of surroundings. For conditions, T = 30 °C, S = 1.25, and impurity % = 0. A 100µm scale bar is also present.

Appendix B: Single Crystal Growth with and without Ultrasound Intervention

For this condition, determining the growth rates in the A and B directions of crystals 1, 2, and particularly 4 (Figure 101) was challenging. This is because multiple faces are expressed in the habit, and there is a tendency for the crystal faces to be less distinct. A similar rounding of the faces of crystal 1 was observed at 20 °C, S = 1.25. The faces of crystal 1 were estimated using the edges of the shadows and observation of the growth through the captured images. Again, for crystals 2 and 4, the growing faces are not those typically found; some faces appear elongated relative to others, resulting in different observed habits. In the final image of crystal 2, additional unusually shaped crystals were not measured. All three observed crystals resulted in various shapes and thicknesses.

The relationship between the growth rates of faces A and B is similar, excluding crystal 4 (Table 20). The ratios between growth rates for faces A and B were 1.16, 1.10, 1.18, and 0.54, respectively, for crystals 1, 2, 3, and 4. The difference is that the measured growth rate is more pronounced. For face A, the average growth rate was 0.18 ± 0.10 µm min^{-1} and for face B, 0.22 ± 0.17 µm min^{-1}; there is a larger variance for face B as well as a faster growth rate.

For T = 30 °C, S = 1.75 and impurity % = 0, the corresponding growth rates are as follows:

Table 21: Single crystal growth rate measurements for pairs of faces A and B at T = 30 °C, S = 1.75, and impurity % = 0.

Crystal	Face A	Face B
1	0.24	0.19
2	0.04	0.02
3	0.04	0.03
4	0.91	0.56

Appendix B: Single Crystal Growth with and without Ultrasound Intervention

Crystal 1	Crystal 2	Crystal 3	Crystal 4
0 min	0 min	0 min	0 min
44 min	44 min	44 min	
Final image 44 min	Final image 44 min	Final image 44 min	Final image 44 min
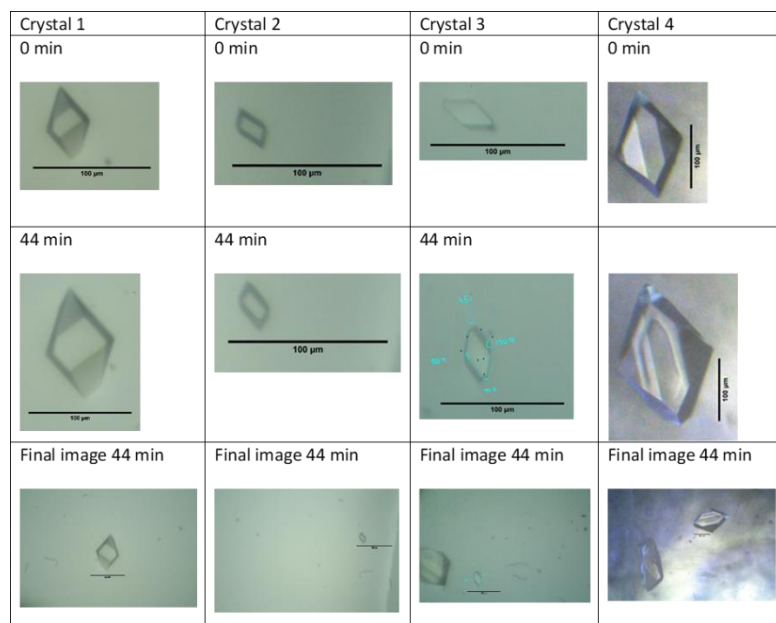
Figure 102: Images of single crystal habits for the first image at 0 mins, the last image at 44 mins and the final image of surroundings. For conditions, T = 30 °C, S = 1.75, and impurity % = 0. A 100μm scale bar is also present.

For this condition, the crystals have apparent habit differences (Figure 102). With similarities between crystals 2 and 3, 3 grew more in the A direction when compared with crystal 2. Crystal 1 habits were observed with the addition of impurities but were not found in other pure-condition experiments. Crystal 4 is more commonly observed in the pure condition, e.g., T = 15 °C, S = 1.25, and 1.75 (Figure 99-Figure 100) and T = 20 °C, S = 1.25 (Figure 103). In the final images of crystals 3 and 4, thicker and larger crystals are present with different habits to the crystals measured.

The relationship between the growth rates of faces A and B is similar to the lower supersaturation, excluding crystal 4 (Table 21). The growth rate of face A is faster than that of B, but the overall size and growth rate are faster than those of the other measured crystals. The ratios between growth rates for faces A and B were 1.29, 1.92, 1.34, and 1.64, respectively, for crystals 1, 2, 3, and 4. For face A, the average growth rate was 0.31 ± 0.41 μm min^{-1} and for face B, 0.20 ± 0.25 μm min^{-1}. This condition's variation is more significant compared to the lower supersaturation. This is likely due to the various habits observed.

Appendix B: Single Crystal Growth with and without Ultrasound Intervention

1.1b Effect of temperature

For T = 20 °C, S = 1.25, and impurity % = 0. There are growth rates for faces A and B on three crystals:

Table 22: Single crystal growth rate measurements for pairs of faces A and B at T = 20 °C, S = 1.25, and impurity % = 0.

Crystal	Face A	Face B
1	0.47	0.42
2	0.52	0.39
3	0.36	0.37
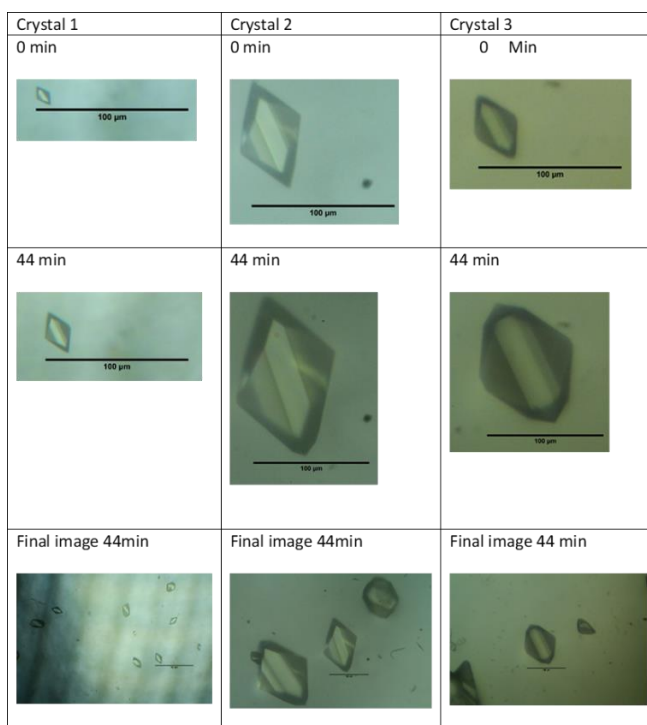
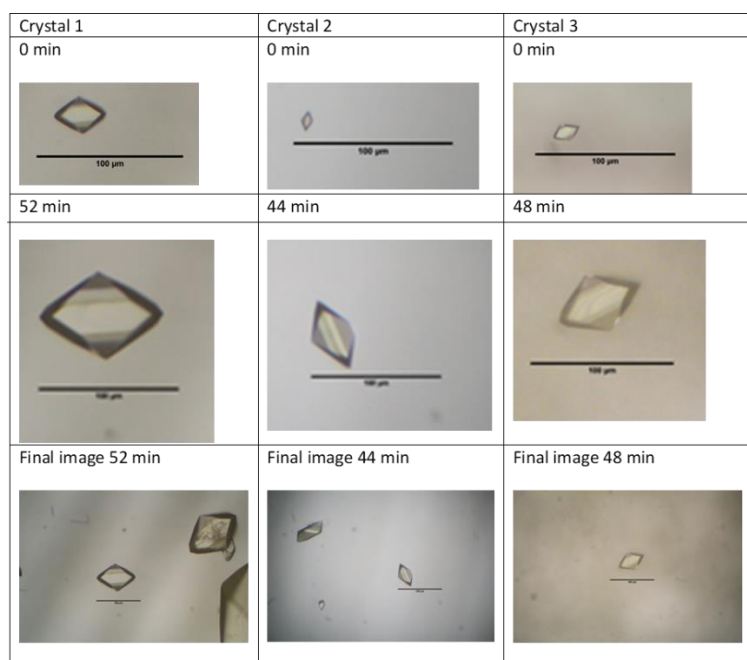**Figure 103:** Images of single crystal habits for the first image at 0 mins the last image at 44 mins and the final image of surroundings. For conditions, T = 20 °C, S = 1.25, and impurity % = 0. A 100µm scale bar is also present.

Appendix B: Single Crystal Growth with and without Ultrasound Intervention

In this condition, the habits (Figure 103) are similar to T = 15 °C and S = 1.25 (Figure 99). Crystals 1, 2, and 3 have similar habits and relationships between their growth rates. face A of crystals 1 and 2 is the fastest-growing face, and face B of crystal 3 is slightly quicker (Table 22); this is also evident from the appearance of the crystal habit, which is subtly different. The ratios between growth rates for faces A and B are 1.12, 1.32, and 0.97, respectively, for crystals 1, 2, and 3. For face A, the average growth rate is 0.45 ± 0.08 µm min^{-1} and for face B, 0.39 ± 0.02 µm min^{-1}.

Crystals grown at 20 °C were compared to those grown at 15 °C (Figure 103-Figure 99) to examine the effect of growth temperature. The average growth rate for faces A and B decreases with an increase in temperature at both supersaturations. The crystal habits produced at each temperature show some similarities. However, there was evidence of face growth rates changing with an increase in temperature; e.g., at 30 °C, S =1.25 (Figure 101), there was a crystal that favoured growth in the Z direction, i.e., appeared thicker, which was like a crystal at 20 °C, S = 1.25 (Figure 103). However, its growth in the B direction appears to be retarded, creating a more rounded appearance at the bottom of the crystal.

For T = 20 °C, S = 1.75 and impurity % = 0. There are growth rates for faces A and B on three crystals:

Table 23: Single crystal growth rate measurements for pairs of faces A and B at T = 20 °C, S = 1.75, and impurity % = 0.

Crystal	Face A	Face B
1	1.03	1.02
2	0.51	0.13
3	0.98	0.69

Appendix B: Single Crystal Growth with and without Ultrasound Intervention

| Crystal 1	Crystal 2	Crystal 3
0 min	0 min	0 min
44 min	36 min	36 min
Final image 44 min	Final image 40 min	Final image 40 min

Figure 104: Images of single crystal habits for the first image at 0 mins the last image at 44 mins and final image of surroundings. For the conditions, T = 20 °C, S = 1.75, and impurity % = 0. A 100µm scale bar is also present.

Appendix B: Single Crystal Growth with and without Ultrasound Intervention
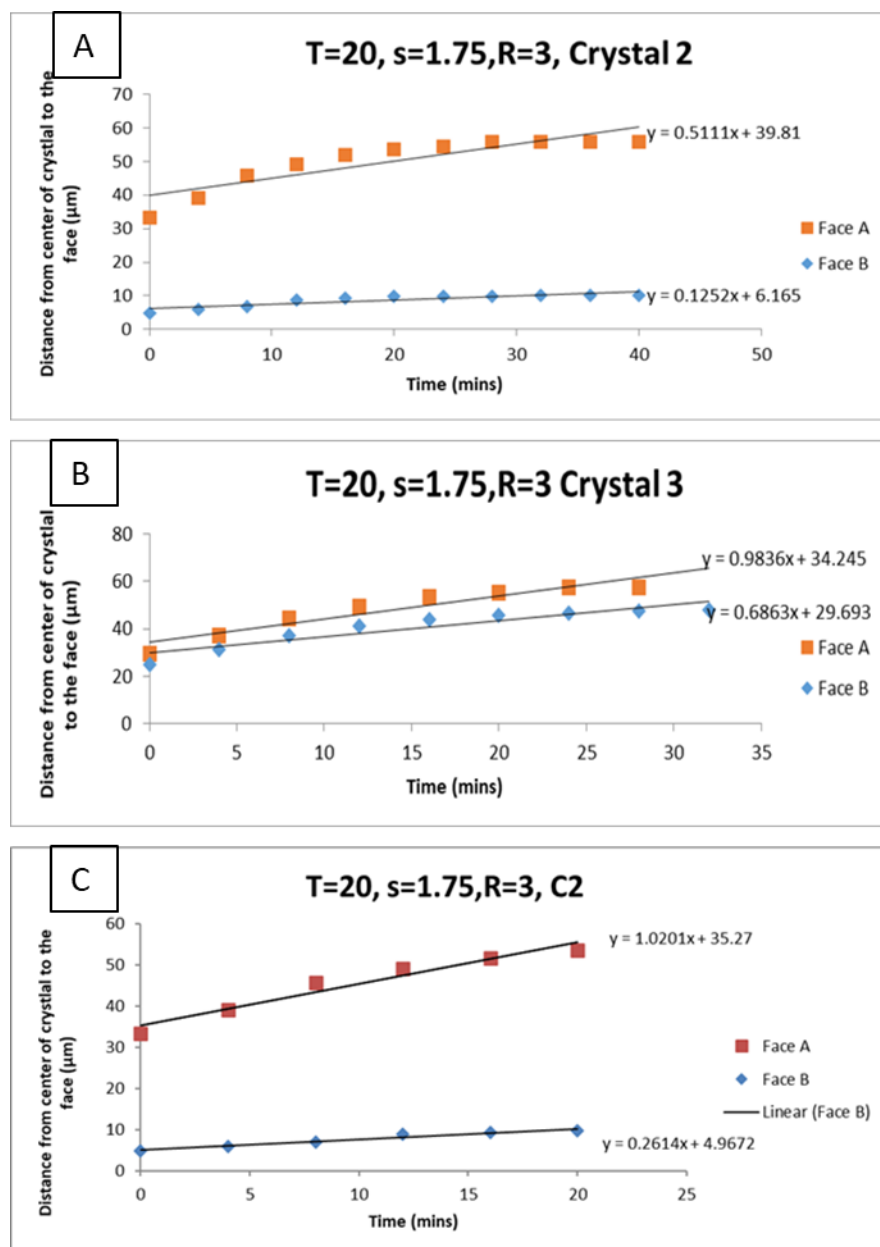
Figure 105: Image of graphs plotted of single crystal growth rate measurements (distance from the centre of the crystal to the face/ time (4-minute intervals)).

At this condition, the habits between the crystals vary (Figure 104). The thickness of crystal 1 is clearly different from that of crystals 2 and 3, as seen by its shadows, i.e., growth in the Z direction and truncation of some corners are also observed. Crystal 1 shows potential defects present on the crystal surface. These are likely to be screw dislocations, as they have some similar characteristics to a potential lattice plane shift (289). Face A is the fastest growing for all crystals. However, crystal 2 has a noticeably lower growth rate for face B, which is consistent with the habit observed. Crystal 3 is

Appendix B: Single Crystal Growth with and without Ultrasound Intervention

thin, indicating inhibited growth in the Z direction. In the final image, a mixture of crystal habits is observed. For crystal 1, the habits are all very similar. Crystals 2 and 3 were selected from the same system. However, the difference in habits is quite significant, similarly seen for crystals 1 and 2, T = 15 °C, S = 1.75.

The relationships between face A and B vary in this case (Table 23). The ratios between growth rates of faces A and B were 1.01, 4.08 and 1.43, respectively, for crystals 1, 2, and 3, respectively. The difference in the average measured growth rate was larger. For face A, the mean growth rate was 0.84 ± 0.29 μm min^{-1}, and for face B, it was 0.61 ± 0.45 μm min^{-1}.

In the graphs of crystals 2 and 3, a slight curve of faces A and B is observed; this indicates that the supersaturation is being consumed by a larger crystal, which can be observed in Figure 105 (A) and (B). The growth rate measurements for crystal 2 were cut in half every 20 seconds, as the curving off of the graph in Figure 105 (C) indicated depletion of supersaturation past 20 seconds. Face A almost doubles from 0.51 μm min^{-1} to 1.02 μm min^{-1}and face B increases slightly from 0.13 μm min^{-1} to 0.26 μm min^{-1}. If this approach were applied to the other crystals measured, then the overall growth rate would increase from 0.84 $\pm$ 0.29 in the A direction to 1.16 $\pm$ 0.14 and in the B direction from 0.61 $\pm$ 0.45 to 0.79 $\pm$ 0.46. Showing a slight increase in overall growth rate. This is still significantly lower than the growth rates at 15 °C.

Between the temperatures, the habits at 20 °C (Figure 103-Figure 104) are very similar to those at 15 °C (Figure 99-Figure 100), with the presence of diamonds, needle-like crystals and truncated crystals being observed. However, the habits are quite different at 30 °C. As stated above, the average growth rate was found to decrease with an increase in temperature (Table 23); this is not usually what is found with single crystal analysis. For example, Omar (257) investigated single paracetamol crystals and found them to be temperature dependent, where the growth rate of all faces measured increased with an increase in temperature. This is clearly not what has been found in this study. However, the method was different as they grew single crystals and then harvested them to measure the growth, whereas this study analysed the crystal in real time. This investigation shows not only the variability while the crystals are growing

but also the entire picture of the crystals surrounding each single crystal. When additional habits are not excluded or individualised in an analysis, this is likely to skew the resulting average data, e.g., having diamonds and needles present.

1.1c Effect of impurities

For the experimental conditions T = 15 °C, S = 1.25, and impurity = 4% metacetamol and 4% acetanilide, growth rates for faces A and B were obtained on three crystals per condition**.** Table 24 provides an overview of the effect of the impurities on growth behaviour.

Table 24: Single crystal growth rate measurements for pairs of faces A and B at T = 15 °C, S = 1.25, impurity % = 0, 4% metacetamol, and 4% acetanilide with images of habits. Each vertical column of three images comprises of the individual crystal at the start and end of the growth measurement and then a wider view showing surrounding crystals, if any.

No impurity			4% Metacetamol			4% Acetanilide		
Crystal	Face A $\mu m\ min^{-1}$	Face B $\mu m\ min^{-1}$	Crystal	Face A $\mu m\ min^{-1}$	Face B $\mu m\ min^{-1}$	Crystal	Face A $\mu m\ min^{-1}$	Face B $\mu m\ min^{-1}$
1	1.16	1.06	1	0.27	0.04	1	0.06	0.02
2	0.87	0.67	2	0.23	0.03	2	0.43	0.09
3	0.66	0.90	3	0.11	0.02	3	0.14	0.23

When comparing the effect impurities have on single crystal growth, it is instantly clear that impurities slow the growth rate in both the A and B directions (Table 24). When 4% metacetamol is added to the system, the growth rate of both faces is reduced, the greatest reduction being in the B direction of the crystals. The ratios in growth rates of face A to B are much higher than in the system with no added impurity; this is consistent with the change in observed crystal habit. These ratios in face growth rate

Appendix B: Single Crystal Growth with and without Ultrasound Intervention

A/B were 7.15, 6.80, and 5.37, respectively, for crystals 1, 2, and 3. The corresponding values for crystals grown from a pure solution are 1.09, 0.97 and 0.97. The difference in measured average growth rates for face A is 0.20 ± 0.08 µm min^{-1} and for face B is 0.03 ± 0.01 µm min^{-1}, indicating that the impurity reduced the average growth rate by 77% in the A direction and 96% in the B direction.

As previously mentioned, the difference in rate affects the ultimate crystal size reached; a similarity in the ratio between the faces will lead to an equant crystal habit, whereas a large difference between the ratios results from an elongated habit. Comparing the starting and final images used to measure the growth of the crystals shows consistency in habit, even though individual crystals exhibit different habits. Although the habits are mostly similar, there are a few notable differences. Crystals 1 and 2, in the presence of 4% metacetamol, appear to be the thickest, indicating notable growth in the z direction (which could not be measured) (Figure 106). There is also truncation evident on some of the edges of the crystals, which alters their habits. In the final image of crystals 2 and 3 (grown in the same field of view), a cluster of agglomerated crystals is observed, as well as a habit with a more rounded appearance seen just below crystal 2, which was not previously observed.

When 4% acetanilide is added to the system, the growth rate in the A direction is the fastest for crystals 1 and 2 but not for crystal 3; it is clear from the image and the scale bar that crystal 3 is a lot bigger compared to the others measured (Figure 107). The ratios between growth rates for faces A and B were higher for crystals 1 and 2 when compared with the system with no added impurity but lower when compared with 4% metacetamol; these were 4.09, 4.71, and 0.56, respectively, for crystals 1, 2, and 3. The difference in measured average growth rates for face A was 0.21 ± 0.19 µm min^{-1} and for face B 0.12 ± 0.12 µm min^{-1}; the error is smaller when compared to the purer system for face A but not B and higher when compared to the error of 4% metacetamol. Acetanilide was found to reduce the average growth rate by 76% in the A direction and 86% in the B direction. This has less of an effect on the average growth rate when compared with metacetamol.

Appendix B: Single Crystal Growth with and without Ultrasound Intervention

As seen above, the similarity in ratio between the faces of crystals 1 and 2 leads to similar-looking habits. Crystal 3 has a much smaller ratio; however, looking at the appearance of the crystal, it is also evidently similar in shape and has a slight truncation of the corners, which is also seen with crystals 1 and 2. The starting and ending images show a progressive growth rate. With no additional crystals found to cause any hindrance to the growth, the final image in crystal 2 showed the appearance of more needle-like habits forming.

In this case, the addition of impurities significantly affects the crystal growth rate and habits. The habits were relatively consistent with and without the addition of impurities (Table 24). With the addition of impurities slowing the growth rate, there was less potential for issues with the depletion of supersaturation due to surrounding larger crystals. However, there was an indication of agglomeration occurring with 4% metacetamol, which could be a problem for downstream processes. Needle-like habits are also usually less favourable due to their compaction behaviours during tabletting.

Crystal 1	Crystal 2	Crystal 3
0 min	0 min	0 min
44 min	44 min	44 min
Final image 44 min	Final image 44 min	Final image 44 min

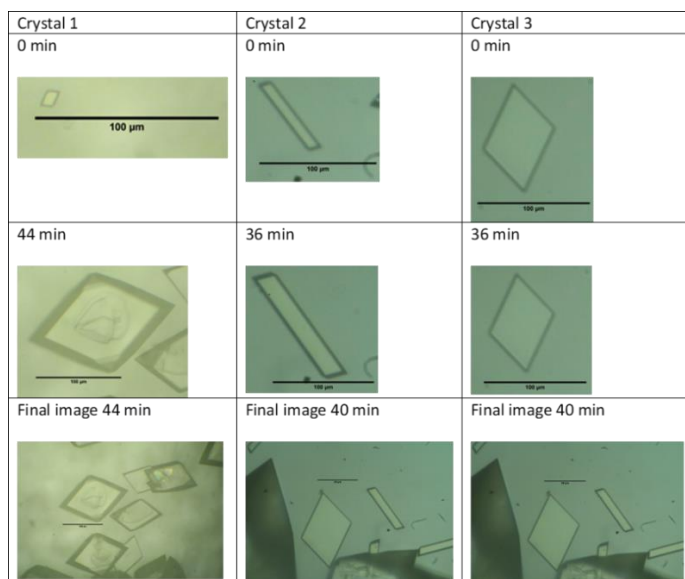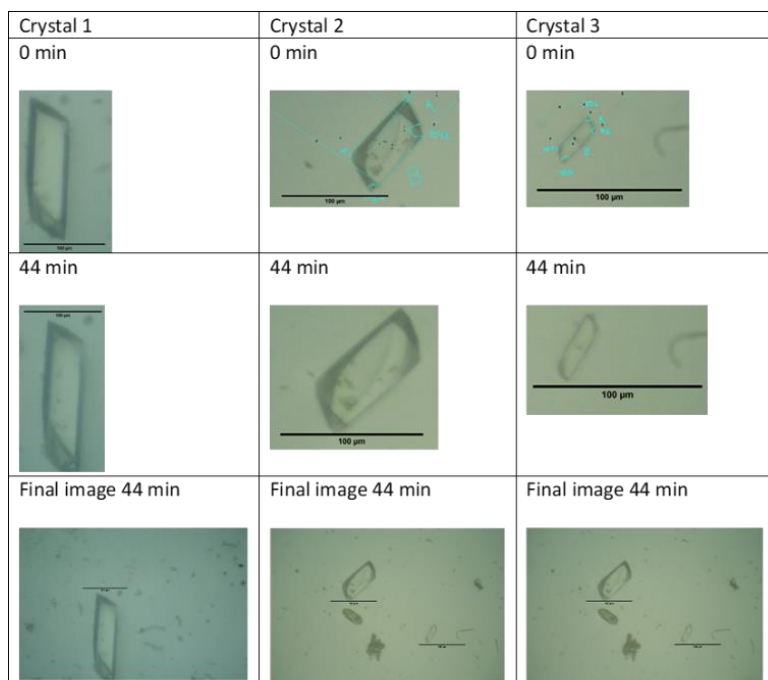Appendix B: Single Crystal Growth with and without Ultrasound Intervention

Figure 106: Images of single crystal habits for the first image at 0 mins, the last image at 44 mins and the final image of surroundings. For conditions, at T = 15 °C, S = 1.25, and impurity % = 4% metacetamol. A 100µm scale bar is also present.
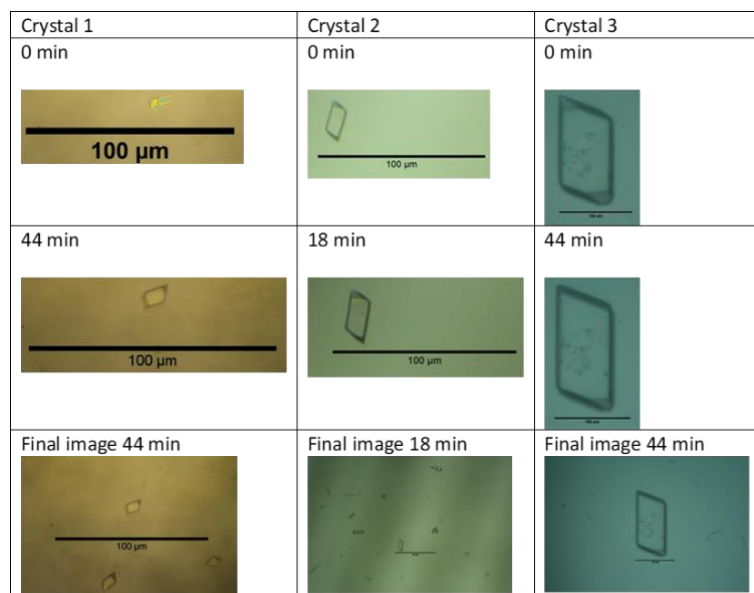
Figure 107: Images of single crystal habits for the first image at 0 mins the last image at 44 mins and the final image of surroundings. For conditions, T = 15 °C, S = 1.25 and impurity % = 4% acetanilide. A 100µm scale bar is also present.

1.1d Effect of impurities and supersaturation

For the experimental conditions, T = 15 °C and S = 1.75 with paracetamol and the addition of 4% metacetamol and 4% acetanilide. The growth rates for faces A and B were obtained for four and three crystals per condition. Table 25 provides an overview of the effect of the impurities on growth behaviour.

In Table 25, impurities are again found to reduce the growth rate. When compared with the pure system, the average growth rate is reduced by 87.5% in the A direction and 95.3% in the B direction when metacetamol is added, and it is reduced by 76.2% in the A direction and 74.1% in the B direction. The comparison between face growth rates indicates that the impurities favour inhibiting growth in the B direction.

35

Appendix B: Single Crystal Growth with and without Ultrasound Intervention

Table 25: Single crystal growth rate measurements for pairs of faces A and B at T = 15 °C, S = 1.75 and impurity % = 0 and 4% metacetamol, and 4% acetanilide. Each vertical column of three images comprises of the individual crystal at the start and end of the growth measurement and then a wider view showing surrounding crystals, if any.

No impurity				4% Metacetamol			4% Acetanilide		
Crystal	Face A μm min^{-1}	Face B μm min^{-1}	Crystal	Face A μm min^{-1}	Face B μm min^{-1}	Crystal	Face A μm min^{-1}	Face B μm min^{-1}	Crystal
1	5.01	2.61	0.52	1	0.59	0.10	1	0.43	0.39
2	1.14	2.36	2.07	2	0.27	0.14	2	0.76	0.47
3	1.27	2.48	1.95	3	0.08	0.01	3	0.58	0.46
4	1.09	2.47	2.26						

When 4% metacetamol is added to the system, the growth rate of both faces is reduced. The greatest reduction is in the B direction of crystal growth (Table 25). The ratios in growth rates of faces A and B are much higher than in the system with no added impurity; this is consistent with the change in observed crystal habits. These ratios in face growth rate A/B were 6.12, 1.89, and 5.54, respectively, for crystals 1, 2, and 3. The corresponding values for crystals grown from pure solution were 5.01, 1.14, 1.28, and 1.09, respectively, for crystals 1, 2, 3, and 4. The difference in measured average growth rates for face A is 0.31 ± 0.25 μm min^{-1} and for face B is 0.08 ± 0.06 μm min^{-1}.

Consistency in habits is found when analysing the images of the growth rates from the first to the final image of the crystals (Figure 108). There are similarities between crystals 1 and 2 and crystal 1 in the pure condition. However, crystal 3 shows a more progressive truncated habit, similar to crystal 4 in the pure conditions. In the final

images, fewer crystals are observed, unlike in the pure condition. There is also an odder shape found in the crystal 2 and 3 system, which has not been found in other systems or conditions; the impurity seems to be inhibiting growth all over, resulting in different angled faces appearing with an almost star-like appearance.

When 4% acetanilide is added to the system, the growth rate in the A direction is the fastest, indicating that the impurity favours inhibiting the B direction of crystal growth. The ratios between growth rates for faces A and B were more consistent for crystals 1, 2, and 3; these were 1.17, 1.62, and 1.25, respectively. This is also lower in comparison to metacetamol. The difference in measured average growth rates for face A is 0.59 ± 0.16 µm min^{-1} and for face B is 0.44 ± 0.04 µm min^{-1}, which is lower in comparison to the purer system but is higher in both the A and B directions when compared with metacetamol.

The images of the first and final crystals analysed show consistency during the growth and capture of images (Figure 109). Crystal 1 and 2, found in the same system, show similarities in the crystals' habit, shape, and thickness; there is obvious growth in the Z direction for these crystals, similar to crystal 2 in the pure system but not as well defined. Crystal 1 also shows an indication of steps forming on the surface; however, it is not possible to be certain about the images taken. Crystal 3 has a similar shape; however, it is not thick and is more plate-like, as previously seen with crystal 3 in its pure condition.

Acetanilide was found to have a lower ratio between growth rates for faces A and B when compared to metacetamol in this system, similar to the results found at supersaturation 1.25. It was also found that acetanilide had less of an effect on reducing the overall growth rate in the A/B direction when compared with metacetamol. This links with Thompson's (164) research, where acetanilids' uptake was discussed as being less than metacetamol. Metacetamol was also noted to cause a higher degree of morphological change.

Needle-like crystals are usually less favourable for downstream processes, which would again show that acetanilide, in this case, is the better of the two impurities if it were required at these set conditions to try and alter or have more control over the habits. When comparing supersaturation 1.25, 1.75, and 4% metacetamol, it was found that the habits are like the ones found in the purer system, although less defined. The ratios between growth rates are slightly lower at higher supersaturation, and the average growth rate increases with an increase in supersaturation. When comparing the supersaturations of 4% acetanilide, the habits at the higher supersaturations were more consistent with what was found in its correlating purer system. The ratios between growth rates are more consistent at higher supersaturation, showing more of a similarity between habits, and the average growth rate increased with an increase in supersaturation. A higher level of supersaturation seems more favourable if control over the habits is required when impurities are a factor.

Figure 108: Images of single crystal habits for the first image at 0 mins the last image at 44 mins and the final image of surroundings. For conditions, T = 15 °C, S = 1.75 and impurity % = 4% metacetamol. A 100μm scale bar is also present.

Figure 109: Images of single crystal habits for the first image at 0 mins the last image at 44 mins and the final image of surroundings. For conditions, T = 15 °C, S = 1.75 and impurity % = 4% acetanilide. A 100µm scale bar is also present.
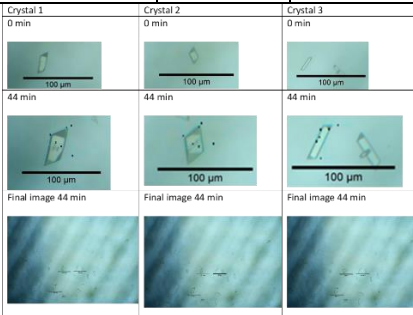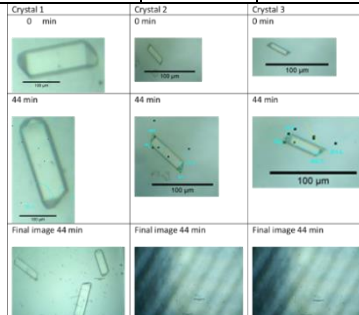
1.1e Effect of impurities and temperature

For the experimental conditions T = 30 °C, S = 1.25, and impurity = 4% metacetamol. Growth rates for faces A and B were obtained for three crystals per condition. Table 26 provides an overview of the effect of the impurities on growth behaviour.

In Table 26, metacetamol was found to reduce the growth rate in the A and B directions. However, acetanilide, on the other hand, was found to increase the growth rate in both the A and B directions. Again, both metacetamol and acetanilide are found to favour inhibiting growth in the B direction.

Table 26: Single crystal growth rate measurements for pairs of faces A and B at T = 30 °C, S = 1.25, and impurity % = 0 and 4% metacetamol and 4% acetanilide with images of habits. Each vertical column of three images comprises of the individual crystal at the start and end of the growth measurement and then a wider view showing surrounding crystals, if any.

No impurity			4% Metacetamol			4% Acetanilide		
Crystal	Face A µm min^{-1}	Face B µm min-1	Crystal	Face A µm min-1	Face B µm min-1	Crystal	Face A µm min-1	Face B µm min-1
1	0.14	0.13	1	0.07	0.06	1	0.24	0.02
2	0.28	0.24	2	0.06	0.05	2	0.65	0.12
3	0.06	0.05	3	0.07	0.02	3	0.24	0.08
4	0.24	0.45						

When 4% metacetamol is added to the system, the growth rate in the A direction is slightly faster, indicating that the impurity favours inhibiting the B direction of crystal growth (Table 26). The ratios in growth rates of face A to B were slightly higher when compared to the system with no added impurity; these were 1.30, 1.30, and 3.35, respectively, for crystals 1, 2, and 3. The corresponding values for crystals grown from pure solution were 1.16, 1.10, 1.18, and 0.54, respectively, for crystals 1, 2, 3, and 4. The difference in measured average growth rates for face A was 0.07 ± 0.01 µm min-1 and face B was 0.04 ± 0.02 µm min-1. The ratios between the growth rates were consistent for crystals 1 and 2 but not crystal 3; this can be seen from the habits presented.

Consistency in habits is found when analysing the images of the growth rate from the first image to the final image of the crystal's growth (Figure 110). There are similarities between crystals 1 and 2 and slight similarities to crystal 3 in the pure condition. However, crystal 3 is more needle-like. It is important to note that all three measured crystals are from the same system. In the final image, there are a few crystals with the truncation observed in crystals 1 and 2, as well as various needles and some clustering of agglomeration towards the lower end of the image. These habits are not like pure

conditions; they are more consistent and predictable. They resemble the crystals found at T = 15 °C and S = 1.25 with 4% metacetamol; however, with these crystals, the truncation at the corners was found at the opposite ends of the crystal. The needle-like habits, on the other hand, were usually found at lower temperatures in purer conditions.

When 4% acetanilide is added to the system, the growth rate in the A direction is the fastest, indicating that the impurity favours inhibiting the B direction of crystal growth (Table 26). The ratios between growth rates for faces A and B varied, with one of the biggest ratios noted; these were 11.34, 5.52, and 2.86 for crystals 1, 2, and 3, respectively; this was a lot higher in comparison to the purer condition and metacetamol. However, this could be down to how well the crystals grow in the A direction as well as the similarities in habits found. The difference in measured average growth rates for face A is 0.37 ± 0.24 µm min-1 and face B was 0.07 ± 0.05 µm min-1, which is higher in the A direction when compared with the purer system but lower in the B direction. When compared with metacetamol, the average growth rate was higher in both the A and B directions.

The images of the first and final crystals analysed show consistency during growth and the capture of images (Figure 111). Crystal 1 seems slightly rounder at the top of the crystals with clear evidence of truncation as well as an easily identified thicker and larger crystal in comparison to crystal 2 and 3, which were found in the same system, showing similarities in habit and shape of the crystals, there are no similarities to the crystals in the purer condition, however, there are similarities to crystal 3 with the addition of 4% metacetamol in this system (Figure 110). A few crystals were found in the final images. However, the addition of this impurity resulted in a more consistent habit and shape.

When comparing this system to T = 15 °C, S = 1.25, and impurity = 4% metacetamol (Figure 106), the first comparison that can be made is that the shapes are quite different at higher temperatures; it is clear that the crystals were more prone to truncation at the corners when compared to the lower temperatures, and they also appear smaller in scale. The average growth rate decreases in the A direction but increases in the B direction with an increase in temperature. The average ratio is found

to be higher at lower temperatures. When comparing this system to T = 15 °C, S = 1.25, and impurity = 4% acetanilide (Figure 107). The first comparison that can be made is that habits are quite different; at the lower temperatures, they are more diamond-shaped with some truncated edges, whereas at higher temperatures, the habits are more needle-like. The average ratio is higher at lower temperatures, and the overall growth rate was found to increase in the A direction but decrease in the B, direction with an increase in temperature.
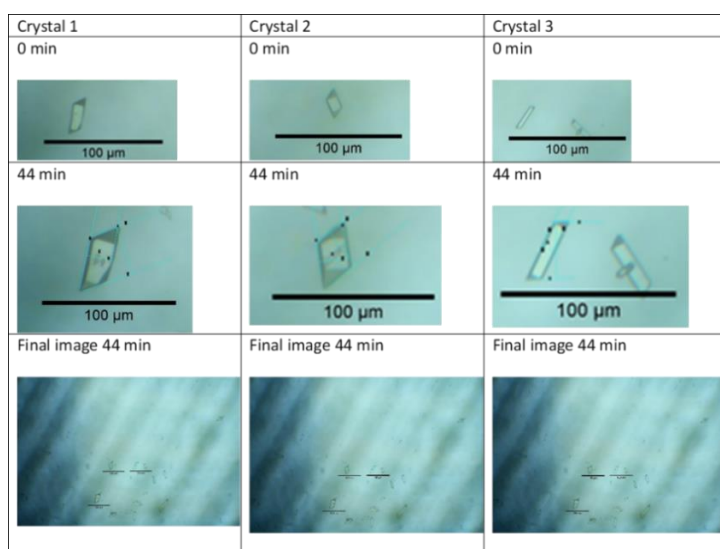
Figure 110: Images of single crystal habits for the first image at 0 mins the last image at 44 mins and the final image of surroundings. For conditions, T = 30 °C, S = 1.25 and impurity % = 4% metacetamol. A 100µm scale bar is also present.

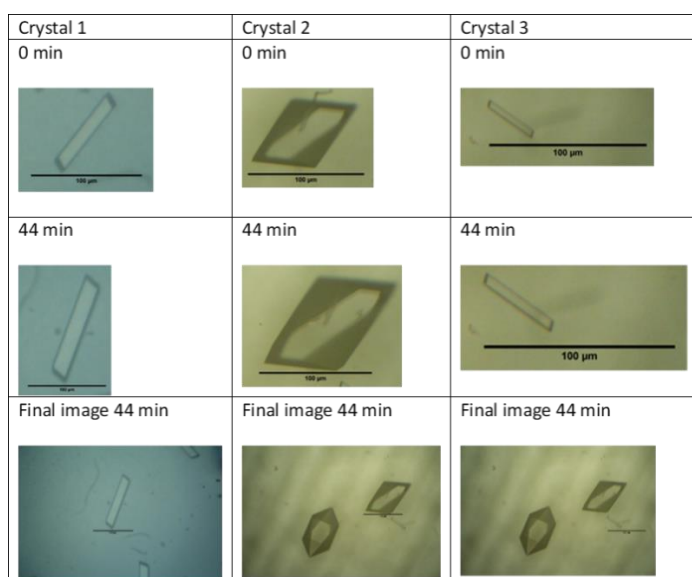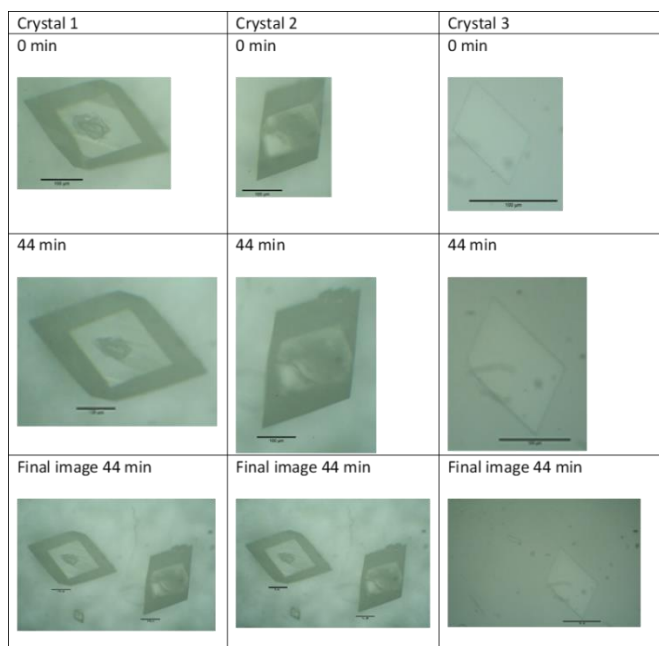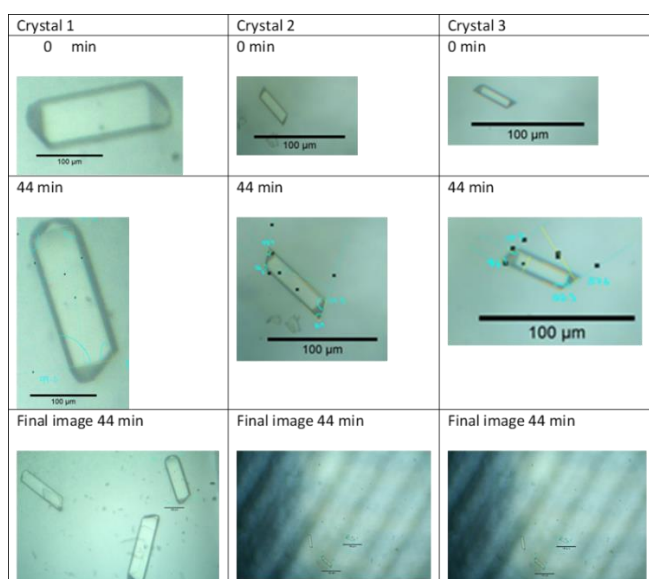Appendix B: Single Crystal Growth with and without Ultrasound Intervention

Figure 111: Images of single crystal habits for the first image at 0 mins the last image at 44 mins and the final image of surroundings. For conditions, T = 30 °C, S = 1.25 and impurity % = 4% acetanilide. A 100µm scale bar is also present.

For the experimental conditions T = 30 °C, S = 1.75, and impurity = 4% metacetamol. There are growth rates for faces A and B were obtained on four, three, and five crystals per condition. Table 27 provides an overview of the effect of the impurities on growth behaviour.

Table 27: Single crystal growth rate measurements for pairs of faces A and B at T = 30 °C, S = 1.75, and impurity % = 0, 4% metacetamol and 4% acetanilide with images of habits.

No impurity			4% Metacetamol			4% Acetanilide		
Crystal	Face A µm min^{-1}	Face B µm min^{-1}	Crystal	Face A µm min^{-1}	Face B µm min^{-1}	Crystal	Face A µm min^{-1}	Face B µm min^{-1}
1	0.24	0.19	1	1.53	0.42	1	0.11	0.11
2	0.04	0.02	2	0.18	0.03	2	0.21	0.20
3	0.04	0.03	3	1.57	0.54	3	0.04	0.02
4	0.91	0.56				4	0.28	0.17
						5	0.80	0.34

In Table 27, metacetamol was found to increase the average growth rate in the A and B directions. Acetanilide, on the other hand, decreased the growth rate in both directions. Again, both metacetamol and acetanilide are found to favour inhibiting growth in the B direction (Table 27).

When 4% metacetamol is added to the system, the growth rate in the A direction is faster, indicating that the impurity favours inhibiting the B direction of crystal growth. The ratios in growth rates of faces A and B were higher when compared with the system with no added impurity; these were 3.63, 5.63, and 2.90, respectively, for

crystals 1, 2, and 3. The corresponding values for crystals grown from pure solution were 1.29, 1.92, 1.34, and 1.64, respectively, for crystals 1, 2, 3, and 4. The difference in measured average growth rates for face A was 1.09 ± 0.79 µm min^{-1} and for face B was 0.33 ± 0.27 µm min^{-1}. The ratios between the growth rates were not consistent; however, this can be linked to the varying habits observed; this is also a lot larger than the ratio in the pure system.

Consistency in habit is found when analysing the images of the growth rate from the first image to the final image of the crystal's growth (Figure 112). There are similarities between crystals 1 and 2. However, crystal 1 is thicker, which is clear from the shadows and the obvious growth in the Z direction; it is harder to determine the thickness of crystal 2; it has a more elongated appearance and is a lot smaller in comparison to crystal 1, looking at the scale bar. Crystal 3 is similar to crystal 4 in its purer condition. However, the truncation in the B direction of the crystal is more pronounced; the crystal also looks to have grown well in thickness (Z direction and size). In the final images of crystal 1, some stranger-looking habits are observed that have not been identified previously. In the final image of crystal 3, there is a crystal identical to the one measured. In terms of similarities between the purer conditions, only crystal 3 is found to have a slight resemblance, as stated previously.

When 4% acetanilide is added to the system, the growth rate in the A direction is the fastest, indicating that the impurity favours inhibiting the B direction of crystal growth. The ratios between growth rates for faces A and B varied slightly; these were 0.99, 1.06, 2.80, 1.67, and 2.32 for crystals 1, 2, 3, 4 and 5, respectively; this was slightly higher when compared to the purer conditions but significantly lower to 4% metacetamol. The difference in measured average growth rates for face A is 0.29 ± 0.30 µm min^{-1} and for face B is 0.17 ± 0.12 µm min^{-1}, which is lower in both the A and B directions when compared with the purer system and 4% metacetamol.

The images of the first and final crystals analysed show consistency during growth and the capture of images. The first striking observation when looking at all of the crystals is the differences in habits between the runs. Crystal 1 and 2 were taken from the same system; these crystals were similar in shape and thickness; however, crystal 1 has truncation occurring on the top corner of the crystal. There are also some

twinning crystals that have made an appearance and some different shapes. These are slightly similar to crystals 2 and 3 of the pure condition. Crystal 3 is more needle-like, with more needle crystals in the final image. Needles were not observed in the pure condition of this system; however, they were observed with 4% metacetamol crystals 1 and 2. Crystal 4 and 5 were in the same system. These crystals were similar in habit; it's difficult to judge how thick they were. However, there is a similarity between these crystal habits and crystals 1 and 2 of the pure condition.

When comparing this system to T = 15 °C, S = 1.75 and impurity = 4% metacetamol (Figure 108), the first comparison that can be made is that the shapes are a little similar, i.e., they both have needle-like habits as well as diamond habits with some truncation on the edges. The average growth rate in both the A and B directions increases with an increase in temperature. The average ratio is found to be higher at lower temperatures. When comparing this system to T = 15 °C, S = 1.75, and impurity = 4% acetanilide (Figure 109), the first comparison that can be made is that habits are again slightly similar. However, the crystals at lower temperatures seem thicker in comparison; the higher temperatures also have truncation at the corners of crystals, which was not seen at lower temperatures. The average ratio is lower at lower temperatures, and the overall growth rate was found to decrease with an increase in temperature.
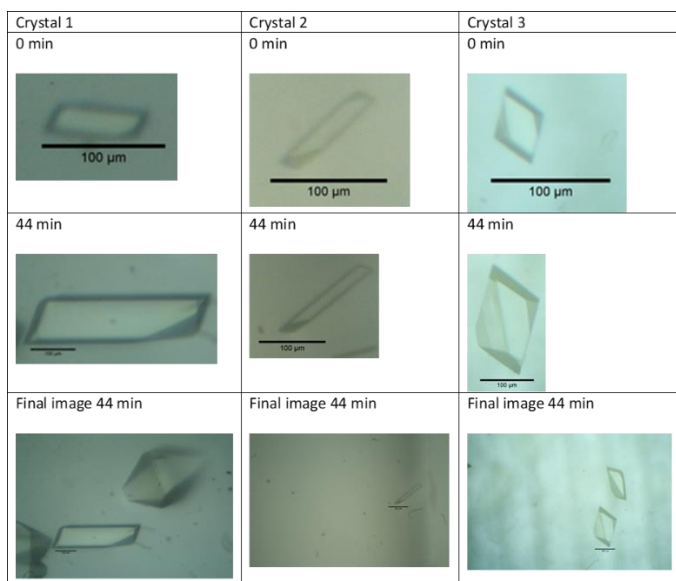
Figure 112: Images of single crystal habits for the first image at 0 mins, the last image at 44 mins and the final image of surroundings. For conditions, T = 30 °C, S = 1.75 and impurity % = 4% metacetamol. A 100µm scale bar is also present.
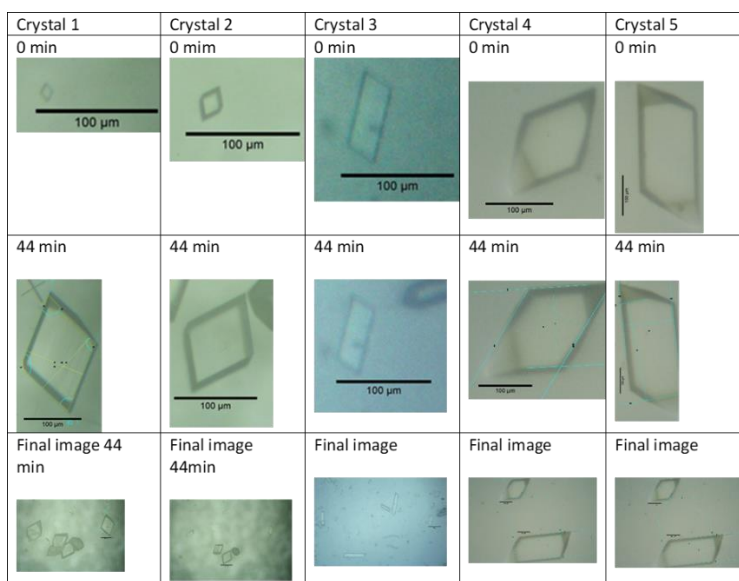
Figure 113: Images of single crystal habits for the first image at 0 mins the last image at 44 mins and the final image of surroundings. For conditions, T = 30 °C, S = 1.75 and impurity % = 4% acetanilide. A 100µm scale bar is also present.

Appendix B: Single Crystal Growth with and without Ultrasound Intervention

Table 28: Single crystal growth rate data at 15 °C σ = 1.25 with ultrasound.

No impurity			4% Metacetamol			4% Acetanilide		
Crystal	Face A $\mu m\ min^{-1}$	Face B $\mu m\ min^{-1}$	Crystal	Face A $\mu m\ min^{-1}$	Face B $\mu m\ min^{-1}$	Crystal	Face A $\mu m\ min^{-1}$	Face B $\mu m\ min^{-1}$
1	0.54	0.48	1	0.04	0.56	1	1.04	0.91
2	0.42	0.35						

Table 29: Single crystal growth rate data at 15 °C σ = 1.75 with ultrasound.

No impurity			4% Metacetamol			4% Acetanilide		
Crystal	Face A $\mu m\ min^{-1}$	Face B $\mu m\ min^{-1}$	Crystal	Face A $\mu m\ min^{-1}$	Face B $\mu m\ min^{-1}$	Crystal	Face A $\mu m\ min^{-1}$	Face B $\mu m\ min^{-1}$
1	0.18	0.97	1	0.14	0.72	1	1.41	1.07
						2	0.08	0.49

Appendix B: Single Crystal Growth with and without Ultrasound Intervention

Table 30: Single crystal growth rate data at 20 °C σ = 1.25 with ultrasound.

No impurity			4% Metacetamol			4% Acetanilide		
Crystal	Face A µm min⁻¹	Face B µm min⁻¹	Crystal	Face A µm min⁻¹	Face B µm min⁻¹	Crystal	Face A µm min⁻¹	Face B µm min⁻¹
1	0.57	0.67	1	0.01	0.04	1	0.26	0.16
2	0.68	0.70						

Table 31: Single crystal growth rate data at 20 °C σ = 1.75 with ultrasound.

No impurity			4% Metacetamol			4% Acetanilide		
Crystal	Face A µm min⁻¹	Face B µm min⁻¹	Crystal	Face A µm min⁻¹	Face B µm min⁻¹	Crystal	Face A µm min⁻¹	Face B µm min⁻¹
1	0.23	1.20	1	0.17	0.26	1	1.72	0.96
			2	0.33	0.50	2	0.07	0.56

Appendix B: Single Crystal Growth with and without Ultrasound Intervention

Table 32: Single crystal growth rate data at 30 °C σ = 1.25 with ultrasound.
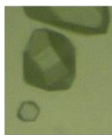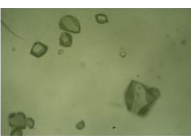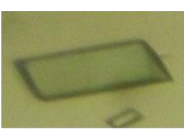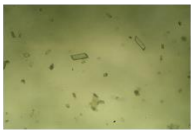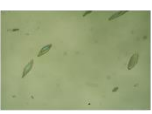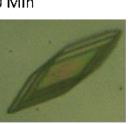
No impurity			4% Metacetamol			4% Acetanilide		
Crystal	Face A µm min^{-1}	Face B µm min^{-1}	Crystal	Face A µm min^{-1}	Face B µm min^{-1}	Crystal	Face A µm min^{-1}	Face B µm min^{-1}
1	0.73	0.83	1	0.03	0.05	1	0.15	0.47

Table 33: Single crystal growth rate data at 30 °C σ = 1.75 with ultrasound.

No impurity			4% Metacetamol			4% Acetanilide		
Crystal	Face A µm min^{-1}	Face B µm min^{-1}	Crystal	Face A µm min^{-1}	Face B µm min^{-1}	Crystal	Face A µm min^{-1}	Face B µm min^{-1}
1	3.01	5.12	1	0.17	0.52	1	0.19	0.27
2	3.51	3.64						
3	0.93	4.71						

APPENDIX C: Bulk Suspension Measurements

1.0: Stereomicroscope images
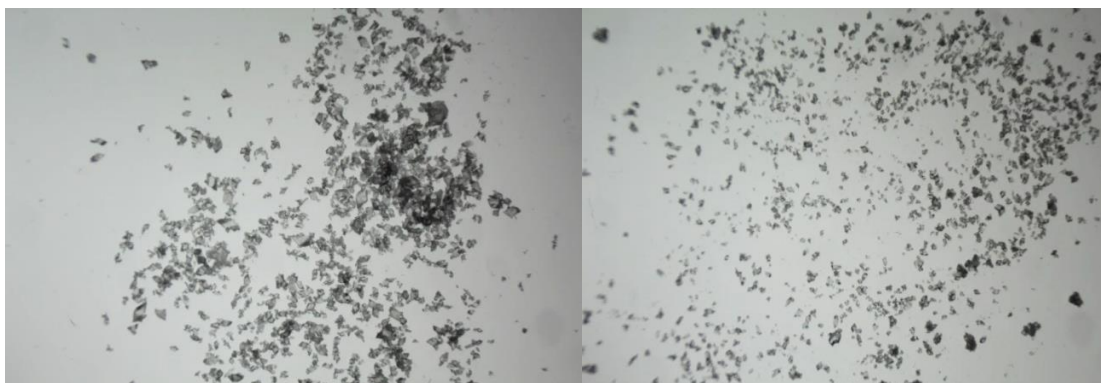
Figure 114: Images of 2% and 4% acetanilide, taken with the Brunel Zoom Stereomicroscope.

1.1: Material data for bulk suspension crystallisation

Data		
Temperature		55
Solubility paracetamol (mg g^{-1})		373
Mass ethanol alcohol (g)		99
Mass paracetamol (g)	Solubility of paracetamol/ mass ethanol alcohol	373*99/1000 = 36.927
Molecular weight paracetamol (g mol^{-1})		151.16
Molecular Weight acetanilide (g mol^{-1})		135.17
Molecular weight metacetamol (g mol^{-1})		151.16
Density of ethanol (g l^{-1})		0.789
Density of n-heptane (g l^{-1})		0.684

Appendix C: Bulk Suspension Measurements

Required ethanol alcohol and impurities		
Mass ethanol alcohol (g)		99
Volume of ethanol (g)	Mass ethanol alcohol / density of ethanol	99/0.789 = 125.475
paracetamol (g)		36.927
2% acetanilide (g)	(Mass paracetamol/molecular weight paracetamol)*0.02*molecular weight of acetanilide	(36.927/151.16)*0.02*135.17 = 0.660
4% acetanilide (g)	(Mass paracetamol/molecular weight paracetamol)*0.04*molecular weight of acetanilide	(36.927/151.16)*0.04*135.17 = 1.321
2% metacetamol (g)	(Mass paracetamol/molecular weight paracetamol)*0.02*molecular weight of metacetamol	(36.927/151.16)*0.02*151.16 = 0.739
4% metacetamol (g)	(Mass paracetamol/molecular weight paracetamol)*0.04*molecular weight of metacetamol	(36.927/151.16)*0.04*151.16 = 1.477

1.2: Calculation for maximum yield output with 99g of solvent

Solubility of paracetamol at 55°C (g g^{-1})	0.373	373	
Density of ethanol 0.789	Mass of solvent (g) 99	Volume 125.4752852	
Density of paracetamol (g cm^{-3}) 1.26	Mass (g) 36.927	Volume (mL) 29.30714286	
Total		154.782428	
Solubility of paracetamol at 15°C (mg g^{-1}) 167	Mass of solvent (g) 99		16533
Mass of material weigh out			36927
Maximum yield			0.55227882
			55.23

1.3: Example of filtration data

Exp 3 (0% power, 2% aceta and 2% m,eta) 20/09/2016

Nucleation point					
Observation	Exp start (time)	Bath cool down (time)	Crystallised (time)	Probe (°C)	Bath (°C)
	07:27	07:47	05:57	31.04	28.74

Sample 1

Data		
Parameter	Value	Units
Temp	15	C
Pressure	800	mbar
Mass filter tube (dry)	19	g
Mass cylinder (mother liq dry)	49.53	g
Mass cylinder (wash 1 dry)	49.63	g
Mass cylinder (wash 2 dry)	49.53	g

Filtration rate		
Volume (mL)	Time (s)	t/V
5	1.5	0.30
10	3.9	0.39
15	6.4	0.43
20	13.5	0.68
25	17.3	0.69
30	21.3	0.71
35	26.1	0.75
43	28.4	0.66
M wet cake	26.34	g

Washing		
Parameter	Value	Units
Vol cake	2.5	cm
Vol wash	2.5	mL
Mass wash 1	26.99	g
Mass wash 2	26.64	g
Time wash 1	1.08	s
Time wash 2	1.39	s
Mass cake + tube dry	23.12	g
Mass cake	4.12	g
Mass cylinder (mother liq)	84.69	g
Mass mother liq	35.16	g
Mass cylinder (wash1)	50.44	g
Mass wash 1	0.81	g
M cylinder (wash 2)	51.23	g
Mass wash 2	1.7	g

Sample 2

Data		
Parameter	Value	Units
Temp	15	C
Pressure	800	mbar
Mass filter tube (dry)	18.8	g
Mass cylinder (mother liq dry)	47.84	g
Mass cylinder (wash 1 dry)	48.99	g
Mass cylinder (wash 2 dry)	47.8	g

Appendix C: Bulk Suspension Measurements

Filtration rate

Volume (mL)	Time (s)	t/V
5	2.5	0.50
10	6.2	0.62
15	10.4	0.69
20	15.7	0.79
25	21.5	0.86
30	26.7	0.89
35	32.2	0.92
40	38	0.95
44	40.3	0.92
M wet cake	26.24	g

Washing

Parameter	Value	Units
Vol cake	2	cm
Vol wash	2	mL
Mass wash 1	26.93	g
Mass wash 2	26.6	g
Time wash 1	1.34	s
Time wash 2	1.74	s
Mass cake + tube dry	23.23	g
Mass cake	4.43	g
Mass cylinder (mother liq)	84.62	g
Mass mother liq	36.78	g
Mass cylinder (wash1)	49.27	g
Mass wash 1	0.28	g
M cylinder (wash 2)	49.43	g
Mass wash 2	1.63	g

Sample 3

Data		
Parameter	Value	Units
Temp	15	C
Pressure	800	mbar
Mass filter tube (dry)	18.67	g
Mass cylinder (mother liq dry)	49.7	g
Mass cylinder (wash 1 dry)	49.69	g
Mass cylinder (wash 2 dry)	49.55	g

Filtration rate		
Volume (mL)	Time (s)	t/V
5	1.7	0.34
10	2.9	0.29
15	5.1	0.34
20	8.1	0.41
25	11.1	0.44
30	14.9	0.50
35	18.1	0.52
39	21.1	0.54
M wet cake	28.64	g

Appendix C: Bulk Suspension Measurements

Washing		
Parameter	Value	Units
Vol cake	2.5	cm
Vol wash	2.5	mL
Mass wash 1	29.6	g
Mass wash 2	29.1	g
Time wash 1	1.16	s
Time wash 2	1.57	s
Mass cake + tube dry	24.74	g
Mass cake	6.07	g
Mass cylinder (mother liq)	81.65	g
Mass mother liq	31.95	g
Mass cylinder (wash1)	50.72	g
Mass wash 1	1.03	g
M cylinder (wash 2)	52.16	g
Mass wash 2	2.61	g

Yield	
Total mass cake	14.62
Theoretical mass	39.165
Yield	37.32924805

1.4: In-depth sample purity tracking and discussion

Figure 115: Diagrammatic representation of HPLC analysis of paracetamol with 2% acetanilide, with 0% US (ultrasound) and 100% US (ultrasound), the input material total (%), the total amount of acetanilide found in the cake and waste streams (mother liquor, wash 1 and wash 2) (%), the total amount of paracetamol through each stage (%), and the final calculated yield (%) discussed in Section 6.4.7.

Figure 115 gives the relative composition from HPLC analysis of the isolated product and waste streams after crystallisation with an input containing 2% acetanilide, showing the effect of 0 and 100% ultrasound. The amount of acetanilide found within the product (cake) was 0.46% in the experiment with 0% ultrasound and 0.37% in 100% ultrasound. This result indicates that ultrasound and washing were effective in reducing the total amount of impurity by 0.09%.

The amount of acetanilide found within the waste streams comprised of the mother liquor and the two collected washes. The mother liquor contained 3.83% acetanilide in the absence of ultrasound and 4.06% when 100% ultrasound power was applied. For wash 1, acetanilide was 3.6% in the absence of ultrasound and 4.03% with 100% ultrasound power. The corresponding values for wash 2 were 4.91% without ultrasound and 3.79% with 100% ultrasound. This data is consistent with successfully removing the acetanilide impurity through the waste stream analysis. The mother

liquor and first wash can be expected to be somewhat similar in composition based on the wash volume of one cake volume since the make-up of wash 1 is a mixture of mother liquor displaced from the voids in the cake and the first portion of the wash solvent breaking through the cake, which can be expected to be relatively rich in both the impurity and paracetamol. A larger amount of acetanilide was found in the mother liquors (0.23%) and wash 1 (0.43%) with 100% ultrasound than in the absence of ultrasound. In wash 2, 100% ultrasound was found to have less impact, with a 1.12% difference. The overall effect is that more acetanilide was removed from the material produced with ultrasound since the combined mother liquor and first wash volume comprise of rather more (ca. 50 mL) than the second wash volume (ca.10 mL).

The solid blue (0% ultrasound) and dotted blue (100% ultrasound) lines indicate the amount of paracetamol found in the samples taken at each stage. This shows that the input material, paracetamol, made up 98% of the total sample, as anticipated, from the composition of the solution prepared. The paracetamol composition increased in the cake sample to 99.5% at 0% ultrasound and 99.6% at 100% ultrasound. This improvement in the purity of the paracetamol fell in line with the reduction of impurities and the increase in yield noted in the figure and discussed in Section 6.4.7 above. The amount of paracetamol relative to acetanilide decreased in the waste streams analysed. There is a minor deviation of less than a 0.4% decrease in paracetamol in the mother liquors and wash 1 for 100% ultrasound compared to 0% ultrasound. However, at wash 2, the total paracetamol amount decreased by 1.12% with 0% ultrasound compared with 100%.

Figure 116: Diagrammatic representation of HPLC analysis of paracetamol with 4% acetanilide, with 0% US (ultrasound) and 100% US (ultrasound), the input material total (%), the total amount of acetanilide found in the cake and waste streams (mother liquor, wash 1 and wash 2) (%), the total amount of paracetamol through each stage (%), and the final calculated yield (%) discussed in Section 6.4.7.

Figure 116 gives the relative composition from HPLC analysis of the isolated product and waste streams after crystallisation with an input containing 4% acetanilide, showing the effect of 0 and 100% ultrasound. The amount of acetanilide found within the product (cake) was 0.74% in the experiment with 0% ultrasound and 0.77% in the experiment with 100% ultrasound. This result indicates that ultrasound and washing were not as effective as 0% ultrasound, with a 0.03% of a difference found.

The amount of acetanilide found within the waste streams comprised of the mother liquor and the two collected washes. The mother liquor contained 6.83% acetanilide in the absence of 0% ultrasound and 8.16% when 100% ultrasound power was applied. For wash 1, the amount of acetanilide was 6.52% in the absence of ultrasound and 7.65% with 100% ultrasound applied. The corresponding values for wash 2 were 5.18% without ultrasound and 7.79% with 100% ultrasound. This data is consistent with successfully removing the acetanilide impurity through the waste stream analysis.

Appendix C: Bulk Suspension Measurements

The solid blue (0% ultrasound) and dotted blue (100% ultrasound) lines indicate the amount of paracetamol found in the samples taken at each stage. This shows that the input material, paracetamol, made up 96% of the total sample, as anticipated, from the composition of the solution prepared. The paracetamol composition increased in the cake sample to 99.23% at 0% ultrasound and 99.26% at 100% ultrasound. This improvement in the purity of the paracetamol fell in line with the increase in yield noted in the figure and discussed in Section 6.4.7 above. The amount of paracetamol relative to acetanilide then decreased in the waste streams analysed. There is a moderate deviation of less than 1% decrease in paracetamol in the mother liquors, wash 1 and wash 2, for 100% ultrasound compared to 0% ultrasound.

Figure 117: Diagrammatic representation of HPLC analysis of paracetamol with 2% metacetamol, with 0% US (ultrasound) and 100% US (ultrasound), the input material total (%), the total amount of metacetamol found in the cake and waste streams (mother liquor, wash 1 and wash 2) (%), the total amount of paracetamol through each stage (%), and the final calculated yield (%) discussed in Section 6.4.7.

Figure 117 gives the relative composition from HPLC analysis of the isolated product and waste streams after crystallisation with an input containing 2% metacetamol, showing the effect of 0 and 100% ultrasound. The amount of metacetamol found within the product (cake) was 0.49% in an experiment with 0% ultrasound and 0.38% in 100% ultrasound; this result indicates that ultrasound and washing effectively reduced the impurity by 0.11%.

Appendix C: Bulk Suspension Measurements

The amount of metacetamol found within the waste streams comprised of the mother liquor and the two collected washes. The mother liquor contained 3.14% metacetamol in the absence of ultrasound and 2.67% when 100% ultrasound power was applied. For wash 1, the amount of metacetamol was 3.58% in the absence of ultrasound and 3.32% with 100% ultrasound applied. The corresponding values for wash 2 were 3.3% without ultrasound and 3.52% with 100% ultrasound. This data is consistent with successfully removing the metacetamol impurity through the waste stream analysis. The mother liquor and first wash can be expected to be somewhat similar in composition based on the wash volume of one cake volume since the make-up of wash 1 is a mixture of mother liquor displaced from the voids in the cake and the first portion of the wash solvent breaking through the cake, which can be expected to be relatively rich in both the impurity and paracetamol. A larger amount of metacetamol was found with no ultrasound in the mother liquors (0.47%) and wash 1 (0.26%). In wash 2, 100% ultrasound was found to have a greater impact with a 0.22% difference. The overall effect is that more metacetamol was removed from the material produced with ultrasound since the combined mother liquor and first wash volume comprised more (ca. 50 mL) than the second wash volume (ca.10 mL).

The solid blue (0% ultrasound) and dotted blue (100% ultrasound) lines indicate the amount of paracetamol found in the samples taken at each stage. This shows that the input material, paracetamol, made up 98% of the total sample, as anticipated, from the composition of the solution prepared. The paracetamol composition increased in the cake sample to 99.51% at 0% ultrasound and 99.62% at 100% ultrasound. This improvement in the purity of the paracetamol fell in line with the reduction of impurities and the increase in yield noted in the figure and discussed in Section 6.4.7 above. The amount of paracetamol relative to metacetamol then decreased in the waste streams analysed. There is a minor deviation of less than 0.4% decrease in paracetamol in the mother liquors and wash 1 for 0% ultrasound compared to 100% ultrasound. However, at wash 2, the total paracetamol amount decreased by 0.2% with 100% ultrasound when compared with 0%.
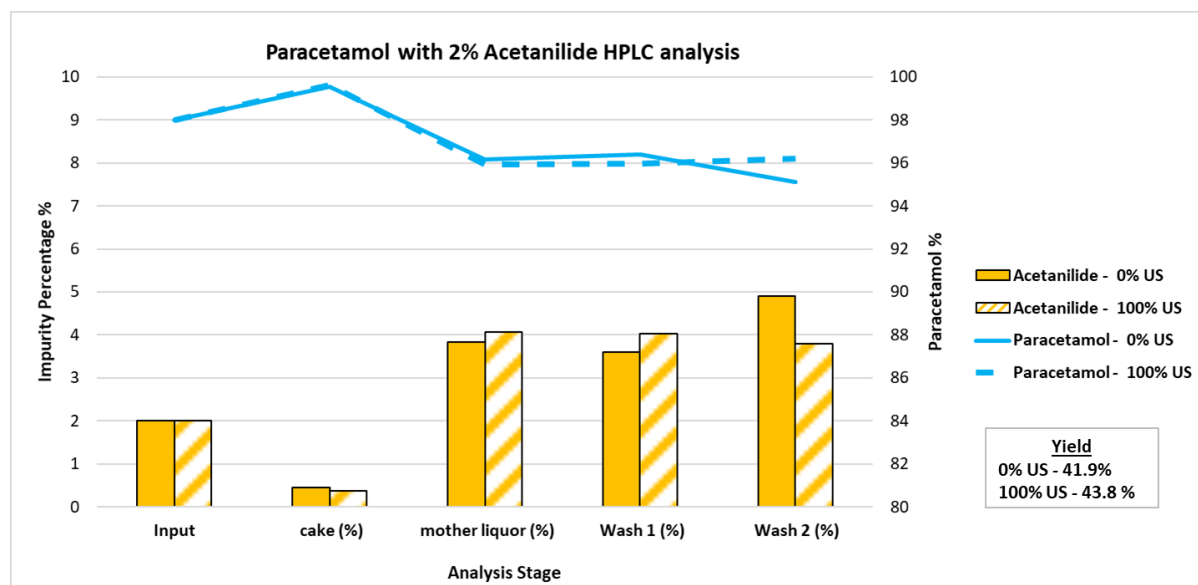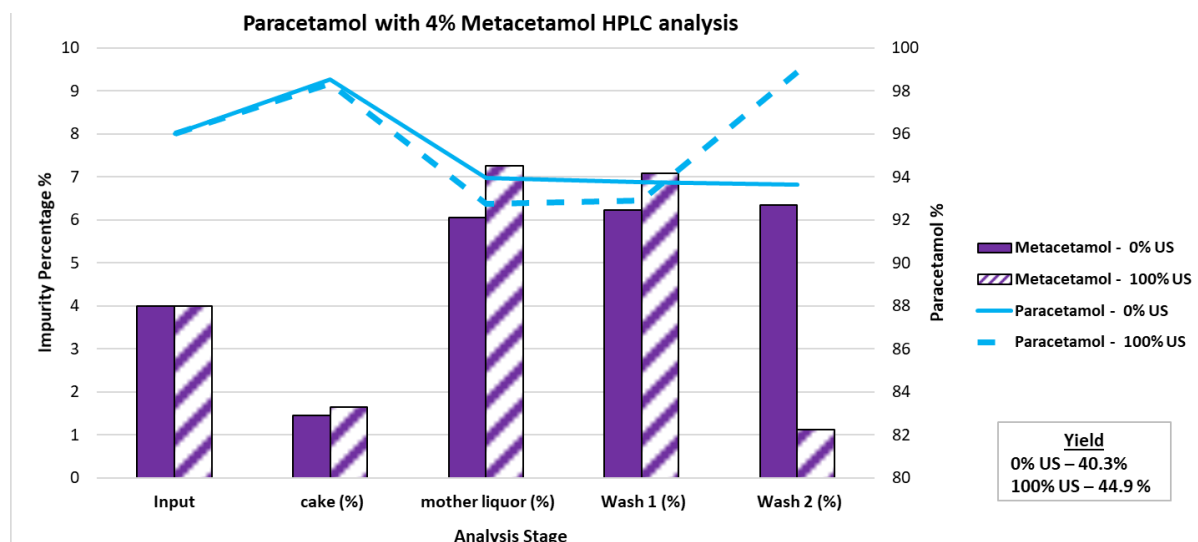
Figure 118: Diagrammatic representation of HPLC analysis of paracetamol with 4% metacetamol, with 0% US (ultrasound) and 100% US (ultrasound), the input material total (%), the total amount of metacetamol found in the cake and waste streams (mother liquor, wash 1 and wash 2) (%), the total amount of paracetamol through each stage (%), and the final calculated yield (%) discussed in Section 6.4.7.

Figure 118 gives the relative composition from HPLC analysis of the isolated product and waste streams after crystallisation with an input containing 4% metacetamol, showing the effect of 0 and 100% ultrasound. The amount of metacetamol found within the product (cake) was 1.49% in experiments with 0% ultrasound and 1.64% with 100% ultrasound. Ultrasound, in this case, was not as effective as no ultrasound in reducing the impurity incorporation, with a difference of 0.19% noted. It is clear from this that metacetamol is harder to remove.

The amount of metacetamol found within the waste streams comprised of the mother liquor and the two collected washes. The mother liquor contained 6.05% metacetamol in the absence of ultrasound and 7.26% when 100% ultrasound power was applied. For wash 1, the amount of metacetamol was 6.23% in the absence of ultrasound and 7.08% with 100% ultrasound applied. The corresponding values for wash 2 were 6.35% without ultrasound and 1.11% with 100% ultrasound. This data is consistent with successfully removing the metacetamol impurity through the waste stream analysis.

The solid blue (0% ultrasound) and dotted blue (100% ultrasound) lines indicate the amount of paracetamol found in the samples taken at each stage. This shows that the input material, paracetamol, made up 96% of the total sample, as anticipated, from the composition of the solution prepared. The paracetamol composition increased in the cake sample to 99.55% at 0% ultrasound and 98.36% at 100% ultrasound. This improvement in the purity of the paracetamol fell in line with the reduction of impurities and the increase in yield noted in the figure and discussed in Section 6.4.7 above. The amount of paracetamol relative to metacetamol then decreased in the 0% ultrasound waste streams analysed; similarities can be seen with 100% ultrasound. However, there is an outlier, unlike the rest of the data, where the total amount of paracetamol increases to 98.89% in wash 2, which surpasses the paracetamol cake concentration by 0.5%. There is a reduction of 0.84% of paracetamol in the mother liquors and wash 1 for 100% ultrasound compared to 0% ultrasound. However, at wash 2, the total paracetamol amount decreased by 5.24% with 0% ultrasound compared with 100%.
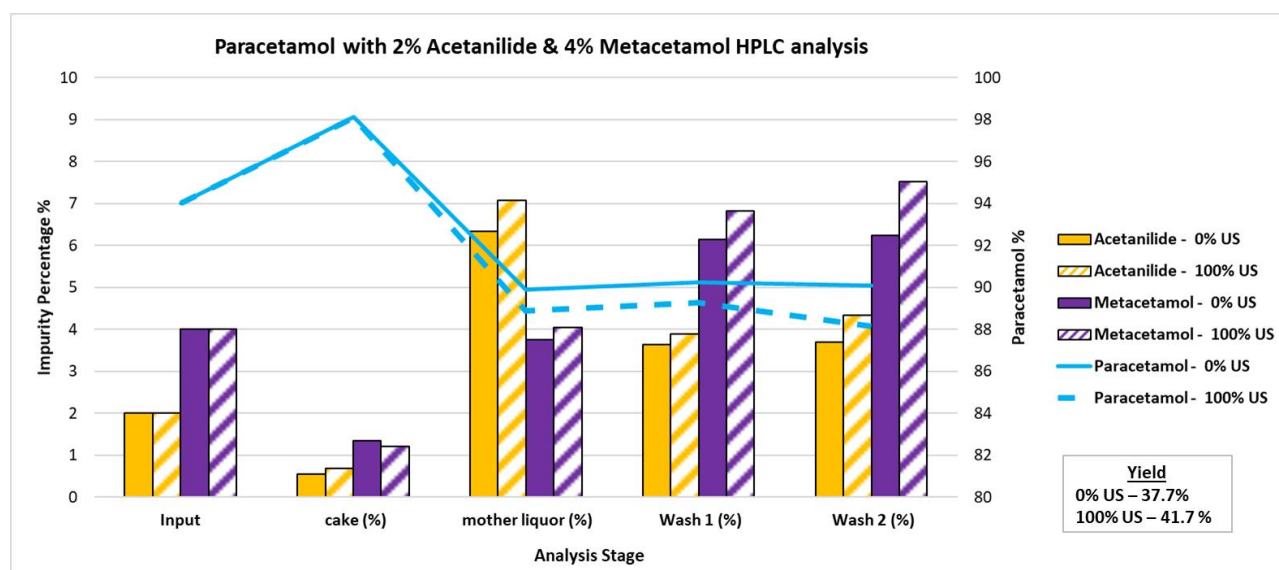
Figure 119: Diagrammatic representation of HPLC analysis of paracetamol with 2% acetanilide and 4% metacetamol, with 0% US (ultrasound) and 100% US (ultrasound), the input material total (%), the total amount of acetanilide and metacetamol found in the cake and waste streams (mother liquor, wash 1 and wash 2) (%), the total amount of paracetamol through each stage (%), and the final calculated yield (%) discussed in Section 6.4.7.

Appendix C: Bulk Suspension Measurements

Figure 119 gives the relative composition from HPLC analysis of the isolated product and waste streams after crystallisation with an input containing 2% acetanilide and 4% metacetamol, showing the effect of 0 and 100% ultrasound. The amount of acetanilide found within the product (cake) was 0.54% in 0% ultrasound and 0.69% in 100% ultrasound; this result indicates that ultrasound and washing were not as effective as 0% ultrasound, with a 0.15% difference found. The amount of metacetamol found within the product (cake) was 1.34% in 0% ultrasound and 1.2% in 100% ultrasound; this result indicates that 100% ultrasound and washing were successful, with a 0.14% difference found.

The amount of acetanilide found within the waste streams comprised of the mother liquor and the two collected washes. The mother liquor contained 6.34% acetanilide in the absence of ultrasound and 7.07% when 100% ultrasound power was applied. For wash 1, the amount of acetanilide was 3.63% in the absence of ultrasound and 3.89% with 100% ultrasound applied. The corresponding values for wash 2 were 3.69% without ultrasound and 4.33% with 100% ultrasound.

The amount of metacetamol found within the waste streams comprised of the mother liquor and the two collected washes. The mother liquor contained 3.75% in 0% ultrasound and 4.04 % in 100% ultrasound. For wash 1: 6.14% in 0% ultrasound and 6.83% in 100% ultrasound, and for wash 2 were 6.23% in 0% ultrasound and 7.53% in 100% ultrasound. Impurity removal in the case of waste streams was successful >0.3% in 100% ultrasound. This data is consistent with successfully removing 2% acetanilide and 4% metacetamol impurities through the waste stream analysis.

The solid blue (0% ultrasound) and dotted blue (100% ultrasound) lines indicate the amount of paracetamol found in the samples taken at each stage. This shows that the input material, paracetamol, made up 94% of the total sample, as anticipated, from the composition of the solution prepared. The paracetamol composition increased in the cake sample to 98.12% at 0% ultrasound and 98.11% at 100% ultrasound. This improvement in the purity of the paracetamol fell in line with the increase in yield noted in the figure and discussed in Section 6.4.7 above. The amount of paracetamol relative to 2% acetanilide and 4% metacetamol then decreased in the waste streams

analysed. There is a moderate deviation of less than 0.95% decrease in paracetamol in the mother liquors, wash 1 and wash 2, for 100% ultrasound compared to 0% ultrasound. This shows that 100% ultrasound was more successful in removing impurities in this case.
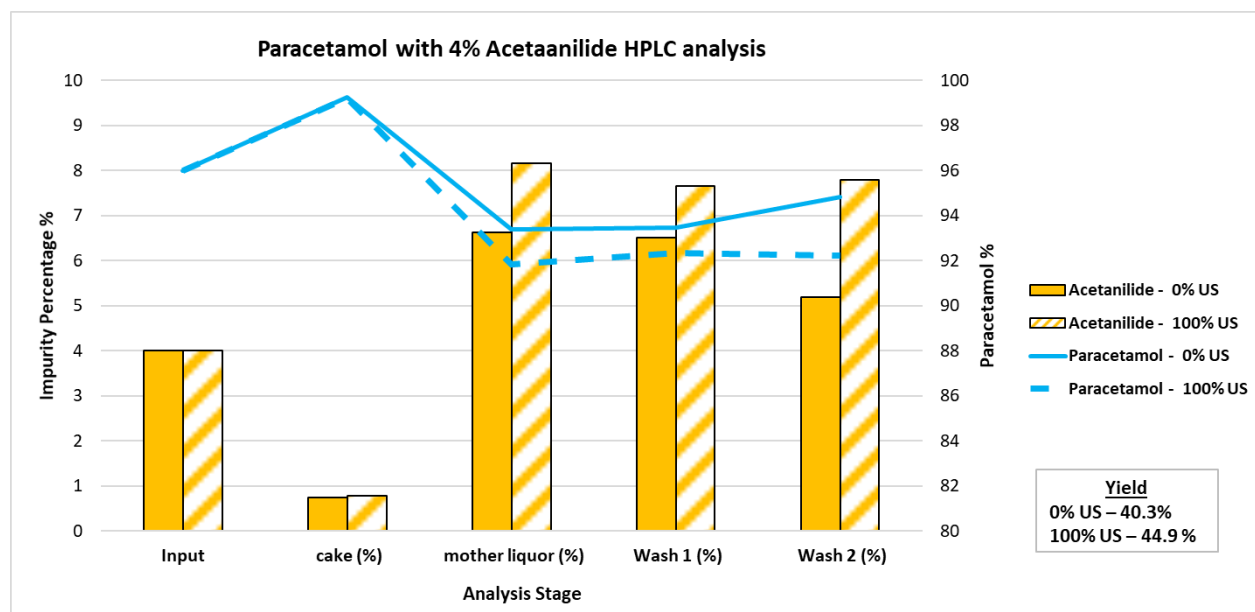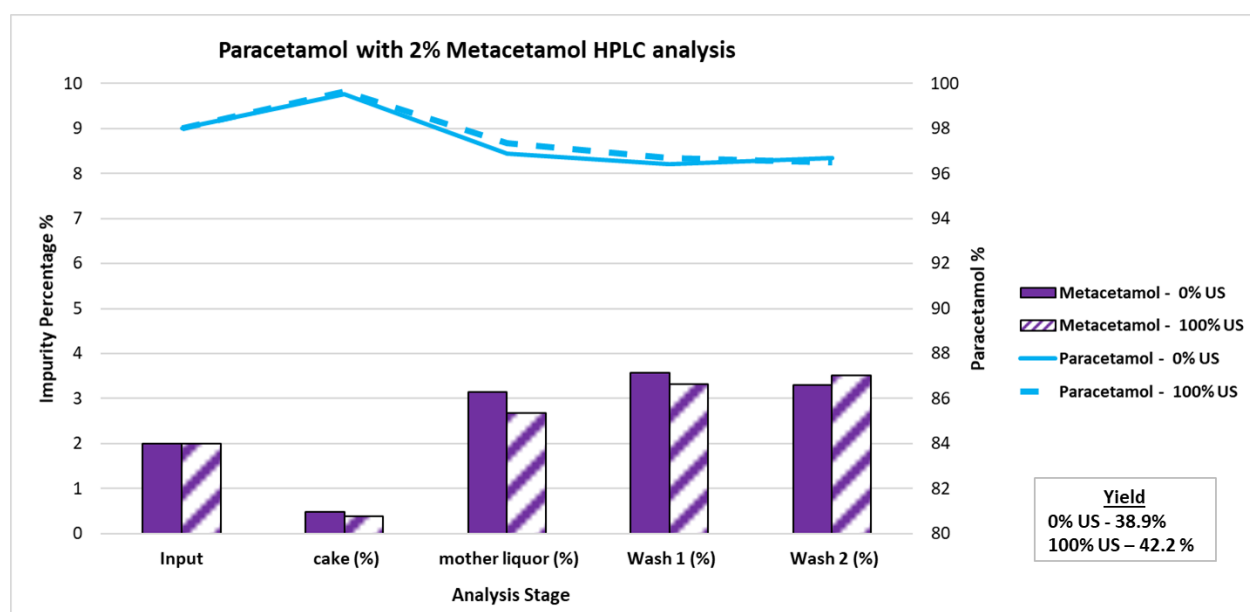

Figure 120: Diagrammatic representation of HPLC analysis of paracetamol with 4% acetanilide and 2% metacetamol, with 0% US (ultrasound) and 100% US (ultrasound), the input material total (%), the total amount of acetanilide and metacetamol found in the cake and waste streams (mother liquor, wash 1 and wash 2) (%), the total amount of paracetamol through each stage (%), and the final calculated yield (%) discussed in Section 6.4.7.

Figure 120 gives the relative composition from HPLC analysis of the isolated product and waste streams after crystallisation with an input containing 4% acetanilide and 2% metacetamol, showing the effect of 0 and 100% ultrasound. The amount of acetanilide found within the product (cake) was 0.57% in 0% ultrasound and 0.78% in 100% ultrasound; this result indicates that ultrasound and washing were not as effective as 0% ultrasound, with a 0.21% difference found. The amount of metacetamol found within the product (cake) was 0.82% in 0% ultrasound and 0.46% in 100% ultrasound; this result indicates that 100% ultrasound and washing were successful, with a 0.36% difference found.

Appendix C: Bulk Suspension Measurements

The amount of acetanilide found within the waste streams comprised of the mother liquor and the two collected washes. The mother liquor contained 6.34% acetanilide in the absence of ultrasound and 7.07% when 100% ultrasound power was applied. For wash 1, the amount of acetanilide was 6.57% in the absence of ultrasound and 7.94% with 100% ultrasound applied. The corresponding values for wash 2 were 9.61% without ultrasound and 8.04% with 100% ultrasound. This data is consistent with successfully removing the acetanilide impurity through the waste stream analysis. The amount of metacetamol found within the waste streams comprised of The mother liquor and the two collected washes. The mother liquor contained 3.75% metacetamol in the absence of ultrasound and 4.04% when 100% ultrasound power was applied. For wash 1, the amount of metacetamol was 3.13% in the absence of ultrasound and 3.63% with 100% ultrasound applied. The corresponding values for wash 2 were 4.05% without ultrasound and 3.65% with 100% ultrasound. This data is consistent with successfully removing the metacetamol impurities through the waste stream analysis.

The solid blue (0% ultrasound) and dotted blue (100% ultrasound) lines indicate the amount of paracetamol found in the samples taken at each stage. This shows that the input material, paracetamol, made up 94% of the total sample, as anticipated from the composition of the solution prepared. The paracetamol composition increased in the cake sample to 98.61% at 0% ultrasound and 98.76% at 100% ultrasound. This improvement in the purity of the paracetamol fell in line with the increase in yield noted in the figure and discussed in Section 6.4.7 above. The amount of paracetamol relative to 4% acetanilide and 2% metacetamol then decreased in the waste streams analysed. There is a moderate deviation of less than 1.2% decrease in paracetamol in the mother liquors and wash 1 for 100% ultrasound compared to 0% ultrasound. However, a larger dip of 2% paracetamol is found in wash 2 between 100% and 0% ultrasound. This could be due to the success of wash 2 and 0% ultrasound in removing a larger number of impurities when compared with 100% ultrasound.
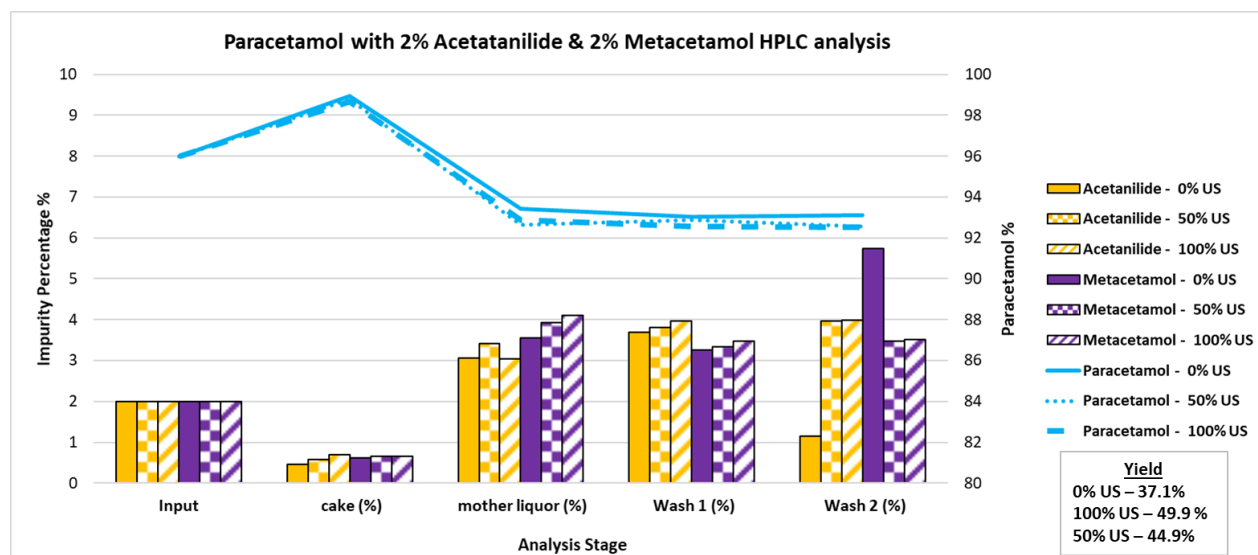
Figure 121: Diagrammatic representation of HPLC analysis of paracetamol with 2% acetanilide and 2% metacetamol, with 0% US (ultrasound), 50% US (ultrasound), and 100% US (ultrasound), the input material total (%), the total amount of acetanilide and metacetamol found in the cake and waste streams (mother liquor, wash 1 and wash 2) (%), the total amount of paracetamol through each stage (%), and the final calculated yield (%) discussed in Section 6.4.7.

Figure 121 gives the relative composition from HPLC analysis of the isolated product and waste streams after crystallisation with an input containing 2% acetanilide and 2% metacetamol, showing the effect of 0, 50, and 100% ultrasound. The amount of acetanilide found within the product (cake) was 0.45% in 0% ultrasound, 0.57% in 50% ultrasound and 0.7% in 100% ultrasound. The amount of metacetamol found within the product (cake) was 0.62% in 0% ultrasound, 0.65% in 50% ultrasound and 0.66% in 100% ultrasound. This result indicates that 50 and 100% of the ultrasound was not successful in the removal of acetanilide by 0.12% (50% ultrasound) and 0.25% (100% ultrasound) or for metacetamol by 0.03% (50% ultrasound) and 0.04% (100% ultrasound).

The amount of acetanilide found within the waste streams comprised of the mother liquor and the two collected washes. The mother liquor contained 3.06% acetanilide in the absence of ultrasound, 3.42% with 50% ultrasound, and 3.04% with 100% ultrasound power applied. For wash 1, the amount of acetanilide was 3.69% in the

69

absence of ultrasound, 3.81% with 50% ultrasound, and 3.98% with 100% ultrasound applied. The corresponding values for wash 2 were 1.15% without ultrasound, 3.97% with 50% ultrasound and 3.98% with 100% ultrasound. This data is consistent with successfully removing the acetanilide impurity through the waste stream analysis, particularly for the non-sonicated case.

The mother liquor and first wash can be expected to be somewhat similar in composition based on the wash volume of one cake volume since the make-up of wash 1 is a mixture of mother liquor displaced from the voids in the cake and the first portion of the wash solvent breaking through the cake, which can be expected to be relatively rich in both the impurity and paracetamol. 50% ultrasound was more successful in removing acetanilide in the mother liquor, giving a 0.36% difference; in wash 1, 100% ultrasound was more successful by 0.27%; and in wash 2, again, 100% ultrasound was more successful, giving a 2.83% difference. The overall effect is that more metacetamol was removed from the material produced with ultrasound since the combined mother liquor and first wash volume comprised of more (ca. 50 mL) than the second wash volume (ca.10 mL).

The amount of metacetamol found within the waste streams comprised of the mother liquor and the two collected washes. The mother liquor contained 3.55% metacetamol in the absence of ultrasound, 3.93% with 50% ultrasound, and 4.1% when 100% ultrasound power was applied. For wash 1, the amount of metacetamol was 3.26% in the absence of ultrasound, 3.33% with 50% ultrasound, and 3.47% with 100% ultrasound applied. The corresponding values for wash 2 were 5.74% without ultrasound, 3.47% with 50% ultrasound, and 3.51% with 100% ultrasound. This data is consistent with successfully removing the metacetamol impurity through the waste stream analysis. The mother liquor and first wash can be expected to be somewhat similar in composition based on the wash volume of one cake volume since the make-up of wash 1 is a mixture of mother liquor displaced from the voids in the cake and the first portion of the wash solvent breaking through the cake, which can be expected to be relatively rich in both the impurity and paracetamol. In the mother liquor and wash 1, 100% removed more impurity incorporation compared with 50% ultrasound, by 0.17% in the mother liquor and 0.14% in wash 1. In wash 2, 50 and 100% ultrasound

were found to have less of an effect than 0% ultrasound. The overall effect is that more metacetamol was removed from the material produced with ultrasound since the combined mother liquor and first wash volume comprised of more (ca. 50 mL) than the second wash volume (ca.10 mL).

The solid blue (0% ultrasound), small dashes (50% ultrasound), and dotted blue (100% ultrasound) lines indicate the amount of paracetamol found in the samples taken at each stage. This shows that the input material, paracetamol, made up 96% of the total sample, as anticipated from the composition of the solution prepared. The paracetamol composition increased in the cake sample to 98.93% at 0% ultrasound, 98.78% at 50% ultrasound, and 98.65 % at 100% ultrasound. This improvement in the purity of the paracetamol fell in line with the reduction of impurities and the increase in yield noted in the figure and discussed in Section 6.4.7 above.

The amount of paracetamol relative to 2% acetanilide and 2% metacetamol then decreased in the waste streams analysed, with 50 and 100% of ultrasound having the least amount of paracetamol per stage. The deviation between 50 and 100% ultrasound is minimal; however, 100% is slightly less at the wash 1 and wash 1 stages by 0.29% and 0.05%, respectively; the difference in the mother liquors was 0.21% with 50% ultrasound. In the mother liquor, the deviation between 0% and 50% in ultrasound was 0.76%. The deviation between 0% and 100% ultrasound in wash 1 and two were 0.48% and 0.6% respectively.
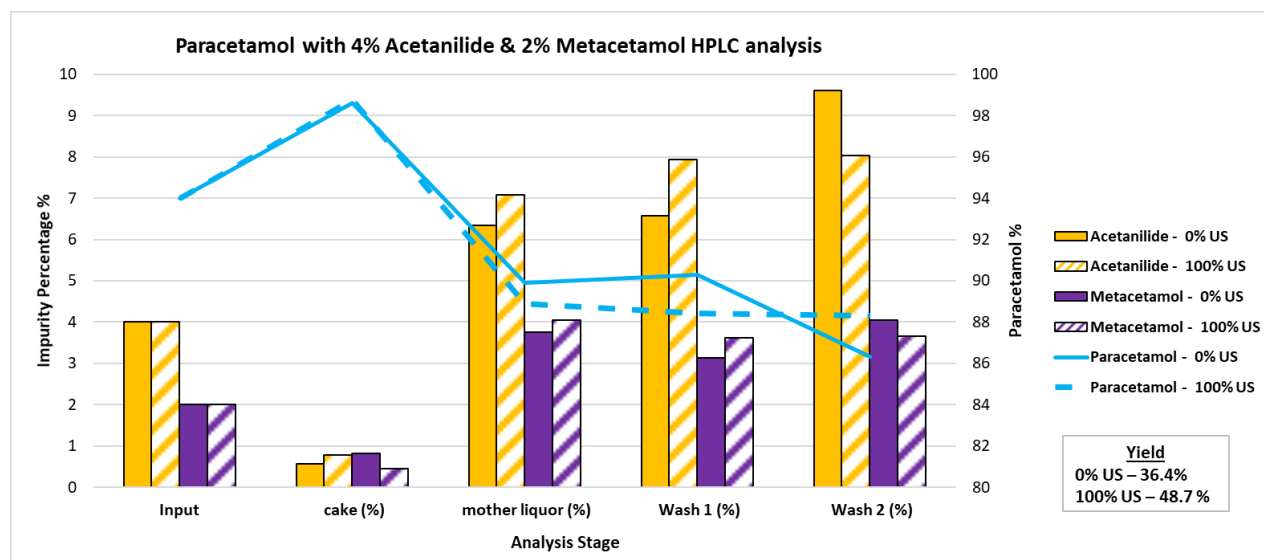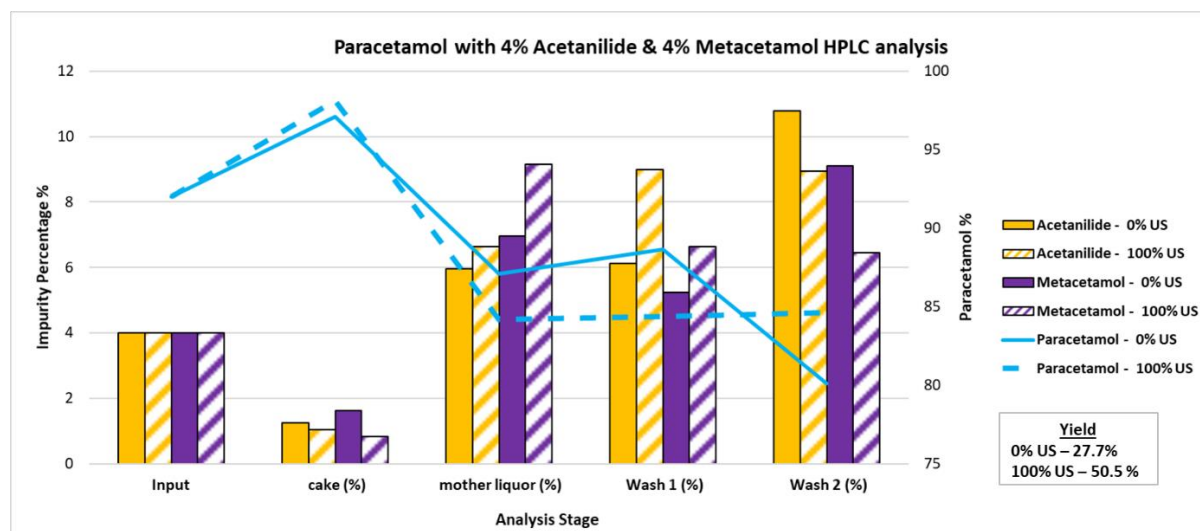
Figure 122: Diagrammatic representation of HPLC analysis of paracetamol with 4% acetanilide and 4% metacetamol, with 0% US (ultrasound) and 100% US (ultrasound), the input material total (%), the total amount of acetanilide and metacetamol found in the cake and waste streams (mother liquor, wash 1 and wash 2) (%), the total amount of paracetamol through each stage (%) and the final calculated yield (%) discussed in Section 6.4.7.

Figure 122 gives the relative composition from HPLC analysis of the isolated product and waste streams after crystallisation with an input containing 4% acetanilide and 4% metacetamol, showing the effect of 0 and 100% ultrasound. The amount of acetanilide found within the product (cake) was 1.26% in 0% ultrasound and 1.04% in 100% ultrasound. The amount of metacetamol found within the product (cake) was 1.63% in 0% ultrasound and 0.83% in 100% ultrasound. This result indicates that 100% ultrasound and washing effectively reduced acetanilide by 0.22% and metacetamol by 0.8%.

The amount of acetanilide found within the waste streams comprised of the mother liquor and the two collected washes. The mother liquor contained 5.95% acetanilide in the absence of ultrasound and 6.64% when 100% ultrasound power was applied. For wash 1, the amount of acetanilide was 6.11% in the absence of ultrasound and 9% with 100% ultrasound applied. The corresponding values for wash 2 were 10.79% without ultrasound and 8.94% with 100% ultrasound. This data is consistent with successfully removing the acetanilide impurity through the waste stream analysis.

Appendix C: Bulk Suspension Measurements

The amount of metacetamol found within the waste streams comprised of the mother liquor and the two collected washes. The mother liquor contained 6.97% metacetamol in the absence of ultrasound and 9.16% when 100% ultrasound power was applied. For wash 1, the amount of metacetamol was 5.23% in the absence of ultrasound and 6.64% with 100% ultrasound applied. The corresponding values for wash 2 were 9.1% without ultrasound and 6.44% with 100% ultrasound. This data is consistent with successfully removing the metacetamol impurity through the waste stream analysis.

The solid blue (0% ultrasound) and dotted blue (100% ultrasound) lines indicate the amount of paracetamol found in the samples taken at each stage. This shows that the input material, paracetamol, made up 92% of the total sample, as anticipated from the composition of the solution prepared. The paracetamol composition increased in the cake sample to 97.11% at 0% ultrasound and 98.13% at 100% ultrasound. This improvement in the purity of the paracetamol fell in line with the reduction of impurities and the increase in yield noted in the figure and discussed in Section 6.4.7 above. The amount of paracetamol relative to 4% acetanilide and 4% metacetamol then decreased in the waste streams analysed.

The results show some variation in the outcome with the application of ultrasound to the system. In the following cases: paracetamol with 2% acetanilide, paracetamol with 2% metacetamol, paracetamol with 2% metacetamol and 4% acetanilide, and paracetamol with 4% acetanilide and 4% metacetamol, the ultrasound-treated samples contain less impurity than the non-sonicated samples, which are anticipated. Of the other four samples, two are very close in concentration and have the following results: paracetamol with 4% acetanilide impurity in non-sonicated samples was 0.74% and 0.77% in the ultrasonic-treated samples. Paracetamol with 4% metacetamol and 2% acetanilide showed a reduction of metacetamol from 1.34% to 1.20 % but an increase in acetanilide from 0.54% to 0.69%. At the conditions of 2% acetanilide and 2% metacetamol, 50% ultrasonic power produced a higher purity of paracetamol (98.78%) than 100% power (98.65%). However, the non-sonicated condition yielded the highest purity of 98.93%. Given the close similarity of these assays, it is fair to conclude there is an improvement in the overall purity within the cakes; however, this is only demonstrated in some cases. Similarly, in the study by Nguyen (128), it was found that the ultrasound-treated samples contained less

impurity than the non-treated samples, e.g., when comparing no ultrasound with 50 and 100% ultrasound, the particle size decreased with an increase in ultrasound power. This would result in particles being easier to wash at 50% ultrasound when compared with smaller, more compact particles at 100% ultrasound. There is also a danger of the wash solvent driving dissolved material out of solution if the contact time is long, and although this was managed as well as it could be, it could still be a possibility.

In the filtrate of mother liquor and wash solvents, the percentage of impurity is consistently higher than that of the cake product, confirming that the filtration and washing steps successfully remove impurities. The liquor collected after processing the cake with wash 1 contains a significant portion of displaced mother liquor, as the wash volume was selected to match the saturated cake volume. Typically, the concentration of both impurities in the liquor displaced by performing wash 1 is similar to the concentration of impurities in the mother liquor and the composition of the liquors collected during the application of wash 2. For example, when 2% acetanilide is added to paracetamol, the percentage of this impurity found in a non-sonicated cake was 0.46% and 0.37% for a sonicated sample; in the mother liquor, the acetanilide represented 3.38% and 4.06%, respectively. In wash 1, it was 3.60% and 4.03%, respectively; in wash 2, it was 4.91% and 3.79%, respectively. As impurities are rejected by the growing crystal surfaces, this leads to an increase in the concentration of the impurities in the solution. In this example, the impurity concentration increases through the following steps: To wash a product thoroughly, it is recommended to wash it at least twice to achieve the desired effect of the selected wash solvent. The wash solvent selected for this experiment was n-heptane; this was chosen due to n-heptane's miscibility with ethanol. There are not many literature examples of ultrasound being deployed to improve product purity, although there has been mention of improvements to product purity with smoother surfaces and fewer inclusions at low intensities (171); in another case, it was also found that ultrasound degraded a growth inhibitor as well as improving the growth rate (201). While the mechanisms of sonocrystallisation are not established, it is reasonable to argue that the localised heating plays a part in removing structurally similar impurities from the growing crystal just as they adsorb onto the surface. Since ultrasound also reduces particle size and

results in breakage at high power outputs, giving more surface area for the impurities to attach, the ultrasound must also be effective in removing them from the growing surfaces. Another theory could be that ultrasound was found to reduce agglomeration, reducing the extent of inclusion of mother liquor in multi-particle clusters. The reduction in particle size and extent of agglomeration tend to work in opposite directions regarding impurity removal. Generally, smaller particles are more challenging to wash with a larger wetted surface area and narrower pores between the crystals forming the filter cake, whereas disrupting agglomerates prevents impurities from becoming trapped in the inaccessible space between agglomerated particles. The combined effect resulted in improved purification during isolation (see Table 17).

Looking at the quantity of impurities in the cake, the impurity fraction is seen to increase with an increase in added impurity amount; metacetamol is found at a higher impurity fraction in the product crystals in comparison to acetanilide's uptake individually and in impurity mixtures of 2% and 4%. This is described by (i) the segregation coefficient of metacetamol, where it is found to have moderate levels of uptake in comparison to acetanilide, the uptake of which was SC = 0.25 for metacetamol and SC = 0.11 for acetanilide (251); this indicates that metacetamol has a strong docking ability (164). (ii) Acetanilide is more soluble in ethanol than metacetamol, and (iii) looking at all results for metacetamol, it was found to inhibit the growth rate of single crystals more than acetanilide. It also inhibited the nucleation rate, resulting in nucleation occurring at lower temperatures. The overall PSD was smaller, therefore hindering the filtration process, and finally, its presence resulted in a smaller yield. There are several mechanisms proposed as to how impurities incorporate into crystalline materials: (i) surface adhesion/adsorbed onto the crystal surface; (ii) molecular substitution at the lattice site; (iii) mother liquor incorporation into the lattice, and (iv) bulk phase inclusion of mother liquor during agglomeration (128, 290). As previously mentioned in other chapters, the acetamido group in metacetamol and acetanilide is identical to paracetamol. The segregation coefficient of metacetamol uptake was higher than acetanilide, as described by Hendrikson (251); this is in agreement with the cake% analysis above, where this study found that there was a larger percentage of metacetamol traced within the samples when compared with acetanilide. When comparing the habits of 2 and 4% of each impurity again, it is

clear that habits are altered; however, mother liquor substitution is not evident from the images. This leads to the assumption that for bulk suspension crystallisation, both (i) surface adhesion/adsorbed onto the crystal surface and (ii) molecular substitution at the lattice site are both very probable ways in which the impurities are incorporated into the growing crystals.

References

Refrences

1.   Nguyen TTH. Influence of crystallisation environment on the nucleation and growth of single crystals of (RS)-Ibuprofen, Published PhD thesis. Leeds: Institute of Particle Science & Engineering

School of Process, Environmental and Materials Engineering; (2013).

2.   Agricola G. DE RE METALLICA. (trans. from H. Hoover and L. Hoover) , London: The Mining   Magazine;   (1912)   [cited   2014   17/12].   Available   from: http://www.gutenberg.org/files/38015/38015-h/38015-h.htm.

3.   Pharmaceutical industry in the United Kingdom (UK) - Statistics & Facts [Internet]. Available   from: https://www.statista.com/topics/5056/pharmaceutical-industry-in-the-uk/#topicOverview.

4.   Research A. Pharmaceutical and Biotechnology Construction Sector Report - UK 2014-2018 Analysis: AMA Research Ltd; (n.d.) [cited 2016 16/09]. Available from: http://www.amaresearch.co.uk/pharmaceutical_construction_14s.html.

5.   Price C. Transforming industrial crystallization by sono-manipulation of crystal surfaces. Swindon: Research Council UK; (2014).

6.   Davey R, Garside J. From molecules to crystallizers.: Oxford University Press, pp. 1; (2000).

7.   Mullin JW. Crystallization. 4th ed. ScienceDirect, editor: Oxford ; Boston : Butterworth-Heinemann; (2001) 1/09/2014. 594 p.

8.   Thompson C, Davies MC, Roberts CJ, Tendler SJ, Wilkinson MJ. The effects of additives on the growth and morphology of paracetamol (acetaminophen) crystals. International journal of pharmaceutics. (2004);280(1):pp. 137-50.

9.   Sangwal K. Additives and Crystallization Processes: From Fundamentals to Applications. West Sussex: John wiley & Sons, Ltd, pp. 109-143; (2007). 437 p.

10.   Biscans B. Industrial crystallization- challanges and scientific issues (2011) [cited 2014 06/12]. Available from: http://www.aidic.it/isic18/webpapers/309Biscans.pdf.

11.   Hendriksen BA, Grant DJ, Meenan P, Green DA. Crystallisation of paracetamol (acetaminophen) in the presence of structurally related substances. Journal of crystal growth. 1998;183(4):629-40.

12.   Tahri Y. Investigation of the l-Glutamic acid polymorphism: Comparison between stirred and stagnant conditions. Journal of Crystal Growth. 2016:Pages 98-104.

13.   Graaf Jvd. Sonocrystallization: Nucleation of ammonium sulfate and alfa-lactose monohydrate due to ultrasonic irradiation [Published Master of Science Thesis, Netherlands]. Netherlands: Delft University of Technology; (2011).

References

14.   Martini S. An Overview of Ultrasound. Sonocrystallization of Fats: Springer; 2013. p. 7-16.

15.   Sander JRG, Zeiger BW, Suslick KS. Sonocrystallization and sonofragmentation. Ultrasonics Sonochemistry. (2014);21(6):pp. 1908-15.

16.   Ruecroft G, Hipkiss D, Ly T, Maxted N, Cains PW. Sonocrystallization: the use of ultrasound for improved industrial crystallization. Organic Process Research & Development. (2005);9(6):923-32.

17.   Zhang HQ, Barbosa-Cánovas GV, Balasubramaniam VB, Dunne CP, Farkas DF, Yuan JT. Nonthermal processing technologies for food: John Wiley & Sons; (2011).

18.   Prasad KVR, Ristic RI, Sheen DB, Sherwood JN. Crystallization of paracetamol from solution in the presence and absence of impurity. International Journal of Pharmaceutics. (2001);215(1–2):29-44.

19.   Kim HN, Suslick KS. The Effects of Ultrasound on Crystals: Sonocrystallization and Sonofragmentation. Crystals (2073-4352). (2018);8(7).

20.   Kiss AA, Geertman R, Wierschem M, Skiborowski M, Gielen B, Jordens J, et al. Ultrasound-assisted emerging technologies for chemical processes. (2018);93(5):1219-27.

21.   Chen Z, Wu Y, Yang Y, Li J, Xie B, Li X, et al. Multilayered carbon nanotube yarn based optoacoustic transducer with high energy conversion efficiency for ultrasound application. Nano energy. (2018);46:314-21.

22.   Paniwnyk L, Alarcon-Rojo A, Rodriguez-Figueroa JC, Toma M. The Use of Ultrasound as an Enhancement Aid to Food Extraction. Ingredients Extraction by Physicochemical Methods in Food: Elsevier; (2017). p. 399-440.

23.   Umbdenstock RR. Preparation of procaine penicillin. Google Patents; (1955).

24.   Principe JR, Skauen DMJJops. Preparation of microcrystalline progesterone using ultrasound. (1962);51(4):389-90.

25.   Silvana M. Sonocrystallization of Fats (SpringerBriefs in Food, Health, and Nutrition). Springer. (2013):65.

26.   Leighton T. Chapter 1: The sound field. The acoustic bubble Academic Press, New York. (1994):1-66.

27.   Narducci O. Particle Engineering via Sonocrystallization: The Aqueous Adipic Acid System: UCL (University College London); (2013).

28.   Chatel G, Colmenares JC. Sonochemistry: from basic principles to innovative applications. Springer; (2017).

29.   McClements DJ. Ultrasonic characterisation of emulsions and suspensions. Advances in Colloid and Interface Science. (1991);37(1-2):33-72.

30.   Tang WZ. Physicochemical treatment of hazardous wastes: CRC Press; (2016).

References

31.   Vajnhandl S, Le Marechal AM. Ultrasound in textile dyeing and the decolouration/mineralization of textile dyes. Dyes and Pigments. (2005);65(2):89-101.

32.   Hugo Miguel Santos, Carlos Lodeiro, Capelo-Martinez J-L. 1) The Power of Ultrasound. Ultrasound in Chrmistry: Analystical Applications: WILEY-VCH; (2009).

33.   Chen D. 15 Applications of Ultrasound in Water and Wastewater Treatment. Handbook on Applications of. (2012):373.

34.   Guo Z. Ultrasonic effects on Crystallization Processes: Univeristy College London; (2007).

35.   Bhatia AB. Ultrasonic absorption: an introduction to the theory of sound absorption and dispersion in gases, liquids, and solids: Courier Corporation; (1985).

36.   Suslick KS. The Chemistry of Ultrasound (2018) [Available from: http://www.scs.illinois.edu/suslick/sonochembrittanica.html.

37.   Yusvika M, Prabowo AR, Baek SJ, Tjahjana DDDP. Achievements in observation and prediction of cavitation: Effect and damage on the ship propellers. Procedia Structural Integrity. 2020;27:109-16.

38.   Price CJ. Application of Ultrasound in Crystallization (Sonocrystallization). Engineering Crystallography: From Molecule to Crystal to Functional Form: Springer; (2017). p. 301-13.

39.   Chow R, Blindt R, Chivers R, Povey M. A study on the primary and secondary nucleation of ice by power ultrasound. Ultrasonics. (2005);43(4):227-30.

40.   Devarakonda S, Evans JM, Myerson AS. Impact of ultrasonic energy on the crystallization of dextrose monohydrate. Crystal growth & design. (2003);3(5):741-6.

41.   Chow R, Blindt R, Kamp A, Grocutt P, Chivers R. The microscopic visualisation of the sonocrystallisation of ice using a novel ultrasonic cold stage. Ultrasonics sonochemistry. (2004);11(3-4):245-50.

42.   Chow R, Blindt R, Chivers R, Povey M. The sonocrystallisation of ice in sucrose solutions: primary and secondary nucleation. Ultrasonics. (2003);41(8):595-604.

43.   Wu TY, Guo N, Teh CY, Hay JXW. Advances in ultrasound technology for environmental remediation: Springer Science & Business Media; (2012).

44.   Adewuyi YG. Sonochemistry: environmental science and engineering applications. Industrial & Engineering Chemistry Research. (2001);40(22):4681-715.

45.   Wood RJ, Lee J, Bussemaker MJJUs. A parametric review of sonochemistry: Control and augmentation of sonochemical activity in aqueous solutions. (2017);38:351-70.

46.   Peters D. Ultrasound in materials chemistry. Journal of materials chemistry. (1996);6(10):1605-18.

References

47.   Ince N, Tezcanli G, Belen R, Apikyan İG. Ultrasound as a catalyzer of aqueous reaction systems: the state of the art and environmental applications. Applied Catalysis B: Environmental. (2001);29(3):167-76.

48.   Lee J, Hallez L, Touyeras F, Ashokkumar M, Hihn JYJUS. Influence of frequency sweep on sonochemiluminescence and sonoluminescence. (2020):105047.

49.   Nalesso S, Bussemaker MJ, Sear RP, Hodnett M, Lee JJUs. A review on possible mechanisms of sonocrystallisation in solution. (2019).

50.   Jordens J, Gielen B, Xiouras C, Hussain MN, Stefanidis GD, Thomassen LC, et al. Sonocrystallisation: observations, theories and guidelines. (2019).

51.   Hua I, Hoffmann MR. Optimization of ultrasonic irradiation as an advanced oxidation technology. Environmental Science & Technology. (1997);31(8):2237-43.

52.   Mason T, Petrier C. Ultrasound processes. Advanced oxidation processes for water and wastewater treatment. (2004):185-208.

53.   Chowdhury P, Viraraghavan T. Sonochemical degradation of chlorinated organic compounds, phenolic compounds and organic dyes–a review. Science of the total environment. (2009);407(8):2474-92.

54.   Mason TJ. Ultrasound in synthetic organic chemistry. Chemical Society Reviews. (1997);26(6):443-51.

55.   Instruments G. XUB Digital Ultrasonic Bath Range (2018) [Available from: https://www.grantinstruments.com/scientific/xub-digital-ultrasonic-bath-range.

56.   Klima J, Frias-Ferrer A, González-García J, Ludvik J, Saez V, Iniesta J. Optimisation of 20 kHz sonoreactor geometry on the basis of numerical simulation of local ultrasonic intensity and qualitative comparison with experimental results. Ultrasonics sonochemistry. (2007);14(1):19-28.

57.   Berlan J, Mason TJ. Dosimetry for power ultrasound and sonochemistry. Advances in sonochemistry. (1996);4(1).

58.   Muthukumaran S, Kentish S, Lalchandani S, Ashokkumar M, Mawson R, Stevens GW, et al. The optimisation of ultrasonic cleaning procedures for dairy fouled ultrafiltration membranes. Ultrasonics Sonochemistry. (2005);12(1-2):29-35.

59.   Lee D, Son YJJoKSoWE. Sonochemial and Sonophysical Effects in Heterogeneous Systems. (2019);35(2):115-22.

60.   Bromberger Soquetta M, Schmaltz S, Wesz Righes F, Salvalaggio R, de Marsillac Terra LJJoFP, Preservation. Effects of pretreatment ultrasound bath and ultrasonic probe, in osmotic dehydration, in the kinetics of oven drying and the physicochemical properties of beet snacks. (2018);42(1):e13393.

References

61.   Sonics & Materials I. CAVITATION EROSION OF ULTRASONIC PROBES (n.d) [Available from: https://www.sonics.com/site/assets/files/2962/cavitation_erosion_of_ultrasonic_probes.pdf.

62.   Prasad KV, Ristic RI, Sheen DB, Sherwood JN. Crystallization of paracetamol from solution in the presence and absence of impurity. International journal of pharmaceutics. 2001;215(1):29-44.

63.   Pahari A, Chauhan B. Engineering chemistry: Laxmi Publications; (2006).

64.   ScienceHQ. Crystalline and Amorphous Solids (2013) [cited 2016 26/05]. Available from: http://www.sciencehq.com/chemistry/crystalline-and-amorphous-solids.html.

65.   Schoen HM, Grove Jr C, Palermo JA. The early history of crystallization. Journal of Chemical Education. (1956);33(8):373.

66.   Weinert F. The scientist as philosopher: Philosophical consequences of great scientific discoveries: Springer Science & Business Media; (2004).

67.   Lowitz J. Bemerkungen über das Krystallisiren der Salze, und Anzeige eines sichern Mittels, regelmässige Krystallen zu erhalten. Chemische Annalen. (1795);1:3-11.

68.   davies PAPaPP. SOLID STATE CHEMISTRY Key concepts, Handouts, supplemental information.
Reading in Zumdahl: Chapter 16 (2007) [cited 2015 20/03]. Available from: http://www.seas.upenn.edu/~chem101/sschem/solidstatechem.html.

69.   Miller WH. A treatise on crystallography: For J. & JJ Deighton; (1839).

70.   Zhang X, Yang Z, Chai J, Xu J, Zhang L, Qian G, et al. Nucleation kinetics of lovastatin in different solvents from metastable zone widths. Chemical Engineering Science. (2015).

71.   Lovette MA, Browning AR, Griffin DW, Sizemore JP, Snyder RC, Doherty MF. Crystal shape engineering. Industrial & engineering chemistry research. (2008);47(24):9812-33.

72.   Klug D. The influence of impurities and solvents on crystallization: Butterworth-Heinemann: Boston. pp. 67-100; (1993a). Available from: http://books.google.co.uk/books?id=gJ7KNvbMtREC&pg=PA67&lpg=PA67&dq=The+influence+of+impurities+and+solvents+in+crystallization&source=bl&ots=oQU0MkspCC&sig=0BVo7jBB94LeyDyYkYD1UTwkkDg&hl=en&sa=X&ei=lGNbVP_NA4mV7AayxIHgBA&ved=0CCYQ6AEwAA#v=onepage&q&f=false.

73.   Pritula I, Sangwal K. Fundamentals of Crystal Growth from Solutions. In: Rudolph P, editor. Handbook of Crystal Growth (Second Edition). Boston: Elsevier; (2015). p. pp. 1185-227.

74.   Ilic D, Nikolic V, Stankovic M, Nikolic L, Stanojevic L, Mladenovic-Ranisavljevic I, et al. Transformation of Synthetic Allicin: The Influence of Ultrasound, Microwaves, Different Solvents and Temperatures, and the Products Isolation. ScientificWorldJournal. 2012;2012:561823-7.

References

75.   Davey RJ, Mullin JW. Growth of the {100} faces of ammonium dihydrogen phosphate crystals in the presence of ionic species. Journal of Crystal Growth. (1974);26(1):45-51.

76.   Zhong X, Huang C, Chen L, Yang Q, Huang Y. Effect of ultrasound on the kinetics of anti-solvent crystallization of sucrose. Ultrason Sonochem. 2022;82:105886-.

77.   Jansens P, Matsuoka M. Melt Crystallization. Encyclopedia of Separation Science, Eds Wilson ID, Adlard ER, Cook M, and Poole CF, Academic Press, San Diego, New York London, Sidney, Tokyo. (2000):966-75.

78.   Jones AG. Crystallization process systems: Butterworth-Heinemann; (2002).

79.   Granberg RA, Rasmuson ÅC. Solubility of paracetamol in pure solvents. Journal of Chemical & Engineering Data. (1999);44(6):1391-5.

80.   Keshavarz L, Steendam RR, Blijlevens MA, Pishnamazi M, Frawley PJJCG, Design. Influence of Impurities on the Solubility, Nucleation, Crystallization, and Compressibility of Paracetamol. (2019);19(7):4193-201.

81.   Jambrak AR, Mason TJ, Lelas V, Herceg Z, Herceg IL. Effect of ultrasound treatment on solubility and foaming properties of whey protein suspensions. Journal of Food Engineering. (2008);86(2):281-7.

82.   Nyvlt J, Soehnel O, Matuchova M. The kinetics of industrial crystallization. Chemical engineering monographs (ISSN 0167-4188. (1985);19.

83.   O'Grady D, Barrett M, Casey E, Glennon B. The effect of mixing on the metastable zone width and nucleation kinetics in the anti-solvent crystallization of benzoic acid. Chemical Engineering Research and Design. (2007);85(7):945-52.

84.   Sahin O, Dolas H, Demir H. Determination of nucleation kinetics of potassium tetraborate tetrahydrate. Crystal Research and Technology. (2007);42(8):766-72.

85.   Omar W, Ulrich J. Solid liquid equilibrium, metastable zone, and nucleation parameters of the oxalic acid-water system. Crystal growth & design. (2006);6(8):1927-30.

86.   Barrett P, Glennon B. Characterizing the metastable zone width and solubility curve using Lasentec FBRM and PVM. Chemical Engineering Research and Design. (2002);80(7):799-805.

87.   Sangwal K. Effect of impurities on the metastable zone width of solute–solvent systems. Journal of Crystal Growth. (2009);311(16):pp. 4050-61.

88.   Lyczko N, Espitalier F, Louisnard O, Schwartzentruber J. Effect of ultrasound on the induction time and the metastable zone widths of potassium sulphate. Chemical Engineering Journal. (2002);86(3):233-41.

89.   Maharana A, Sarkar D. Effects of Ultrasound and Its Amplitude on the Metastable Zone Width, Induction Time, and Nucleation Kinetics of Pyrazinamide in Acetone. Industrial & Engineering Chemistry Research. 2022;61(30):11262-75.

References

90.   Mitchell NA, Frawley PJ, Ó'Ciardhá CT. Nucleation kinetics of paracetamol–ethanol solutions from induction time experiments using Lasentec FBRM®. Journal of Crystal Growth. (2011);321(1):91-9.

91.   Lenka M, Sarkar D. Determination of metastable zone width, induction period and primary nucleation kinetics for cooling crystallization of l-asparaginenohydrate. Journal of Crystal Growth. (2014);408:85-90.

92.   Kashchiev D, Verdoes D, van Rosmalen GM. Induction time and metastability limit in new phase formation. Journal of Crystal Growth. (1991);110(3):373-80.

93.   POORNACHARY SK. Effects of impurities on crystal growth processes: NATIONAL UNIVERSITY OF SINGAPORE; (2007).

94.   Veesler S, Puel F. 21 - Crystallization of Pharmaceutical Crystals. In: Nishinaga T, editor. Handbook of Crystal Growth (Second Edition). Boston: Elsevier; 2015. p. 915-49.

95.   Davey RJ, Schroeder SL, ter Horst JH. Nucleation of organic crystals—a molecular perspective. Angewandte Chemie International Edition. (2013);52(8):2166-79.

96.   ten Wolde PR, Frenkel D. Enhancement of protein crystal nucleation by critical density fluctuations. Science. (1997);277(5334):1975-8.

97.   Knezic D, Zaccaro J, Myerson AS. Nucleation induction time in levitated droplets. The Journal of Physical Chemistry B. (2004);108(30):10672-7.

98.   Turnbull D. Kinetics of solidification of supercooled liquid mercury droplets. The Journal of chemical physics. (1952);20(3):411-24.

99.   Jiang S, ter Horst JH. Crystal nucleation rates from probability distributions of induction times. Crystal Growth & Design. (2010);11(1):256-61.

100.   Auer S, Frenkel D. Prediction of absolute crystal-nucleation rate in hard-sphere colloids. Nature. (2001);409(6823):1020-3.

101.   Ting HH, McCabe WL. Solubility of magnesium sulfate heptahydrate. Industrial & Engineering Chemistry. (1934);26(11):1207-8.

102.   Kane S, Evans T, Brian P, Sarofim A. Determination of the kinetics of secondary nucleation in batch crystallizers. AIChE Journal. (1974);20(5):855-62.

103.   Mason R, Strickland-Constable R. Breeding of crystal nuclei. Transactions of the Faraday Society. (1966);62:455-61.

104.   Mersmann A, Bartosch K. How to predict the metastable zone width. Journal of crystal growth. (1998);183(1):240-50.

105.   Ulrich J, Strege C. Some aspects of the importance of metastable zone width and nucleation in industrial crystallizers. Journal of crystal Growth. (2002);237:2130-5.

106.   Sangwal K, Mielniczek-Brzoska E. Effect of impurities on metastable zone width for the growth of ammonium oxalate monohydrate crystals from aqueous solutions. Journal of crystal growth. (2004);267(3):pp. 662-75.

References

107. Lahav M, Leiserowitz L. Tailor-made auxiliaries for the control of nucleation, growth and dissolution of two-and three-dimensional crystals. Journal of Physics D: Applied Physics. (1993);26(8B):B22.

108. Thomson R-H, N. and Murphy, D. . Significance of controlling crystallization mechanisms and kinetics in pharmaceutical systems. J Pharm. (1999); 88:651-60.

109. Milisavljevic I, Wu Y. Current status of solid-state single crystal growth. BMC materials. 2020;2:1-26.

110. Yadav J, Srivastava A, Patel SA. Analysis of Thermal Characteristics of Batch Cooling Sonocrystallization: Effect on Crystal Attributes. Crystal research and technology (1979). 2023;58(3):2200156-n/a.

111. Lin H, Petsev DN, Yau S-T, Thomas BR, Vekilov PG. Lower incorporation of impurities in ferritin crystals by suppression of convection: modeling results. Crystal Growth & Design. (2001);1(1):73-9.

112. Hoyer JR, Asplin JR, Otvos L. Phosphorylated osteopontin peptides suppress crystallization by inhibiting the growth of calcium oxalate crystals. Kidney international. (2001);60(1):77-82.

113. Sangwal K, Benz K. Impurity striations in crystals. Progress in crystal growth and characterization of materials. (1996b);32(1):pp. 135-69.

114. Dabrowska N. Influence of Impurities on the Crystallisation of Pharmaceutical Materials: University of Strathclyde; (2017).

115. Sangwal K. Effects of impurities on crystal growth processes. Progress in crystal growth and characterization of materials. (1996a);32(1):pp. 3-43.

116. Sharon C. Crystallization Kinetics handout (n.d.) [cited 2015 22/01]. this is a calss handout]. Available from: http://community.dur.ac.uk/sharon.cooper/lectures/cryskinetics/handoutsalla.html.

117. Finnie S, Prasad KV, Sheen DB, Sherwood JN. Microhardness and dislocation identification studies on paracetamol single crystals. Pharmaceutical research. (2001);18(5):674-81.

118. Noyes AA, Whitney WR. The rate of solution of solid substances in their own solutions. Journal of the American Chemical Society. (1897);19(12):930-4.

119. Nernst W. Theorie der Reaktionsgeschwindigkeit in heterogenen Systemen. Zeitschrift für physikalische Chemie. (1904);47(1):52-5.

120. Car R, Kelly PJ, Oshiyama A, Pantelides ST. Microscopic theory of impurity-defect reactions and impurity diffusion in silicon. Phys Rev Lett. 1985;54(4):360-3.

121. Coleman S, Roy S. Effect of ultrasound on mass transfer during electrodeposition for electrodes separated by a narrow gap. Chemical engineering science. 2014;113:35-44.

References

122.   J.W. Morris J. Chapter 4: Defects in crystals: Materials Science; (n.d) [Available from: http://www.mse.berkeley.edu/groups/morris/MSE205/Extras/defects.pdf.

123.   Gutwald T, Mersmann A. Evaluation of kinetic parameters of crystallization from batch and continuous experiments. Separations Technology. (1994);4(1):2-14.

124.   Prasad KV, Ristic RI, Sheen DB, Sherwood JN. Dissolution kinetics of paracetamol single crystals. International journal of pharmaceutics. (2002);238(1):29-41.

125.   Ottoboni S, Chrubasik M, Mir Bruce L, Nguyen TTH, Robertson M, Johnston B, et al. Impact of Paracetamol Impurities on Face Properties: Investigating the Surface of Single Crystals Using TOF-SIMS. Crystal Growth & Design. 2018;18(5):2750-8.

126.   Steendam RR, Keshavarz L, de Souza B, Frawley PJJTJoCT. Thermodynamic properties of paracetamol impurities 4-nitrophenol and 4′-chloroacetanilide and the impact of such impurities on the crystallisation of paracetamol from solution. (2019);133:85-92.

127.   Keshavarz L, Pishnamazi M, Khandavilli UR, Shirazian S, Collins MN, Walker GM, et al. Tailoring crystal size distributions for product performance, compaction of paracetamol. (2021);14(4):103089.

128.   Nguyen TT, Khan A, Bruce LM, Forbes C, O'Leary RL, Price CJ. The Effect of Ultrasound on the Crystallisation of Paracetamol in the Presence of Structurally Similar Impurities. Crystals. (2017);7(10):294.

129.   Nguyen TTH, Turner TD, Matinong AM, Marziano I, Hammond RB, Roberts KJJCE, et al. Measured growth rates of Ibuprofen: comparing single crystal and bulk suspensions data. (2021).

130.   Durak L, Kennedy M, Langston M, Mitchell C, Morris G, Perlman ME, et al. Development and scale-up of a crystallization process to improve an API's physiochemical and bulk powder properties. (2018);22(3):296-305.

131.   Eder RJ, Schmitt EK, Grill J, Radl S, Gruber-Woelfler H, Khinast JGJCr, et al. Seed loading effects on the mean crystal size of acetylsalicylic acid in a continuous-flow crystallization device. (2011);46(3):227-37.

132.   Ristic R, Finnie S, Sheen D, Sherwood J. Macro-and micromorphology of monoclinic paracetamol grown from pure aqueous solution. The Journal of Physical Chemistry B. (2001);105(38):9057-66.

133.   Phan CU, Shen J, Yu K, Mao J, Tang G. Impact of crystal habit on the dissolution rate and in vivo pharmacokinetics of sorafenib tosylate. Molecules (Basel, Switzerland). 2021;26(11):3469.

134.   Guo M, Wei M, Li W, Guo M, Guo C, Ma M, et al. Impacts of particle shapes on the oral delivery of drug nanocrystals: Mucus permeation, transepithelial transport and bioavailability. J Control Release. 2019;307:64-75.

References

135.   Dandekar P, Kuvadia ZB, Doherty MF. Engineering crystal morphology. Annual Review of Materials Research. (2013);43:359-86.

136.   Weissbuch I, Popovitz-Biro R, Lahav M, Leiserowitz L. Understanding and control of nucleation, growth, habit, dissolution and structure of two-and three-dimensional crystals usingtailor-made'auxiliaries. Acta Crystallographica Section B: Structural Science. (1995);51(2):pp. 115-48.

137.   Berglund K, Myerson A. Handbook of industrial crystallization. Butterworth-Heinemann, London. (1993b):65.

138.   Braga D, Grepioni F, Maini L, Polito M. Crystal polymorphism and multiple crystal forms. Molecular Networks: Springer; (2009). p. 87-95.

139.   Tamura R, Miyata M. Advances in Organic Crystal Chemistry: Comprehensive Reviews 2015: Springer; (2015).

140.   Mitscherlich E. Über die Körper, welche in zwei vershiedenen kristallisieren Formen [Considerering the materials which can crystallize in two different crystal forms]. Abhl Akad Berlin. (1823):43-8.

141.   Stahly GP. Diversity in single-and multiple-component crystals. The search for and prevalence of polymorphs and cocrystals. Crystal growth & design. (2007);7(6):1007-26.

142.   Aitipamula S. Polymorphism in Molecular Crystals and Cocrystals. Advances in Organic Crystal Chemistry: Springer; (2015). p. 265-98.

143.   Bernstein J. Polymorphism in molecular crystals: Oxford University Press; (2007).

144.   Sudha C, Srinivasan K. Nucleation control and separation of paracetamol polymorphs through swift cooling crystallization process. Journal of Crystal Growth. (2014);401:248-51.

145.   Hilfiker R. Polymorphism: in the pharmaceutical industry: John Wiley & Sons; (2006).

146.   Ostwald W. Studies on formation and transformation of solid materials. Z Phys Chem. (1897);22:289-330.

147.   Ostwald W. Grundriss der allgemeinen Chemie: W. Engelmann; (1899).

148.   Ostwald W. On the assumed isomerism of red and yellow mercury oxide and the surface-tension of solid bodies. Z Phys Chem. (1900);34:495.

149.   Oswald ID, Allan DR, McGregor PA, Motherwell WS, Parsons S, Pulham CR. The formation of paracetamol (acetaminophen) adducts with hydrogen-bond acceptors. Acta Crystallographica Section B: Structural Science. (2002);58(6):1057-66.

150.   Datapharm-Communications-Limited. Electronic Medicines Compendium (eMC) (2021)   [cited   2021.   Available   from: https://www.medicines.org.uk/emc/search?q=paracetamol.

151.   Bosch ME, Sanchez A, Rojas FS, Ojeda CB. Determination of paracetamol: Historical evolution. Journal of pharmaceutical and biomedical analysis. (2006);42(3):291-321.

References

152. MHRA mahpra-. Paracetamol overdose: Simplification of the use of intravenous acetylcysteine London: MHRA - medicines and healthcare products regulatory agency; (2013) [cited 2015 23/01]. Available from: http://www.mhra.gov.uk/home/groups/pl-p/documents/drugsafetymessage/con178655.pdf.

153. Ms L Gordon, Dr G Jackson, Sandilands DEA. National Poisons Information Service Report 2016/17 [Annual Report]. Public Health England; (2013/14) [cited 2018 22/08/18]. Available from: https://www.toxbase.org/upload/Public%20Content/NPIS%202016-17%20report.pdf.

154. Silverman M, Lee PR. Bad medicine: The prescription drug industry in the third world: Stanford University Press; (1992).

155. Ellis F. Paracetamol- a curriculum resource: Royal Society of Chemistry; (2002) [cited 2015 19/01/2015]. Available from: http://www.rsc.org/learn-chemistry/content/filerepository/CMP/00/000/047/Paracetamol_web.pdf.

156. Quartarone G, Rancan E, Ronchin L, Vavasori A. Beckmann rearrangement of acetophenone oximes to the corresponding amides organo-catalyzed by trifluoroacetic acid for sustainable NSAIDs synthesis. Applied Catalysis A: General. (2014);472:167-77.

157. Haisa M, Kashino S, Kawai R, Maeda H. The monoclinic form of p-hydroxyacetanilide. Acta Crystallographica Section B: Structural Crystallography and Crystal Chemistry. (1976);32(4):1283-5.

158. Haisa M, Kashino S, Maeda H. The orthorhombic form of p-hydroxyacetanilide. Acta Crystallographica Section B: Structural Crystallography and Crystal Chemistry. (1974);30(10):2510-2.

159. Perlovich G, Volkova TV, Bauer-Brandl A. Polymorphism of paracetamol. Journal of Thermal Analysis and Calorimetry. 2007;89(3):767-74.

160. Di Martino P, Guyot-Hermann A, Conflant P, Drache M, Guyot J. A new pure paracetamol for direct compression: the orthorhombic form. International journal of pharmaceutics. (1996);128(1):1-8.

161. Agnew LR, McGlone T, Wheatcroft HP, Robertson A, Parsons AR, Wilson CC. Continuous crystallization of paracetamol (acetaminophen) form II: selective access to a metastable solid form. Crystal Growth & Design. (2017).

162. Nichols G, Frampton CS. Physicochemical characterization of the orthorhombic polymorph of paracetamol crystallized from solution. Journal of pharmaceutical sciences. (1998);87(6):684-93.

163. Espeau P, Céolin R, Tamarit JL, Perrin MA, Gauchi JP, Leveiller F. Polymorphism of paracetamol: Relative stabilities of the monoclinic and orthorhombic phases inferred from topological pressure-temperature and temperature-volume phase diagrams. Journal of pharmaceutical sciences. (2005);94(3):524-39.

References

164. Thompson C. Investigating the fundamentals of drug crystal growth using Atomic Force Microscopy: University of Nottingham; (2003).

165. Chen D, Sharma SK, Mudhoo A. Handbook on applications of ultrasound: Sonochemistry for sustainability: CRC press; (2011).

166. Guo Z, Jones AG, Li N. The effect of ultrasound on the homogeneous nucleation of BaSO4 during reactive crystallization. Chemical Engineering Science. (2006);61(5):1617-26.

167. Li H, Li H, Guo Z, Liu Y. The application of power ultrasound to reaction crystallization. Ultrasonics sonochemistry. (2006);13(4):359-63.

168. Bari AH, Chawla A, Pandit AB. Sono-crystallization kinetics of K2SO4: Estimation of nucleation, growth, breakage and agglomeration kinetics. Ultrasonics sonochemistry. (2017);35:196-203.

169. Mastan TH, Lenka M, Sarkar DJUs. Nucleation kinetics from metastable zone widths for sonocrystallization of l-phenylalanine. (2017);36:497-506.

170. Ni X, Liao A. Effects of cooling rate and solution concentration on solution crystallization of L-glutamic acid in an oscillatory baffled crystallizer. Crystal Growth and Design. (2008);8(8):2875-81.

171. Anderson HW, Carberry JB, Staunton HF, Sutradhar BC. Crystallization of adipic acid. Google Patents; (1995).

172. Ramisetty KA, Rasmuson ÅC. Controlling the Product Crystal Size Distribution by Strategic Application of Ultrasonication. Crystal Growth & Design. (2018);18(3):1697-709.

173. Kim W-S, Kim D-W, Koo K-KJJoI, Chemistry E. Effect of a surface-active agent on nucleation kinetics in ultrasound-assisted crystallization of paracetamol. (2019);77:441-8.

174. Sánchez-García YI, Bhangu SK, Ashokkumar M, Gutiérrez-Méndez N. Sonocrystallization of Lactose from Whey. Technological Approaches for Novel Applications in Dairy Processing first: IntechOpen London; (2018). p. 51-69.

175. Gracin S, Uusi-Penttilä M, Rasmuson ÅC. Influence of ultrasound on the nucleation of polymorphs of p-aminobenzoic acid. Crystal growth & design. (2005);5(5):1787-94.

176. Ike Y, Hirasawa IJCE, Technology. Polymorph Control of L-Phenylalanine in Cooling Crystallization by Ultrasonication. (2018);41(6):1093-7.

177. Belca LM, Ručigaj A, Teslič D, Krajnc MJUs. The use of ultrasound in the crystallization process of an active pharmaceutical ingredient. (2019);58:104642.

178. Narducci O, Jones A. Seeding in situ the cooling crystallization of adipic acid using ultrasound. Crystal Growth & Design. (2012);12(4):1727-35.

179. De Castro ML, Priego-Capote F. Ultrasound-assisted crystallization (sonocrystallization). Ultrasonics sonochemistry. 2007;14(6):717-24.

References

180.   Kordylla A, Koch S, Tumakaka F, Schembecker G. Towards an optimized crystallization with ultrasound: effect of solvent properties and ultrasonic process parameters. Journal of Crystal Growth. (2008);310(18):4177-84.

181.   Miyasaka E, Ebihara S, Hirasawa I. Investigation of primary nucleation phenomena of acetylsalicylic acid crystals induced by ultrasonic irradiation—ultrasonic energy needed to activate primary nucleation. Journal of crystal growth. (2006);295(1):97-101.

182.   Leighton T. The acoustic bubble: Academic press; (2012).

183.   Hem SL. The effect of ultrasonic vibrations on crystallization processes. Ultrasonics. (1967);5(4):202-7.

184.   Zeiger BW, Suslick KS. Sonofragmentation of molecular crystals. Journal of the American Chemical Society. (2011);133(37):14530-3.

185.   Ratsimba B, Biscans B, Delmas H, Jenck J. Sonocrystallization: the end of empiricism? A review on the fundamental investigations and the industrial developments. KONA Powder and particle Journal. 1999;17:38-48.

186.   Gielen B, Kusters P, Jordens J, Thomassen LC, Van Gerven T, Braeken L. Energy efficient crystallization of paracetamol using pulsed ultrasound. Chemical Engineering and Processing: Process Intensification. (2017);114:55-66.

187.   Sánchez-García YI, Ashokkumar M, Mason TJ, Gutiérrez-Méndez NJJofe. Influence of ultrasound frequency and power on lactose nucleation. (2019);249:34-9.

188.   Crespo R, Martins PM, Gales L, Rocha F, Damas AM. Potential use of ultrasound to promote protein crystallization. J Appl Cryst. 2010;43(6):1419-25.

189.   Guo Z, Zhang M, Li H, Wang J, Kougoulos E. Effect of ultrasound on anti-solvent crystallization process. Journal of Crystal Growth. (2005);273(3–4):pp. 555-63.

190.   Qiu L, Shi L, Liu Z, Xie K, Wang J, Zhang S, et al. Effect of power ultrasound on crystallization characteristics of magnesium ammonium phosphate. Ultrason Sonochem. 2017;36:123-8.

191.   Maharana A, Sarkar D. Effects of Ultrasound and Its Amplitude on the Metastable Zone Width, Induction Time, and Nucleation Kinetics of Pyrazinamide in Acetone. Ind Eng Chem Res. 2022;61(30):11262-75.

192.   Jordens J, Gielen B, Braeken L, Van Gerven T. Determination of the effect of the ultrasonic frequency on the cooling crystallization of paracetamol. . Chemical Engineering and Processing: Process Intensification. (2014):38-44.

193.   Wohlgemuth K, Ruether F, Schembecker G. Sonocrystallization and crystallization with gassing of adipic acid. Chemical Engineering Science. (2010):1016-27.

194.   Li H, Wang J, Bao Y, Guo Z, Zhang M. Rapid sonocrystallization in the salting-out process. Journal of Crystal Growth. (2003);247(1-2):192-8.

References

195.   Jordens J, Gielen B, Braeken L, Van Gerven T. Determination of the effect of the ultrasonic frequency on the cooling crystallization of paracetamol. Chemical Engineering and Processing: Process Intensification. 2014;84:38-44.

196.   Kaur Bhangu S, Ashokkumar M, Lee J. Ultrasound assisted crystallization of paracetamol: crystal size distribution and polymorph control. Crystal Growth & Design. (2016);16(4):1934-41.

197.   De Castro ML, Priego-Capote F. Ultrasound-assisted crystallization (sonocrystallization). Ultrasonics sonochemistry. (2007);14(6):717-24.

198.   Eder RJP, Schrank S, Besenhard MO, Roblegg E, Gruber-Woelfler H, Khinast JG. Continuous Sonocrystallization of Acetylsalicylic Acid (ASA): Control of Crystal Size. Cryst Growth Des. 2012;12(10):4733-8.

199.   Boels L, Wagterveld R, Mayer M, Witkamp G. Seeded calcite sonocrystallization. Journal of Crystal Growth. (2010);312(7):961-6.

200.   Hatkar UN, Gogate PR. Process intensification of anti-solvent crystallization of salicylic acid using ultrasonic irradiations. Chemical Engineering and Processing: Process Intensification. (2012);57:16-24.

201.   Boels L, Wagterveld R, Witkamp G. Ultrasonic reactivation of phosphonate poisoned calcite during crystal growth. Ultrasonics sonochemistry. (2011);18(5):1225-31.

202.   Kusters KA, Pratsinis SE, Thoma SG, Smith DM. Ultrasonic fragmentation of agglomerate powders. Chemical engineering science. (1993);48(24):4119-27.

203.   Guo Z, Jones A, Li N, Germana S. High-speed observation of the effects of ultrasound on liquid mixing and agglomerated crystal breakage processes. Powder technology. (2007);171(3):146-53.

204.   Horie T, Akao S, Suzuki T, Tanaka K, Jia N, Taniya K, et al. Process development for ultrasonic fracturing of zirconium phosphate particles. Journal of Chemical Engineering of Japan. (2014);47(2):124-9.

205.   Kabalnov AS, Shchukin ED. Ostwald ripening theory: applications to fluorocarbon emulsion stability. Advances in colloid and interface science. (1992);38:69-97.

206.   Mason TJ. Sonochemistry and the environment–Providing a "green" link between chemistry, physics and engineering. Ultrasonics sonochemistry. (2007);14(4):476-83.

207.   Price CJ. Take some solid steps to improve crystallization. Chemical engineering progress. 1997;93(9):34-6.

208.   Forbes C. Investigations on the mechanisms of non-photochemical laser-induced nucleation and sonocrystallisation. 2022.

209.   Inc TFS. Agilent Technologies 1100 Series User Manual: the ultimate manuals library; (2007) [cited 2021. Available from: https://www.manualslib.com/manual/2853/Agilent-Technologies-1100-Series.html?page=2#manual.

References

210.   Worlitschek J, De Buhr J. Crystallization studies with Focused Beam Reflectance Measurement and MultiMax(2005). Available from: http://uk.mt.com/mt_ext_files/Editorial/Generic/4/Crystallization_MultiMax_FBRM_Editorial-Generic_1117648389578_files/Application_note_Crystallization_Studies_on_MultiMax_with_FBRM.pdf.

211.   GmbH S. QICPIC (2017-2018) [Available from: https://www.sympatec.com/en/particle-measurement/sensors/dynamic-image-analysis/qicpic/.

212.   Clark C, M , Dutrow, B,L. Single-crystal X-ray Diffraction Montana state univeristy(2015) [updated 24/04/2015; cited 2015 13/05]. Available from: http://serc.carleton.edu/research_education/geochemsheets/techniques/SXD.html.

213.   Nave CRR. HyperPhysics Atlanta, Georgia: Georgia State Univeristy; (2012) [cited 2015 16/06]. Available from: http://hyperphysics.phy-astr.gsu.edu/hbase/quantum/bragg.html.

214.   Database JSE. *Inorganic Chemistry.* Single Crystal and Powder X-ray Diffraction 2023 [Available from: https://www.jove.com/v/10462/single-crystal-and-powder-x-ray-diffraction.

215.   Beyer T, Day GM, Price SL. The prediction, morphology, and mechanical properties of the polymorphs of paracetamol. Journal of the American Chemical Society. 2001;123(21):5086-94.

216.   K O. Separation Technology. 2nd ed
John Wiley and Sons Inc. (2008);2.

217.   Bai R, Tien C. Further work on cake filtration analysis. Chemical engineering science. (2005);60(2):301-13.

218.   Bürger R, Concha F, Karlsen KH. Phenomenological model of filtration processes: 1. Cake formation and expression. Chemical Engineering Science. (2001);56(15):4537-53.

219.   Tien C, Teoh S, Tan R. Cake filtration analysis—the effect of the relationship between the pore liquid pressure and the cake compressive stress. Chemical Engineering Science. (2001);56(18):5361-9.

220.   Birch M, Marziano I. Understanding and avoidance of agglomeration during drying processes: A case study. Organic Process Research & Development. (2013);17(10):1359-66.

221.   Tamrakar A, Gunadi A, Piccione PM, Ramachandran R. Dynamic agglomeration profiling during the drying phase in an agitated filter dyer: Parametric investigation and regime map studies. Powder Technology. (2016);303:109-23.

222.   Ottoboni S, Simurda M, Wilson S, Irvine A, Ramsay F, Price CJ. Understanding effect of filtration and washing on dried product: Paracetamol case study. Powder technology. 2020;366:305-23.

223.   Ottoboni S PCJ, Steven C1, Meehan E, Barton A, Firth P, Mitchell A5 Tahir, F. Development of a novel continuous filtration unit for pharmaceutical process development and manufacturing. JPS(2018).

References

224.   Umetrics M. MODDE user guide to(2015).

225.   Leardi R. Experimental design in chemistry: A tutorial. Elsevier. (2009).

226.   Perrin M-A, Neumann MA, Elmaleh H, Zaske L. Crystal structure determination of the elusive paracetamol Form III. Chemical Communications. (2009)(22):3181-3.

227.   Finnie S, Ristic R, Sherwood J, Zikic A. Morphological and growth rate distributions of small self-nucleated paracetamol crystals grown from pure aqueous solutions. Journal of crystal growth. (1999);207(4):308-18.

228.   Sudha C, Srinivasan K. Understanding the effect of solvent polarity on the habit modification of monoclinic paracetamol in terms of molecular recognition at the solvent crystal/interface. Crystal Research and Technology. (2014);49(11):865-72.

229.   Druzhbin D, Drebushchak T, Min'kov V, Boldyreva E. Crystal structure of two paracetamol polymorphs at 20 K: A search for the "structure-property" relationship. Journal of Structural Chemistry. (2015);56(2):317-23.

230.   Ripperger S, Gösele W, Alt C, Loewe T. Filtration, 1. fundamentals in Ullmann's Encyclopedia of industrial chemistry. Wiley-VCH. (2013).

231.   Beckmann W. Crystallization: Basic Concepts and Industrial Applications: John Wiley & Sons; (2013).

232.   Sciences P, Services DD. Solubility (2011) [Available from: http://www.particlesciences.com/docs/technical_briefs/TB_2011_6.pdf.

233.   Behera S, Ghanty S, Ahmad F, Santra S, Banerjee S. UV-visible spectrophotometric method development and validation of assay of paracetamol tablet formulation. J Anal Bioanal Tech. (2012);3(6):2-6.

234.   Ungnade HE. Ultraviolet Absorption Spectra of Acetanilides1. Journal of the American Chemical Society. (1954);76(20):5133-5.

235.   Capellades G, Bonsu JO, Myerson AS. Impurity incorporation in solution crystallization: diagnosis, prevention, and control. CrystEngComm. 2022;24(11):1989-21.

236.   Thomas LH, Wales C, Zhao L, Wilson CC. Paracetamol Form II: An Elusive Polymorph through Facile Multicomponent Crystallization Routes. Cryst Growth Des. 2011;11(5):1450-2.

237.   Food U, Administration D. Laboratory analysis of ranitidine and nizatidine products. 2020.

238.   Woodcock J. Statement alerting patients and health care professionals of NDMA found in samples of ranitidine. Food and Drug Administration Statement Director-Center for Drug Evaluation and Research. 2019.

239.   group Cn. Isoamyl Alcohol (n.d) [22/08/2018]. Available from: https://www.chemoxy.com/products-and-applications/products/intermediates/isoamyl-alcohol/.

References

240. ROMERO S, REILLO A, ESCALERA B, BUSTAMANTE P. The behavior of paracetamol in mixtures of amphirotic and amphiprotic-aprotic solvents. Relationship of solubility curves to specific and nonspecific interactions. Chemical and pharmaceutical bulletin. 1996;44(5):1061-4.

241. Grant D, Mehdizadeh M, Chow A-L, Fairbrother J. Non-linear van't Hoff solubility-temperature plots and their pharmaceutical interpretation. International journal of pharmaceutics. 1984;18(1-2):25-38.

242. BmbH C. Chemical Properties of Metacetamol (CAS 621-42-1) (2016) [cited 2017 03/07]. Available from: https://www.chemeo.com/cid/12-642-5/Metacetamol.

243. Gmehling J, Krafczyk J, Ahlers J, Nebig S, Hunecker I, Eisel M, et al. Pure compound data from DDB. Dortmund Data Bank. (1983).

244. Gaisford S. W*hat is ideal solubility?* 2023 [Available from: https://www.pharmaexcipients.com/news/what-is-ideal-solubility/.

245. Chew CM, Ristic RI, Dennehy RD, De Yoreo JJ. Crystallization of Paracetamol under Oscillatory Flow Mixing Conditions. Cryst Growth Des. 2004;4(5):1045-52.

246. Mikhailenko MA. Growth of large single crystals of the orthorhombic paracetamol. Journal of crystal growth. 2004;265(3):616-8.

247. Turner TD, Nguyen TTH, Nicholson P, Brown G, Hammond RB, Roberts KJ, et al. A temperature-controlled single-crystal growth cell for the in situ measurement and analysis of face-specific growth rates. Journal of applied crystallography. 2019;52(2):463-7.

248. Altaher H, Frohberg P, Ulrich J. Crystal Growth Rate Measurements in Pure and Impure Solutions: Single Crystal vs. Crystal Collectives. Chemie ingenieur technik. 2015;87(10):1418.

249. Vizman D. Flow Control by Magnetic Fields during Crystal Growth from Melt. 2015;2:909-50.

250. Hendriksen BA, Grant DJ. The effect of structurally related substances on the nucleation kinetics of paracetamol (acetaminophen). Journal of crystal growth. (1995);156(3):252-60.

251. Hendriksen BA, Grant DJW, Meenan P, Green DA. Crystallisation of paracetamol (acetaminophen) in the presence of structurally related substances. Journal of Crystal Growth. (1997);183(4):629-40.

252. Shekunov BY, Grant DJ, Latham RJ, Sherwood JN. In situ optical interferometric studies of the growth and dissolution behavior of paracetamol (acetaminophen) crystals. 3. Influence of growth in the presence of p-acetoxyacetanilide. The Journal of Physical Chemistry B. (1997);101(44):9107-12.

References

253.   Kempkes M, Vetter T, Mazzotti M. Monitoring the particle size and shape in the crystallization of paracetamol from water. Chemical Engineering Research and Design. (2010);88(4):447-54.

254.   David J. Effect of temperature on crystal growth and crystal properties of paracetamol. Journal of the Chemical Society, Faraday Transactions. 1996;92(3):439-44.

255.   Gibbs JW. The scientific papers of J. Willard Gibbs: Longmans, Green and Company; (1906).

256.   Randolph A, White EJCES. Modeling size dispersion in the prediction of crystal-size distribution. (1977);32(9):1067-76.

257.   Omar W, Al-Sayed S, Sultan A, Ulrich J. Growth rate of single acetaminophen crystals in supersaturated aqueous solution under different operating conditions. Crystal Research and Technology. (2008);43(1):22-7.

258.   Barrett M, McNamara M, Hao H, Barrett P, Glennon B. Supersaturation tracking for the development, optimization and control of crystallization processes. Chemical Engineering Research and Design. (2010);88(8):1108-19.

259.   Tari T, Ambrus R, Szakonyi G, Madarász D, Frohberg P, Csóka I, et al. Optimizing the crystal habit of glycine by using additive for impinging jet crystallization. Chemical Engineering & Technology. (2017).

260.   Yang Y, Zhang C, Pal K, Koswara A, Quon J, McKeown R, et al. Application of Ultra-Performance Liquid Chromatography as an Online Process Analytical Technology Tool in Pharmaceutical Crystallization. Crystal Growth & Design. (2016);16(12):7074-82.

261.   Yang Y, Song L, Zhang Y, Nagy ZK. Application of wet milling-based automated direct nucleation control in continuous cooling crystallization processes. Industrial & Engineering Chemistry Research. (2016);55(17):4987-96.

262.   Ruecroft GH, David ; Ly, Tuan ; Maxted, Neil ; Cains, Peter W. ; Cains, Peter W. Sonocrystallization: The Use of Ultrasound for Improved Industrial

Crystallization. Organic process research & development. (2005);9 (60:923-32.

263.   Richards WTLAL. The chemical effects of high frequency sound waves I. A preliminary survey. Journal of the American Chemical Society. (1929);49.

264.   Kapustin A. The effects of ultrasound on the kinetics of crystallization. US Academy of Sciences Press. (1963).

265.   Reshetnyak I. Effect of ultrasound on crystallization kinetics in small volumes of solutions. Akust Zh. (1975):99-103.

266.   Turner C, Galkowski T, Radle W, VanHook A. Grain formation by sonic irradiation. Int Sugar J. (1950);52:298-9.

References

267.   Renuka Devi K, Raja A, Srinivasan K. Ultrasound assisted nucleation and growth characteristics of glycine polymorphs – A combined experimental and analytical approach. Ultrasonics Sonochemistry. (2015);24(0):107-13.

268.   Dodds J, Espitalier F, Louisnard O, Grossier R, David R, Hassoun M, et al. The Effect of Ultrasound on Crystallisation-Precipitation Processes: Some Examples and a New Segregation Model. Particle & Particle Systems Characterization. (2007);24(1):18-28.

269.   Luque de Castro MD, Priego-Capote F. Ultrasound-assisted crystallization (sonocrystallization). Ultrasonics Sonochemistry. (2007);14(6):717-24.

270.   Stelzer T, Pertig D, Ulrich J. Ultrasonic crystallization monitoring technique for simultaneous in-line measurement of liquid and solid phase. Journal of Crystal Growth. (2013);362:71-6.

271.   Shtukenberg AG, Ward MD, Kahr B. Crystal growth inhibition by impurity stoppers, now. Journal of Crystal Growth. 2022;597:126839.

272.   Urwin S, Martin A, Ter Horst J, editors. Paracetamol habit modification by impurities. 50th Annual Conference of the British Association of Crystal Growth; (2019).

273.   Ruecroft G, Hipkiss D, Fennell M. Improving the Bayer process by power ultrasound induced crystallization (sonocrystallization) of key impurities. TMS Light Metals. 2005:163-6.

274.   Evrard Q, Houard Fl, Daiguebonne C, Calvez G, Suffren Y, Guillou O, et al. Sonocrystallization as an Efficient Way to Control the Size, Morphology, and Purity of Coordination Compound Microcrystallites: Application to a Single-Chain Magnet. Inorg Chem. 2020;59(13):9215-26.

275.   Amara N, Ratsimba B, Wilhelm A-M, Delmas H. Crystallization of potash alum: effect of power ultrasound. Ultrasonics sonochemistry. (2001);8(3):265-70.

276.   Dhumal R, Biradar S, Paradkar A, York P. Ultrasound assisted engineering of lactose crystals. 2008.

277.   Lee J. Importance of sonication and solution conditions on the acoustic cavitation activity. Handbook of Ultrasonics and Sonochemistry. (2016):137-75.

278.   Frawley PJ, Mitchell NA, Ó'Ciardhá CT, Hutton KW. The effects of supersaturation, temperature, agitation and seed surface area on the secondary nucleation of paracetamol in ethanol solutions. Chemical Engineering Science. (2012);75:183-97.

279.   Agrawal S, Paterson A. Secondary nucleation: Mechanisms and models. Chemical Engineering Communications. (2015);202(5):698-706.

280.   Louisnard O GF, Grossier R. Segregation of a liquid mixture by a radially oscillating bubble. Journal of Fluid Mechanics. (2007):385-415.

281.   Mingxi W, Yi F, Gail tH. Cavitation in Biomedicine (2017). Available from: https://books.google.com/books/about/Cavitation_in_Biomedicine.html?id=smJ1CgAAQBAJ.

References

282.   Kordylla A, Krawczyk T, Tumakaka F, Schembecker G. Modeling ultrasound-induced nucleation during cooling crystallization. Chemical Engineering Science. (2009):1635-42.

283.   Ghazi N, Liu Z, Bhatt C, Kiang S, Cuitino AJAP. Investigating the Effect of APAP Crystals on Tablet Behavior Manufactured by Direct Compression. (2019);20(5):168.

284.   Hagenson LC, Doraiswamy L. Comparison of the effects of ultrasound and mechanical agitation on a reacting solid-liquid system. Chemical Engineering Science. (1998);53(1):131-48.

285.   Narducci O, Jones A, Kougoulos E. Continuous crystallization of adipic acid with ultrasound. Chemical engineering science. (2011):1069-76.

286.   Gielen B, Jordens J, Thomassen LC, Braeken L, Van Gerven TJC. Agglomeration control during ultrasonic crystallization of an active pharmaceutical ingredient. (2017);7(2):40.

287.   Zamanipoor MH, Dincer TD, Zisu B, Jayasena V. Nucleation and growth rates of lactose as affected by ultrasound in aqueous solution (Retraction of vol 93, pg 995, 2013). SPRINGER FRANCE 22 RUE DE PALESTRO, PARIS, 75002, FRANCE; (2016).

288.   Kim S, Wei C, Kiang S. Crystallization process development of an active pharmaceutical ingredient and particle engineering via the use of ultrasonics and temperature cycling. Organic process research & development. (2003);7(6):997-1001.

289.   Uwaha M. 8 - Growth Kinetics: Basics of Crystal Growth Mechanisms. In: Nishinaga T, editor. Handbook of Crystal Growth (Second Edition). Boston: Elsevier; 2015. p. 359-99.

290.   Moynihan HA, Horgan DE. Impurity Occurrence and Removal in Crystalline Products from Process Reactions. Organic Process Research & Development. (2017);21(5):689-704.